

CONSTRUCTION NOISE PREDICTION USING
STOCHASTIC DEEP LEARNING

OOI WEI CHIEN

MASTER OF ENGINEERING SCIENCE

LEE KONG CHIAN FACULTY OF ENGINEERING AND
SCIENCE
UNIVERSITI TUNKU ABDUL RAHMAN
APRIL 2022

**CONSTRUCTION NOISE PREDICTION USING STOCHASTIC DEEP
LEARNING**

By

OOI WEI CHIEN

A dissertation submitted to the Department of Civil Engineering,
Faculty of Lee Kong Chian Engineerin and Science,
Universiti Tunku Abdul Rahman,
in partial fulfillment of the requirements for the degree of
Master of Engineering Science
April 2022

APPROVAL SHEET

This dissertation entitled “CONSTRUCTION NOISE PREDICTION USING STOCHASTIC DEEP LEARNING” was prepared by OOI WEI CHIEN and submitted as partial fulfilment of the requirements for the degree of Master of Engineering and Science in Civil Engineering at Universiti Tunku Abdul Rahman.

Approved by:



(Dr. Lim Ming Han)

Date:...22nd April 2022.....

Assistant Professor/Supervisor

Department of Civil Engineering

Faculty of Lee Kong Chian Faculty of Engineering and Science

Universiti Tunku Abdul Rahman



(Dr. Lee Yee Ling)

Date:... 22nd April 2022.....

Assistant Professor/Co-supervisor

Department of Civil Engineering

Faculty of Lee Kong Chian Faculty of Engineering and Science

Universiti Tunku Abdul Rahman

SUBMISSION SHEET

LEE KONG CHIAN FACULTY OF ENGINEERING AND SCIENCE

UNIVERSITI TUNKU ABDUL RAHMAN

Date: 22nd APRIL 2022

SUBMISSION OF FINAL YEAR PROJECT /DISSERTATION/THESIS

It is hereby certified that **Ooi Wei Chien** (ID No: **20UEM00218**) has completed this dissertation entitled "**CONSTRUCTION NOISE PREDICTION USING STOCHASTIC DEEP LEARNING**" under the supervision of Dr. Lim Ming han (Supervisor) from the Department of Civil Engineering, Lee Kong Chian Faculty of Engineering and Science, and Dr. Lee Yee Ling (Co-Supervisor) from the Department of Civil Engineering, Lee Kong Chian Faculty of Engineering and Science.

I understand that University will upload softcopy of my dissertation in pdf format into UTAR Institutional Repository, which may be made accessible to UTAR community and public.

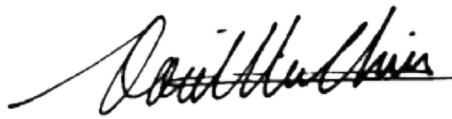
Yours truly,



Ooi Wei Chien

DECLARATION

I hereby declare that the dissertation is based on my original work except for quotations and citations which have been duly acknowledged. I also declare that it has not been previously or concurrently submitted for any other degree at UTAR or other institutions.



Name : OOI WEI CHIEN

Date : 22nd APRIL 2022

The copyright of this report belongs to the author under the terms of the Copyright Act 1987 as qualified by Intellectual Property Policy of Universiti Tunku Abdul Rahman. Due acknowledgement shall always be made of the use of any material contained in, or derived from, this report.

© 2022, OOI WEI CHIEN. All right reserved.

ACKNOWLEDGEMENTS

I would like to thank everyone who had contributed to the successful completion of this project. I would like to express my gratitude to my research supervisor, Dr. Lim Ming Han and Dr. Lee Yee Ling for their invaluable advice, guidance and their enormous patience throughout the development of the research.

In addition, I would also like to express my gratitude to my loving parents and friends who had helped and encouraged me.

ABSTRACT

CONSTRUCTION NOISE PREDICTION USING STOCHASTIC DEEP LEARNING

OOI WEI CHIEN

Construction noise is an occupational noise that is potentially harmful, and it usually originates from earth-moving machines in construction sites. The impact of construction noise on the health and safety of construction workers is one of the main concerns in the industry. The adverse impacts arising from construction noise may jeopardize public welfare, particularly for those who live nearby the construction site. Therefore, this research aims to develop a reliable noise prediction model on the basis of stochastic modelling and deep learning technique. Stochastic modelling was applied in this study to manipulate the several major parameters such as the randomness of three different duty cycles, coverage angle of the noise receiver, and position of dynamic machinery in the construction site, to generate a set of randomized data as the input for the deep learning model. The deep learning model was trained with stochastic data to predict the noise levels emitted from the construction site. The programming algorithm of stochastic modelling was executed in MATLAB, whereas the deep learning model was established by using Python 3.6 programming language in Spyder. Ten case studies were conducted in this study to validate the predictive performance of the stochastic deep learning noise prediction model. The stochastic deep learning model showed high accuracy of prediction results with an average absolute difference of less than 1.2 dBA having the relative percentage error of less than 4 % among the case studies as compared to the measurement. The reliability of the results from the prediction model was high. In conclusion, the stochastic deep learning model was established and provided a promising outcome with satisfactory predictive performance. Lastly, the

model is worthwhile to be further developed to fully exploit the potential of the stochastic deep learning noise prediction model in construction industries as a planning, managerial, and monitoring tool.

TABLE OF CONTENTS

	Page
APPROVAL SHEET	i
SUBMISSION SHEET	ii
DECLARATION	iii
ACKNOWLEDGEMENTS	v
ABSTRACT	vi
TABLE OF CONTENTS	viii
LIST OF TABLES	xii
LIST OF FIGURES	xiv
LIST OF SYMBOLS / ABBREVIATIONS	xxi

CHAPTER

1	INTRODUCTION	1
1.1	General Introduction	1
1.2	Importance of the Study	4
1.3	Problem Statement	5
1.4	Aim and Objectives	7
1.5	Scope of the Study	8
1.6	Report Structure	9
2	LITERATURE REVIEW	12
2.1	Introduction	12
2.2	Sound	12
2.3	Sound Power, Sound Intensity and Sound Pressure	13
2.4	Sound Propagation	14
2.5	Geometrical Divergence of Point Source	15
2.6	Human Hearing	17
2.7	Noise	18
	2.7.1 Types of Noise	20
	2.7.2 Occupational Noise Exposure	21
	2.7.3 Construction Noise	24
2.8	Hierarchy of Controls for Noise Exposure	27
2.9	Noise Regulation and Guidelines	30
	2.9.1 Occupational Regulation and Guidelines	30
	2.9.2 Guidelines for Environmental Noise Limits and Control	32
2.10	Noise Prediction	36
2.11	Construction Noise Prediction	36
2.12	Stochastic Modelling	38
	2.12.1 Probabilistic Approach for Noise Modelling	39
	2.12.2 Stochastic Monte Carlo Method	40
	2.12.3 Stochastic Simulation Framework	41

2.12.4	Simple Prediction Charts Method	42
2.13	Reliability and Accuracy Assessment for Predicted Data	48
2.14	Artificial Intelligence	51
2.15	Machine Learning	52
2.16	Supervised Learning	54
	2.16.1 Regression	54
	2.16.2 Classification	56
2.17	Unsupervised Learning	58
	2.17.1 Clustering	58
	2.17.2 Association	60
2.18	Semi-supervised Learning	60
2.19	Reinforcement Learning	62
2.20	Deep Learning	63
2.21	Multilayer Perceptron	64
2.22	Convolutional Neural Network	65
2.23	Recurrent Neural Network	67
2.24	Input Layer	68
2.25	Activation Function	69
	2.25.1 Linear Activation Function	70
	2.25.2 Sigmoid Activation Function	70
	2.25.3 Hyperbolic Tangent Function (Tanh)	71
	2.25.4 Rectified Linear Unit Function (ReLU)	72
2.26	Backpropagation	75
	2.26.1 Learning Rate	78
2.27	Loss Function and Cost Function	79
2.28	Optimization Techniques	80
	2.28.1 Gradient Descent (GD)	80
	2.28.2 SGD with Momentum	82
	2.28.3 Adaptive Gradient Algorithm (AdaGrad)	83
	2.28.4 Root Mean Square Propagation (RMSprop)	84
	2.28.5 Adaptive Moment Estimation (Adam)	85
2.29	Dropout Rate	87
2.30	Application of Deep Learning in Prediction Models	88
2.31	Concluding Remarks	89
3	METHODOLOGY	91
3.1	Introduction	91
3.2	Research Framework	92
3.3	Configuration of Stochastic Deep Learning Framework	92
3.4	Development of Programming Algorithms and Coding	96
3.5	Model Configuration	102
	3.5.1 Data Split	103
	3.5.2 The Architecture of the Neural Network	103
	3.5.3 Activation Function	104
	3.5.4 Optimizer and Learning Rate	104
	3.5.5 Learning Rate	105

3.5.6	Batch Size	105
3.5.7	Epoch	106
3.5.8	Optimal Hyperparameters	106
3.5.9	Performance Evaluation	111
3.6	Data Analysis, Data Validation and Publications	112
3.7	Field Measurement	113
3.7.1	Noise Measurement Equipment	113
3.7.2	Software	115
3.7.3	Selection Criteria for Case Studies	115
3.8	Data Analysis	123
3.8.1	Background Noise Level	123
3.8.2	Sound Pressure Level	125
3.8.3	Sound Power Level	125
3.8.4	Prediction of Sound Pressure Level using Simple Prediction Charts	126
3.8.5	Data Validation between the Prediction and Measurement	128
3.9	Concluding Remarks	130
4	DEVELOPMENT OF STOCHASTIC DEEP LEARNING MODEL	130
4.1	Introduction	131
4.2	Stochastic Modelling	132
4.2.1	Mean Level Deviation	132
4.2.2	Standard Deviation	135
4.2.3	Distribution of the Data at Different Angles	137
4.3	Configuration of Stochastic Deep Learning Model	139
4.3.1	Data Split	140
4.3.2	Number of Hidden Layers and Neurons	144
4.3.3	Activation Function in Hidden Layers	144
4.3.4	Number of Epoch	146
4.3.5	Learning Rate	146
4.3.6	Batch Size	149
4.3.7	Optimizer	151
4.4	Performance of Stochastic Deep Learning Models	153
4.5	Concluding Remarks	155
5	RESULTS AND DISCUSSION	158
5.1	Introduction	158
5.2	Proposed Case Studies	159
5.2.1	Noise Emission Levels from Individual Machine	159
5.2.2	Construction Activity of the Case Studies	163
5.3	Background Noise of Construction Site	165
5.4	Noise Emission Levels from Construction Activities	166
5.5	Construction Noise Prediction using Simple Prediction Charts	170

5.6	Construction Noise Prediction using Stochastic Deep Learning Model	185
5.7	Comparison of Simple Prediction Charts Technique (SPC) and Stochastic Deep Learning (SDL) Model Prediction	199
5.8	Comparison of the Prediction and Actual Measurement	203
5.9	Concluding Remark	214
6	CONCLUSION AND RECOMMENDATION	216
6.1	Introduction	217
6.2	Conclusion	217
6.2.1	Feasibility of using Artificial Neural Network to Predict Construction Noise Levels	217
6.2.2	Limitation	219
6.3	Recommendation	220
	REFERENCES	222
	APPENDIX A	239
	APPENDIX B	248

LIST OF TABLES

Table		Page
2.1	The Noise Exposure Level of Heavy Machines Operators.	24
2.2	Noise Emitted from Construction Machines	26
2.3	Maximum allowable sound level ($L_{A_{\text{Freq}}}$) by for Different Category of Land Use for New Development and Planning	33
2.4	Maximum Allowable Sound Levels (percentile L10 and Lmax) for Different Land Use in Demolition Work, Construction Activities and Maintenance Purposes	34
2.5	Application of Stochastic Modelling in Noise Prediction	38
2.6	Determination of Association Strength based on R^2	49
2.7	Determination of Association Strength based on Correlation Coefficient Value	50
3.1	Configuration of the noise prediction model for aspect ratio of 1:1	106
3.2	Coordinate system of microphone position	121
3.3	Coordinate system of microphone position	122

3.4	Determination of background noise correction factor	124
4.1	Performance of model of different variations of hyperparameters	140
4.2	Performance of the stochastic deep learning models	154
5.1	Construction activities and sound power level of the machines	161
5.2	Input data for the sound power level of the earth-moving machine	162
5.3	Description of the case studies	163
5.4	Background noise of the construction sites	165
5.5	Summary of the sound pressure levels at the control points for the case studies	168
5.6	Noise prediction using Simple Prediction Charts.	172
5.7	Noise Prediction using Stochastic Deep Learning Model	188
5.8	Comparison between the prediction of SPC technique and DL model	201
5.9	Comparison between the prediction and measurement	206

LIST OF FIGURES

Figures		Page
2.1	Propagation of sound wave	15
2.2	Point source above a rigid hard surface	16
2.3	Auditory system anatomy	18
2.4	Tolerability of ear	18
2.5	Types of noise (a) steady continuous noise; (b) steady non-continuous noise; (c) fluctuating noise; (d) intermittent noise; (e) impulsive noise	21
2.6	Noise-induced hearing loss compensation	23
2.7	Hierarchy of controls	27
2.8	Effect of distance for square sites (50 m x 50 m; 100 m x 100 m) (a) site configuration with same r: w : d; (b) design layout of construction site and position of receiver; (c) effect of distance on noise level distribution on square site (- - - - :100 m x 100 m; — : 50 m x 50 m); (d) standard deviation vs. distance normalised with w or d; (e) mean level variation; (f) deviation from tangent line	46
2.9	Relationship of variables	48

2.10	Venn diagram of artificial intelligence, machine learning and deep learning	51
2.11	Classification of machine learning	53
2.12	Visualization of linear regression	55
2.13	Types of classification (a) binary classification; (b) multi-class classification	57
2.14	Visualization of clustering	58
2.15	Semi-supervised learning	60
2.16	Illustration of reinforcement learning	62
2.17	Architecture of multilayer perceptron	63
2.18	Architecture of simple, shallow and deep neural network	64
2.19	Convolutional neural network	65
2.20	Recurrent neural network	66
2.21	Shallow neural network	67
2.22	Activation functions (a) linear function (b) sigmoid; (c) tanh; (d) ReLU	72
2.23	Training the neural network using the back-propagation algorithm	75

2.24	Propagate backwards to hidden nodes and calculate the data	75
2.25	Equation derivation to adjust the weight	76
2.26	Derive the equation again to adjust the weight	76
2.27	Influence of learning rate (a) variation of learning rate; (b) illustration of local minimum and global minimum	77
2.28	Illustration of gradient descent	80
2.29	Influence of momentum in learning process (a) without momentum and causing violent oscillation; (b) with momentum shows that it takes less oscillation to reach the optimum point	81
2.30	During each minibatch of training, dropout makes each neuron in the network inactive with a random probability	85
3.1	Stages of work plan	91
3.2	The framework of stochastic modelling for aspect ratio 1:1	93
3.3	The conceptual framework of the deep learning model	94
3.4	The programming algorithm of stochastic modelling for aspect ratio 1:1	98

3.5	The process of finding the optimal set of hyperparameters for the model	108
3.6	The architecture of the optimal model for the aspect ratio of 1:1	109
3.7	Calibration of sound level meter	113
3.8	The procedures of measurement	116
3.9	Configuration of sub-area	117
3.10	Site configuration (a) case study 1 drainage system; (b) case study 2 and 3 sewerage system; (c) case study 4 water distribution system; (d) case study 5 and 6 road construction; (e) case study 7 site clearance; (f) case study 8 mountain hacking; (g) case study 9 pile boring activity for pile with the diameter of 1.2 m; (h) pile boring activity for contiguous bored pile with the diameter of 750 mm	117
3.11	Configuration of sound power level measurement	121
4.1	Graph of r/w ratio vs. MLD (mean level deviation) with different aspect ratios (a) 1:1; (b) 1:2; (c) 1:4; (d) 1:8; (e) 2:1; (f) 4:1; (g) 8:1	132
4.2	Graph of r/w ratio vs. STD (standard deviation) with different aspect ratios (a) 1:1; (b) 1:2; (c) 1:4; (d) 1:8; (e) 2:1; (f) 4:1; (g) 8:1	135

4.3	Graph of angle vs. MLD (mean level deviation) with different aspect ratios (a) 1:1; (b) 1:2; (c) 1:4; (d) 1:8; (e) 2:1; (f) 4:1; (g) 8:1	137
4.4	Training and testing of the model based on different data split ratios (a) 60:20:20 training; (b) 60:20:20 testing; (c) 70:15:15 training; (d) 70:15:15 testing; (e) 80:10:10 training; (f) 80:10:10 testing	142
4.5	Comparison of training and testing of the model using different activation functions in the hidden layers (a) validation curve using ReLU; (b) testing curve using ReLU; (c) validation curve using Sigmoid; (d) testing using Sigmoid	144
4.6	Comparison of different learning rates in training and testing of the model (a) lr of 10^{-4} on training; (b) lr of 10^{-4} on testing; (c) lr of 10^{-3} on training; (d) lr of 10^{-3} on testing; (e) lr of 10^{-2} on training; (f) lr of 10^{-2} on testing	147
4.7	Comparison of validation and testing of the model using different batch size (a) batch size 32 on validation; (b) batch size 32 on testing; (c) batch size 64 on validation; (d) batch size 64 on testing; (e) batch size 128 on validation; (f) batch size 128 on testing	149

4.8	Comparison of validation and testing of the model using different optimizers (a) Adam on validation; (b) Adam on testing; (c) RMSprop on validation; (d) RMSprop on testing; (e) Adagrad on validation; (f) Adagrad on testing	151
5.1	Case study 1 for the simple prediction charts technique	175
5.2	Case study 2 for the simple prediction charts technique	176
5.3	Case study 3 for the simple prediction charts technique	176
5.4	Case study 4 for the simple prediction charts technique	177
5.5	Case study 5 for the simple prediction charts technique	178
5.6	Case study 6 for the simple prediction charts technique	179
5.7	Case study 7 for the simple prediction charts technique	180
5.8	Case study 8 for the simple prediction charts technique	181
5.9	Case study 9 for the simple prediction charts technique	182

5.10	Case study 10 for the simple prediction charts technique	183
5.11	Case study 1 for stochastic deep learning model	190
5.12	Case study 2 for stochastic deep learning model	191
5.13	Case study 3 for stochastic deep learning model	191
5.14	Case study 4 for stochastic deep learning model	192
5.15	Case study 5 for stochastic deep learning model	193
5.16	Case study 6 for stochastic deep learning model	194
5.17	Case study 7 for stochastic deep learning model	195
5.18	Case study 8 for stochastic deep learning model	195
5.19	Case study 9 for stochastic deep learning model	196
5.20	Case study 10 for stochastic deep learning model	197
5.21	Comparison of sound pressure level between the SPC technique and DL model	200
5.22	Comparison of sound pressure level between the SPC technique, SDL and actual measurement	204
5.23	Absolute difference between the prediction and the actual measurement	205

LIST OF SYMBOLS / ABBREVIATIONS

Combined σ	Combined standard deviation where the number of the earth-moving machine was more than 1 dBA, dBA
Combined L_p	Predicted sound pressure level where the number of the earth-moving machine was more than 1 dBA, dBA
d	Depth of the sub-area, m
I	Sound intensity generated from machine, W/m ²
K_1	Background noise correction factor, dBA
K_2	Environmental correction, dBA
l	Basic length, m
L	Mean noise level, dBA
L_{Aeqn}	Combined equivalent mean noise levels, dBA
L_{AFeq}	Equivalent continuous noise level, dBA
$L_{(i,j)}$	Sound pressure level at the selected location, dBA
L_I	Sound intensity level, dBA
L_{max}	Maximum noise level, dBA
$L_{measurement}$	Measured sound pressure level at a control point, dBA
L_{min}	Minimum noise level, dBA
L_P	Sound pressure level, dBA
$L_{prediction}$	Predicted sound pressure level at a control point, dBA
L_{pn}	Mean noise level, dBA
L_W	Sound power level, dBA

L_{10}	Noise level that exceeded 10 % of the time measurement duration, dBA
L_{50}	Noise level that exceeded 50 % of the time measurement duration, dBA
L_{90}	Noise level that exceeded 90 % of the time measurement duration, dBA
$\overline{L'_{p(ST)}}$	Averaged or mean equivalent continuous noise level from all the points surrounding the machine, dBA
$\overline{L_{p(B)}}$	Mean equivalent sound pressure level of the background noise, dBA
$L'_{p(ST)}$	Equivalent continuous level of the background noise from all the points surrounding the machine, dBA
ΔL	Mean level deviation, dBA
ΔL_p	Difference between noise level from measurement point and background noise, dBA
r	Distance between the noise source and the centre of the site, m
$R_{(i,j)}$	Distance between the receiver and the source position (x_i, y_j, z_s), m
S	Area that covers the sound radiation during the measurement, m ²
S_o	Reference surface that covers the sound radiation, m ²
SDL L_{AFeq}	Predicted sound pressure level using the stochastic deep learning model, dBA

$SDL \sigma$	Predicted standard deviation using the stochastic deep learning model, dBA
$SPC L_{AFeq}$	Predicted sound pressure level using the simple prediction charts technique, dBA
$SPC \sigma$	Predicted standard deviation using the simple prediction charts technique, dBA
$SPL1$	Mean of sound pressure levels when the noise source was located at the site centre, dBA
$SPL2$	Mean of sound pressure levels when the noise source was moving randomly within the sub-area, dBA
W_a	Acoustic power of the noise source which is equivalent to 1 Watt, Watt
\bar{x}	Mean of measured noise level at a control point, dBA
\bar{y}	Mean of predicted noise level at a control point, dBA
θ	Coverage angle from site centre, °
σ	Standard deviation, dBA
$r_{correlation}$	Pearson's correlation coefficient, dBA
A_i	Scaling factor (exponentially averaged value of i th parameter W_i)
α	Learning rate (ranging from 0 – 1)
α_t	Learning rate α_t in the t th iteration
b	Bias (constant to enhance the performance of prediction)
β	Momentum parameter or friction parameter

β_1	Decay factor, (default values of 0.9)
β_2	Decay factor, (default values of 0.999)
d_n	Corrected output from training data
e_n	Error of the output node
$e^{(l)}$	Error of the hidden node
ε	10^{-8} , to avoid ill-conditioning
F_i	Estimates of the first moment (the mean) of the gradients
n	Number of output nodes
N	Total number of points surrounding the machine
N_i	random number ranging from 0 - 1 for randomized x coordinate
N_j	random number ranging from 0 - 1 for randomized y coordinate
N_T	Total number of samples collected
ρ	Decay factor (ranging from 0 – 1)
P_{on}	Ratio of the time when machine operated at full power
P_{idle}	Ratio of the time when the machine was idling
P_{off}	Ratio of the time when the machine was turned off
r/w ratio	Ratio of distance to the width of the sub-area
v_i	Weighted sum of corresponding node
V_{t-1}	Product of learning rate and the derivative of loss function with respect to the weight from previous iteration
$v^{(l)}$	Weight sums of the forwards signals at the node
w	Weighting

$w:d$ ratio	Width to depth ratio of the sub-area
w_n	Weighting (random number)
W_t	Weight of current iteration
W_{t-1}	Weight from previous iteration
w_0	y-axis intercept
w_l	weight coefficient of the explanatory variable or the slope of the best fit line
x	Explanatory variable
x_i	x coordinate of the randomized location of machine
x_j	Input signal for the corresponding weight
x_n	Input data
x_r	x coordinate of the receiver
y	Target variable
\hat{y}_i	Predicted value
y_i	Observed value
y_j	y coordinate of the randomized location of machine
y_n	Output from the output node
y_r	y coordinate of the receiver
Z	Logit or weighted sum
δ_n	Product of error and derivative of the activation function
$\delta^{(l)}$	Derivative product of error
σ_n	Standard deviation of the mean noise level for each machine
Φ	Derivative of the activation function of the output node

Adagrad	Adaptive Gradient Algorithm
Adam	Adaptive Moment Estimation
ANN	Artificial Intelligence
ARIMAX	Autoregressive Integrated Moving Average with Explanatory Variable
BP	Back pusher
CS	Case study
CE	Crawler excavator
CERB	Crawler excavators with rock breaker
CNN	Convolutional Neural Network
CP	Control point
CPU	Central Processing Unit
DL	Deep learning
DNN	Deep neural network
DOSH	Department of Occupational Safety and Health Malaysia
DOE	Department of Environmen Malaysia
GD	Gradient descent
GRU	Gated recurrent unit
IDE	Integrated Development Environment
IEC	International Electrotechnical Commission
LSTM	Long-short term memory
MAE	Mean absolute error
ML	Machine learning

MLP	Multilayer perceptron
MSE	Mean squared error
NIHL	Noise-Induced Hearing Loss
PM	Rotary piling machines
RAM	Random Access Memory
RMSE	Root mean squared error
RMSProp	Root Mean Square Propagation
RNN	Recurrent Neural Network
RR	Road roller
PPE	Personal Protection Equipment
SDL	Stochastic deep learning model
SGD	Stochastic gradient descent
SPC	Simple prediction chart method
SSA-DNN	Singular Spectrum Analysis and Deep Neural Network

CHAPTER 1

INTRODUCTION

1.1 General Introduction

Acoustic noise is known as an undesirable sound or annoyance that causes irritation and discomfort to humans and wildlife. Noise pollution is a growing and ubiquitous environmental issue that is unnoticed in both developed and developing countries (Bhosale, 2017). Construction noise is claimed to be one of the major noise pollutions in the environment as studies proved that construction activities generate high levels of noise and cause disturbance to sensitive areas (Zolfagharian et al., 2012; Golmohammadi et al., 2013; Foo, 2014; Darus et al., 2015; Zao et al., 2020). The fluctuation and continuity of construction-induced noise have mainly resulted from the different operation modes of machines and equipment that emits blaring noise during the stage when constructing the substructures, and eventually, this stage has become the noisiest stage of all (Ballesteros et al., 2010; Haron et al., 2012; Lee et al., 2016; Zao et al., 2020).

Social Security Organization Malaysia (2020) stated that the number of workers who suffered from noise-induced hearing loss has been increasing since 2005. Besides, researchers proclaimed that there were 18 – 22 % of construction workers were exposed to the noise level of heavy machines that exceed

permissible noise limits (Johnson and Morata, 2010; Said et al., 2014; Li et al., 2016; Mohd Bakhori et al., 2017). The prevalence of noise-induced hearing loss is corresponding to the exposure time, which justified workers who were exposed to blaring noise for more than 6 hours are more likely to suffer from hearing loss problems (Macca et al., 2016; Gan and Mannino, 2018). Moreover, noise exposure may cause minor to severe adverse effects depending on the exposure duration and noise level. These adverse effects can be categorized as physical, physiological, psychological and reduction in work efficiency (Passchier-Vermeer and Passchier, 2000; Foo, 2014; Geetha and Ambika, 2015;). This illness cannot be identified immediately; however, sequelae may occur in a long-term period (Towers, 2001; Zolfagharian et al., 2012; Zao et al., 2020).

Consequently, industrialized countries over the world are obligated to comply with the noise regulation that has been enacted by the government. The basis of regulation and guidelines shares a similar purpose as in, to monitor, assess and control the severity of noise impacts on the employees and the environment. Occupational Safety and Health (Noise Exposure) Regulation (2019) Act 514 governs the regulations and standards regarding occupational noise in Malaysia. On the contrary, limits of ambient noise in the environment are regulated under the Guidelines for Environmental Noise Limits and Control (Department of Environment, 2019).

With regards to the impact of occupational noise and environmental noise as discussed, many researchers developed probabilistic noise prediction

methods to predict excessive noise from construction activities (Lim et al., 2015; Darus et al., 2015; Haron et al., 2012; Haron et al., 2009; Haron et al., 2008). The outcome of the previous studies proved that noise prediction models are reliable and accurate as compared to the deterministic approach such as BS 5228 – Part 1: 2009 (British Standard Institution, 2009). Hence, these noise prediction models are potentially useful to prevent and mitigate potential noise hazards in the workplace.

However, the application of current prediction techniques is time-consuming in computation and required laborious work to achieve a reassuring outcome. Therefore, the concept of artificial intelligence applied in acoustic noise prediction works to reduce the human effort when performing complex calculations. Artificial intelligence can be known as a broad field that consists of machine learning and deep learning. Machine learning can be defined as a type of program that acquires self-learning ability without an individual to command the software. Machine learning comprises four types of basic archetypes which are supervised, unsupervised, semi-supervised and reinforcement learning (Rafique and Velasco, 2018). Deep Learning is a subset of machine learning that consists of an input and output layer, and several hidden layers, each layer of the neural network serves a different purpose. The concept of the artificial neural network is adopted in different types of prediction models such as biological vision prediction, traffic noise prediction, traffic state prediction, sound levels prediction, and environmental noise prediction (Majaj and Pelli, 2018; Do et al., 2018; Navarro et al., 2020; Zhang et al., 2020). Hence, this study has predominately emphasized the incorporation

of stochastic modelling and artificial neural network in the construction noise prediction model.

1.2 Importance of the Study

The application of the noise prediction model in a workplace is a necessity to improve the current noise monitoring practice. The noise prediction model helps in providing insight for the users to prevent and eliminate potential hazardous noise at the workplace. Hence, it can be utilized as a powerful supervisory tool in every stage of construction. However, current noise prediction techniques are time-consuming and inefficient. Therefore, this study applied the concept of stochastic modelling along with deep learning to generate a more accurate, reliable, and promising outcome.

This study contributed its novelties in noise prediction technology by applying both stochastic modelling and deep neural network. The model was expected to predict the sound pressure levels at a selected location within a construction site, by using several major parameters such as random movement of machinery, different duty cycles of machinery, coverage angle and aspect ratio of the determined sub-area in the construction site. The contribution of this study was to establish a stochastic deep learning noise prediction model that is capable to outperform the simple prediction chart technique in computational time and varieties of parameters. Stochastic modelling was applied to determine the random positions of the machinery (Haron et al., 2012), whereas Monte Carlo was adopted in the study to predict the noise level emitted from earth-

moving machines depending on the variation of operation modes (Haron et al., 2009). The output of stochastic modelling was utilized as the input data for the deep learning model. Then, the stochastic deep learning model was analysed based on given parameters to predict construction noise levels at a selected location.

The target users of this technology are local authorities, consultants, contractors, noise practitioners and planners. Existing noise prediction methods applied the deterministic approach which required complex calculation and laborious processes. On that account, this model has the potential to be introduced to the construction industries as an improved version of the noise prediction model that is capable to enhance the effectiveness of noise monitoring and management.

1.3 Problem Statement

Construction noise is unpreventable when there is the presence of construction activities. Besides, most of the construction machinery induced loud noise during operation, which explained the majority of the construction workers are under exposure to loud noise due to the nature of the job scopes. Irreversible Noise-Induced Hearing Loss (NIHL) problems among construction workers often arise due to overexposure to loud noise (Mirza et al., 2018). According to Social Security Organization Malaysia (2018), the number of workers that suffered from NIHL had been increasing from 53 in 2005 to 540 in 2016. Moreover, the Department of Occupational Safety and Health Malaysia (2018)

stated that there were 2478 occupational hearing loss cases in the year 2017. Hence, effective noise management is one of the essential solutions to manage this issue. It is the obligation of the management to ensure the noise levels are maintained under an acceptable limit in the workplace, but the importance of noise management was neglected and often resulted from ineffective noise attenuation at construction sites. Other than ineffective noise management and planning, the ignorance of construction workers for not using personal protection equipment (PPE) and lack of personal safety concerns is a major factor that contributed to NIHL problems. Thus, the establishment of a planning and managerial tool is a necessity for the management to handle the noise exposure issues. The tool can be deployed during the early phase of construction works to foresee potential noise hazards and maintain noise levels below the permissible level during the construction phase.

Previous studies proved that the application of stochastic modelling in construction noise prediction is feasible, reliable and able to provide acceptable performance. Several prediction methods adopted the concept of stochastic modellings such as the simple prediction charts method, Monte Carlo approach and probabilistic approach (Haron et al., 2008; Haron et al., 2009; Haron et al., 2012). These prediction techniques were mainly applied in the sound pressure level prediction at a construction site. However, current stochastic modelling prediction techniques required a laborious process to predict noise levels at a chosen location. In particular, users have to refer to the simple prediction charts based on the aspect ratio of the site and angle away from the site centre to calculate the approximate sound pressure level at the specific location.

Although the current stochastic modelling technique can predict noise levels with the inclusion of randomness of machine movement and duty cycles of machinery from a workplace; however, this technique is inefficacious for complex and dynamic workplaces due to the time-consuming prediction process (Lim, 2017). Therefore, stochastic modelling can be further enhanced by considering additional parameters for better performance. The accuracy and reliability of the prediction model are the key elements to rendering efficient occupational noise monitoring. As a result, this study is conducted to develop a noise prediction model with the association of stochastic modelling and deep learning technique.

1.4 Aim and Objectives

This study aims to develop a reliable noise prediction model using the stochastic deep learning technique. To attain the outcome of this study, several objectives are required to be achieved:

1. To establish the framework for the stochastic deep learning model.
2. To develop the programming algorithms and coding for the stochastic deep learning models.
3. To validate the accuracy and the reliability of the stochastic deep learning models by comparing the predicted results with actual measurements from the construction sites.

1.5 Scope of the Study

This study comprised the development of a stochastic modelling framework and a deep learning framework. The output generated from the stochastic modelling was applied as the historical data or input for the stochastic deep learning model. Then, based on the given parameters the model will predict the noise level at any location within a construction site. The stochastic modelling programming algorithm was developed using MATLAB software, whereas the deep learning model was established in Spyder software using Python programming language. The performance of the stochastic deep learning model was evaluated with statistical measures.

This study limited the scope of field works only to construction industries. The measurement of the case studies consisted of different types of works and conducted in Selangor, Malaysia. The sound level measurement was performed by using a calibrated Larson Davis sound level meter. Measurement tape and distometer were used to measure the distance between the noise receiver and the source, the distance of control points, as well as the site layouts. The intention of conducting the case studies was to obtain the actual measurement data at the control points and to validate the performance of the noise prediction model when it is applied in different construction activities. The measurement procedures were in accordance with British Standard International Organisation for Standardisation, BS ISO 6395:2008, BS 5228-1:2009 and BS EN ISO 3744:2010 (British Standard Institution, 2008; British Standard Institution, 2009; British Standard Institution, 2010). Pearson's

correlation coefficient and R-squared were adopted in this study to assess the model reliability. Contrarily, the model accuracy was assessed by using absolute difference and relative error.

1.6 Report Structure

This thesis comprises six main components which introduce the conceptual idea of this study, the background and literature review of this study, the procedures of fieldwork, the establishment of the conceptual framework and the programming algorithms of the stochastic deep learning model, the preliminary results, the comparison and justification of the actual measurement and the prediction, as well as conclusion and recommendation for this study. Concluding remarks are clearly presented at the end of the chapters.

Chapter 1 (Introduction) covers the background of acoustic noise and artificial intelligence, the importance of the study, the existing problem statement, the objectives to be achieved to attain the aim, the scope coverage of the study and lastly the thesis structure.

Chapter 2 (Literature Review) provides the types and characteristics of discrete acoustic noise, the hierarchy of controls for noise exposure, noise regulation and guidelines of current practice and the findings of previous literature on construction noise prediction and stochastic modelling. Besides, the fundamentals of artificial intelligence such as machine learning and deep learning, as well as comprehensive reviews on the feasibility of the noise

prediction model with the association of artificial neural networks are expressed in this chapter. Research gaps are determined from the preceding studies and form the foundation of the present study.

Chapter 3 (Methodology) presents a meticulous illustration and explanation, of the planning, design and implementation of this study. This chapter includes the research framework, configuration of stochastic framework and deep learning framework, field measurement procedure and equipment and lastly the demonstration of formulation application from previous studies in construction noise prediction.

Chapter 4 (Development of the Stochastic Deep Learning Model) contains the results from the development of the stochastic deep learning model. The results from stochastic modelling are discussed in this chapter. The deep learning model with different variations of hyperparameters is employed in construction noise prediction to determine the optimum hyperparameters and viability of this study. The findings from the preliminary tests are crucial to manifest the feasibility of applying artificial neural networks to construction noise prediction.

Chapter 5 (Results and Discussion) presents the main results of this study. The preferential neural network configuration is determined by the hyperparameters that contribute to the highest accuracy and reliability during the noise prediction. Comparisons between the present study, previous studies and case studies are made and discussed concerning the hypothesis of this study.

Lastly, Chapter 6 (Conclusion and Recommendation) concludes the significant findings obtained from this study. The discussion of the current study on the limitation and the future research recommendation is also presented in this chapter.

CHAPTER 2

LITERATURE REVIEW

2.1 Introduction

This chapter provides an intuition into the sound fundamentals, types of noise, methods of noise prediction, current noise monitoring techniques, rules and regulation of permissible noise in the current practice, fundamentals and applications of deep learning in noise prediction.

2.2 Sound

Sound is essential in human daily life as it helps a person to differentiate and learn from the sound sources to react. In addition, prehistoric human communicates with one another through the first mode of communication, voice. Sound is generated when there is a disturbance propagated through an elastic medium such as air and causes variation in pressure which can be detected by humans (Beranek and Mellow, 2012). Sound can be identified as pleasant and unpleasant sounds. Pleasant sounds can be related to music, whereas unpleasant sounds can be classified as noise (Hewitt, 2014).

2.3 Sound Power, Sound Intensity and Sound Pressure

According to Murphy and King (2014), the pressure level of sound (L_P), the intensity level of sound (L_I) and the power level of sound (L_W) shall all be measured in the units of decibels (dB) because it is more convenient, as the measurement is more closely to the nature of human hears the sound loudness (Everest and Pohlmann, 2015). The sound power level determination, sound intensity level calculation and the sound pressure level computational formula are expressed in Equations 2.1, 2.2 and 2.3 correspondingly. Sound power is present when a sound source produced an amount of acoustic energy within a timeframe. A quantum that determines the emission rate of the acoustic energy throughout a unit area in a certain direction is called the sound intensity. Sound pressure can be defined as the alteration of atmospheric pressure caused by a sound wave or vibration of an object (Crocker, 2007).

$$\text{Sound power, } L_W = 10 \log_{10} \left(\frac{W}{W_o} \right) \quad (2.1)$$

Where reference value for sound power,

W = sound power of a source (Watt);

$W_o = 10^{-12}$ (Watt)

$$\text{Sound Intensity, } L_I = 10 \log_{10} \left(\frac{I}{I_o} \right) \quad (2.2)$$

Where reference value for sound intensity,

I = component of the sound intensity in a given direction (W/m^2);

$I_o = 10^{-12}$ (W/m^2)

$$\text{Sound pressure, } L_p = 10 \log_{10} \left(\frac{p^2}{p_o^2} \right) \quad (2.3)$$

Where reference value for sound pressure,

p_s = sound pressure being measure (Pa);

$p_{ref} = 2 \times 10^{-5}$ (Pa) for airborne

2.4 Sound Propagation

A sound from a source transmits uniformly, spherically and omnidirectionally in an unbounded medium (Pierce, 2019). As the sound propagates farther from the source, the intensity of sound sources will reduce due to the inverse-square law. Figure 2.1 depicts that the surface area of the same acoustic energy from the sound source will increase radially outward when the radius increases (Everest and Pohlmann, 2015). This justifies the relationship between the intensity of sound and the square of the distance from the origin of the sound is inversely proportional. The sound intensity can be computed by using Equation 2.4.

$$I = \frac{W}{4\pi r^2} \quad (2.4)$$

Where

I = intensity of sound (W/m^2);

W = sound source power (Watt);

r = distance away from the source in radius (m)

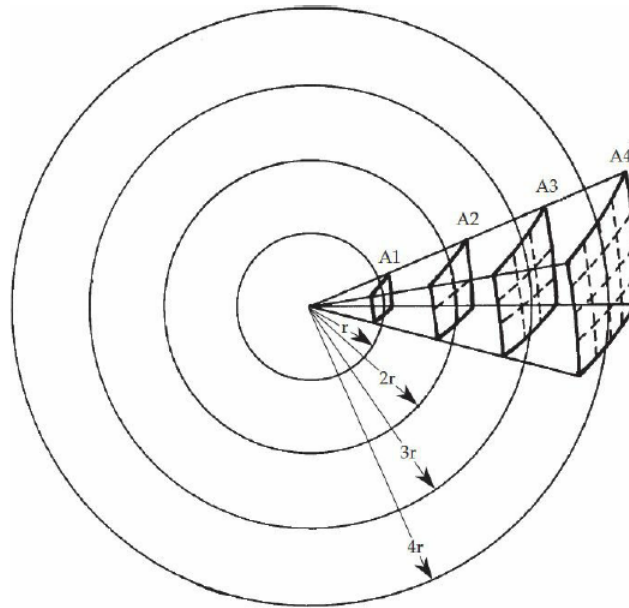


Figure 2.1: Propagation of sound wave (Everest and Pohlmann, 2015)

2.5 Geometrical Divergence of Point Source

It is crucial to identify the ambience of the sound source because the accuracy of the measurement can be significantly affected by the surroundings (Crocker, 2007). For a free field without any reflection and obstacles, the sound pressure level can be computed by using Equation 2.5. However, construction machines are mostly mounted on a hard surface in the industry. Therefore, Equation 2.6 is adopted to determine the sound pressure level (L_p) when the sound source is located on a rigid hard surface. Figure 2.2 exemplifies the propagation of sound when the source is mounted on the ground (Ning, 2017).

$$L_p = L_w - 20 \log r - 11 \quad (2.5)$$

Where

L_w = sound power noise source (dBA);

r = distance away from the sound source (m)

$$L_p = L_w - 20 \log r - 8 \quad (2.6)$$

Where

L_w = sound power noise source (dBA);

r = distance away from the sound source (m)

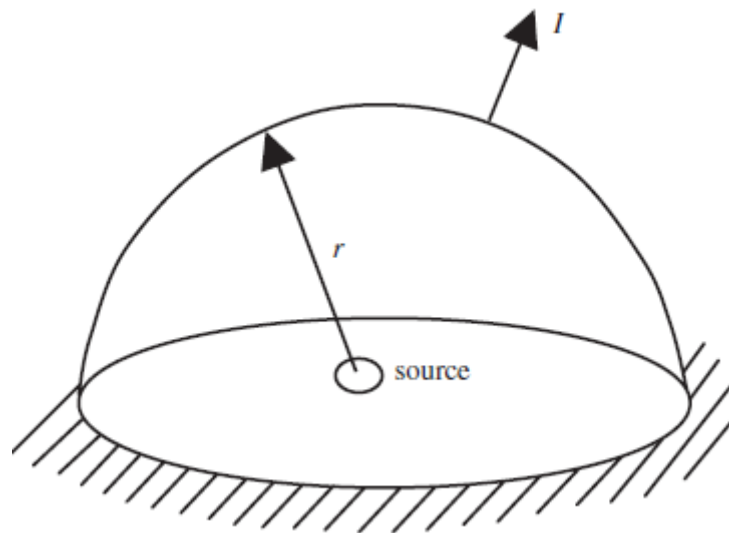


Figure 2.2: Point source above a rigid hard surface (Ning, 2017)

2.6 Human Hearing

Hearing enables humans to identify and recognize the sound produced by living and non-living creatures in the world (Peterson, 1980). Besides, hearing is one of the essential components of effective communication. Sound is produced when an object vibrates and causes variation of pressure in a sound-transmitting medium such as air. The generated pressure wave is usually transmitted away from the vibrating object. Hence, the pressure wave will travel through the ear canal, and the eardrum of a listener will capture the sound transmitted by the vibrating object and the hearing process will be initiated as depicted in Figure 2.3. The sound will be converted into vibration by the eardrum once it passed through the outer ear canal. The converted vibrations will propagate through the hammer, anvil and stirrup then into the cochlea. According to Crocker (2007), Figure 2.4 shows the maximum tolerability of sound for an auditory system is 130 dBA, a sound pressure level that exceeds the threshold will cause pain to the listener. Murphy and King (2014) signified that the typical frequency ranges for human hearing are 20 Hz – 20, 000 Hz.

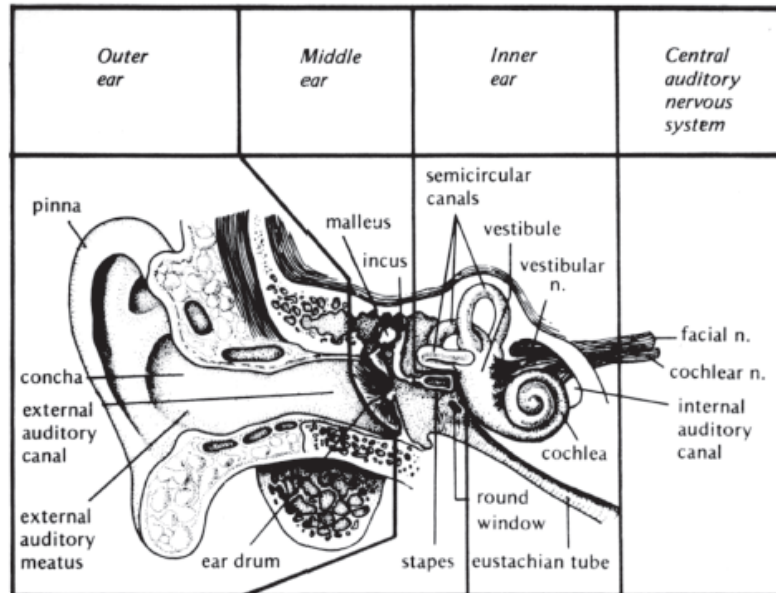


Figure 2.3: Auditory system anatomy (Dobie and Hemel, 2005)

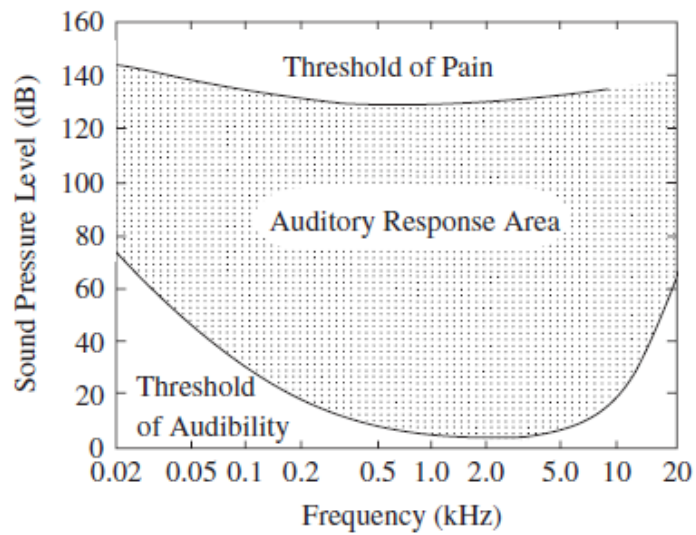


Figure 2.4: Tolerability of ear (Crocker, 2007)

2.7 Noise

An undesirable sound that can bring negative impacts on humans and other walking creatures is defined as noise (Murphy and King, 2014). World Health Organization (2011) emphasized that noise should be identified as a consequential menace to humans. Noise pollution has been identified as one of the catastrophes that may jeopardize the welfare of humans and also the quality of life in cities all over the world (Hunashal and Patil, 2012). Additionally, World Health Organization (2011) proved that there is overwhelming evidence that noise exposure has adverse impacts on humans.

Geetha and Ambika (2015) revealed that noise pollution from the construction industry resulted in severe negative impacts on humans and the environment. Noise exposure may lead to a different level of adverse effects depending on the exposure duration and volume. These adverse effects can be classified in the form of physical, physiological, psychological and also reduced work efficiency (Passchier-Vermeer and Passchier, 2000; Foo, 2014; Geetha and Ambika, 2015). For instance, noise-induced hearing loss is a common result of physical effects. Additionally, loud noise exposure will inflict an increase in blood pressure and inconsistency of heartbeat rhythms whereas psychological effects are sleep disturbance, disorders and irritability. Moreover, noise may affect social performance during work due to interference in communication. According to Gan and Mannino (2018), workers that suffered from bilateral high-frequency hearing impairment had a higher heart rate, a higher chance of getting diastolic blood pressure, and the prevalence of hypertension compared to individuals that were exposed under normal high-frequency hearing.

2.7.1 Types of Noise

Noise can be categorized into steady, fluctuating, intermittent and impulsive noise. According to the Department of Environment Malaysia (2019), steady noise is defined as noise that remains constant and stagnant for a specific period. The continuous noise is comprised of steady-continuous noise and steady-noncontinuous noise. Steady-continuous noise has minor changes, less than 3 dBA in sound level within a specific time as depicted in Figure 2.5a. Steady-noncontinuous noise has the same behaviour as steady-continuous noise except for the sound level varies upon the time frame as shown in Figure 2.5b. Fluctuating noise is a type of noise that has a variation of more than 3 dBA in sound level within a specific time. The sound level of fluctuating noise is unconstant and varies over the observation period as depicted in Figure 2.5c. For intermittent noise, the sound level has a sudden drop to ambient level several times over an observation period whereby the sound level over the observation is stable and consistent. The characteristic of intermittent noise is illustrated in Figure 2.5d. Lastly, impulsive noise occurs for a period that lasts for less than a second, accompanied by a very short burst of loud noise as shown in Figure 2.5e.

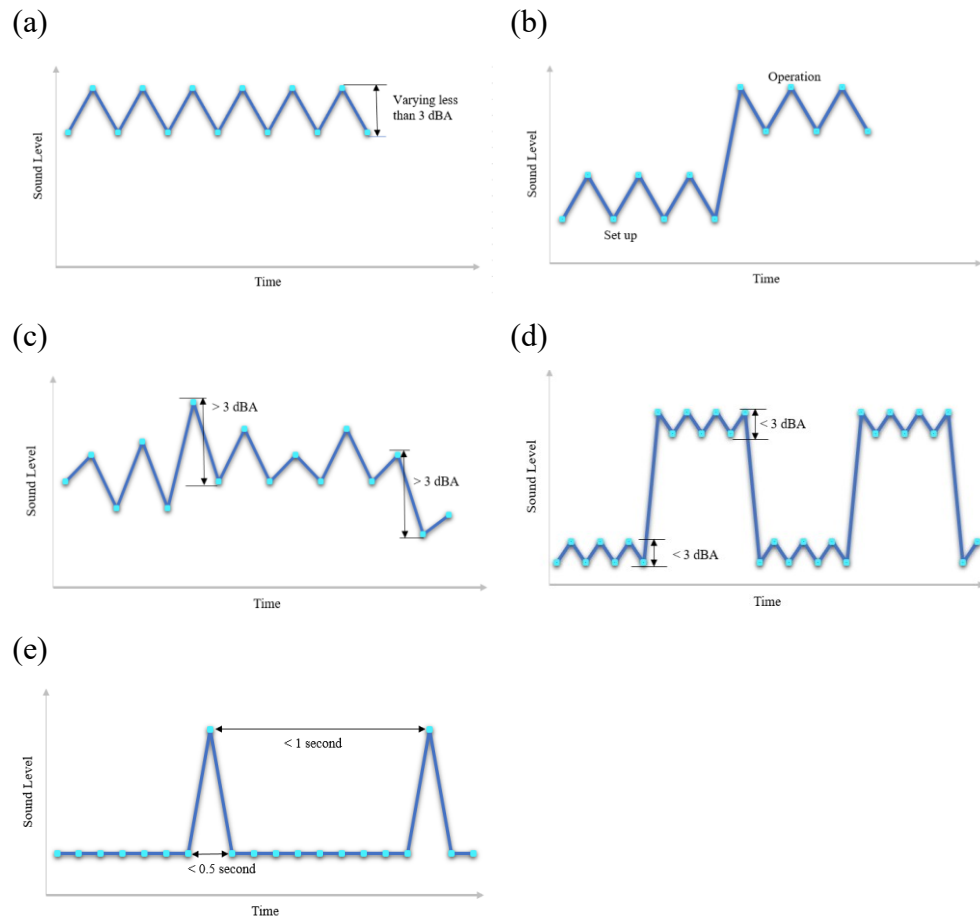


Figure 2.5: Types of noise (a) steady continuous noise; (b) steady non-continuous noise; (c) fluctuating noise; (d) intermittent noise; (e) impulsive noise (Department of Environment, 2007)

2.7.2 Occupational Noise Exposure

Occupational safety and health is an awareness that concerns the safety, health, and welfare of individuals when they are engaged in employment (Lord Robens, 1972). A study mentioned that the main cause of employees suffering from the irreversible occupational noise-induced hearing loss was due to extensive exposure to blaring noise in a workplace (Mirza et al., 2018). In the United States, an estimation of 22 million workers is currently exposed to perilous occupational noise (Themann and Masterson, 2019). Moreover, 11.2

million workers in Canada are overexposed to occupational noise and one-third of the workers experienced acute effects of hearing loss (Feder et al., 2017). According to Social Security Organization Malaysia (2020), the number of workers that claimed noise-induced hearing loss compensation increased gradually every year as shown in Figure 2.6. Department of Occupational Safety and Health Malaysia (2019) stated that there were 2478 occupational hearing loss cases out of 6020 occupational disease and poisoning cases in the year 2017.

A study estimated prolonged occupational noise exposure accounts for 16 % of hearing impairment in adults globally (Nelson et al., 2005). Besides, workers that were afflicted with hearing loss issues were mostly from economic sectors such as mining, manufacturing, and construction was proved to be the largest proportion among all the occupations (Fernández et al., 2009). A study has shown that construction workers were exposed to loud noise that exceeds the stipulated permissible noise level (Mohd Bakhori et al., 2017). Based on the findings, Johnson and Morata (2010) mentioned that 18 – 22 % of construction workers were under exposure to occupational noise above 85 dBA during working hours. Cantley et al. (2014) discovered that aluminium workers are more likely to get injured when they were exposed to noise levels exceeding 88 dBA. Moreover, a quantitative assessment revealed that the majority of heavy machine operators are under exposure to noise levels exceeding 85 dBA as depicted in Table 2.1 (Li et al., 2016). Heavy machines that generate noise levels exceeding 85 dBA may cause risks of overexposure among workers and operators. Gan and Mannino (2018) proved that the accumulated noise exposure

time will increase the chances of an individual having bilateral high-frequency hearing loss, which explained that workers that were exposed to a blaring noise for a long duration, are more likely to suffer from hearing impairment. Macca et al. (2015) reported that 41.6 % of welding workers suffered from tinnitus and sleep disorders after daily noise exposure of 6 hours. Based on a study, 45 % of workers from trade work were diagnosed with hearing problems; the following 32 % of workers that suffer from hearing impairment came from the road work stage and 23 % were from the pavement construction stage (Said *et. al.*, 2014).

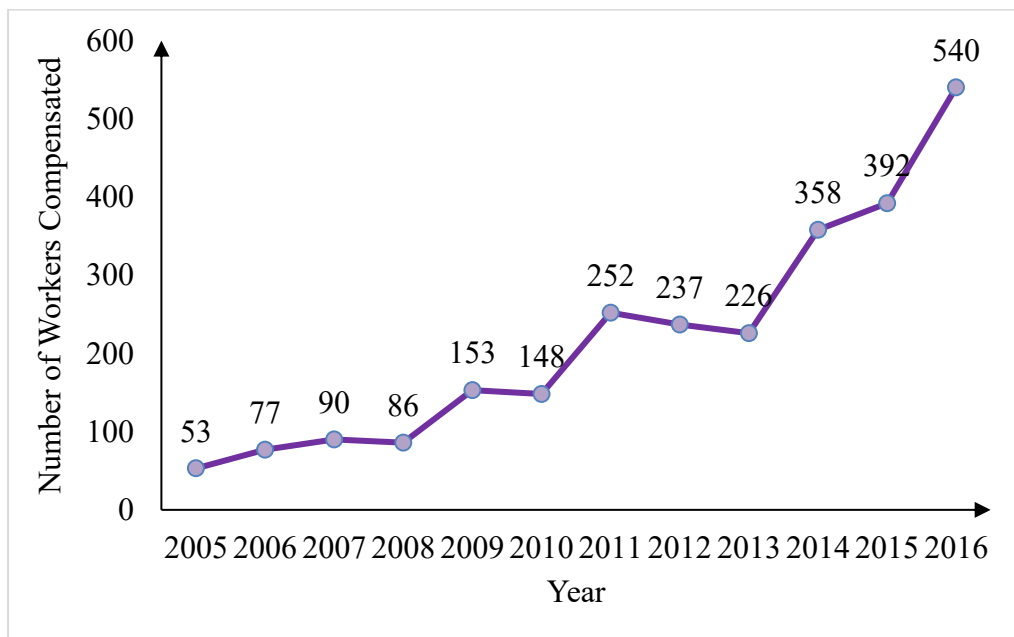


Figure 2.6: Noise-induced hearing loss compensation (Social Security Organization, 2018)

Table 2.1: The noise exposure level of heavy machines operators. (Li et al., 2016)

Construction Stage	Construction Trades	Noise Levels (dBA)
	Excavator Operator	80.5
Earthwork	Sand Ejector Operator	87
	Pile Driver Operator	88.3
	Steel Bender	85.6
Earthwork and	Steel Fixer	87
	Superstructure	Scaffolder
construction	Formwork Fixer	91.9
	Concreteer	92.4

2.7.3 Construction Noise

During the industrial revolution, heavy machines have been invented by the pioneers to reduce human effort in the construction industry (Haycraft, 2011). However, the application of heavy machines in the construction industry will cause setbacks such as inducing construction noise. The fluctuation and continuity of construction-induced noise will cause irritation and discomfort to humans (Zao et al., 2020).

A study in Malaysia proclaimed that construction sites are one of the sources that create noise pollution in the surroundings (Zolfagharian et al., 2012). Foo (2014) claimed that the construction industry was identified as the second most impactful source that contributed to noise pollution in the

surroundings. In recent years, the effects of construction noise are no longer tolerable due to the increased consciousness of government and the public regarding environmental issues, and escalation in the growth of “megaprojects” (Towers, 2001). From the perspective of the construction industry, the noise level is determined by the emitted sound level of construction machines, the number of machines operating simultaneously, the distance between the sound receiver and sound source, the presence of reflective objects between the receiver and source, as well as the machine acoustic power under different duty cycles (Carpenter, 1997; Haron and Yahya, 2009; Lim et al., 2015).

Geetha and Ambika (2015) classified the types of potentially hazardous noise effects from construction activities as noise hazards and nuisance. Noise hazards will cause irreversible hearing loss and neural stress to the human body. Besides, noise nuisance will cause irritation, mental stress, and negatively affect the performance and concentration of construction workers. Furthermore, studies proved that high levels of noise exposure on construction sites are a significant matter and distress to labours; apart from affecting the construction workers, construction noise may affect the public as well (Haron et al., 2014; Darus et al., 2015; Bhosale, 2017). A study proved that the initial construction stage such as earthwork and substructure produced the highest noise levels compared to other stages (Ballesteros et al., 2010; Darus et al., 2015).

The main sources of noise at a construction site consists of construction machines that emit high levels of noise such as heavy machine, pile driving machine and pneumatically driven device (Haron et al., 2008). On the other

hand, Lee et al. (2015) and Lee et al. (2016) revealed the sound power level of different types of construction equipment as shown in Table 2.2. Nonetheless, the responses of the people vary in accordance with the level of noise pollution; however, the prevalence of getting affected negatively by the construction noise is higher, when the noise levels reach a certain extent (Darus et al., 2015). The impacts cannot be identified immediately; however, they will escalate in a long-term period (Towers, 2001; Zolfagharian et al., 2012; Zao et al., 2020).

Table 2.2: Noise emitted from construction machines (Lee et al., 2015; Lee et al., 2016)

Peak L_p in dBA	Types of Machine
100.9	Vibratory pile driver
93.1	Hacking machine
89.5	Excavator
95.2	Bull Dozer
87.3	Trench cutter
99.8	Earth Gauger
109.6	Breaker

2.8 Hierarchy of Controls for Noise Exposure

Noise is a potential hazard that may cause negative effects on the health of the employees and also jeopardize the welfare of the public. Hence, construction noise that has been emitted from the activities shall be monitored and controlled by the noise creator. Therefore, noise monitoring is mandatory to supervise and control the hazard caused by noise.

Department of Occupational Safety and Health (2019) has adopted a hierarchy of controls to develop the objectives that are more precise and systematic to assess the hazards in a workplace. A hierarchy of controls can be defined as the establishment of the sequence for the types of measures to be taken to control the encountered risks. The hierarchy of controls consists of 5 major components as illustrated in Figure 2.7.

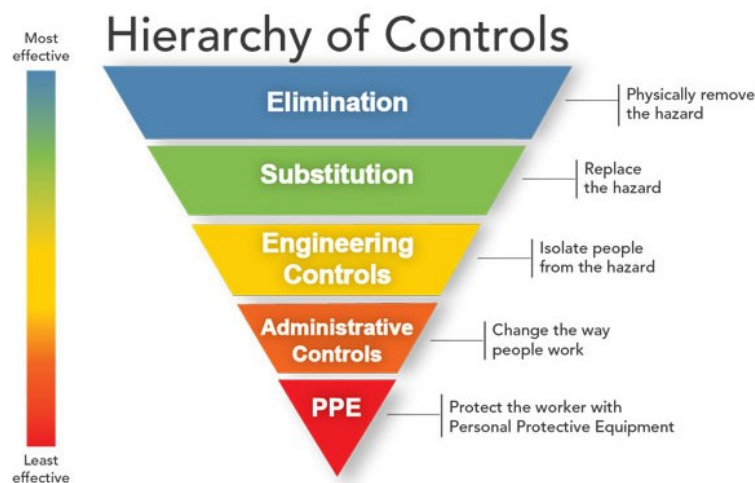


Figure 2.7: Hierarchy of controls (Department of Occupational Safety and Health, 2019)

According to the Department of Occupational Safety and Health (2019), the most effective way to prevent an employee from suffering occupational noise is to remove the machinery and equipment from the workplace. Other than that, the employer should eliminate dangerous jobs and substances that will cause injury and fatality to the employees. Department of Occupational Safety and Health (2019) defined substitution is to replace a conventional material, machinery or process with a less harmful alternative. For instance, replacing the existing machine with a quieter machine.

According to Canadian Centre for Occupational Health and Safety (2019), engineering controls are the methods or procedures adopted in the design of processes, plants or equipment to minimize exposure to hazards. For the construction industry, a noise barrier is one of the most effective solutions to prevent workers exposed to loud and blaring noise. Halim et al., (2015) mentioned that the concrete hollow blocks and concrete panels can reduce the noise level up to 5 - 10 dBA, which proved that it is feasible to use the noise barrier as one of the engineering controls. Suter (2010) stated that noise control is the most practical solution to lower the impact of noise-induced hearing loss, and it can reduce the risk of fatal accidents occurring.

The concept of administrative controls is to alter the work practice of the employee that exceeds the permissible noise level, validate the management policies, supervise and monitor the working behaviour of employees (Morata, 2016). Department of Occupational Safety and Health (2019) mentioned that safe work procedures must be carried out by the employer and employee as well.

Standardized safety practices have to be conducted and the employer is expected to ensure that the employee complies with the practices. Besides, work procedures must be assessed periodically and the procedures must be updated to the employee.

According to the United States Department of Labor (2019), supervision and training are mandatory to be provided to supervisors on safety concepts and their responsibility. Other than that, proper and appropriate supervision is expected to be conducted by the supervisor to assist the employees to identify potential hazards and assessing work procedures.

Moreover, the Department of Occupational Safety and Health (2019) stated PPE and clothing are adopted when extra protection is needed and the other control measures are not practically achievable. Fernández et al., (2009) mentioned that PPE for hearing protection must be chosen appropriately for different workplaces regarding attenuation spectrum and global attenuation.

Proper training and instruction must be given to the employees to ensure they are capable of equipping PPE. It is the obligation of the employer to ensure the employees are equipped with PPE when exposed to potential hazards. Different specifications are applied for different types of PPE used to protect different body parts of an individual in terms of hearing, visual and respiratory. PPE has to be checked thoroughly to ensure it is functioning well. Otherwise, PPE may jeopardize the welfare of the worker by providing an illusion of protection.

2.9 Noise Regulation and Guidelines

The noise regulation had been inaugurated by the government and adopted in industrialized countries over the world because the hearing health of construction workers emerged significantly over the past decades (Foo, 2014). Hence, all the regulations and guidelines share the same objective, which is mainly emphasized hearing loss and annoyance to the surroundings. Most of the industrialized countries had established noise regulatory limits correlated with hearing protection. However, only occupational noise sources and noise sources corresponding to public exposure can be supervised and regulated authoritatively. Although occupational safety is the priority, the existing noise regulations enforcement is relatively poor, particularly in the construction sector; and improvement is yet to be made in the future to strengthen the regulation in Malaysia (Suter, 2010; Foo, 2014).

2.9.1 Occupational Regulation and Guidelines

Regulations and standards regarding noise monitoring for employees in Malaysia are governed by Occupational Safety and Health Act (2019) under Act 514. According to regulations, the daily noise exposure level of an individual shall not exceed 85 dBA for 8 hours. Besides that, employees are restricted to be exposed to noise levels that are beyond 115 dBA. Thereafter, employees shall not be exposed to impulsive noise levels exceeding 140 dBC at the workplace.

Under Occupational Safety and Health Act (2019), employee exposure monitoring shall be conducted by employers to detect any exposure to noise levels exceeding the permissible level for their employees. Department of Occupational Safety and Health Malaysia (DOSH) adopted the occupational exposure level to determine the allowable noise level that required noise monitoring and control. There are three types of noise monitoring such as initial employee exposure monitoring is to be conducted for a single or more employee representing a category with the same work or from the same workplace. For a positive initial employee exposure monitoring, where the noise exposure level exceeds the permissible level, then the monitoring period for employees of the same work or workplace is to be determined within six months; whereas if the initial employee exposure meeting does not show exposure level exceeding permissible level, noise monitoring is not required at the workplace, this is termed as negative initial employee exposure monitoring.

Occupational Safety and Health Act (2019) indicated that additional monitoring shall be conducted in the event of any changes regarding work activities or employees. Besides, the employer shall announce the noise monitoring results to every employee upon the reception of the results. The noise measuring equipment approved by the Industrial Hygiene and Ergonomics Division shall be used during the noise exposure monitoring under the supervision of Noise Competent Person registered with DOSH. The monitoring report will be submitted to DOSH for further compliance validation and documentation.

Occupational noise regulation is mainly emphasized on the potential hazards relating to hearing loss problems. It is globally proven that exposure to the noise level of 85 to 90 dBA daily for 8 hours will result in sensorineural hearing loss in the majority of workers after 5 years of exposure and will suffer from significant loss of hearing after 20 years of exposure (Cowan, 2016).

2.9.2 Guidelines for Environmental Noise Limits and Control

In Malaysia, Guidelines for Environmental Noise Limits and Control enacted by the Department of Environment enacted served as technical guidance and cover the scope of providing recommendations on ambient noise standards to reduce the adverse impacts on the environment. The guidelines presented the noise limits in the environment for new projects and development to protect the public welfare from unpleasant noise (Department of Environment Malaysia, 2019). Procedures to conduct the environmental noise measurements, assessment and mitigation are mentioned in the guidelines as well.

The purpose of these guidelines is to provide an insight for the parties involved in the initial stage to propose the required precautionary measures and planning (Department of Environment, 2019). Besides, noise impact assessments, before and after Environmental Impact Assessment compliance verification are explained in the guideline. These guidelines are applied to quantify the noise disturbance throughout a given time and lastly serve as guidance in the mitigation of environmental noise.

According to the Department of Environment Malaysia (2019), the maximum permissible sound level for different land development is categorized into five receiving land use categories as presented in Table 2.3. Next, Table 2.4 presented the recommended maximum allowable noise levels such as statistical percentile (L_{10}), and maximum instantaneous sound pressure level (L_{max}) for demolition activities, construction phases and maintenance purposes. According to the guidelines, measured values of (L_{10}) and (L_{max}) levels are applied to assess and quantify fluctuating and impulsive noise generated from piling activity and pneumatic tools.

Table 2.3: Maximum allowable sound level (L_{AFeq}) by for Different Category of Land Use for New Development and Planning (Department of Environment, 2019)

Night time	Day time	Category of Receiving Land Use
10.00 pm – 7.00 am	7.00 am – 10.00pm	
50 dBA	55 dBA	Low-Density Residential
55 dBA	60 dBA	Medium Density Residential
60 dBA	65 dBA	High Density Residential
60 dBA	65 dBA	Commercial Business Zones
65 dBA	70 dBA	Industrial Zones

Table 2.4: Maximum allowable sound levels (percentile L_{10} and L_{max}) for Different Land Use in Demolition Work, Construction Activities and Maintenance Purposes (Department of Environment, 2019)

Night 10.00 pm - 7.00am	Evening 7.00 pm – 10.00 pm	Day 7.00 am - 7.00 pm	Category of Receiving Land Use	Parameter of Noise
			Designated	
80 dBA	80 dBA	80 dBA	Industrial Zones	L_{10}
			Commercial,	
75 dBA	80 dBA	80 dBA	Mixed Development	L_{10}
70 dBA	70 dBA	75 dBA		L_{10}
85 dBA	85 dBA	90 dBA	Residential	L_{max}
Existing	Existing	Existing	Sensitive	
$L_{AFeq} + 1.5$ dBA	$L_{AFeq} + 3$ dBA	$L_{AFeq} + 3$ dBA	Areas	L_{AFeq}

2.9.2.1 Noise Measurement and Monitoring

The necessity of conducting noise levels measurement is to serve the purpose of determining the current noise climate, evaluating the noise limits for noise sources and the development of projects that complies with the regulations.

Lastly, it is used to identify the environmental impact and potential hazards to the community.

Department of Environment Malaysia (2019) explained that noise measurement shall include the ambient sound pressures level at the location of the noise receptor, or the coverage boundary of the noise source, and shall be undertaken without the presence of the noise source. Secondly, measurement of the noise levels at a noise receiver's location shall be conducted in the presence of a noise source. Next, the determination of the contribution of each source to the surroundings shall be based on the sound pressure levels of each noise source during the assessment.

In accordance with the Guidelines for Environmental Noise Limits and Control, noise assessment shall be performed in the areas that are noise-sensitive, and the selected monitoring locations shall be located beyond the receiver's real property border (Department of Environment, 2019). Besides, the noise measurements are conducted at the height of 1.5 m to 4.0 m above ground level. However, alteration of noise monitoring locations at the site boundary is allowed when there are measurement difficulties due to constraints that may cause inaccurate results.

Moreover, measured values of L_{AFeq} , L_{max} , L_{10} and L_{90} shall be recorded and kept along with the information of the measured periods. Besides, the methodology of noise measurement, instrumentation specification, system calibration data of the sound level meter, the position of the noise receiver regarding the site and details of sampling techniques, plans of the site, and site

activities during the monitoring periods shall be documented as well. Besides that, factors that may result in unreliable and inaccurate measurement, wind speed and direction, the presence of precipitation, weather conditions, relative humidity and temperature shall be diarized.

2.10 Noise Prediction

Acoustic noise caused by factories, construction sites, and traffic noise has been increasing over the past decades due to urbanization and transportation. This issue has to be managed appropriately to prevent the seriousness of noise pollution from getting intensified (Koi et al., 1993; Foo, 2014). Acoustic noise is considered during the tendering stage and construction phase to confirm the contractor complies with the permissible limit prescribed by the local authority (Haron et al., 2008). Noise prediction is usually conducted to assess the seriousness of adverse impacts arising from excessive noise on the surroundings. Consequently, there are many noise prediction methods available especially for traffic noise prediction (Wang et al., 2018; Al-Mosawe et al., 2018; Konbattulwar et al., 2016; Petrovici, 2015) but construction noise prediction methods are very limited and only a few can be found (Haron et al., 2008; Haron et al., 2009; Idris, 2012; Darus et al., 2015; Lim et al., 2015).

2.11 Construction Noise Prediction

Construction noise prediction is very essential in the planning phase of construction to ensure potential noise hazards can be monitored, controlled and

mitigation of noise may be made (Carpenter, 1997). Many techniques are being adopted in noise prediction such as BS 5228-1:2009, stochastic Monte Carlo approach, simple prediction chart technique and artificial neural network. (Haron et al., 2008; Haron and Yahya, 2009; Haron et al., 2012; Lim et al., 2015; Mansourkhaki et al., 2018). These noise prediction models can be utilized as a supervisory and planning tool in construction activities.

Darus et al. (2015) compared the results of noise prediction methods from BS 5228-1: 2009 with the actual measurement and obtained a significant difference with the highest value of 5 dBA. The prediction included several factors such as the sound power machine, the distance between receiver and noise source, the operating facility, the reflected sound, the reduction due to noise absorption of earth and the presence of screening. Moreover, Jahya (2014) conducted a comparative study on a construction site on a larger scale and discovered that the random movement of machines resulted in an observable difference between the measurement and prediction results.

Findings showed that the simple prediction chart technique is capable of providing reasonable and reliable outcomes and has absolute differences of 3 dBA (Haron et al., 2012). Besides, Lim et al. (2015) developed a noise prediction stochastic framework that considered the earth-moving machines' complexity and randomness along with the emitted noise levels; the outcome of this study showed reliable accuracy with the absolute differences of 2 dBA.

2.12 Stochastic Modelling

A stochastic model is applied to predict a set of possible results based on the possibilities or likelihood within a given time (Taylor and Karlin, 1998). Stochastic modelling is found to be feasible, especially in the construction noise prediction based on previous studies (Haron et al., 2008; Lim et al., 2015; Lim, 2017). Table 2.5 shows the findings of researchers that applied the concept of the stochastic process to their studies (Haron, 2008; Haron and Yahya, 2009; Haron et al., 2012; Lim et al., 2015).

Table 2.5: Application of stochastic modelling in noise prediction

Authors	Application and Findings
Lim et al. (2015)	This study adopted a stochastic model in noise prediction and it shows a satisfactory outcome (Absolute differences not more than 2 dBA). Besides, noise mapping quality was enhanced by using the results from the prediction.
Haron et al. (2012)	The noise prediction was conducted using the simple chart method based on stochastic modelling, the charts can be used to manually approximate construction noise at the planning stage with plausible accuracy.

Table 2.5: Application of stochastic modelling in noise prediction (Cont'd)

Authors	Application and Findings
Haron and Yahya (2009); Haron et al. (2008)	Monte Carlo approach and probabilistic approach are applied on the basis of stochastic modelling to obtain the temporal noise level dispersion emitted from construction activities. The findings of this study revealed that either for a single noise source or multiple noise sources, this technique can be applied to predict the temporal distribution of the construction activities.

2.12.1 Probabilistic Approach for Noise Modelling

The application of the probabilistic approach in noise modelling was to obtain a set of quantitative data to evaluate the seriousness of noise issues from traffic noise (Nelson, 1973). The probabilistic approach can be used to determine the noise level that exceeded 10 % of the time measurement duration, L_{10} and ambient noise level, L_{90} with the collaboration of multiple Gaussian traffic noise distributions. The conditions between construction noise and traffic noise are relatively similar as each involves different noise sources, operating concurrently or non concurrently, operating under random locations, noise sources with different sound power and operating under different conditions (Haron et al., 2008).

Haron et al. (2008) extended the work of Nelson (1973) on traffic noise prediction and developed a new method for construction noise prediction. Several factors that may influence the noise variability in terms of the position of machines or equipment, sound power and duty cycle of the machine, the amount of equipment within a hypothetical subarea, and the possibility of different activities operating concurrently were considered in the model to enhance the prediction model accuracy. This technique is capable of predicting a set of noise levels during a working day period based on their probabilities of cumulative or temporal distribution. Moreover, the probabilistic approach is proved as a reliable technique to predict equivalent noise levels, as the comparison of the result between BS 5228-1:2009 and the probability approach has a slight difference of 1 dBA.

2.12.2 Stochastic Monte Carlo Method

Monte Carlo can be defined as the concept of using randomness to predict an estimation (Brandimarte, 2014). Monte Carlo is a random number generator and a method that generates a set of boundless independent random variables that are uniformly distributed (Kroese et al., 2011). In this modern world, the concept of Monte Carlo has already been adopted in most computer languages. The user is required to insert an initial number, namely the seed as input. Then, a series of independent uniform random variables in the range of 0 to 1 will be simulated by the random number generator based on the input.

Carpenter (1997) was the first that introduced Monte Carlo in construction noise prediction. Gilchrist et al. (2003) deployed a model using the deterministic approach in corporate with the Monte Carlo technique. The model can forecast the frequency as well as the magnitude of noise levels emitted by equipment that is involved in construction activities within the site. Subsequently, Haron and Yahya (2009) obtained the temporal noise level distribution of the construction activities by using the Monte Carlo approach in the noise prediction model.

2.12.3 Stochastic Simulation Framework

Based on the studies of Haron and Yahya (2009) and Lim et al. (2015), the duty cycles and the random position of the machinery must be taken into consideration as the parameter of the noise prediction modelling. Lim et al. (2015) proclaimed that the duty cycles of the construction machinery are required to be categorized into several modes such as off, fully operating and idling to improve the noise prediction model reliability and accuracy. Subsequently, application of Monte Carlo theory is applied to generate a set of random output between these modes. Lim et al. (2015) stated randomness of activities and temporal distribution of noise levels were taken into account in the random walk approach. This technique can effectively forecast the strategic noise mapping from the moving workers and the dynamic machines within an area for noise exposure prediction.

2.12.4 Simple Prediction Charts Method

In this study, simple prediction charts were developed using a stochastic approach with some alterations from previous researchers to estimate the level of noise arising from construction noise (Haron et al., 2008; Haron and Yahya, 2009). This method was enhanced with the implication of three parameters to increase the accuracy of the prediction. The first parameter is the fluctuation in generated noise levels arising from the random position of an item of the machine within a confined area. Secondly, assuming the sound power level of the noise source as 120 dBA. Thirdly, the screening was excluded between the receiver and source during the simulation.

The mean noise level for a sub-area is computed by averaging the total number of sound pressure levels obtained based on the random movement of the machine in the sub-area. The mean noise level can be calculated by using Equation 2.7. Next, Figure 2.8a illustrates the design layout of the site, and the site is assumed as an ideal rectangular area with depth (d), width (w), and a receiver is positioned out of the area with a random angle (θ) and distance between the site centre and noise source (r). The sound pressure level is enumerated under the assumption, that the acoustic energy radiated in the form of hemispherical when the source is mounted on a rigid hard surface and can be calculated by using Equation 2.8. The distance from the sound source is quantified by using Equation 2.9. Besides, the x and y coordinates of the receiver with different radii can be calculated by using Equations 2.10 and 2.11. The randomness of the machine working at a random position is defined by using

two random numbers N_i and N_j , with the coordinates of x_i and y_j in Equations 2.12 and 2.13.

$$L = 10 \log_{10} \left(\frac{1}{N_T} \sum_{i=1, j=1}^{i=n, j=m} I_{(i,j)} / 10^{-12} \right) \quad (2.7)$$

Where,

N_T = total number of samples collected;

I = sound intensity generated from the machine (W/m^2);

L = mean noise level (dBA)

$$L_{(i,j)} = 10 \log_{10} \left(\frac{W_a}{2\pi R_{(i,j)}^2} \cdot 10^{12} \right) \quad (2.8)$$

Where,

W_a = acoustic power of the noise source which is equivalent to 1 Watt;

$R_{(i,j)}$ = the distance between the receiver and the source position (x_i, y_j, z_s);

$L_{(i,j)}$ = sound pressure level at the selected location (dBA)

$$R_{(i,j)} = \sqrt{(x_i - x_r)^2 + (y_j - y_r)^2 + (z_i - z_s)^2} \quad (2.9)$$

$$x_r = r \sin \theta \quad (2.10)$$

$$y_r = r \cos \theta \quad (2.11)$$

$$x_i = w(N_i - 0.5) \quad (2.12)$$

$$y_j = d(N_j - 0.5) \quad (2.13)$$

Where

w = sub-area width (m);

d = sub-area depth (m);

x_r = coordinate from horizontal axis of the receiver;

y_r = coordinate from the vertical axis of the receiver;

x_i = coordinate from horizontal axis of the randomized location of machine;

y_j = coordinate from the vertical axis of the randomized location of machine;

N_i = random number (from zero to one) for randomized x coordinate;

N_j = random number (from zero to one) for randomized y coordinate

Haron et al. (2012) studied the characteristics of noise level distribution between construction sites with a site aspect ratio (width : depth) and distance to width ratio (r/w) of 50 m x 50 m site with receiver distance of 50 m, 100 m x 100 m site with receiver distance of 100 m and 150 m x 150 m site with receiver distance of 150 m. The receiver was placed orthogonally to the site while the acoustic power of the source is 1 Watt during full-power operation. Based on the findings, Haron et al. (2012) proved that the noise level distribution for a construction site with the same $r : w : d$ ratio is identical and hence the same standard deviation as shown in Figure 2.8b.

With the same methodology but different variables, Haron et al. (2012) studied the relationship between the receiver coordinate and the noise level distribution on the square site. The dimensions of the sites in width and depth

were 50 m x 50 m and 100 m x 100 m. The sound power of the noise source is 1 Watt when it is operating at full power. The distance between the centre of the site and the receiver was calculated by Equation 2.14. The noise level distribution based on different receiver distances is depicted in Figure 2.8c. The distribution of mean noise level and the standard deviation reduced systematically as the distance increased. The findings explained that the same noise level distribution is generated when the site has the same ratio of width : depth. Figure 2.8d illustrates the relationship between standard deviation and $r:d$ or $r:w$. The results justified that all the sub-areas with a similar aspect ratio $w : d$ of 1 : 1 will generate data sets that appear to be on the same curve in the graph.

Haron et al. (2012) revealed the mean level variation curves are not directly normalised against the size of the site as well as in standard deviation. Figure 2.8e exemplifies the variation in mean levels for sites with the size of 50 m x 50 m and 100 m x 100 m is close to the sound pressure level at the site centre when the receiver distance increase. This explained that the mean level is not dependent on the dimension of the site in w and d . However, the mean level deviation can be plotted against the distance to site width ratio (r/w ratio) as illustrated in Figure 2.8f. It was observed that the mean level deviation against the r/w ratio for 50 m x 50 m and 100 m x 100 m has an identical curve in the graph. The relationship between the mean level deviation and radius : width ratio along with the mean level at any distance for the site with a homogeneous aspect ratio (width : depth) can be conveyed in Equation 2.15.

$$r = d1 + 1,2,4 \dots, 2048 \quad (2.14)$$

Where,

$d1$ = depth of the site (m);

r = distance between the centre of site and receiver (m)

$$L = L_w - 20\log_{10}(r) - 8 + \Delta L \quad (2.15)$$

Where,

L = mean level, sound pressure level correspond to the source at centre of site (dBA);

L_w = sound power level (dBA);

ΔL = mean level deviation (dBA)

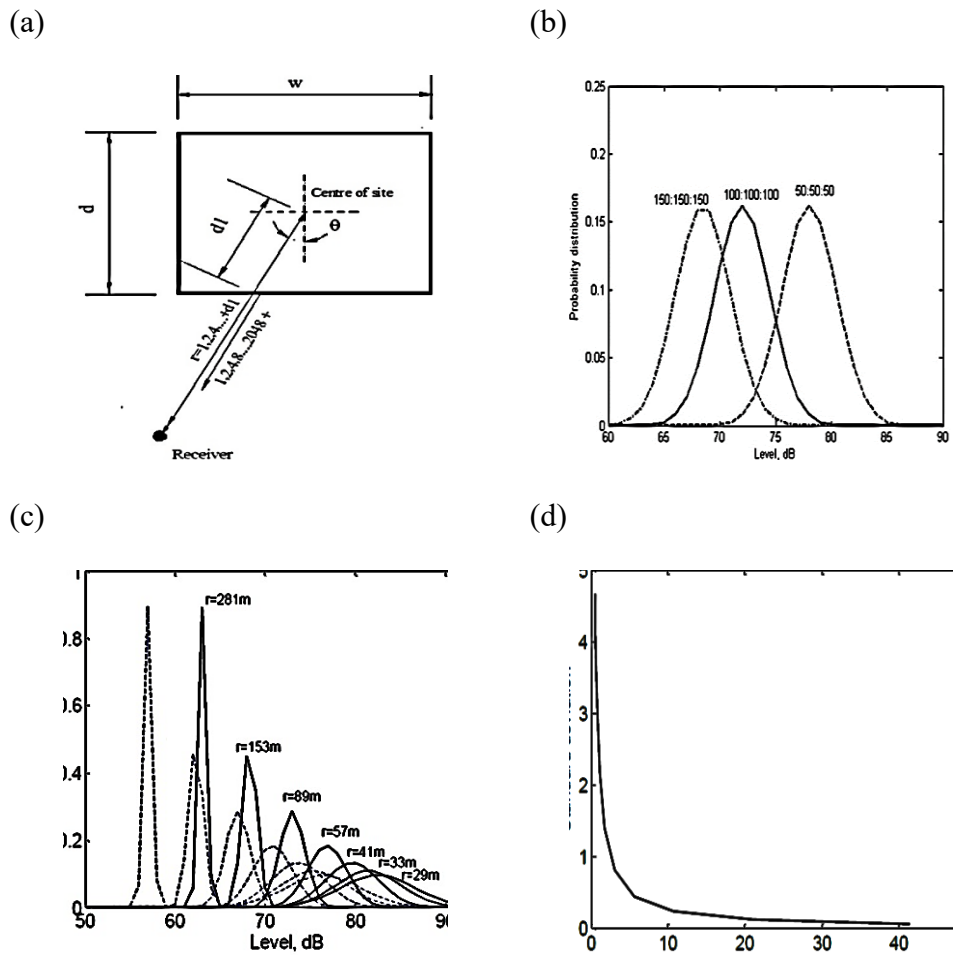
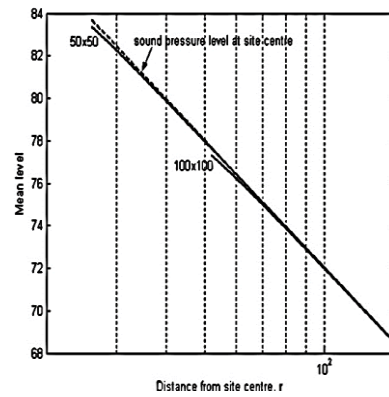


Figure 2.8: Effect of distance for square sites (50 m x 50 m; 100 m x 100 m)
 (a) site configuration with same r : w : d ; (b) design layout of construction site and position of receiver; (c) effect of distance on noise level distribution on square site (- - - : 100 m x 100 m; — : 50 m x 50 m); (d) standard deviation vs. distance normalised with w or d ; (e) mean level variation; (f) deviation from tangent line (Haron et al., 2012)

(e)



(f)

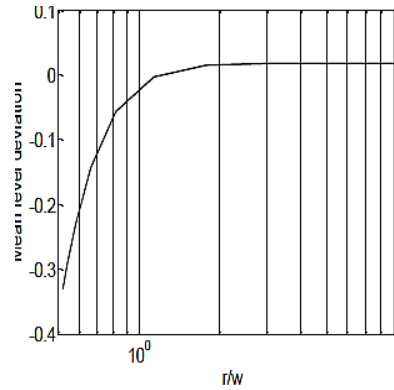


Figure 2.8: Effect of distance for square sites (50 m x 50 m; 100 m x 100 m)
(a) site configuration with same $r : w : d$; (b) design layout of construction site and position of receiver; (c) effect of distance on noise level distribution on square site (- - - :100 m x 100 m; — : 50 m x 50 m); (d) standard deviation vs. distance normalised with w or d; (e) mean level variation; (f) deviation from tangent line (Haron et al., 2012) (Cont'd)

2.13 Reliability and Accuracy Assessment for Predicted Data

The reliability of the deep learning model is assessed by the strength of association between the predicted data and actual measured data. The consistency of measurement can be defined as reliability. Several types of reliability measurement such as R-squared and Pearson correlation coefficient are applied in the predictive model (Lim et al., 2015; Lim, 2017). These techniques are used to validate the consistency between the predicted data and actual measured data.

R-squared shows the variations of the discrepancy between independent and dependent variables in a regression model (Weisberg, 2014). Figure 2.9 illustrated the correlation between the predictor and response, along with the best fit line in the scatter plot. Each circle represents each data point and the vertical line indicates the difference from the best fit line. The association strength of the R-squared is clearly presented in Table 2.6 (Henseler, Ringle, and Sinkovics, 2009).

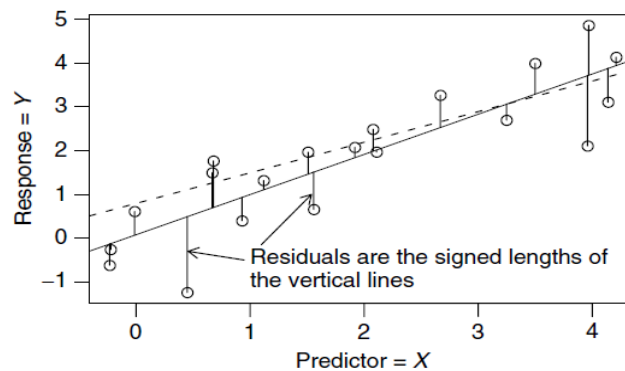


Figure 2.9: Relationship of variables (Henseler, Ringle, and Sinkovics, 2009)

Pearson correlation coefficient was applied in this study as this technique was used by previous research in determining the reliability of noise prediction results (Lim, 2017). The strength of the association of Pearson's Coefficient Value can be assessed by using Table 2.7 (Silver et al., 2013). The table consists of 5 categories of association strength which are very strong, moderate to strong, weak to moderate, weak and non-existent to very weak to comprehend the association of the data.

The deep learning model accuracy is assessed with several statistical measures such as absolute difference, mean absolute difference and root mean square deviation. The absolute difference is the amount of error in a statistical measure. It is the difference between the predicted and the actual value. The mean absolute difference is the average value of the difference between all observations in a sample set. Next, root mean square deviation is also applied in this study to assess the accuracy, it shows the positive or negative deviation of typical points that are away from the regression line (Freedman, Pisani and Purves, 2007).

Table 2.6: Determination of association strength based on R^2 (Henseler, Ringle, and Sinkovics, 2009)

Strength of Association	Range of Correlation Coefficient
Strong	Greater than 0.67
Moderate	0.33 – 0.66
Weak	0.19 – 0.32
Non-existent to very weak	0.00 – 0.18

Table 2.7: Determination of association strength based on correlation coefficient value (Silver et al., 2013)

Correlation Coefficient Range	Association Strength
0.00 to 0.20	Non-existent to very weak
0.21 to 0.40	Weak
0.41 to 0.60	Weak to moderate

0.61 to 0.80	Moderate to strong
Greater than 0.80	Very strong

2.14 Artificial Intelligence

Artificial intelligence is the area that studies the response of machines that applies the concept of observation, perspicacity, and intention of a human under different simulations (Shubhendu and Vijay, 2013). In other words, the field of study that discusses the potentiality of machine learning to act like humans and the ability to respond to certain behaviours is called Artificial Intelligence. However, different researchers studied different approaches such as thinking humanly and rationally, acting humanly and rationally, applied to AI (Haugeland, 1985; Winston, 1992; Nilsson, 1998; Kurzweil, 1999;). Artificial Intelligence consists of machine learning and deep learning. Any process that conjoins intelligence into a system or machine to learn independently without involvement from a human is called machine learning (ML). The concept of deep learning (DL) is derived from the biological structure and function of the human brain and enhances the intelligence of machines. Figure 2.10 illustrates the relationship between Deep Learning, Machine Learning and Artificial Intelligence. (Moolayil, 2019).

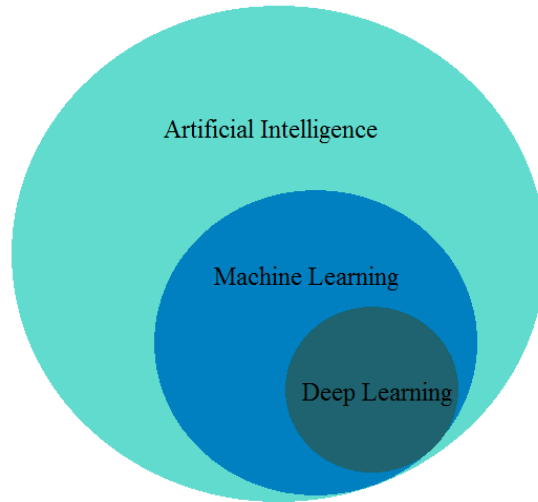


Figure 2.10: Venn diagram of artificial intelligence, machine learning and deep learning (Moolayil, 2019)

2.15 Machine Learning

A type of computer program that acquires the capability of self-learning without an individual to program the software is called machine learning. In other words, machine learning learned from the experience and enhance future performance. Machine learning comprised four main types of basic paradigms which are supervised, unsupervised, semi-supervised and reinforcement learning as exemplified in Figure 2.11 (Rafique and Velasco, 2018). Supervised Learning uses a training data set that requires labelling the inputs and generating the outputs (Dasgupta and Nath, 2016). The function of Semi-supervised learning works like supervised and unsupervised machine learning by applying the combination of both labelled and unlabelled data to enhance the performance of prediction. Lastly, the basis of reinforcement learning is by using reward feedback when a different simulation is given. Reinforcement learning is the

algorithm that is trained to find the optimized action based on the environment by trial and error (Das and Behera, 2017).

Moreover, supervised learning can be subdivided into regression and classification which the applications are housing price prediction and medical imaging to detect abnormalities respectively (Chollet, 2018). On the other hand, unsupervised learning can be ramified to clustering and association that both frequently used in the business sector. Clustering is in customer segmentation which is separating the customers into different groups based on their common traits or similarities. Association is employed to study the purchasing behaviour and patterns of the consumers, which is called market basket analysis (Kurniawan et al., 2018; Singh, 2021). Fan et al. (2014) adopted semi-supervised learning in traffic lane detection, and the result is remarkable even in challenging conditions. Witten et al. (2017) mentioned that the application of semi-supervised learning will improve the accuracy of text and document classification. Wang et al. (2018) conducted a study that proved that the application of reinforcement learning enables the autonomous vehicle to perform an efficient driving policy for lane-change manoeuvres. Lastly, the application of the reinforcement learning classification technique will help the marketing sector in presenting the best-suited advertisement to the users based on their browsing data.

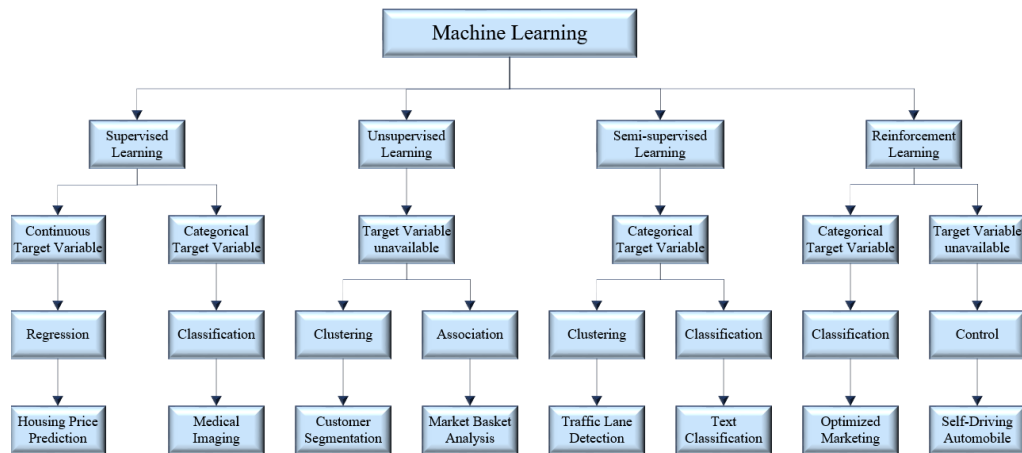


Figure 2.11: Classification of machine learning (Rafique and Velasco, 2018)

2.16 Supervised Learning

Supervised learning is a technique that required references from past data that are precisely categorized and explained in patterns and trends, to make a future prediction. The word ‘supervised’ means the date set where the targeted outputs are already known. The input dataset will be distributed into two components which are the training dataset and the test dataset. In other words, the algorithms will learn from the date set during the training and will predict a test data set. Supervised learning is targeted to develop a regressor or classifier that is able to determine the output value for unknown inputs from earlier on (Raschka and Mirjalili, 2017).

2.16.1 Regression

A regression model is a derivation of supervised learning and it is a problem of predicting a real value or quantity. A regression problem with

various input parameters is usually known as a multivariate regression problem (Campeato, 2020; Singh and Manure, 2020). A regression model predicts a quantity and hence, and the regression model's performance is usually assessed by using the mean absolute and mean squared error. However, there are mainly two types of regression analysis techniques such as linear regression and polynomial regression (Singh and Manure, 2020). The application of these techniques depends on the quantity of the independent variables, the formation of the regression line, and the archetype of the target variable. The function of regression analysis techniques is distinct and each may be applied in constructing a regression model depending on the types and availability of data.

The simplest type of regression in which the goal is to find the best fitting line that represents the relationship between the target and explanatory variable is known as simple linear regression (Raschka and Mirjalili, 2017; Campeato, 2020). However, the non-linearity between the input features and output will result in the data being under-fitted (Patel, 2019). The linear regression model equation with a single explanatory variable can be expressed in Equation 2.16 (Raschka and Mirjalili, 2017). A visualization of linear regression is depicted for a better insight in Figure 2.12.

$$y = w_0 + w_1x \quad (2.16)$$

Where,

y = target variable;

x = explanatory variable;

w_0 = y-axis intercept;

w_1 = weight coefficient of the explanatory variable or the slope of the best fit line

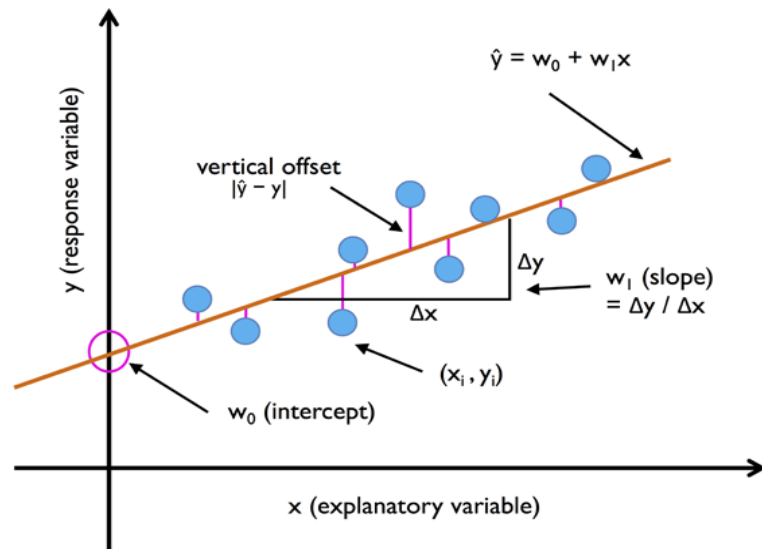


Figure 2.12: Visualization of linear regression (Raschka and Mirjalili, 2017)

2.16.2 Classification

Classification is a subset of supervised learning that utilizes a machine-learning algorithm to assign discrete class labels to input samples from the data set (Campeato, 2020). The class labels are commonly in the form of string values. Logistic regression unlike linear regression is applied in classification problems and applied when the dependent variable is discrete. The logistic regression prediction is a class of probabilities or in the form of a binary state, and it is not used for real values or quantitative prediction. Nonetheless, the weakness of logistic regression is that it will fail to perform when the classes

are not linearly distinguishable (Patel, 2019). The performance of the classification model is usually assessed by the accuracy of prediction. Besides, several types of classification algorithms such as binary, multi-class, multi-label and imbalanced classification are widely used in the computer science industry (Brownlee, 2016).

Binary classification is the classification task that contains two class labels such as normal state and abnormal state. For instance, this technique is popularly used in spam detection (Mallampti, 2018). Multi-class classification or multinomial consists of more than two class labels and the number of class labels on the same problems could be enormous. Multi-class classification is usually applied in face classification and plant species classification (Lee et al., 2018; Khan et al., 2020). The comparison between binary and multi-class classification is illustrated in Figure 2.13. The classification tasks in which an object can be classified into more than two class labels are known as multi-label classification tasks. For a multi-label image classification example, multiple class labels will be assigned to different objects in an image (Singh, 2021). Lastly, an imbalanced classification occurs when the number of samples in the normal and abnormal classes is unequally distributed in which the majority of the samples in the training dataset are usually biased toward the normal state, while the remaining samples are biased toward the abnormal state (Goodfellow et al., 2016). This method is commonly used in medical diagnostic tests (Zhao et al., 2018).

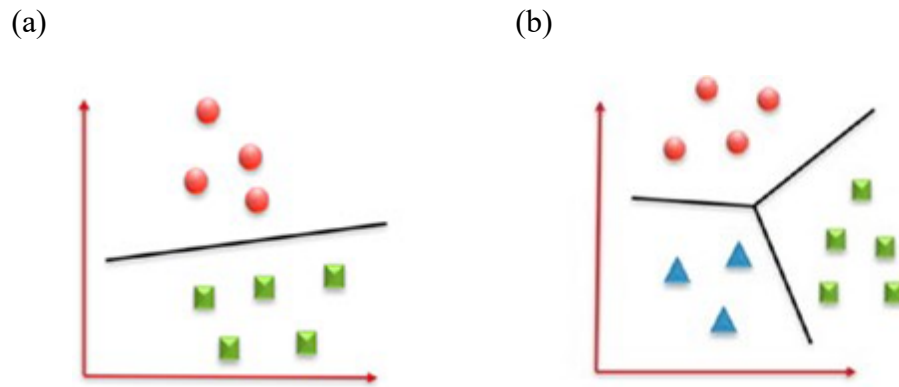


Figure 2.13: Types of classification (a) binary classification; (b) multi-class classification (Singh, 2021)

2.17 Unsupervised Learning

In unsupervised learning, the model is conceptually different from supervised learning. (Raschka and Mirjalili, 2017). Unlike supervised learning, there are target outputs in regression or classification problems to show the algorithm the correct answer to possible inputs. On the contrary, the unsupervised learning algorithm attempts to discover and analyse the hidden pattern and applicable signals of the clusters with similar inputs without being specifically defined that these samples are in the same cluster whereas those in a different cluster (Marsland, 2015). The samples with different attributes and features will be assigned to a different group without a label. There are several types of unsupervised learning such as clustering and association.

2.17.1 Clustering

Clustering in unsupervised learning is the task to separate the unlabelled data into several groups such that in the same group the data contained similar attributes and dissimilar compared to the data in other groups and it can be subdivided into k-means and hierarchy clustering (Goodfellow et al., 2016). To cluster efficiently, different groups have to be determined in a way that the samples within a category are close to each other but dissimilar from samples in the other groups. With the application of the k-means clustering algorithm, the user is allowed to specify the number of targeted clusters, then each sample will be assigned exactly to these clusters. In an attempt to optimize the clustering process, each sample will be assigned randomly to one of the clusters. Then, the cluster's centre point and Euclidean distance between each sample will be minimized after the reassignment of the samples in other clusters. As a result, the least summation within-cluster variation among all clusters will be selected as the optimum separation. Figure 2.14 depicts the organization of unlabelled data based on the given features x_1 and x_2 by using clustering (Raschka and Mirjalili, 2017).

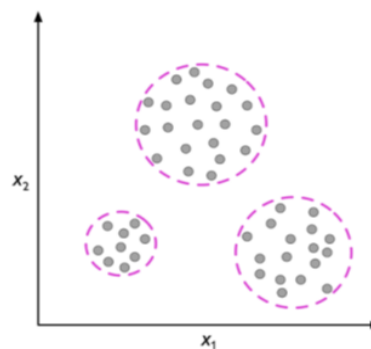


Figure 2.14: Visualization of clustering (Raschka and Mirjalili, 2017)

The user is not restricted to a limited clusters number when using hierarchical clustering. Agglomerative clustering is one of the hierarchical clustering that uses a tree-based clustering method and constructs a dendrogram (Firdaus and Uddin, 2015). Discrete samples in the dataset will start from the bottom of the dendrogram. Hierarchical clustering will join the samples with similarities together vertically towards the top (Vijaya et al., 2017). The samples that are more similar to each other will be clustered sooner whereas the less similar samples are joined together later. In the end, all the samples will converge and form a group at the uppermost of the dendrogram. Then, the dendrogram allows the user to determine of cluster similar to the basis of the k-means clustering algorithm.

2.17.2 Association

The association rule is a technique to discover the relationship between two seemingly unrelated variables in a large dataset. This technique is often named market basket analysis which is an analysis mode conducted on consumer behaviour whilst shopping at a supermarket, and identifying the correlation and association among several items selected by the consumers in their shopping carts; in particular, the objective of market basket analysis is to determine the most frequently purchased items by the consumers (Kurniawan et al., 2018).

2.18 Semi-supervised Learning

Another subset of machine learning which is semi-supervised learning applies the supervised and unsupervised learning techniques concurrently in the training and prediction. This technique is handy when the user is dealing with a mixed-type dataset that consists of unlabelled and labelled data (Singh, 2021). Machine learning learns the labelled data by reducing the error between labelled data along with the predicted data, and unlabelled data based on their closeness or similarities (Jo, 2021). The concept of semi-supervised learning is called pseudo-labelling which utilizes a small portion of the labelled information to train the model and then used the predicted output to label the other remaining data, lastly transforms all the unlabelled data into labelled data (Huang et al., 2006). Semi-supervised learning can be easily trained on a larger size dataset, which is better at prediction. Besides, the benefit of using semi-supervised learning is that it is more time-efficient and reduces the unnecessary laborious effort in manually labelling the data (Goodfellow et al., 2016). The concept of semi-supervised learning is presented as a diagram in Figure 2.15.

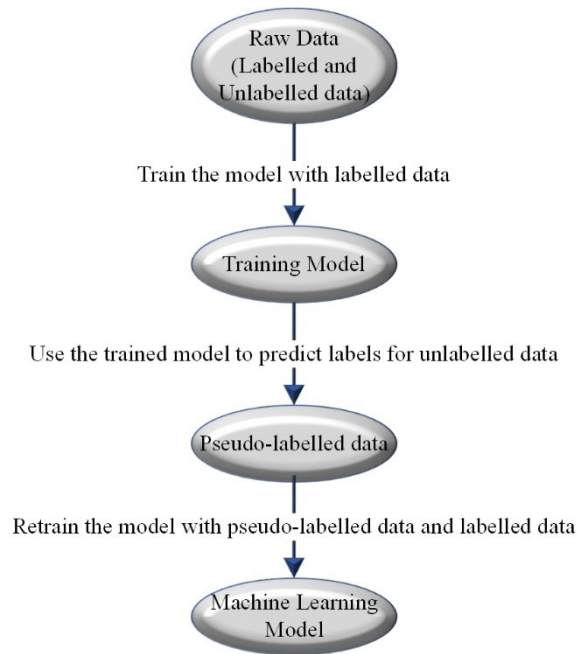


Figure 2.15: Semi-supervised learning (Huang et al., 2006)

2.19 Reinforcement Learning

Machine learning consists of reinforcement learning that works differently from other machine learning in terms of data usage and prediction (Singh, 2021). In fact, supervised, unsupervised and semi-supervised learning required historical data to train the model and make predictions then compare with the correct value or label. However, the main idea of reinforcement learning is a measure of the performance of an action taken by a reward function (Raschka and Mirjalili, 2017). Reinforcement learning is built on the basis of these essential elements such as autonomous agent, action, environment, state, and reward (Marsland, 2015). The relationship of these individual elements can be depicted in Figure 2.16. The autonomous agent is responsible in receiving information from the environment and observing the feedback that will obtain the maximum reward (Goodfellow et al., 2016; Chollet, 2018). Besides, an autonomous agent must

learn to execute the task by trial and error under circumstances without human guidance. Actions are the possible steps that the agent can choose in the task. The action performed by the agent will be determined by the environment whether it takes place in rewards or penalties. The state represents the current situation during the given scenario, the agent has to keep moving in the positive direction to obtain the maximized rewards. The most common application of reinforcement learning is in navigation systems, gaming, and recommender system (Singh, 2021).

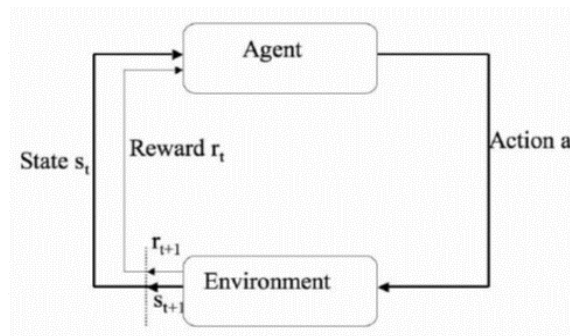


Figure 2.16: Illustration of reinforcement learning (Marsland, 2015)

2.20 Deep Learning

Deep learning is an algorithm that is set out to learn in multiple levels of representation and correspond to a structure of concepts to simplify the data set with high complexity (Benuwa et al., 2016; Li and Dong, 2014). Deep learning mainly uses an artificial neural network that responds to different levels of concepts, where the lower level defined the higher level. Nevertheless, deep learning is broad and consists mainly of three different types of neural work

essentially recurrent neural network, convolutional neural network and artificial neural network.

2.21 Multilayer Perceptron

The idea of a neural network was originated from a perceptron model developed in the 1950s (Rosenblatt, 1958). An artificial neural network (ANN) is an imitation of the human brain (Aggarwal, 2018). An artificial neural network is commonly named multilayer perceptron (MLP), consisting of input, hidden layer, and output layer. Besides, MLP has been commonly adopted in forecasting and predictive problems (Suhartono et al., 2019; Das and Roy, 2019). The shallow neural network is an artificial neural network that only comprises a single hidden layer. The nodes in each hidden layer represent a neuron and a nonlinear activation function is involved in these nodes (Camposato, 2020). The mechanisms of a shallow neural network are based on a simple feedforward propagation algorithm. The architecture of the multilayer perceptron is illustrated in Figure 2.17 (Do et al., 2018). Figure 2.18 shows the architecture of neural networks that consists of multiple hidden layers between the output layer and the input layer (Kim, 2017). The backpropagation algorithm will be applied to update the weights and bias. The state of the backpropagation neural network is always altering continuously until an equilibrium point is achieved. A new equilibrium point will be recalculated once there are new inputs in the ANN.

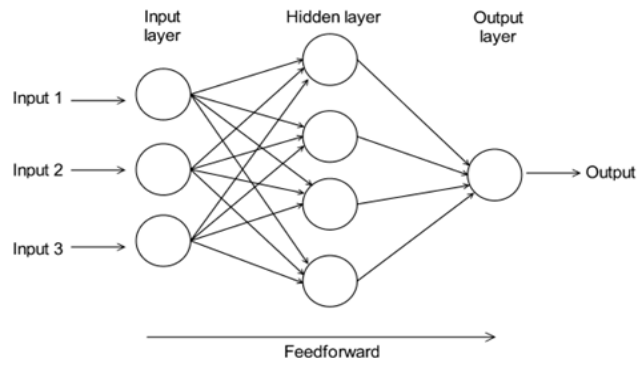


Figure 2.17: Architecture of multilayer perceptron (Do et al., 2018)

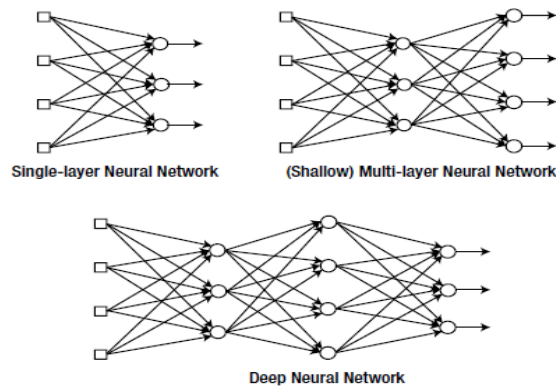


Figure 2.18: Architecture of simple, shallow and deep neural network (Kim, 2017)

2.22 Convolutional Neural Network

Convolutional Neural Network (CNN) is a notable neural network that is designed for the purpose of solving problems in which the input data of the prediction model has a grid-like structure in one dimensional or two dimensional (Ketkar, 2017). CNN-based structures are omnipresent in the computer vision industry and are even widely applied in the commercial sector for image recognition, semantic segmentation, and object detection. For the case

of image recognition, each image that is used in the learning model is divided into dense topological division, then the division will be processed by filters to search for a specific regime (Zaccone and Karim, 2018).

CNN consists of three discrete layers namely convolutional, pooling and fully connected layers (Singh and Manure, 2020). Figure 2.19 demonstrates the mechanisms of the convolutional neural network (Ketkar, 2017; Singh and Manure, 2020). The main function of the convolutional layer is to apply one or more filters to an input, the filter in the convolutional layer is named the convolutional kernels, and it is a matrix of integers, that is used on segments of the input image, wherein the size of the segment is of the filter; values from the segments and kernels will be multiplied and the results of each multiplication will be summed up to a single value, this process will be repeated by sliding horizontally then vertically across the entire image to create an output feature map. This process is executed by using an extracting window namely stride, which is the measure of movement between filter applications to the input image. Next, the convolutional layer output will be relocated to the pooling layer for dimensionality reduction, thus reducing the parameters and intricacy of the model. The max-pooling technique is conventionally adopted in the pooling layer, by selecting the maximum value from the generated output by using stride. Then the output from the pooling layer will propagate to the flattened and fully connected layer or hidden layer consecutively which is identical to an artificial neural network wherein the neurons are fully connected to the activation from the preceding layers (Ketkar, 2017; Singh and Manure, 2020).

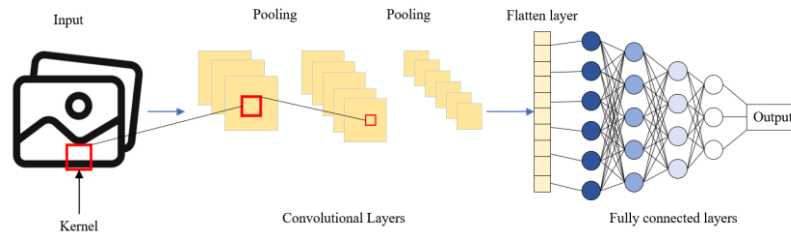


Figure 2.19: Convolutional neural network (Ketkar, 2017; Singh and Manure, 2020)

2.23 Recurrent Neural Network

A recurrent neural network (RNN) is designed to solve sequential problems., wherein the input data for the predictions is in the structure of a sequence (Ketkar, 2017). Unlike multilayer perceptron neural networks, the neurons in the hidden layers may pass their signal laterally to other neurons forming a directed cycle, in addition, to propagating forward to the succeeding layer. Moreover, the output of the neural network could be used as an input vector for the next input vector. In other words, RNN processes the information gradationally while maintaining an internal model of the current process simultaneously, in which the newly updated information is based on the previous data (Chollet, 2018). As opposed to MLP and CNN, RNN is stateful as it has an internal state for its hidden neurons. As a result, RNN is more capable of processing input with high complexity sequences, which makes it more preferable for speech recognition and hand-writing recognition tasks. A visualization of RNN is depicted in Figure 2.20.

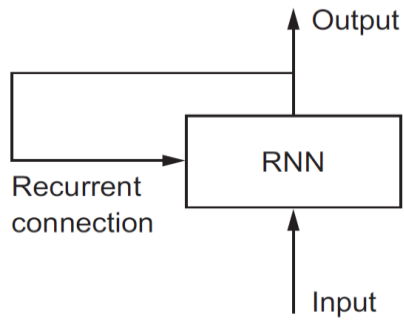


Figure 2.20 Recurrent neural network (Chollet, 2018)

2.24 Input Layer

A perceptron consists of input node (x), weighting (w), and bias (b). Then, the net-input function takes place to calculate a layer of net input by merging its weighted input s and biases as shown in Figure 2.17 (Skansi, 2018). Initially, the weights would all be random during the model training, then the model will learn to generate correct output after these weights are updated iteratively by using the feedforward method (Moolayil, 2019). The weighted sum can be mathematically expressed in Equation 2.17.

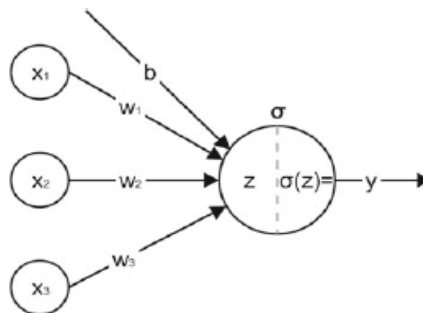


Figure 2.21: Shallow neural network (Skansi, 2018)

$$z = \sum w_n x_n + b \quad (2.17)$$

Where,

w_n = weighting (random number);

x_n = Input data;

b = bias (constant to enhance the performance of prediction);

z = logit or weighted sum,

2.25 Activation Function

Nonlinear functions that lie between the input and output layers in deep learning are named activation functions. Hence, the activation function is applied in the neural network to perform complex calculations in the hidden layers then the outcome will propagate to the output layer. Net input is computed by an activation function such as the sigmoid function, rectified linear unit function, tanh function, and softmax function (Aggarwal, 2018). The main purpose of the activation function is to control the threshold whenever a neuron is activated in a hidden layer, and govern the degree of the output signal. Simple step activation functions were previously applied on the condition that the totalled input was above a threshold, for instance, a value of 0.5 would generate a value of 1.0 when it passes through the neuron, otherwise, the output would be 0. However, simple step activation functions cannot solve problems with non-linearity. As a consequence, nonlinear activation such as logistic function is applied that allows the network to merge the inputs with higher complexity, and render a higher capability in the functions for computation. A logistic function can be

subdivided into a sigmoid function, that outputs a value ranging from 0 to 1 with an s-shaped distribution. Nevertheless, the rectifier activation function has been proven to have better performance in neural networks (Brownlee, 2016).

2.25.1 Linear Activation Function

A linear function is basically an equation of a line, in which it will appear as a straight line when plotted, where the independent variable is equivalent to the dependent variable, preferably used in the output layer (Kim, 2017; Aggarwal, 2018). The relationship of a linear function is depicted in Figure 2.22a and can be expressed in Equation 2.18.

$$\text{output, } y = x \quad (2.18)$$

Where

y = target variables;

x = explanatory variable

2.25.2 Sigmoid Activation Function

A sigmoid activation function is originally used in an artificial neural network as it is considered less complex (Lago et al., 2018). As illustrated in Figure 2.22b, the sigmoid activation function has a limit of 0 to 1, which is very useful in performing computations in the form of probabilities and it is the ideal choice for classification problems as the output layer (Charniak, 2018; Aggarwal, 2018;

Loy, 2019). The sigmoid activation function generates output with a smooth gradient which to prevent the fluctuation between output values. Moreover, the output of the prediction model will be clear and precise for binary classification tasks because the output is very close to 1 or 0. However, the sigmoid activation function has three major disadvantages which are the vanishing gradient problem, function output is not zero-centred and lastly, the computations are time-consuming due to exponential function (Campeato, 2020). The occurrence of the vanishing gradient problem is when the z value is either very high or low, then there will be almost no change to the prediction. As a result, as the loss reaches the first few layers, it has already decreased to the point that the weights did not change much. Updating and training the weights of the first few layers with such a slight loss propagated backwards are relatively difficult (Loy, 2019). This will lead to the neural network refusing from learning further or taking a longer duration to achieve an accurate prediction. The sigmoid activation function can be expressed in Equation 2.19.

$$\text{output, } f(z) = \sigma(z) = \frac{1}{1 + e^{-z}} \quad (2.19)$$

Where

z = logit or weighted sum;

2.25.3 Hyperbolic Tangent Function (Tanh)

Tanh activation function has primarily been applied to natural language processing and speech recognition tasks. Similar to the sigmoid function, the tanh function has a drawback as it is not capable of solving the vanishing gradient problem. The difference between tanh and sigmoid is that the integers of tanh activation function ranged from a negative one to one (-1,1), whereas the sigmoid function ranged between zero to one (0,1). However, unlike sigmoid, the output of tanh is always zero-centred. Hence, tanh nonlinearity is preferable as compared to sigmoid nonlinearity in current practice (Campesato, 2020). An illustration of the tanh activation function is presented in Figure 2.22c, it can be mathematically expressed in Equation 2.20.

$$\text{output, } f(z) = \sigma(z) = \frac{e^{2z} - 1}{e^{2z} + 1} \quad (2.20)$$

Where

z = logit or weighted sum;

x = explanatory variable

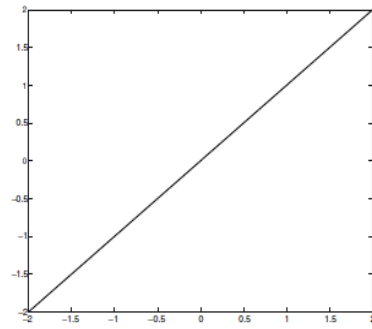
2.25.4 Rectified Linear Unit Function (ReLU)

ReLU function is presently adopted because it helps the training process of the models by reducing vanishing gradient problems (Goulet, 2020). Furthermore, the ReLU function is being recommended as the default function in the feedforward neural network (Goodfellow et al., 2016). This is because whenever the ReLU function is applied to the output of a linear transformation

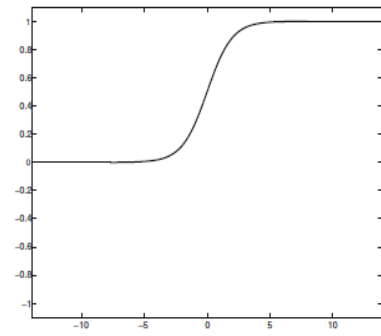
a nonlinear transformation will be produced. Although this function is very close to linear, but it is a piecewise-defined function with two sub-functions. On account, ReLU functions are almost linear, most of the features are preserved and make linear models much easier to be optimized with gradient-based methods. In short, output values that are greater than 0 will remain unchanged whereas output values that are less than 0 will be considered as 0 as shown in Equation 2.21. Besides, studies suggested that the ReLU function is preferable to be used in the hidden layers (Loy, 2019). Moreover, models with the ReLU function converge faster than other activation functions (Campeato, 2020).

$$\text{output}, y = \max(0, x) \quad (2.21)$$

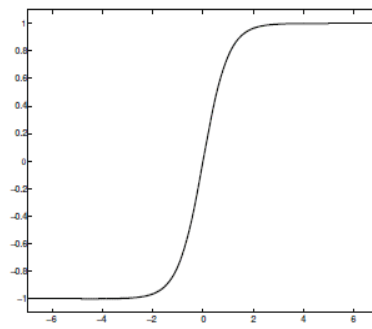
(a)



(b)



(c)



(d)

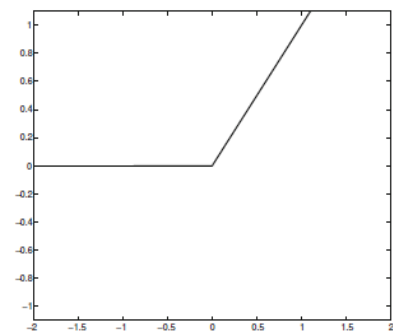


Figure 2.22: Activation functions (a) linear function (b) sigmoid; (c) tanh; (d) ReLU; (Aggarwal, , 2018)

2.26 Backpropagation

Backpropagation is an algorithm in which the error from the output travels in reverse order from the output layer throughout the hidden layers until it propagates back to the input layer to update the weights depending on the loss or cost function. The significance of the back-propagation algorithm in an artificial neural network was that a systematic method was developed to signify the hidden nodes error (Kim, 2017). Then, the delta rule is used to calibrate and update the weights once the errors of hidden layers are identified.

The delta of the output node is expressed identically as the delta rule of the Generalized Delta Rule in the back-propagation algorithm. The output node error will be computed by detecting the difference between the corrected outcome from the training data and the output from the output node as explained in Equations 2.22 and 2.24. In Figure 2.19, the back-propagation algorithm is applied as an initial process of training in the neural network. Delta can be calculated by using Equations 2.23 and 2.25. The error of the output node can be explained as the summation of the deltas that propagated to the hidden layer from the output layer as depicted in Figure 2.20. The process from the output layer to the hidden layer is mathematically expressed from Equations 2.22 to 2.30. Next, the error calculation formulas from Equations 2.26 and 2.28 are combined to obtain the product by multiplying the delta vector with the transposed weight matrix using the product rule that allows the algorithm to execute more easily. Then, once all the deltas have been computed, Equations 2.31 and 2.32 will be applied to adjust the weights of each layer.

$$e_1 = d_1 - y_1 \quad (2.22)$$

$$\delta_1 = \phi^1(v_1)e_1 \quad (2.23)$$

$$e_2 = d_2 - y_2 \quad (2.24)$$

$$\delta_2 = \phi^1(v_2)e_2 \quad (2.25)$$

Where

e_n = error of the output node;

d_n = corrected output from training data;

y_n = output from the output node;

δ_n = product of error and activation function derivative;

v_i = corresponding node weighted sum;

ϕ = derivative of the output node activation function

$$e_1^{(1)} = w_{11}^{(2)}\delta_1 + w_{21}^{(2)}\delta_2 \quad (2.26)$$

$$\delta_1^{(1)} = \phi^1(v_1^{(1)})e_1^{(1)} \quad (2.27)$$

$$e_2^{(1)} = w_{12}^{(2)}\delta_1 + w_{22}^{(2)}\delta_2 \quad (2.28)$$

$$\delta_2^{(1)} = \phi^1(v_2^{(1)})e_2^{(1)} \quad (2.29)$$

$$\begin{bmatrix} e_1^{(1)} \\ e_2^{(1)} \end{bmatrix} = \begin{bmatrix} w_{11}^{(2)} & w_{21}^{(2)} \\ w_{12}^{(2)} & w_{22}^{(2)} \end{bmatrix} \begin{bmatrix} \delta_1 \\ \delta_2 \end{bmatrix} \quad (2.30)$$

$$\Delta w_{ij} = \alpha \delta_i x_j \quad (2.31)$$

$$w_{ij} \leftarrow w_{ij} + \Delta w_{ij} \quad (2.32)$$

Where

$v^{(l)}$ = the weight sums of the forwards signals at the node;

$e^{(l)}$ = error of the hidden node;

$\delta^{(l)}$ = derivative product of error;

x_j = input signal for the corresponding weight;

α = learning rate (ranging from 0 – 1);

w = weighting

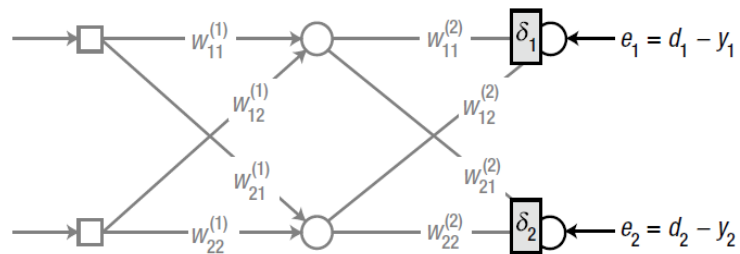


Figure 2.23: Training the neural network using the back-propagation algorithm (Kim, 2017)

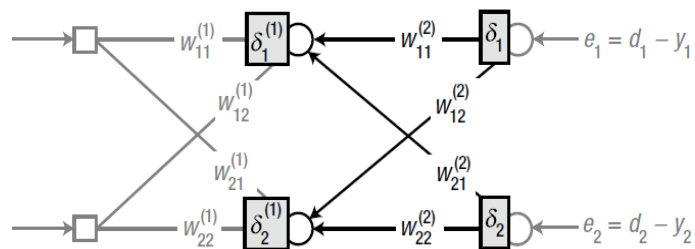


Figure 2.24: Propagate backwards to hidden nodes and calculate the data (Kim, 2017)

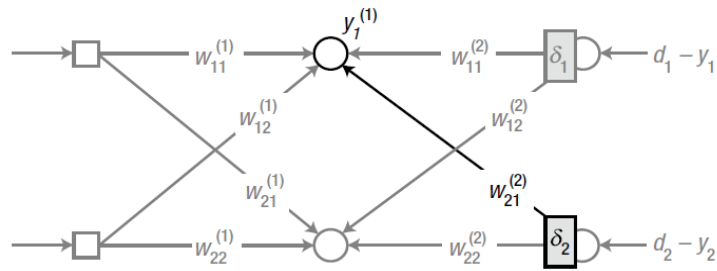


Figure 2.25: Equation derivation to adjust the weight (Kim, 2017)

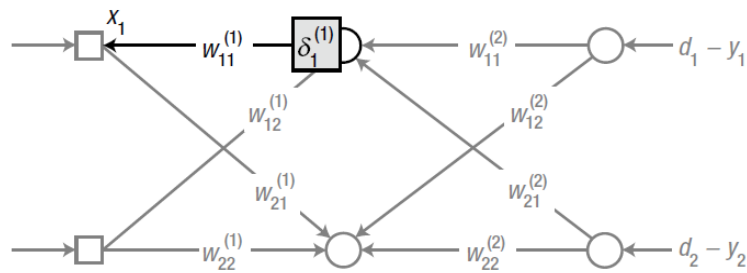


Figure 2.26: Derive the equation again to adjust the weight (Kim, 2017)

2.26.1 Learning Rate

The learning rate is a decimal value that typically lies between 0.001 and 0.05, which will directly influence the magnitude of value that is gradually added to the current weight to train the model with these adjusted weights. The throttling effect might occur when the learning rate is either at a very high value or a very low value. As a supporting statement, a high value of learning rate can cause the learning curve to oscillate violently or the new approximation might exceed the optimal point; and a low learning rate represents slow convergence and resulting in the optimization process remaining at the local minimum instead of moving towards the global minimum as shown in Figure 2.27(a) and 2.27(b) (Ketkar, 2017; Chollet, 2018; Campesato, 2020; Kinsley and Kukiela, 2020).

The targeted learning rate adjustment can be achieved by allowing the learning rate to decay gradually, and eventually mitigate the problems mentioned (Aggarwal, 2018).

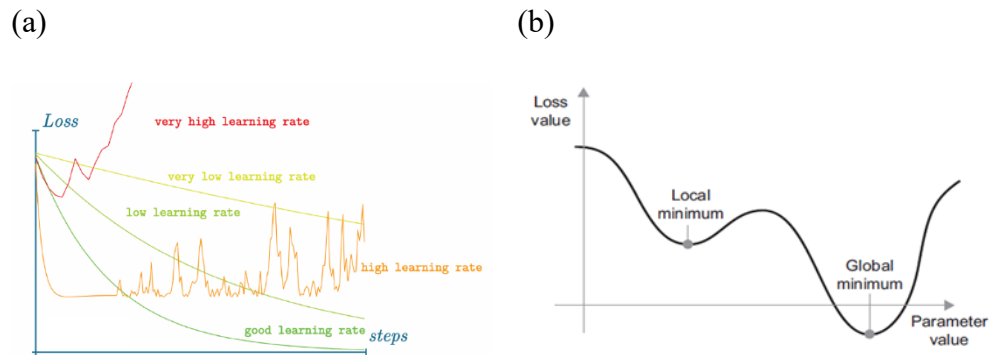


Figure 2.27 Influence of learning rate (a) variation of learning rate; (b) illustration of local minimum and global minimum (Chollet, 2018; Kinsley and Kukiela, 2020)

2.27 Loss Function and Cost Function

The cost function is a statistical theory that utilized the optimization concept and average value of loss functions. The cost function aims to measure the neural network error. Besides, the loss function value is directly proportional to the neural network error. Loss function usually will be included in the layers as it helps the neural network to understand the learning direction and by adding a dropout layer that may prevent overfitting from happening (Srivasta et al., 2014). Overfitting occurs when the prediction trend in a data set is too complex. In other words, the model locates too much emphasis on particular weights.

2.28 Optimization Techniques

Next, optimization of the model is a necessity to enhance its reliability of the model. There are several types of optimization algorithms such as Root Mean Square Propagation (RMSProp), stochastic gradient descent (SGD), gradient descent (GD), Adaptive Gradient Algorithm (Adagard), and Adaptive Moment Estimation (Adam) (Aggarwal, 2018). Hence, during the backpropagation process, these techniques will be employed to update the weights and the biases in the neural network. The most common optimization technique is SGD and it performs error calculation for each training data set accompanied by the weight calibration. When each data point is being adjusted by SGD, the neural network performance is distorted during the training process. In accordance with Loy (2019), the Adam optimizer was found to be the best optimization technique for deep neural networks, whereas the SGD optimizer is more suitable for shallow neural networks.

2.28.1 Gradient Descent (GD)

Vanilla gradient descent or batch gradient descent refers to the optimization algorithms that use the entire training set simultaneously in a large batch and this would be computationally expensive (Goodfellow et al., 2016). This optimization algorithm is applied to compute the differentiable function local minimum. However, GD tends to be trapped at in local optimum and slows down at the region with zero-gradient as shown in Figure 2.28 and can be mathematically expressed in Equations 2.33 and 2.34 (Aggarwal, 2018).

Stochastic gradient descent is an augmentation of the gradient descent algorithm and it refers to an optimizer that fits a single sample at a time (Kinsley and Kukiela, 2020). The scientific term stochastic is the synonym of randomness; in deep learning, SGD is mainly derived from the fact that each batch of data is randomly selected (Chollet, 2018). In practice, it is mandatory to gradually reduce the learning rate progressively. This is because the SGD gradient estimator causes disruption or noises that do not vanish even if the point is at the local minima (Goodfellow et al., 2016).

Most optimization algorithms fall somewhere in between, employing more than one but not all of the training data. These were formerly known as minibatch or minibatch stochastic methods, but they are more commonly called stochastic methods. Larger batches tend to provide gradient with higher accuracy, but with less than linear returns. Due to high oscillation in the estimation of the gradient, training with minimal batch size and a low learning rate is a good option to maintain the stability of the model (Goodfellow et al., 2016).

$$V_{t-1} = -\alpha \frac{\partial L}{\partial W} \quad (2.33)$$

$$W_t \leftarrow W_{t-1} + V_{t-1} \quad (2.34)$$

Where

V_{t-1} = the product of learning rate and the loss function derivative in accordance with the weight from previous iteration;

α = learning rate (ranging from 0 – 1);

W_t = weight of current iteration;

W_{t-1} = weight from previous iteration

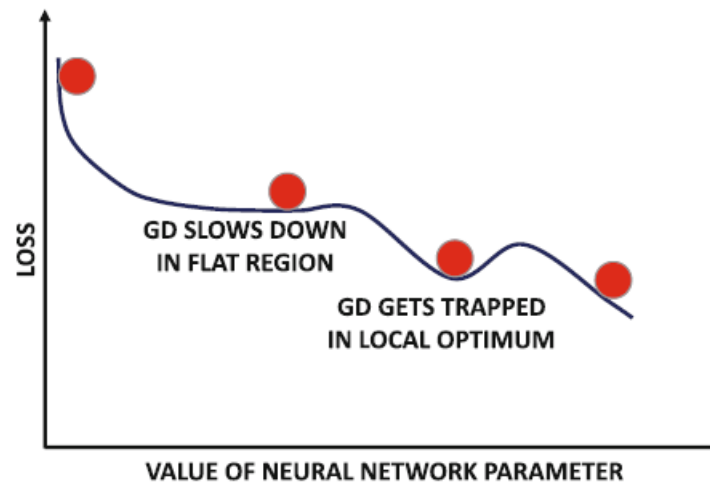


Figure 2.28 Illustration of gradient descent (Aggarwal, 2018)

2.28.2 SGD with Momentum

In order to solve the problem of GD, SGD with momentum is introduced. In the momentum-based descent, modifications were made in the vector of V with a smoothing parameter (Buduma, 2017). With the inclusion of a smoothing parameter namely friction or moment parameter, the learning process is accelerated, helping the process to gain a consistent velocity towards the optimal solution and dampen the irrelevant steps oscillation as shown in Figure 2.29 (Aggarwal, 2018). Equations 2.35 and 2.36 expressed the concept of modification in SGD with momentum.

$$V_{t-1} = \beta V_{t-1} - \alpha \frac{\partial L}{\partial W} \quad (2.35)$$

$$W_t \leftarrow W_{t-1} + V_{t-1} \quad (2.36)$$

Where

β = momentum parameter or friction parameter

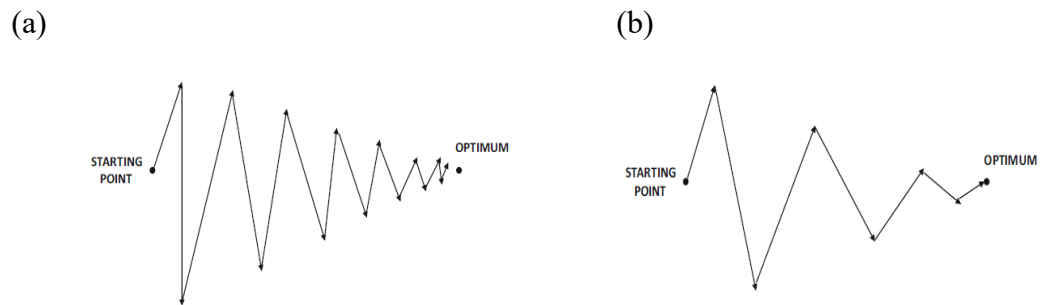


Figure 2.29 Influence of momentum in the learning process (a) without momentum and causing violent oscillation; (b) with momentum shows that it takes less oscillation to reach the optimum point (Aggarwal, 2018)

2.28.3 Adaptive Gradient Algorithm (AdaGrad)

The AdaGrad algorithm adjusts the model parameters learning rates independently, and learning rates will be updated inversely correlated to the square root of every preceding squared values summation of the gradient (Duchi et al., 2011). The learning rate will decrease quickly if the loss of partial derivative of the parameters is high, whereas the parameters with a small loss of partial derivative tend to have a higher learning rate (Moolayil, 2019). AdaGrad is good at convex optimization but not non-convex optimization; this

is because convex optimization has only one minimum point while non-convex optimization has multiple local minima. The purpose of AdaGrad is to asymptote quickly in convex function; whereas in nonconvex function, the learning path may pass through several discrete structures and ultimately trapped a locally convex region (Goodfellow et al., 2016). The mathematical concept of the AdaGrad optimizer can be expressed in Equations 2.37 and 2.38.

$$A_i = A_{i-1} + \left(\frac{\partial L}{\partial W_i}\right)^2 \quad (2.37)$$

$$W_i \leftarrow W_{i-1} - \frac{\alpha}{\sqrt{A_i + \varepsilon}} \left(\frac{\partial L}{\partial W_i}\right) \quad (2.38)$$

Where

A_i = scaling factor (exponentially averaged value of i th parameter W_i);

$\varepsilon = 10^{-8}$, to avoid ill-conditioning

2.28.4 Root Mean Square Propagation (RMSprop)

The design purpose of the RMSprop algorithm was to outperform the Adaptive Gradient algorithm (Adagrad) in non-convex function by altering the gradient aggregation into an exponentially weighted moving average (Hinton and Tieleman, 2012). AdaGrad reduces the learning rate based on the previously squared gradients, which may have resulted in an extremely low learning rate before reaching the convex structure. On the contrary, RMSProp employs an exponentially decaying average to remove historical data in order to converge

swiftly after discovering a convex bowl, as the initialization condition within the convex bowl is similar to the AdaGrad algorithm. Equations 2.39 and 2.40 convey the standard form of RMSProp, with the introduction of a new hyperparameter ρ (decay factor), that governs the moving average length scale (Aggarwal, 2018). The uniqueness of RMSProp is the flexibility to employ momentum within the computational algorithm, and the historical gradients of RMSProp decay exponentially over time; however, in RMSProp second-order moment estimation, there are possibilities that high bias may occur early in the training due to its initialization (Kinsley and Kukiela, 2020).

$$A_i = \rho A_{i-1} + (1 - \rho) \left(\frac{\partial L}{\partial w_i} \right)^2 \quad (2.39)$$

$$W_i \leftarrow W_{i-1} - \frac{\alpha}{\sqrt{A_i + \epsilon}} \left(\frac{\partial L}{\partial w_i} \right) \quad (2.40)$$

Where

ρ = decay factor (ranging from 0 – 1);

2.28.5 Adaptive Moment Estimation (Adam)

Adam is an alternative choice of adaptive learning rate optimization algorithm, which stands for Adaptive Moment Estimation, and is currently the most favourable and commonly used optimizer in deep learning (Kingma and Ba, 2015). Similarly, Adagrad, RMSprop, and Adam employed an identical function in performing the normalization of signal-to-noise; it leverages the

incorporation between momentum and variance of the loss gradient to update the weight parameters resulting in a smooth learning curve and shorter learning process (Aggarwal, 2018; Moolayil, 2019). The momentum and bias corrections are included as an approximation of gradient first-order moment and second-order moments respectively, to initialize the weight and bias as shown in Equations 2.41 - 2.44 (Goodfellow et al., 2016; Aggarwal, 2018; Kinsley and Kukiela, 2020). The adaptive learning rate was computed individually for each parameter by utilizing the Adam optimizer. Adam is substantially recognized as the best optimizer among the others, despite the learning rate having to be altered from the default value (Ketkar, 2017).

$$F_i = \beta_1 F_{i-1} + (1 - \beta_1) \left(\frac{\partial L}{\partial W_i} \right) \quad (2.41)$$

$$A_i = \beta_2 A_{i-1} + (1 - \beta_2) \left(\frac{\partial L}{\partial W_i} \right)^2 \quad (2.42)$$

$$\alpha_t = \alpha \left(\frac{\sqrt{1 - \beta_2^t}}{1 - \beta_1^t} \right) \quad (2.43)$$

$$W_i = W_{i-1} - \alpha_t \frac{F_i}{\sqrt{A_i + \epsilon}} \quad (2.44)$$

Where

β_1 = decay factor, (default values of 0.9);

β_2 = decay factor, (default values of 0.999);

F_i = estimates of the first moment (the mean) of the gradients;

A_i = estimate of the gradient's second moment (the uncentered variance);

α_t = learning rate α_t in the t th iteration

2.29 Dropout Rate

The dropout rate is one of the hyperparameters in configuring a deep learning model, which is a decimal value between 0 and 1, the commonly used values are ranging from 0.2 to 0.5. For instance, if the configured dropout rate is 0.3, then only 70 % of randomly selected neurons will be trained during each step of the forward pass. A series of neurons will be selected on a stochastic basis each time when a new data point is processed in the neural network. However, the neurons still remain in the neural network, just that these neurons are ignored during the forward pass so that the neural network will be trained with less complexity (Campesato, 2020). The dropout layer is typically used when the dataset is too large, and some irrelevant correlation between the data may cause the neurons to convey false information to the succeeding neurons and hence affect the neural network performance. The dropout process can be expressed as an illustration in Figure 2.30 (Buduma, 2017).

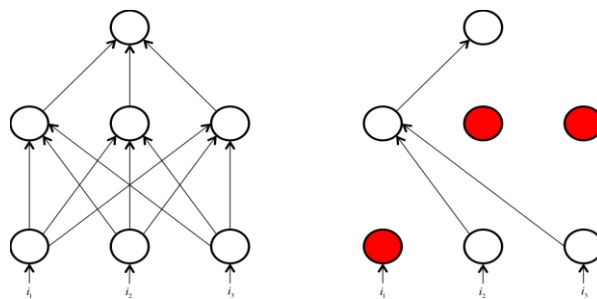


Figure 2.30 During each minibatch of training, dropout makes each neuron in the network inactive with a random probability (Buduma, 2017)

2.30 Application of Deep Learning in Prediction Models

Several works have adopted the concept of deep learning not only in acoustic noise prediction but also in other sectors (Olatunji, et al., 2019; Suhartono et al., 2019; Lago et al., 2018; Mansourkhaki et al., 2018; Zulifqar et al., 2017; Aliabadi et al., 2015). Aliabadi et al. (2015) developed a model with the concept of ANN and advanced fuzzy techniques to predict the excessive noise in industrial embroidery, and the results were confirmed to be reliable. A study stated application of ANN in noise barrier optimization provided results that were in good agreement with the design of experiments, and it can be utilized in environmental acoustics and noise control (Zanin et al., 2018). Guo et al. (2019) applied several algorithms in Radial Basis Neural Network and discovered the optimum algorithms for ship cabin noise prediction. Navarro et al. (2020) developed a noise monitoring model with Long Short-Term Neural Network to forecast the near-time future value of environmental noise in a certain location specifically in sound pressure level (L_p) and loudness values. Moreover, Zhang et al. (2020) deployed a double-layered Long Short-Term Neural Network to forecast environmental noise with respect to large data volume and it outperformed the other existing classic techniques.

Zulifqar et al. (2017) utilized multilayer perceptron to forecast drought in Pakistan and proved that the variation between the observed data and prediction was not high. A study stated that the performance of DNN was better than the long-short term memory (LSTM) model in electricity price forecasting (Lago et al., 2018). Olatunji, et al. (2019) applied multilayer perceptron with different

learning algorithms in heating value prediction of municipal solid waste. Suhartono et al. (2019) proclaimed that the deep neural network (DNN) outperformed the hybrid prediction model of Singular Spectrum Analysis and Deep Neural Network (SSA-DNN), and the statistical model with Autoregressive Integrated Moving Average with Explanatory Variable (ARIMAX) in forecasting monetary inflow and outflow. Genaro et al. (2010) proclaimed that the results of Multilayer Perceptron trained with Backpropagation Levenberg-Marquardt algorithm were a significant enhancement as compared to the existing urban noise predictive model. Arora et al. (2012) predicted the traffic noise along Agra-Firozabad Highway using ANN and discovered the optimum learning algorithms. Aliabadi et al. (2013) presented a technique of industrial noise prediction by using multi-layered neural networks. Cirianni et al. (2015) proved that ANN can predict the continuous equivalent noise level induced by vehicle flow on the roads with a satisfactory outcome. Mansourkhaki et al. (2018) proved that MLP outperformed Radial Basis Function in traffic noise prediction.

2.31 Concluding Remarks

This chapter discusses occupational noise exposure, noise prediction, and deep learning techniques. To conclude, relevant literature reviews of studies related to the current study revealed the feasibility of the application of stochastic modelling in construction noise prediction (Haron et al., 2008; Haron and Yahya, 2009; Haron et al., 2012, Lim *et al*, 2015). Among the various types of ANN, MLP has been commonly applied in traffic and urban noise forecasting and

predictive researches (Mansourkhaki et al., 2018; Arora et al., 2012; Cirianni et al., 2015; Genaro et al., 2010; Aliabadi et al., 2013). However, research related to construction noise prediction using MLP is still very limited. Besides, several research gaps were discovered in the current noise prediction method. For instance, the existing technique, simple prediction charts only cover 0, 15, 30, and 45 degrees of noise emission of machinery in a construction site, which did not achieve full coverage of 360 degrees. Moreover, simple prediction charts are more suitable to predict machine that operates at all time. Hence, the noise levels predicted by using simple prediction charts may be less accurate, as in the actual scenario machine operates with different duty cycles such as full power mode, idling mode, and off mode during construction activities. Besides, another research gap showed that it is time-consuming to use simple prediction charts in noise prediction at specific locations. In addition, it would be overwhelming when there are a large number of noise predictions to be conducted. In current practice, there is no application of the stochastic deep learning method in construction noise prediction. Hence, to fill the existing research gap, this study emphasizes the stochastic deep learning method to develop noise prediction models with high accuracy and reliability, to resolve the issues as mentioned.

CHAPTER 3

METHODOLOGY

3.1 Introduction

The study was initiated by discovering the findings of previous research regarding stochastic modelling and multilayer perceptron by numerous researchers. Critical reviews and research gaps were identified from the outcome of previous studies. The modification of stochastic modelling along with the association of multilayer perceptron in construction noise prediction was the main focus of this study.

This study aims to develop a reliable noise prediction model with high accuracy. To achieve the aim, a stochastic framework and deep learning framework were developed. Next, the programming algorithms for both stochastic and deep learning noise prediction models are devised. Furthermore, field measurement is conducted to gain the actual noise level during different construction activities. Lastly, the predicted data were compared with the actual data for reliability and accuracy assessment. A systematic methodology was constructed in this chapter to attain the aim and objectives as mentioned.

3.2 Research Framework

The research methodology was generally divided into three stages as shown in Figure 3.1. The methodology comprised the establishment of the conceptual framework in the initial stage, followed by the development of programming and algorithms and coding, and lastly, the stage was for data analysis, data validation, and journal publication.

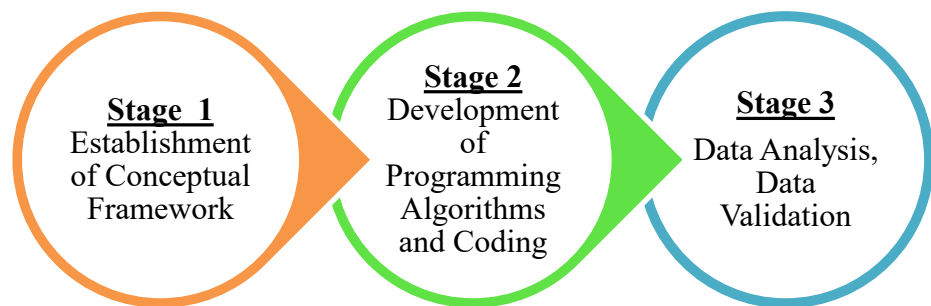


Figure 3.1: Stages of the work plan

3.3 Configuration of Stochastic Deep Learning Framework

The first stage of this research was to search for information, materials and background studies that are relevant to construction noise prediction, stochastic modelling and deep learning. Conceptual ideas and fundamental theories were thoroughly explained in this stage. The stochastic deep learning model was developed with the association of stochastic modelling and multilayer

perceptron or artificial neural network. The purpose of stochastic modelling was to generate training data and these data were utilized as the training data for the multilayer perceptron. Visualization of the conceptual stochastic modelling framework for the aspect ratio of 1: 1 is shown in Figure 3.2. The generated output will be used as the training data in the deep learning model to predict the noise levels as illustrated in Figure 3.3.

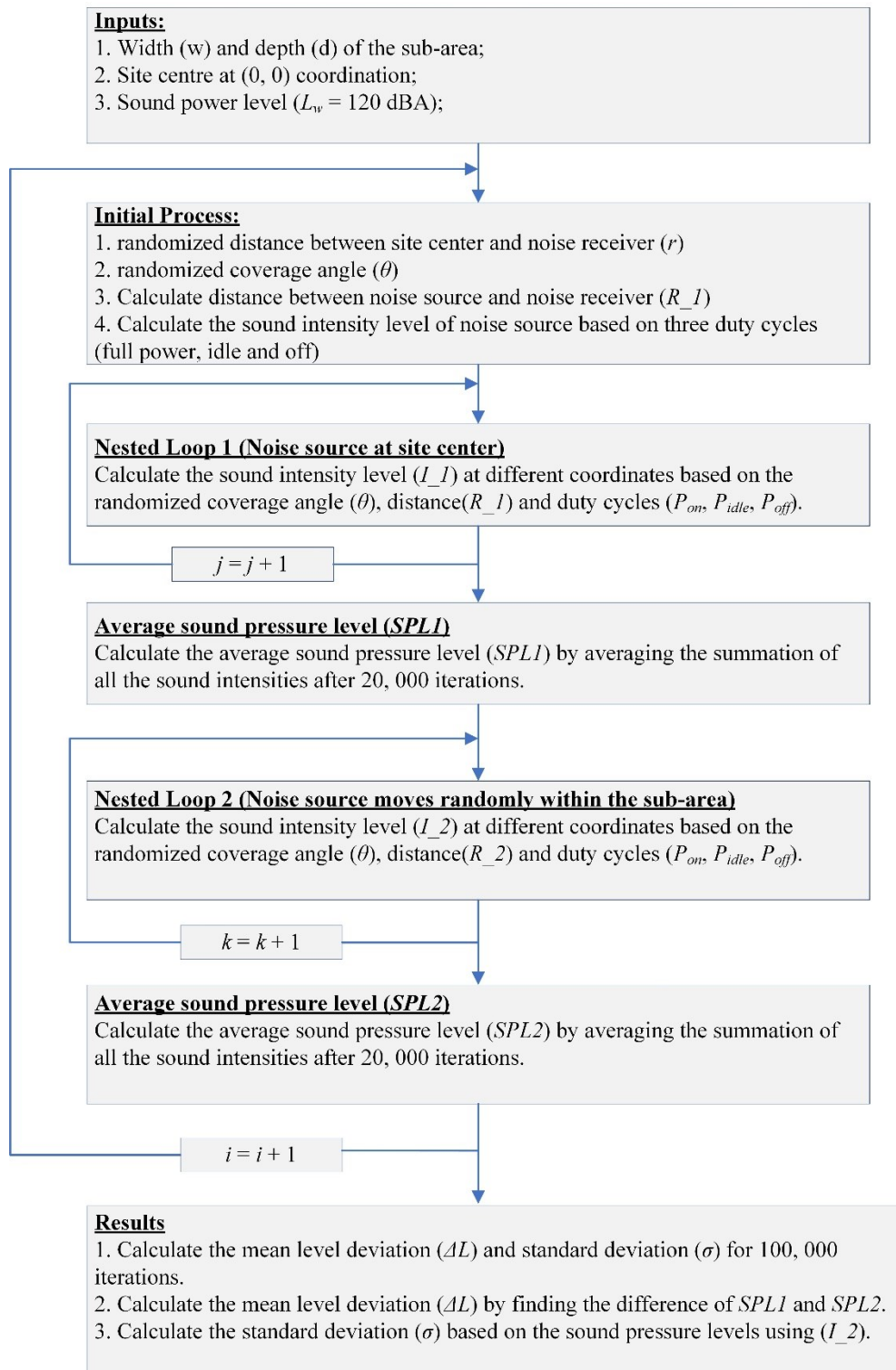


Figure 3.2: The framework of stochastic modelling for aspect ratio 1:1

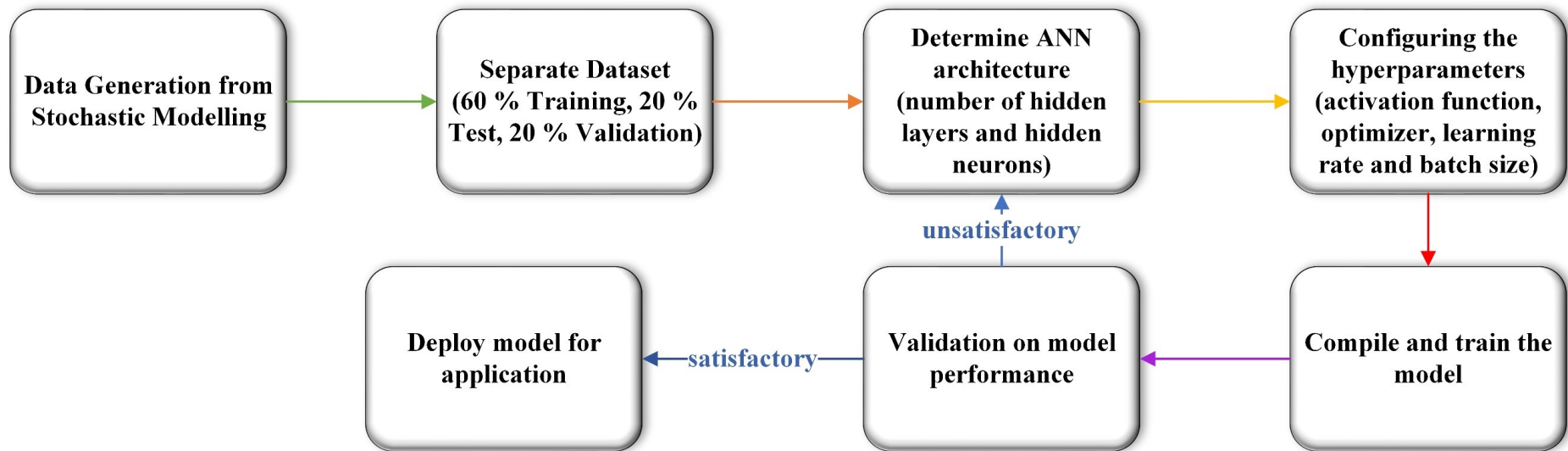


Figure 3.3: The conceptual framework of the deep learning model

3.4 Development of Programming Algorithms and Coding

In the second stage, the programming algorithms for stochastic modelling were developed in MATLAB to validate and compare the outcome of the previous studies and the current stochastic modelling. Stochastic modelling is found to be feasible, especially in construction noise prediction based on previous studies (Haron et al., 2008; Haron and Yahya, 2009; Haron et al., 2012). The application of stochastic modelling is to simulate the activities of the actual scenario at construction sites as a means to predict the sound pressure levels at different locations based on the predetermined randomized parameters. Hence, the concept is adopted in this study to generate the input data for ANN.

The important variables in the prediction model, such as (1) sound properties of dynamic machinery; (2) random movement and position of dynamic machinery; (3) different sizes of working sub-area; (4) distance away from the sound level receiver; (5) coverage angle from the site centre; (6) operational duty cycles of dynamic machinery, were taken into an account in the simulation. The sound pressure level at the noise receiver will be generated depending on the parameters. Haron and Yahya (2009) revealed that it is mandatory to have large samples of up to 20, 000 to generate a smooth probability distribution curve. As a result, the number of iterations for both the nested loops was determined as 20, 000 steps. Hence, 20, 000 sound pressure levels were generated when the noise source was placed at the site centre whereas another 20, 000 sound pressure levels were generated when the noise source was moving randomly within the sub-area.

Then, the mean level deviation was obtained from the variation between the sound pressure levels' average value when the noise source was located at the site centre (*SPL1*) and the mean sound pressure levels when the noise source was moving randomly within the sub-area (*SPL2*). The standard deviations were generated based on the sound pressure levels when the noise source was moving randomly in the sub-area. The generated output of the stochastic modelling consists of 100, 000 sets of mean level deviation and standard deviation with different values due to the randomized parameters during the simulation. The stochastic modelling generated seven sets of datasets with 100, 000 stochastic data each based on different aspect ratios 1:1 (50 m x 50 m), 1:2 (50 m x 100 m), 1:4 (50 m x 200 m), 1:8 (50 m x 400 m), 2:1 (100 m x 50 m), 4:1 (200 m x 50 m) and 8:1 (400 m x 50 m). The dimensions of each aspect ratio were selected according to a study (Haron et al., 2008). The study stated that sites with different dimensions but the same aspect ratio provided the same curve of mean level deviation and standard deviation. The total execution time for each simulation was 19 hours with the hardware specifications of Central Processing Unit (CPU) Ryzen 3 3100 @ 3.9 GHz and random access memory (RAM) 16 GB @ 2666 MHz. Lastly, the output of the stochastic modelling comprised the coverage angle, r/w ratio, fully operating, idling and off duty modes, mean level deviation and standard deviation. The programming algorithm is shown in Figure 3.4.

Almost any modern programming language can be adopted to develop an artificial neural network model; however, certain programming languages are specifically designed for the artificial intelligence field, making these

programming languages more engaging and favourable. Python was selected in this study because its main purpose is to emphasize the quality of software in which it is built to be user-friendly as in readable, maintainable, and applicable for future utilization compared to those traditional programming tools. Python is much easier to be understood by users due to its uniformity and simplicity. Python has a built-in and portable library called the standard library, that supports varieties of programming tasks. On top of that, the libraries of Python can be expanded by importing the libraries from a third-party application and prebuilt libraries. One of the libraries named NumPy has proven that its computation performance is better than the numeric programming system of MATLAB (Lutz, 2013).

The programming algorithms of the stochastic deep learning model were programmed by using the simulated data as the input data for the model to learn the variation of mean level deviation and standard deviation based on the randomized parameters during the stimulation. Programming algorithms were established with Python 3.6 programming language by using Spyder Integrated Development Environment (IDE) in Anaconda. The training model was optimized by updating the loss function then the model was trained multiple times until the desired performance is attained.

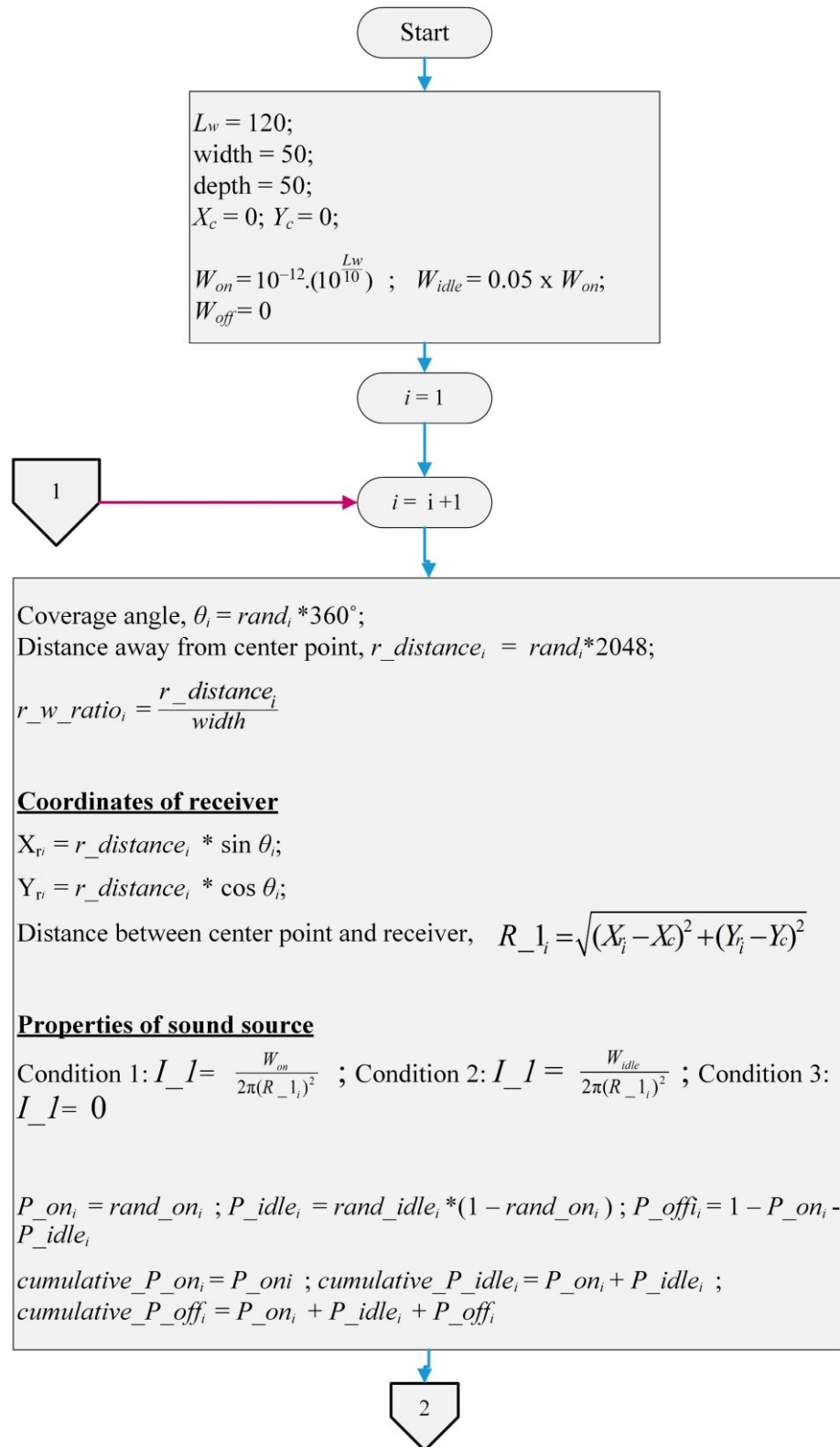


Figure 3.4: The programming algorithm of stochastic modelling for aspect ratio 1:1

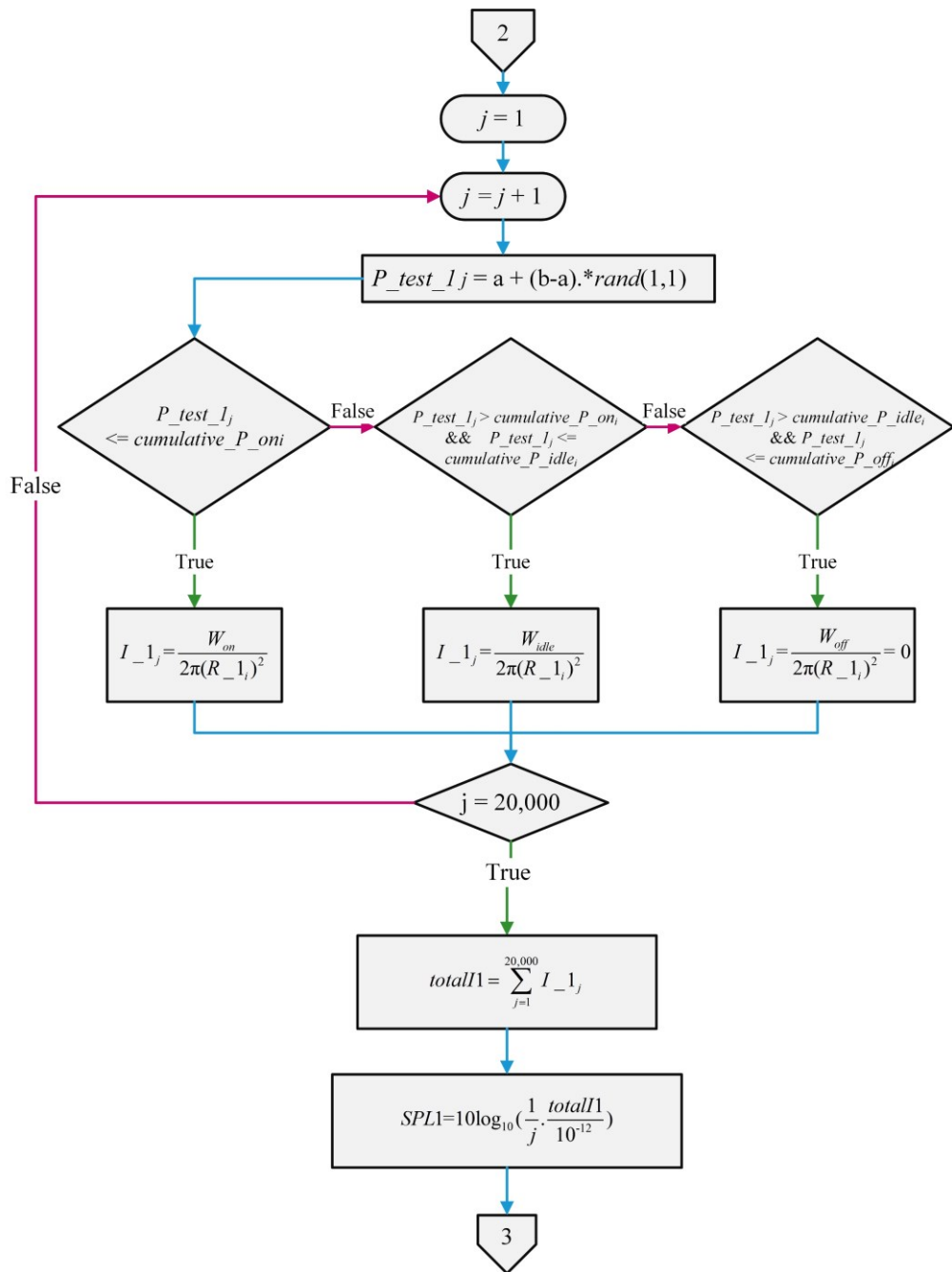


Figure 3.4: The programming algorithm of stochastic modelling for aspect ratio 1:1 (Cont'd)

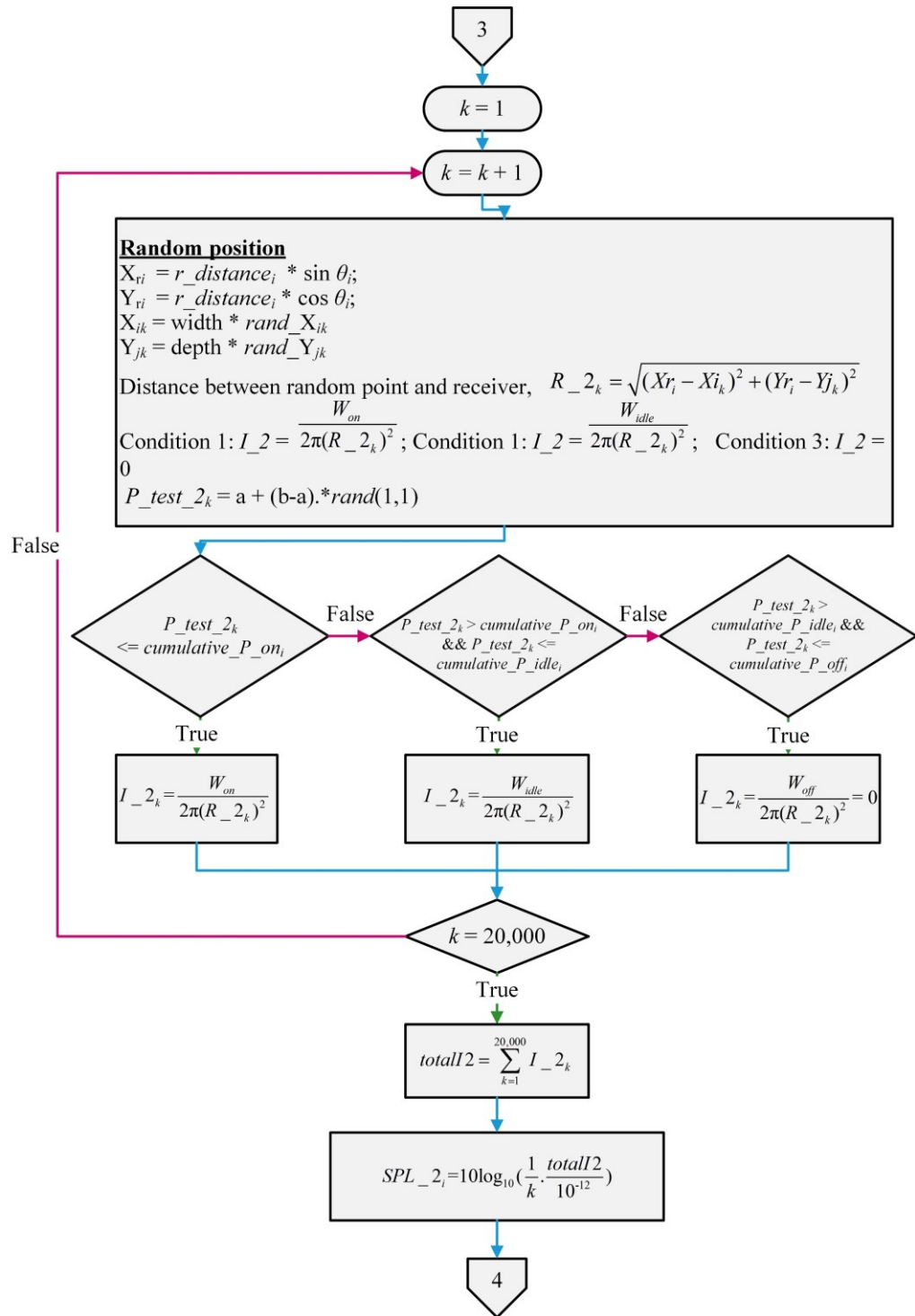


Figure 3.4: The programming algorithm of stochastic modelling for aspect ratio 1:1 (Cont'd)

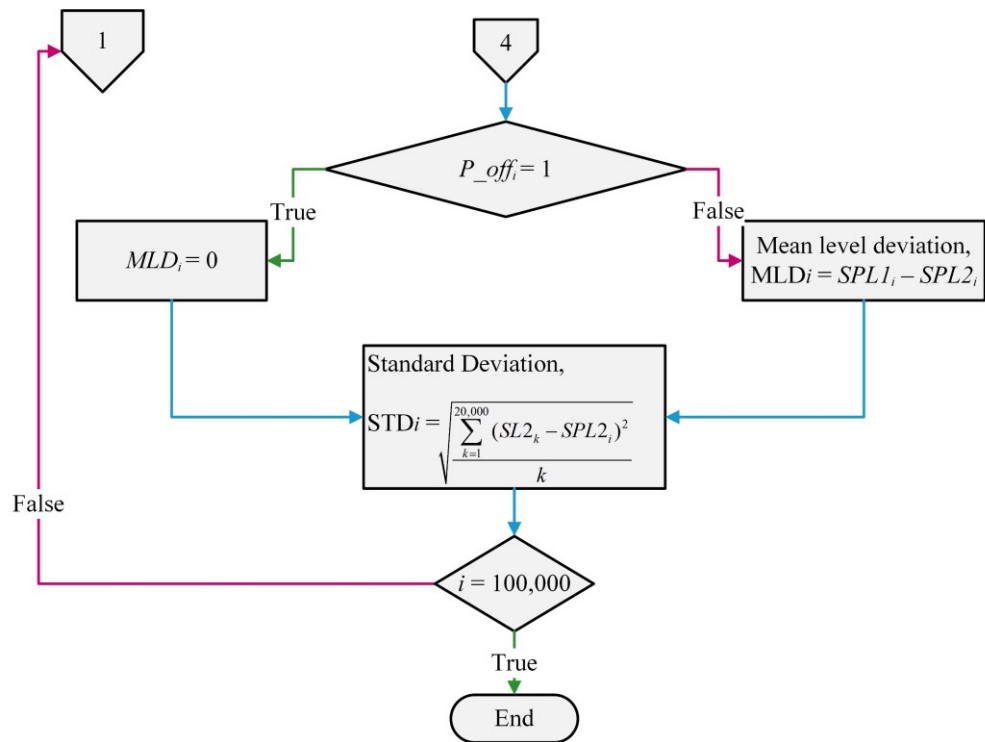


Figure 3.4: The programming algorithm of stochastic modelling for aspect ratio 1:1 (Cont'd)

3.5 Model Configuration

Seven deep learning models with the aspect ratio of 1:1, 1:2, 1:4, 1:8, 8:1, 4:1 and 2:1 were established and each of the models was trained with 100, 000 data points from the stochastic model with the same aspect ratio. The configuration of the neural network is essential to develop a predictive model with satisfactory performance. Hence, hyperparameters such as the data split ratio, the number of hidden layers and neurons, activation function selection criteria, selection of optimizer, learning rate, epochs number and batch size were considered in the model training and optimization. The configured optimal hyperparameters will then be applied in the other models with different aspect ratios.

3.5.1 Data Split

The occurrence of the overfitting problem often happens when the model performs exceedingly good during the training observation whereas the performance is exceptionally poor in the unknown observation; which explains the generalization of the model is ineffectual. The determination of the model's optimal hyperparameters is to find the well-adjusted ratio between the training, validation and testing set (Xu and Goodacre, 2018). The training set extracts the information and learns the pattern of the dataset; the validation set estimates the prediction error of the training set and tunes the model to achieve the optimal hyperparameters based on the lowest validation error which this process is called model selection (Hastie et al., 2009). Lastly, the test set is applied to evaluate the optimal model predictive performance and this set will only be applied once in the model. Harrington (2017) mentioned that the erroneous evaluation of the model can be obtained by separating the test and training set.

3.5.2 The Architecture of the Neural Network

The number of neurons was determined based on quinary which is a base 5 numeral system. Initially, the model was started with one layer and 5 hidden neurons, but the result was unsatisfactory. As a consequence, the number of neurons was increased by adding 5 neurons in each of the 10 hidden layers respectively. Lan et al. (2010) applied the grid search method to determine the optimal neurons number using quinary in the previous research. The architecture of the neural network was selected based on a trial and error

approach as the optimal neural network for every problem was different. Moolayil (2019) mentioned that the neurons and hidden layers numbers shall be enlarged if the previous architecture failed to perform during the training and validation test.

3.5.3 Activation Function

The selected activation function in this study was the ReLU activation function because it is the most suitable activation function to be applied in the hidden layers and regression problems as well as solving the vanishing gradient problem (Loy, 2019; Goulet, 2020) whereas linear activation function was commonly adopted in the output layer; after all, it is more appropriate for the regression model in real number prediction (Kim, 2017; Aggarwal, 2018).

3.5.4 Optimizer and Learning Rate

Optimizer is mainly adopted to increase the neural network predictive performance. It was used to rationalize the neural network weights based on the loss function after each epoch. There are many types of available optimizers but only three types such as Adagrad, RMSProp and Adam were included in this study to find the most suitable optimizer for the model because studies revealed that Adagrad, RMSProp and Adam performed well in the neural network (Lydia and Sagayaraj, 2019; Soydaner, 2020).

3.5.5 Learning Rate

The learning rate is an essential hyperparameter in training the model. Neither the learning rate can be too high nor too low; as a higher learning rate may lead to vigorous oscillation in the curve whereas extremely low learning resulted in a long convergence time (Zhao et al., 2019). Yang et al. (2019) mentioned that it is mandatory to apply an individual learning rate that is suitable for different variables in the model. Hence, three different values (10^{-2} , 10^{-3} , 10^{-4}) of the learning rate were tested in this study.

3.5.6 Batch Size

The batch size is a hyperparameter that determines the data points numbers to be processed before updating the parameters of the internal model. The batch size is generally set in binary such as the numbers 32, 64, 128 (Moolayil, 2019). The purpose of setting a batch size is to reduce high oscillation in the optimizations technique like the stochastic gradient descent method. Another better option is to provide a minibatch to reduce the number of iterations; this would allow the loss to be averaged across all the data points in a batch, and the weights will be updated at the end of the batch; A better result and smooth training process are more likely to be attained by adopting this approach (Brownlee, 2016).

3.5.7 Epoch

The epoch is another hyperparameter that governs the number of iterations that the learning algorithms propagate back and forth from the entire training dataset. The number of epochs is relatively large so that the learning algorithm can effectively minimize the error of the model (Kim, 2017). The number of epochs determined in the preliminary test was 200. The dropout layer was not applied in this study because regularization contributes to a minimal reduction in generalization error for very large datasets. Therefore, it is ineffective to use dropout layers in a model with a larger dataset because the computational cost would be high (Goodfellow et al., 2016).

3.5.8 Optimal Hyperparameters

The approach of the grid search was applied in this study to find out the best hyperparameters for the model. All possible combinations for a predetermined set of hyperparameters values were tested by trials to find the optimal value in the grid search method (Moolayil, 2019). Lastly, in this study, the model for the 1: 1 width to depth aspect ratio was tested with different variations of hyperparameters to find the optimal values using the grid search method as shown in Table 3.1. The process of training the model for the optimal set of hyperparameters is demonstrated in Figure 3.5. The optimal model architecture is depicted in Figure 3.6.

Table 3.1: Configuration of the noise prediction model for aspect ratio of 1:1

Hyperparameter	Trial 1	Trial 2	Trial 3
Data split (Training, Validation, Test)	60 %, 20 %, 20 %	70 %, 15 %, 15 %	80 %, 10 %, 10 %
Number of neurons for each layer	Increasing the depth of the neural network by adding 5 hidden neurons to each of the hidden layers, when the model failed to perform each time		
Number of hidden layers	10		
Number of inputs	5		
Activation function in hidden layers	ReLU activation function		
Number of outputs	2		
Activation function in the output layer	Linear activation function		
Number of epochs	Start at 50, increase by 25 upon every failure		

Table 3.1: Configuration of the noise prediction model for aspect ratio of 1:1 (Cont'd)

Learning rate	i. 10^{-2}		
	ii. 10^{-3}	10^{-4}	10^{-4}
	iii. 10^{-4}		
Batch size	i. 32		
	ii. 64	32	32
	iii. 128		
Optimizer	i. Adam		
	ii. RMSProp	Adam	Adam
	iii. Adagrad		

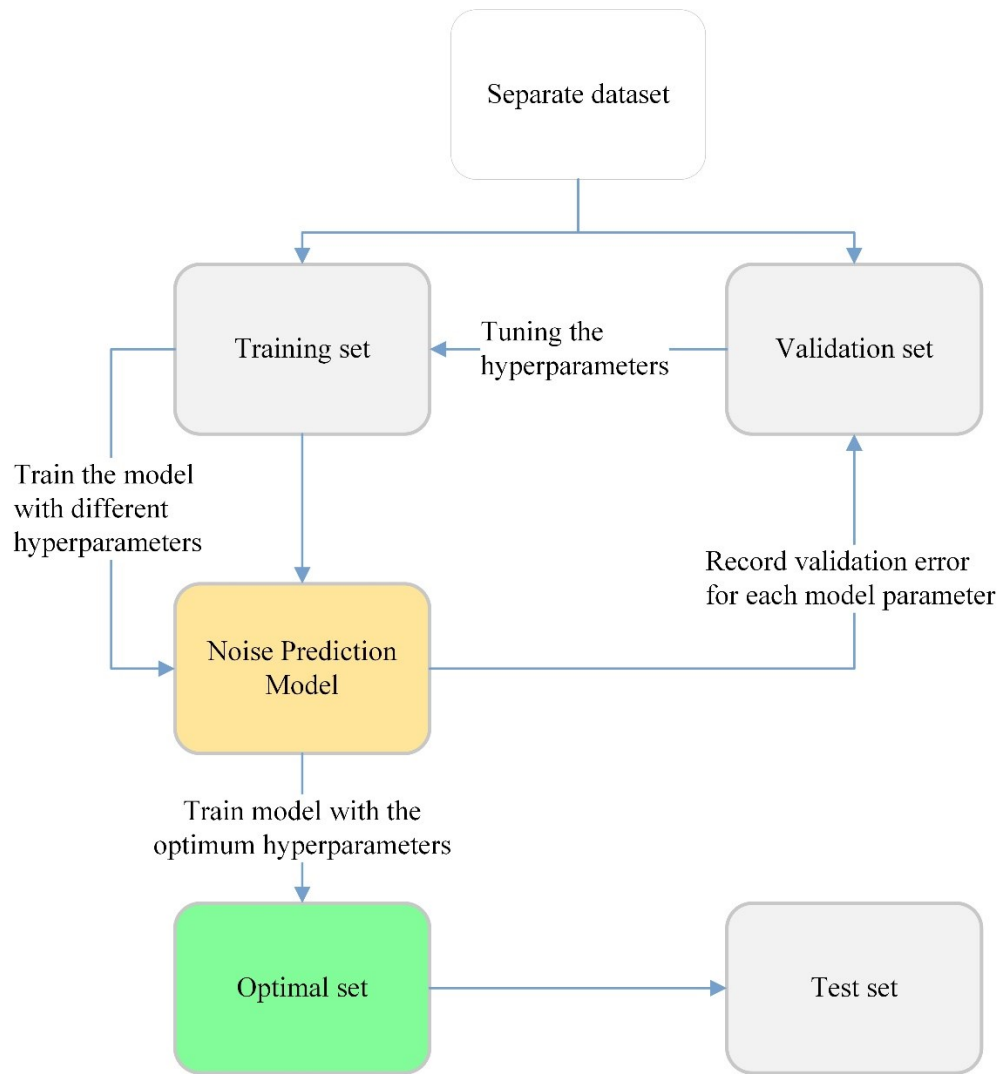


Figure 3.5: The process of finding the optimal set of hyperparameters for the model

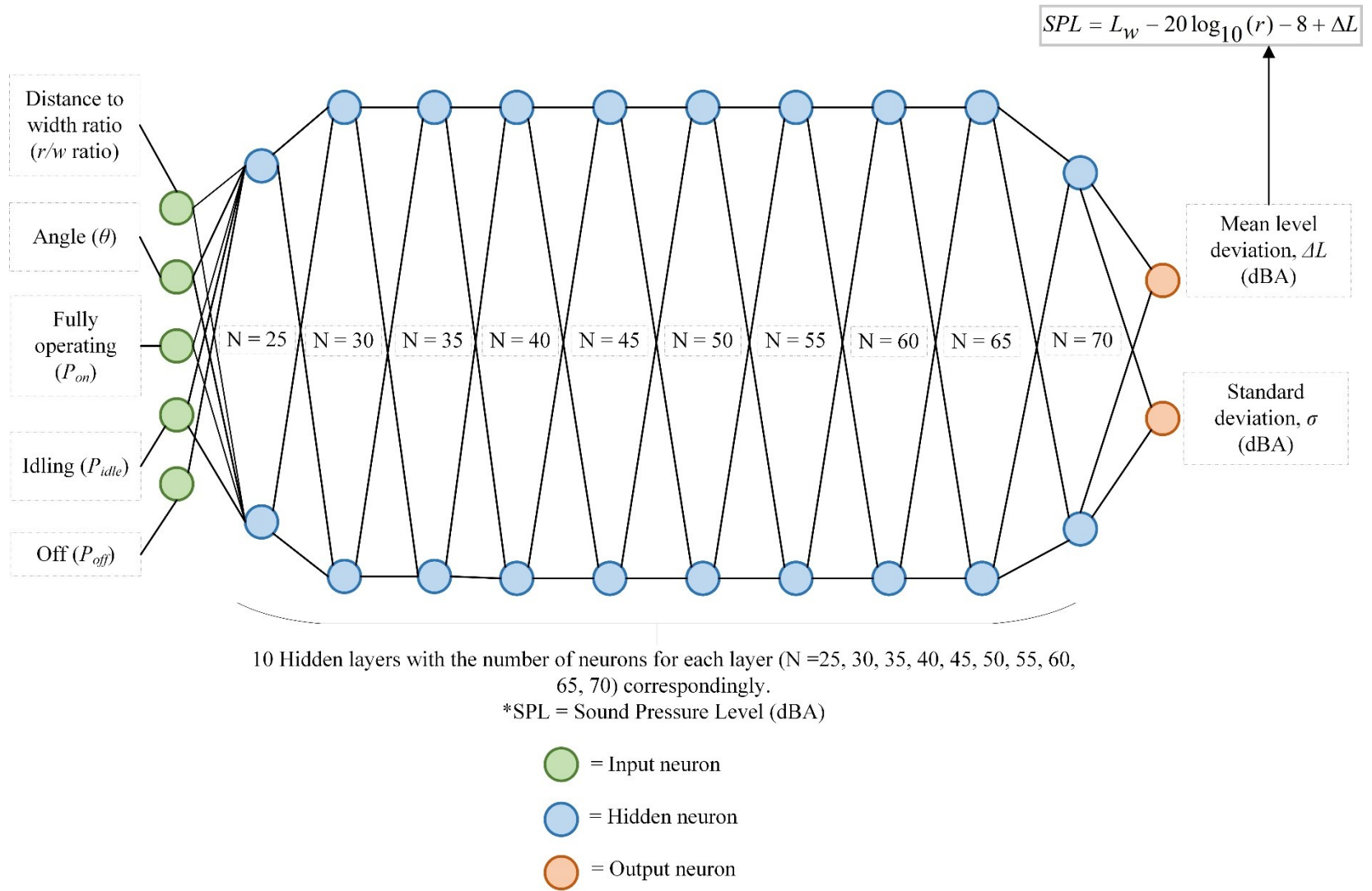


Figure 3.6: The architecture of the optimal model for the aspect ratio of 1:1

3.5.9 Performance Evaluation

All the models with different hyperparameters were evaluated by using mean-squared error, root mean squared error and mean absolute error, as the difference is closer to 0, the better the performance of the model. The R-squared coefficient was adopted in this study to determine the reliability of the model; the closer the coefficient closer to the value of 1, the more reliable the model is. Next, the mean absolute error can be expressed as the average absolute error between actual and predicted; and the mathematical equivalent is shown in Equation 3.1 (Moolayil, 2019). Application of mean squared error in loss function of regression aims to compute the square of the difference between the observed and predicted value (Aggarwal, 2018). Root mean squared error determines the error of squared between the observed value and prediction as expressed in Equation 3.2. The formula of mean squared error is mathematically explained in Equation 3.3.

$$MAE = \frac{1}{n} \sum_{i=1}^n |y_i - \hat{y}_i| \quad (3.1)$$

$$RMSE = \sqrt{\frac{1}{n} \sum_{i=1}^n (y_i - \hat{y}_i)^2} \quad (3.2)$$

$$MSE = \frac{1}{n} \sum_{i=1}^n (y_i - \hat{y}_i)^2 \quad (3.3)$$

Where

MAE = Mean absolute error;

$RMSE$ = Root mean squared error;

MSE = Mean squared error;

\hat{y}_i = predicted value;

y_i = observed value

n = number of output nodes

3.6 Data Analysis, Data Validation and Publications

The third stage involved data analysis, validation processes and publications. Ten case studies will be carried out at the construction sites. The prediction of the ten case studies will be conducted using the stochastic deep learning method. The procedures for conducting the site measurement of noise levels are explained in this section. The data will be collected on construction sites by using a sound level meter mounted on a tripod stand and distometer for distance measurement. According Department of Environment (2019), the sound level meter will be installed at an elevation ranging from 1.2 m to 1.5 m, and 3.5 m offset from the sound reflective structure.

Data validation will be conducted by comparing the measured and predicted results at the different control points by using Pearson's Correlation Coefficient. The absolute differences will be obtained to determine the accuracy of the prediction method. Discussions and conclusions were presented after the validation of the measurement and prediction. On the other hand, one journal article is accepted by the International Journal of Integrated Engineering, and two journal articles with Scopus indexed are under review in this study. A report will be prepared to record and justify all the findings of this study.

3.7 Field Measurement

This research mainly focused on the construction activities related to infrastructure works. A total number of ten case studies with different parameters were carried out at residential projects in Selangor, Malaysia. All the noise level measurement procedures are following BS ISO 6395:2008, BS 5228-1:2009, and BS ISO 3744:2010 (British Standard Institution, 2008; British Standard Institution, 2009; British Standard Institution, 2010). Hence, the background noise of the construction site, dynamic sound power level emission of machinery and noise control points measurement were recorded. The aspect ratio (width : depth) of the construction site will be examined in terms 1:1, 1: 2, 1:4, 1:8, 2:1, 4:1, and 8:1 for the validation of the prediction.

3.7.1 Noise Measurement Equipment

3.7.1.1 Sound Level Meter

SoundTrack LxT of Larson Davis (Type 1 sound level meter) was utilized to conduct all the noise level measurements. This device was developed to fulfil the needs of the industry to achieve higher accuracy in the machinery noise level measurement and occupational noise exposure assessment. The device complied with the requirement of the International Electrotechnical Commission (IEC) stipulated by the Department of Environment (2019) but the acceptable tolerance of error for class 1 is much lower and it covers a broader frequency range compared to class 2.

The SoundTrack LxT is mainly comprised of 3 components which are the microphone, preamplifier and device. The microphone was fixed on the top end of the preamplifier whereas the bottom end was assembled with the top part of the device as shown in Figure 3.7. The usage of mic foam is necessary during the outdoor measurement to avoid the noise of the wind effect. The sound calibrator with the reference sound of 94 dBA at 1 kHz was applied to fine-tune the sound level meter with the maximum difference of 0.5 dBA before conducting the measurement as shown in Figure 3.7 (British Standard Institution, 2010). The Guidelines for Environmental Noise Limits and Control mentioned that the sound level meter shall be positioned at an elevation of 1.2 m - 1.5 m from the ground level and having an offsetting distance of 3.5 m from the reflective structure (Department of Environment Malaysia, 2019).

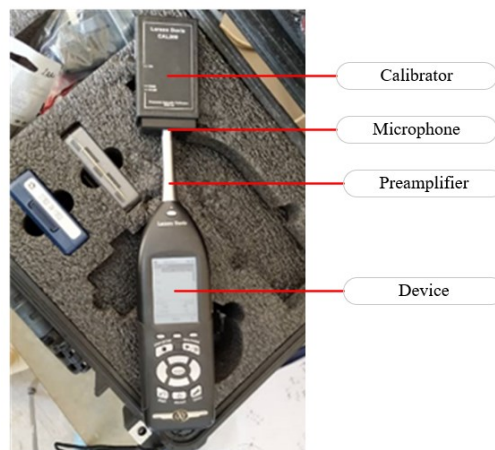


Figure 3.7: Calibration of sound level meter

3.7.1.2 Distometer

Distometer is used instead of measuring during the distance measurement as it is more convenient when measuring both short and long-distance. The model of distometer is SW-T100, a hand-held type laser distance meter manufactured by Sndway. The mechanism of this device uses a laser beam to measure the distance between the target and the datum. However, it does not perform well when there is a presence of strong light intensity in the surroundings.

3.7.2 Software

AutoCAD is a well-known software that has been adopted by construction industries and the users are mainly engineers and architects to produce precise dimensions in the design and construction drawings. Hence, it was utilized in this study to sketch the site layout of the case studies to provide better visualization. Not only that, distance and angle away from the site centre of the case studies were measured by using AutoCAD as well.

3.7.3 Selection Criteria for Case Studies

The case studies selected for this study mainly consisted of the construction activities of the drainage system, sewerage system, water distribution system, road construction, pile boring activities, site clearance and mountain hacking activity. The procedures of measurement are demonstrated in Figure 3.8, and

the theoretical configuration and the actual configuration of the sub-area is illustrated in Figure 3.9 and 3.10.

Machinery such as excavator, road roller, back pusher, hacker, and pile boring machine was involved in these construction activities which is favourable for this study. The chosen locations are suburban areas located in Semenyih, Selangor, Malaysia which is ideal for this study because excessive noise such as traffic noise must be avoided during the noise level measurement. This is because the fluctuation of noise levels resulting from neighbouring noise may adversely affect the accuracy of the measurement to a certain extent. Besides, locations in the city area were avoided due to similar factors.

The criteria to select the suitable locations for case studies were based on the construction activities and the operation duration for the activities. The information on the construction activities must be provided and confirmed by the machine operators and site engineer to ensure there are no interferences during the measurement. The measurement has to be conducted in the early phase of the construction activities so that the data obtained is sufficient and promising as it was recorded throughout the whole operation cycle.

Upon the confirmation of the information provided by the personnel at the construction site, the coverage area of the machine during the particular activities was observed so that the boundary for the sub-area can be determined. Next, the accessibility to set up the instrument is another consideration due to space constraints because other machines might pass through the boundary of

the sub-area. The selected points must be free from obstacles and not disrupt the ongoing construction activities. However, personal safety is still the main concern as the process of measurement must be free from potential hazards, proper personal protective equipment must be equipped, keeping a safe distance from the machine and avoiding standing in the blind spot area of the machines.

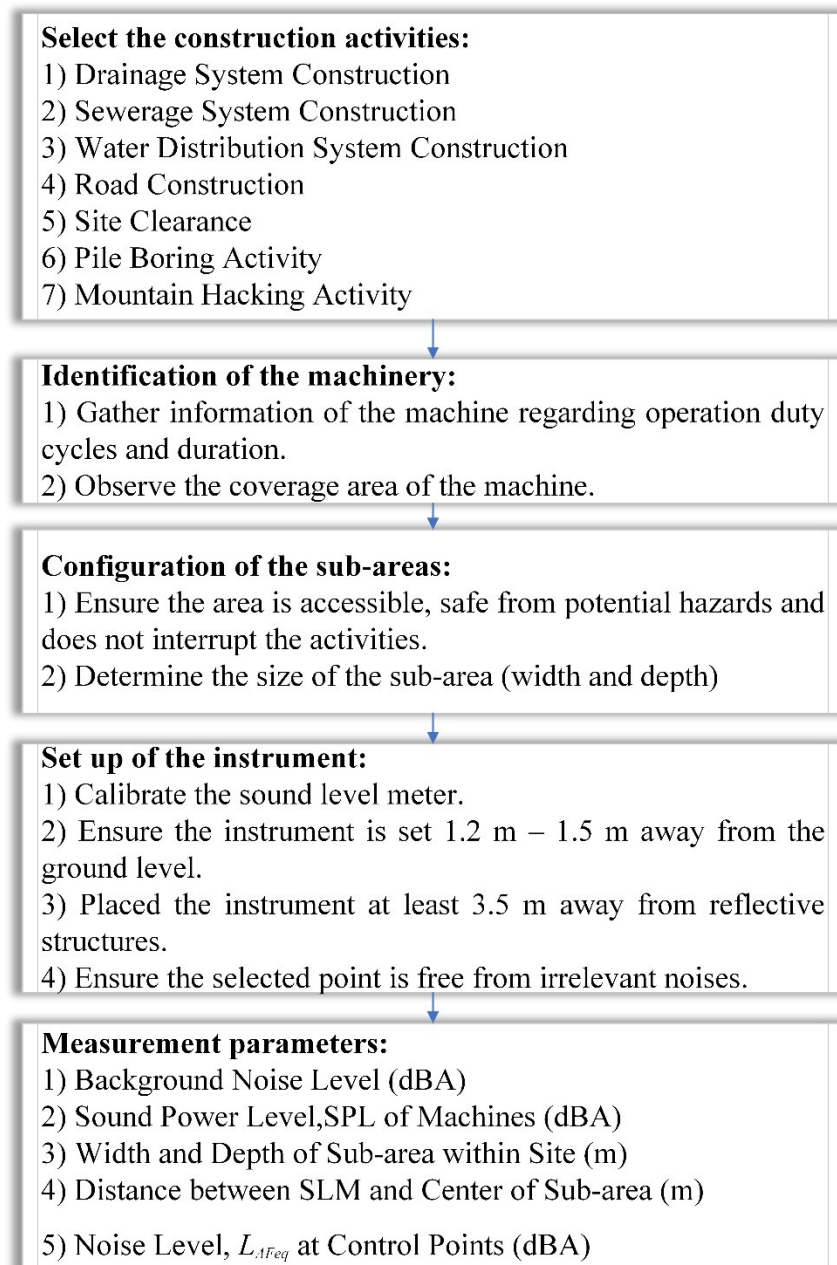


Figure 3.8: The procedures of measurement

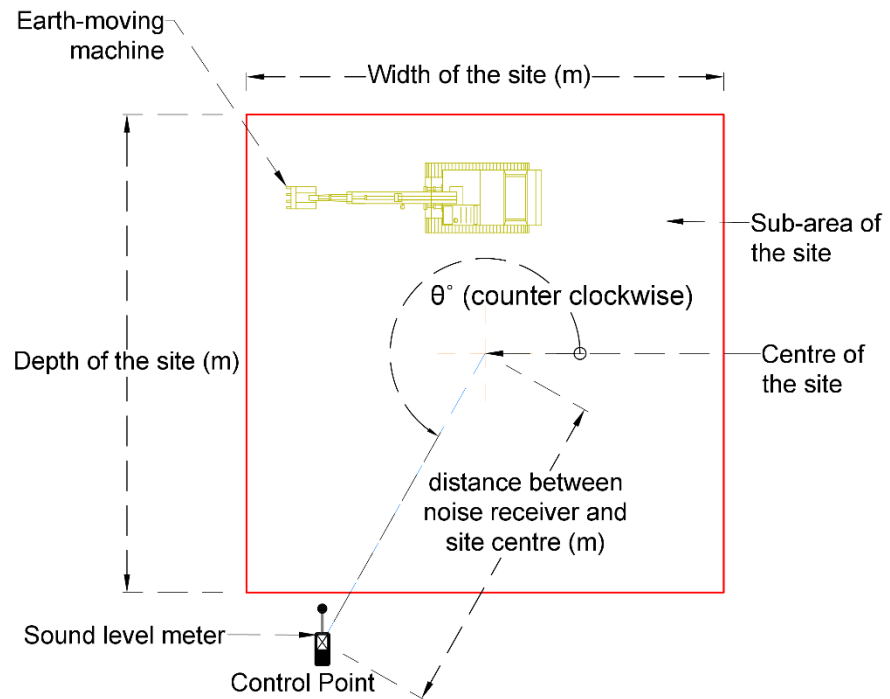


Figure 3.9: Configuration of sub-area

(a)



(b)



Figure 3.10: Site configuration (a) case study 1 drainage system; (b) case study 2 and 3 sewerage system; (c) case study 4 water distribution system; (d) case study 5 and 6 road construction; (e) case study 7 site clearance; (f) case study 8 mountain hacking; (g) case study 9 pile boring activity for pile with the diameter of 1.2 m; (h) pile boring activity for contiguous bored pile with the diameter of 750 mm

(c)



(d)



(e)



(f)



(g)



(h)



Figure 3.10: Site configuration (a) case study 1 drainage system; (b) case study 2 and 3 sewerage system; (c) case study 4 water distribution system; (d) case study 5 and 6 road construction; (e) case study 7 site clearance; (f) case study 8 mountain hacking; (g) case study 9 pile boring activity for pile with the diameter of 1.2 m; (h) pile boring activity for contiguous bored pile with the diameter of 750 mm (Cont'd)

3.7.3.1 Background Noise Level

The definition of background noise can be expressed as the existing noise level in an ambient environment; background noise types consist of environmental noises such as traffic noise in an urban area, airborne sound, noise from structure-borne vibration and bio-acoustic noise from animals in nature (British Standard Institution, 2010). Therefore, the background noise level must be recorded before the commencement of any measurement as it can be used as the reference level of the noise measurement. Any type of momentary noise was avoided during the measurement of background noise to ensure the accuracy of the measurement. Hence, the measurement was conducted an hour before the commencement of any activities at the construction site. However, due to the size of the construction site, the background noise may vary based on different locations; consequently, the measurement was taken at the centre of the site for 30 minutes as a means of recording the average background noise level in the construction site with the acoustic parameter of equivalent continuous noise level, L_{Aeq} (Haron et al., 2008; Haron and Yahya 2009; Lim et al., 2015).

3.7.3.2 Sound Pressure Level

The sound pressure level is an assessment of the noise level when there is the presence of construction activities, using a noise level measuring instrument. The instrument was set up at the selected control point with an elevation of 1.2 m to 1.5 m away from the ground and 3.5 m offset from a sound reflective structure. Control points were set on the outside of the sub-area to record the

sound pressure level following the previous study (Haron et al., 2008). Three control points were assigned for each case study with the presence of at least one earth-moving machine during the construction activities. The duration of the measurement for each control point was 30 minutes, using the short-term sampling stipulated by the Department of Environment (2019). The acoustic parameters considered were the maximum noise level (L_{max}), minimum noise level (L_{min}), sound pressure level exceeding 10 %, 50 % and 90 % of the time of measurement duration (L_{10} , L_{50} , L_{90}) of the time of measurement duration and equivalent continuous noise level (L_{AFeq}), for each case study.

3.7.3.3 Sound Power Level

Earth-moving machine sound power level is a crucial parameter in this study because it was meant to be applied in the noise prediction model. To conduct the sound power level measurement of the earth-moving machine, the basic length, l of the machine will be measured and the radius, r will be determined according to BS ISO 6395:2008 Appendix A. Each location of microphones was calculated by using a set of coordinate systems stated by the British Standard Institution (2010) as shown in Figure 3.11 and Table 3.2. The sound power level of the machine was obtained at 6 locations with different coordinates surrounding the machine. However, for points 5 and 6, it is difficult and impractical to set up the measurement at a very high level. Hence, each point was recorded for 30 seconds with a proposed coordinate system applied by the previous researchers as shown in Table 3.3 (Haron et al., 2008; Haron and Yahya 2009; Lim et al., 2015).

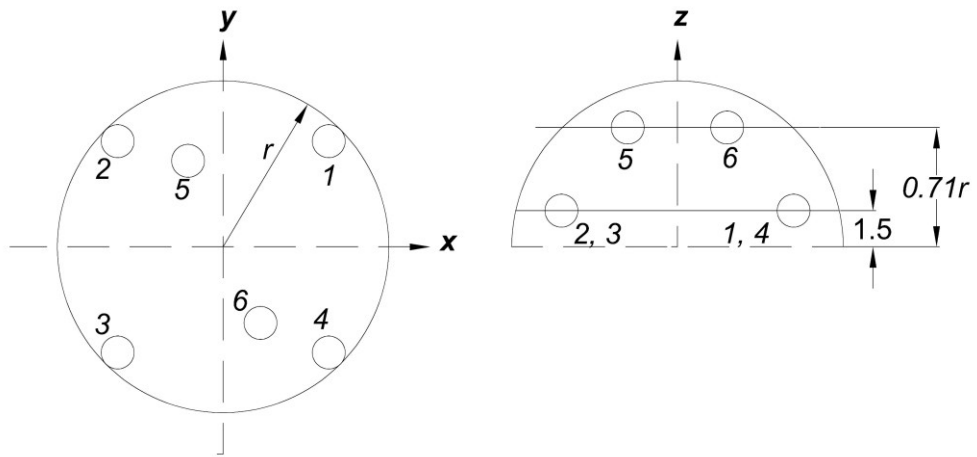


Figure 3.11 Configuration of sound power level measurement (British Standard Institution, 2010)

Table 3.2: Coordinate system of microphone position (British Standard Institution, 2010)

Microphone position	z	y/r	x/r
1	1.5 m	0.7	0.7
2	1.5 m	0.7	-0.7
3	1.5 m	-0.7	-0.7
4	1.5 m	-0.7	0.7
5	0.71 r	0.65	-0.27
6	0.71 r	-0.65	0.27

Table 3.3: Coordinate system of microphone position (Haron et al., 2008; Haron and Yahya 2009; Lim et al., 2015)

Microphone position	z	y/r	x/r
1	1.5 m	0.7	0.7
2	1.5 m	0.7	-0.7
3	1.5 m	-0.7	-0.7
4	1.5 m	-0.7	0.7
5	1.5 m	0.65	-0.27
6	1.5 m	-0.65	0.27

3.8 Data Analysis

All the data obtained from the measurement can directly be applied in this study except for the sound power level, further calculations were required to be performed. The data were recorded and calculations were performed using the spreadsheet in Microsoft Excel. The analysis and calculations of data are explained in this section.

3.8.1 Background Noise Level

The background noise is the noise that originates from all sources apart from the noise generated by the machines during the measurement. The background noise is expressed in decibels (dBA); background noise correction, K_1 is applied to the L_{AFeq} of the six measurement points to calculate the sound power level.

The background noise correction factor, K_1 , is mathematically presented in Equation 3.4, determined by using Equations 3.5 and 3.6, as well as Table 3.4.

$$K_1 = -10 \log(1 - 10^{-0.1 \Delta L_p}) \quad (3.4)$$

$$\Delta L_p = \overline{L'_{p(ST)}} - \overline{L_{p(B)}} \quad (3.5)$$

Where

$\overline{L'_{p(ST)}}$ = Averaged or mean equivalent continuous noise level from all the points surrounding the machine (dBA);

$\overline{L_{p(B)}}$ = Mean equivalent sound pressure level of the background noise, dBA
(Taken as L_{AFeq} from background noise measurement)

ΔL_p = Difference between noise level from measurement point and background noise

$$\overline{L'_{p(ST)}} = 10 \log \left[\frac{1}{N} \sum_{i=1}^N 10^{0.1 L'_{p(ST)}} \right] \quad (3.6)$$

where

$L'_{p(ST)}$ = Equivalent continuous level of the background noise from all the points surrounding the machine (dBA);

N = Total number of points surrounding the machine

Table 3.4: Determination of background noise correction factor (British Standard Institution, 2010)

Condition of ΔL_p	Determination of K_I
ΔL_p greater than 15 dBA	$K_I = 0$
ΔL_p greater than 6 dBA but lesser than 15 dBA	Calculated using Equation 3.2
ΔL_p lesser than 6 dBA	$K_I = 1.3$ dBA (ΔL_p taken as 6 dBA)

3.8.2 Sound Pressure Level

The site measurement for the sound pressure level was to use the recorded data and used to validate the prediction from the model. Besides, the sound pressure levels at the construction sites were assessed by comparing with the permissible level stipulated by Occupational Safety and Health (Noise Exposure) Regulations (2019).

3.8.3 Sound Power Level

The sound power levels of the earth-moving machine are considered as one of the main parameters in this study as it is the source to generate noise during construction activities. The computation of the sound power level, L_w , of an earth-moving machine can be computed by using Equation 3.7 (British Standards Institution, 2010). The sound power level not only can be affected by the background noise but also by environmental factors such as ground

reflection, ground absorption, air humidity, variation of temperature and the altitude of the topography. Nevertheless, the environmental correction, K_2 contributes negligible impact on the measurement of sound power level (Haron et al., 2008; Lim, et al., 2015). According to British Standard Institution (2010), the environmental correction factor can be taken as 0 if the measurement was conducted outdoor. Consequently, the environmental factor will be taken as 0 dBA in the calculation.

$$L_w = \overline{L'_{p(ST)}} + 10 \log \frac{S}{S_0} - K_1 - K_2 \quad (3.7)$$

Where

$\overline{L'_{p(ST)}}$ = Averaged of mean equivalent continuous level from all the points surrounding the machine (dBA)

S = Area that covers the sound radiation during the measurement (m^2) (taken as $2\pi r^2$)

S_0 = Referenced surface 1 (m^2)

K_1 = Background noise correction (dBA)

K_2 = Environmental correction (dBA)

3.8.4 Prediction of Sound Pressure Level using Simple Prediction Charts

The prediction included several factors such as sound power of the machine, the aspect ratio of the site, the distance between receiver and noise source, variation

of angle from the site centre, full power operation of the machine and the reduction due to noise absorption of the earth (Haron et al., 2008).

The first step to adopting the simple prediction charts in the noise prediction is to determine the overall size of the construction site and divide the site into various sub-areas, then the noise levels of the respective areas will be predicted and combined for the overall noise levels of the construction site. Moreover, multiple earth-moving machines that are operating for different construction activities can be clustered within a predetermined sub-area. The noise level at a receiver can be determined by following the procedures of (1) selecting the sound power level of the machine; (2) determining the width and depth of the sub-area; (3) identifying the angle away from the sub-area centre; (4) compute the distance between the earth-moving machine and the noise receiver, and the r/w ratio; (5) determine the standard deviation by referring the simple prediction charts (Haron et al., 2008); (6) determine the mean level deviation by referring the simple prediction charts (Haron et al., 2008); (7) Apply Equation 3.8 to compute the mean noise level. Lastly, combine the mean noise levels from each sub-areas by applying Equation 3.9 to obtain the equivalent mean noise levels and Equation 3.10 is used to compute the combined standard deviation.

$$L = L_w - 20 \log_{10} (r) - 8 + \Delta L \quad (3.8)$$

Where

L = sound pressure level correspond to the source at centre of site (dBA)

L_w = sound power level (dBA)

r = distance between receiver and center of sub-area (m)

ΔL = mean level deviation (dBA).

$$L_{Aeqn} = 10 \cdot \log_{10} \left(10^{\frac{L_{P1}}{10}} + 10^{\frac{L_{P2}}{10}} + \dots + 10^{\frac{L_{Pn}}{10}} \right) \quad (3.9)$$

Where

$L_{p1}, L_{p2}, \dots, L_{pn}$ is the mean noise level of each machine calculated by using Equation 1.

$$\sigma = \sqrt{\sigma_1^2 + \sigma_2^2 + \dots + \sigma_n^2} \quad (3.10)$$

Where

$\sigma_1, \sigma_2, \dots, \sigma_n$, is the noise level standard deviation for each machine.

3.8.5 Data Validation between the Prediction and Measurement

All the data are validated by using the methods mentioned in Chapter 2 Section 2.9.

3.8.5.1 Reliability Test

The R-squared value for the predicted and measured data can be computed by using Microsoft Excel. Equation 3.11 explains the calculation of Pearson's correlation coefficient. The determination of association strength of R-squared

and Pearson's correlation coefficient was determined by using Tables 2.6 and 2.7 correspondingly (Henseler et al., 2009; Silver et al., 2013).

$$r_{correlation} = \frac{\sum(L_{measurement} - \bar{x})(L_{prediction} - \bar{y})}{\sqrt{\sum(L_{measurement} - \bar{x})^2 \sum(L_{prediction} - \bar{y})^2}} \quad (3.11)$$

Where

$r_{correlation}$ = Pearson's correlation coefficient (dBA);

$L_{prediction}$ = Predicted sound pressure level at a control point (dBA);

$L_{measurement}$ = Measured sound pressure level at a control point (dBA);

\bar{x} = mean of measured noise level at a control point (dBA);

\bar{y} = mean of predicted noise level at a control point (dBA)

3.8.5.2 Accuracy Test

Accuracy can be defined as a statistical measure that determines the closeness of prediction to the measurement. Absolute difference was applied in this study to validate the results as this approach was previously adopted in a study (Lim et al., 2015). The absolute difference is to present the difference between the prediction and measurement. This method can be expressed in Equation 3.12. Besides, the relative difference was adopted in this study to evaluate the changes in percentage between the measurement and prediction, and the mathematical formula is presented in Equation 3.13.

$$\text{Absolute Difference} = |L_{\text{measurement}} - L_{\text{prediction}}| \quad (3.12)$$

$$\text{Relative Difference} = \frac{|L_{\text{measurement}} - L_{\text{prediction}}|}{L_{\text{measurement}}} \times 100 \quad (3.13)$$

Where

$L_{\text{prediction}}$ = Predicted sound pressure level at a control point (dBA)

$L_{\text{measurement}}$ = Measured sound pressure level at a control point (dBA);

3.9 Concluding Remarks

This chapter covers the research framework of this study which was generally divided into three stages. Relevant information and study materials for construction noise prediction, stochastic modelling and deep learning were extensively studied in stage one. Followed by stage two, the programming algorithms for the stochastic deep learning model were developed based on the optimal hyperparameters obtained from the trial models. The third stage which is the data analysis and validation consists of actual data measurement from the existing construction activities and the prediction of sound pressure levels from the stochastic deep learning model. Then, the measured values and the prediction were compared and validated by using the reliability and accuracy test.

CHAPTER 4

DEVELOPMENT OF STOCHASTIC DEEP LEARNING MODEL

4.1 Introduction

The preliminary results are demonstrated in this chapter, which is significantly important to determine the feasibility of the stochastic deep learning model in construction noise prediction, before conducting any further extensive development. Since the accuracy and reliability of stochastic modelling were proven to be promising by several previous studies as presented in Chapter 2, the deep learning model was trained with the output from the stochastic modelling to develop the optimum model for construction noise prediction. The variation of hyperparameters during the model configuration is used to determine the optimal results.

This chapter is comprised of two sections, the stochastic modelling and the deep learning model. Firstly, the variation of mean level deviation, standard deviation and the distribution of the data of the stochastic modelling will be explained in Section 4.2. Followed by Section 4.3, the influence of different hyperparameters (data split ratio, architecture of the neural network, activation function, learning rate of the model, epochs numbers, batch size and the optimizer) on the predictive performance was discussed.

4.2 Stochastic Modelling

4.2.1 Mean Level Deviation

Figure 4.1 presents the output of stochastic modelling from different aspect ratios of 1:1 (50 m x 50 m), 1:2 (50 m x 100 m), 1:4 (50 m x 200 m), 1:8 (50 m x 400), 2:1 (100 m x 50 m), 4:1 (200 m x 50 m), and 8:1 (400 m x 50 m). The sound pressure levels within the sub-area were obtained, by assuming a noise receiver that is moving along the radius of a circle at different angles from the site centre. Contrary to the previous research, by collapsing the mean level deviation with r/w ratio, the variation of mean level deviation in all the aspect ratios showed a systematic trend due to the coverage angle of the receiver from the previous research ranging from 0°, 15°, 30° and 45°, whereas the coverage angle for this study was ranging from 0° to 360°.

Figure 4.1 demonstrates the variation of the mean level deviation increases as the depth of the sub-areas for the aspect ratios (width : depth) of 1:2, 1:4 and 1:8 increases. The relationship between the variation of the mean level deviation and the depth of the sub-area can be expressed as a directly proportional trend. On the other side, Figure 4.1 presents that the larger the width of the sub-areas for aspect ratios of 2:1, 4:1 and 8:1, the higher the variation of the mean level deviation. The mean level deviation was primarily affected by the r/w ratio in which the lower the value of the r/w ratio represents the position of the noise receiver was nearer to the boundary of the sub-area during the stochastic modelling simulation. When the noise receiver was

positioned at the edge of the sub-area, *SPL1* was biased to the noise source owing to the short distance between the noise source and receiver; whereas *SPL2* covered all the random points within the sub-area which explained the high value of the mean level deviation when finding the difference between *SPL1* and *SPL2*.

Besides, the mean level deviation was influenced by the duty cycles as well. For example, the sound pressure level at the noise receiver was minimal when the simulated random noise source was configured to operate in the idling mode or off mode. Conversely, when the noise source was set to operate at full power, the sound pressure level was higher as compared to the other modes. As a consequence, this explained that the variation of mean level deviation was governed by the distance between the noise receiver and noises source as well as the operation mode of the noise source.

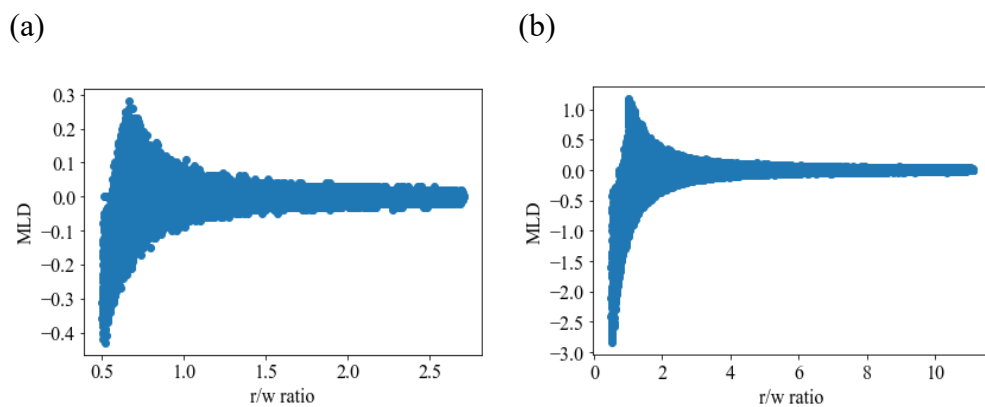


Figure 4.1: Graph of MLD (mean level deviation) vs. r/w ratio with different aspect ratios (a) 1:1; (b) 1:2; (c) 1:4; (d) 1:8; (e) 2:1; (f) 4:1; (g) 8:1

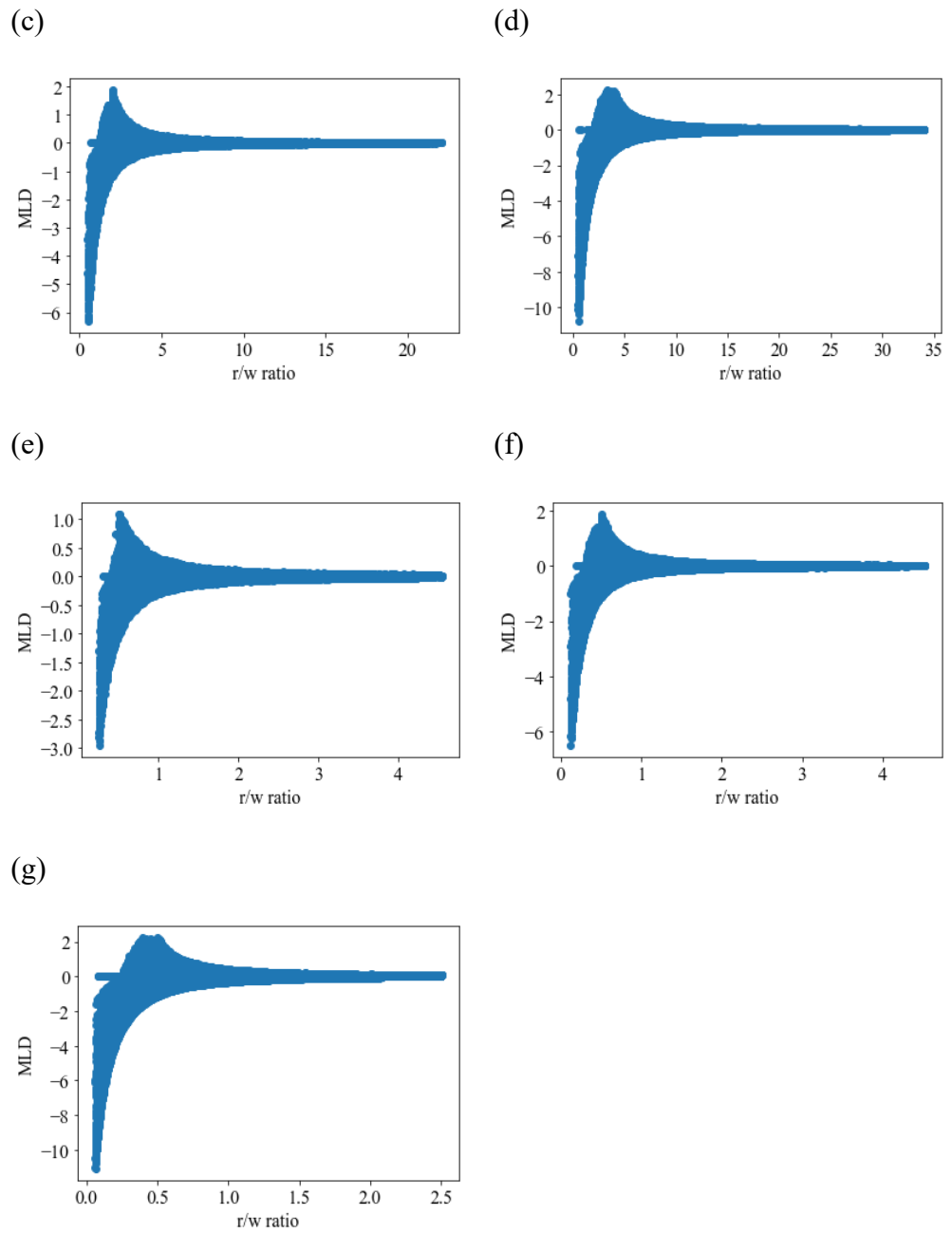


Figure 4.1: Graph of MLD (mean level deviation) vs. r/w ratio with different aspect ratios (a) 1:1; (b) 1:2; (c) 1:4; (d) 1:8; (e) 2:1; (f) 4:1; (g) 8:1 (Cont'd)

4.2.2 Standard Deviation

Figure 4.2 shows the generated standard deviations using stochastic modelling that comprised of the different aspect ratios of 1:1, 1:2, 1:4, 1:8, 2:1, 4:1 and 8:1. The standard deviation was used to explain the noise level distribution based on different parameters during the stochastic simulation.

Despite there being changes in the r/w ratio for each aspect ratio but the standard deviation plotted against the r/w ratio still presents a systematic pattern. This indicates that the randomness of the duty cycles was evenly distributed during the simulation. Unlike the previous research, the overall variation of standard deviation for all the aspect ratios in this study was ranging from 0 dBA to 44 dBA, but for previous research, the standard deviation revolved from 0 dBA to 5 dBA (Haron et al., 2012). This is due to the inclusion of different duty cycles in the simulation; when the majority of the noise sources operated with the combination of idling or off mode within a set (20, 000 steps). Consequently, the minimum and maximum sound pressure levels will have a large difference which eventually leads to a high standard deviation in that particular set. However, 0 dBA of standard deviations were obtained when the noise source was assumed to be completely off.

The maximum standard deviation for aspect ratios 1:8 and 8:1 was lowered as compared to the other aspect ratios because of the inverse squared law. This can be explained by the reduction of sound intensity as it propagates farther away from the noise source. For instance, the noise receiver of each

aspect ratio was positioned at the border of the sub-area but the coverage area of aspect ratios 1:8 and 8:1 was much larger in scale and the distance between the noise receiver and noise source was much farther as compared to other aspect ratios. Moreover, the effect of the inverse square law influenced the maximum standard deviation as well, which gradually decreases with the increment of the r/w ratio.

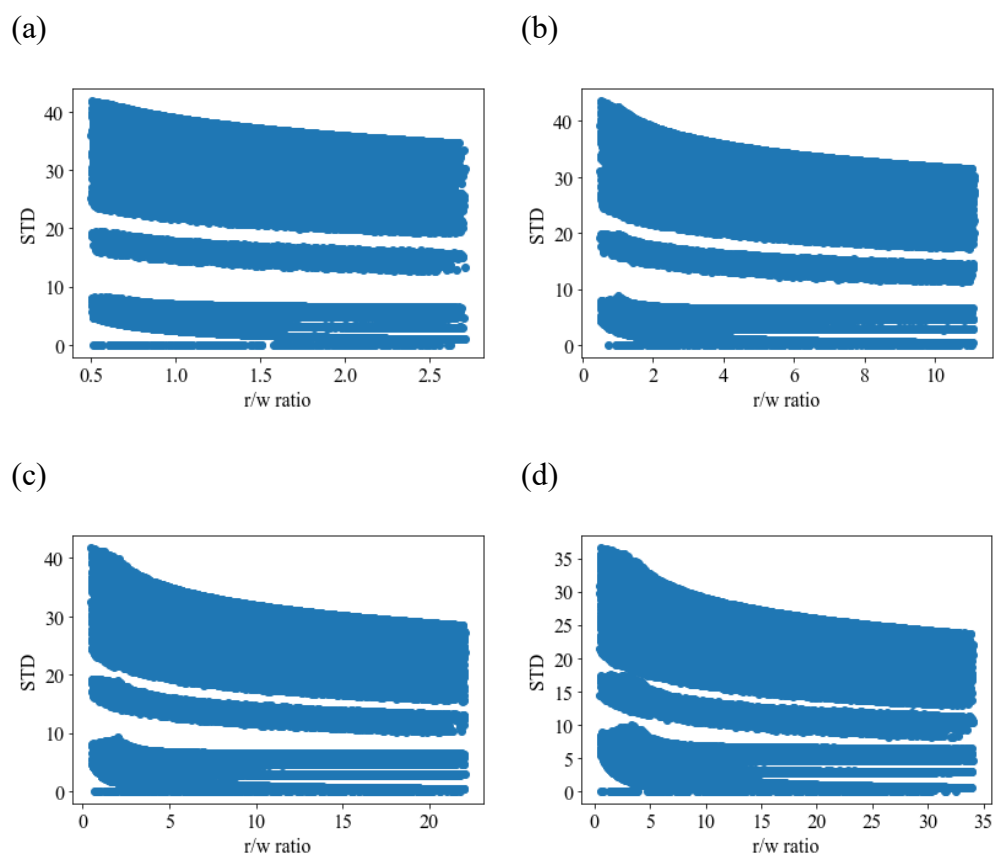


Figure 4.2: Graph of STD (standard deviation) vs. r/w ratio with different aspect ratios (a) 1:1; (b) 1:2; (c) 1:4; (d) 1:8; (e) 2:1; (f) 4:1; (g) 8:1

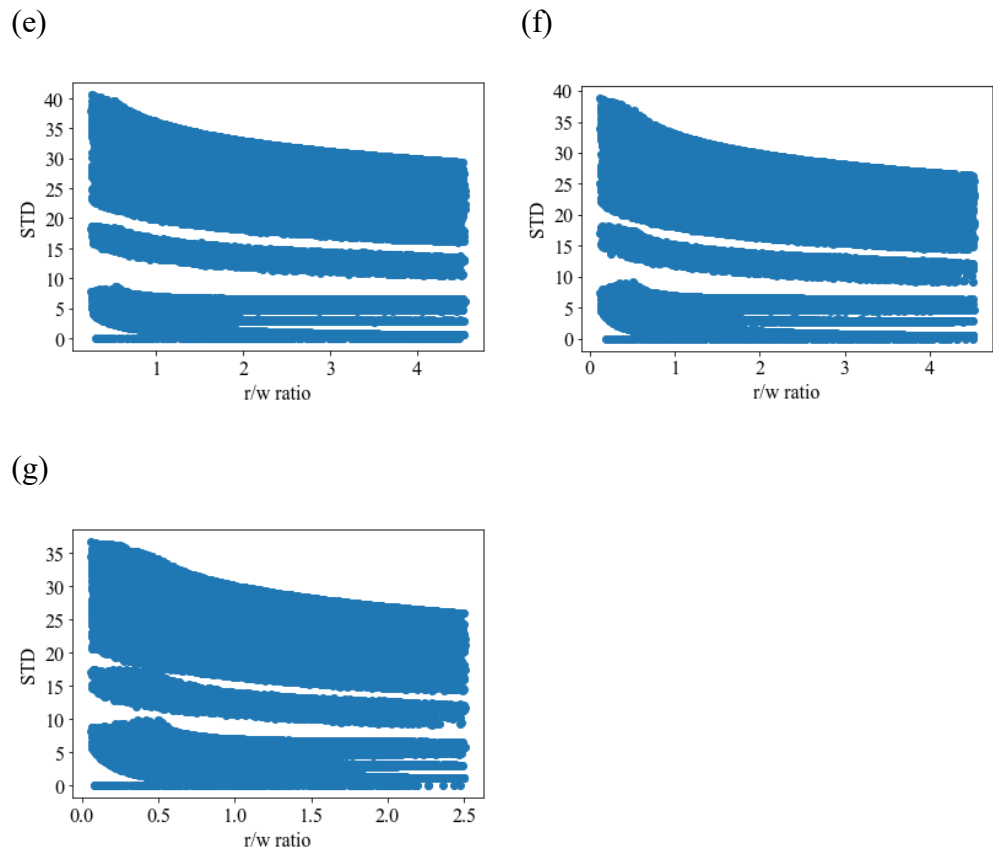


Figure 4.2: Graph of STD (standard deviation) vs. r/w ratio with different aspect ratios (a) 1:1; (b) 1:2; (c) 1:4; (d) 1:8; (e) 2:1; (f) 4:1; (g) 8:1 (Cont'd)

4.2.3 Distribution of the Data at Different Angles

Figure 4.3 presents the correlation between the coverage angle and the mean level deviation from different aspect ratios. For the aspect ratio of 1:1, the data were distributed uniformly at every half quarter in the circular coverage area. However, as the depth of the sub-areas (1:2, 1:4, 1:8) was increasing, the majority of the data were distributed within the angles of 0° to 45° , 136° to 225° and 316° to 360° . This is because the coverage area of the long side of the sub-area (depth) was larger than the short side (width).

Contrastingly, for the aspect ratio of 2:1, 4:1 and 8:1, a preponderance of data was observed within the angle of 46° to 135° and 226° to 315° because the orientation of the sub-areas was rotated. By interpreting the plotted graph, the data for every aspect ratio were distributed proportionally in the respective quadrants which indicates the noise receiver moved in a circular motion to cover all the directions of the sub-areas; this is important information to be considered when the data are being utilized as the input data for the deep learning model.

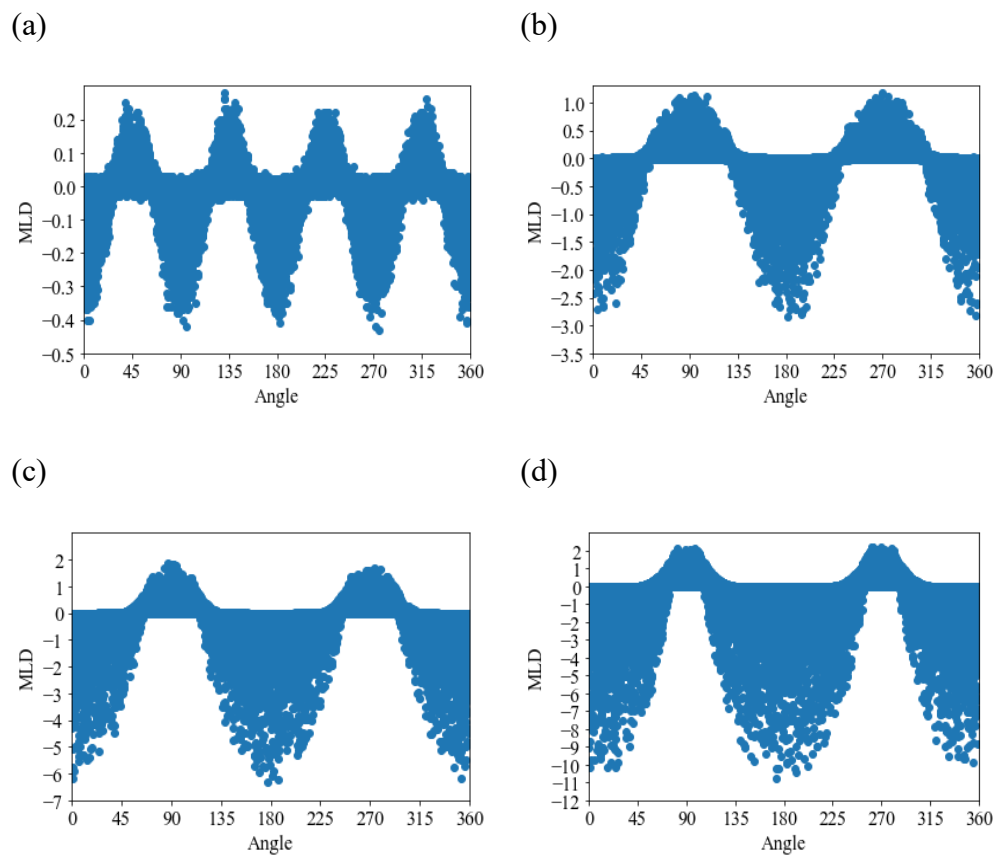


Figure 4.3: Graph of MLD (mean level deviation) vs. angle with different aspect ratios (a) 1:1; (b) 1:2; (c) 1:4; (d) 1:8; (e) 2:1; (f) 4:1; (g) 8:1

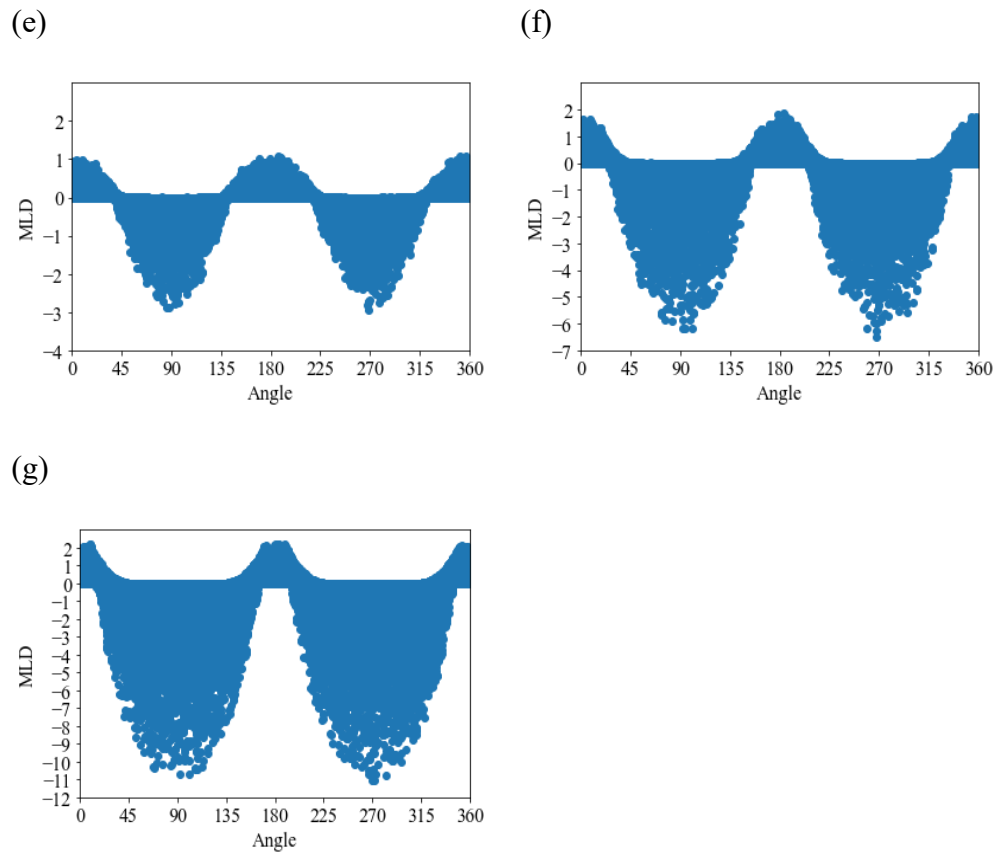


Figure 4.3: Graph of MLD (mean level deviation) vs. angle with different aspect ratios (a) 1:1; (b) 1:2; (c) 1:4; (d) 1:8; (e) 2:1; (f) 4:1; (g) 8:1

(Cont'd)

4.3 Configuration of Stochastic Deep Learning Model

In this section, the hyperparameters such as data split ratio, the architecture of the neural network, activation function, number of epochs, the learning rate of the model, batch size and the optimizer on the predictive performance were tested with different variations. Mean absolute error was applied in the model training (loss), and mean squared error was used in model testing.

4.3.1 Data Split

Figure 4.4 compares the results of the deep learning model based on different data split ratios (training: test: validation) of 60:20:20; 70:15:15; 80:10:10. Figures 4.4a, 4.4c and 4.4e represent the training and validation of the model, Figure 4.4b, 4.4d and 4.4f present the testing of the model for the data split ratios of 60:20:20, 70:15:15, and 80:10:10 correspondingly.

The performance of the models was evaluated and the outcome is demonstrated in Table 4.1. The mean squared error of the model for data split ratio of 60:20:20, 70:15:15 and 80:10:10 was 0.0166, 0.0182 and 0.0409 respectively. Next, the root means squared error of the models for the different data split was 0.1288, 0.1349 and 0.2023 sequentially. For the mean absolute error, the lowest value was 0.0775 for the data split ratio of 60:20:20, followed by 0.0776 and 0.1151 for the succeeding data split ratios. Moreover, the R-squared coefficient of the three different data split ratios was 0.97, 0.57 and 0.64.

Based on the observation, the data split ratio of 60:20:20 outperformed the others having the highest R-squared coefficient but the lowest mean squared error, mean absolute error, root mean squared error. This is because the closer the value of errors to 0, indicates the lower the error of the prediction. Besides, the results show that 97 % of the independent variables of data influenced the dependent variables which explain that the model was reliable.

The oscillation in training and testing of the data split ratio of 60:20:20 stopped after the epochs of 150 as shown in Figures 4.4a and 4.4b whereas the other two remained unstable as illustrated in Figures 4.4c – 4.4f. This can be explained as the prediction being biased to the training because only a small portion of the data was used to validate and test the model. Although the recommended data split ratio was 80:10:10 (Chollet, 2017; Zaccone and Karim, 2018; Loy, 2019), the optimal ratio for the model in this study was 60:20:20 because the dataset was in large size of 100, 000 and the recommended ratio (80:10:10) is only suitable for small dataset. However, the split of 60:20:20 was an acceptable and reasonable choice (Nikhil, 2017).

Table 4.1: Performance of model of different variations of hyperparameters

No.	Model name	Mean	Root Mean	Mean	R ²
		Squared Error	Squared Error	Absolute Error	
1	(60:20:20) ¹ -(ReLU) ² - (10 ⁻⁴) ³ -(32) ⁴ -(Adam) ⁵	0.0166	0.1288	0.0775	0.9720
2	(70:15:15)-(ReLU)-(10 ⁻⁴)-(32)-(Adam)	0.0182	0.1349	0.0776	0.5709
3	(80:10:10)-(ReLU)-(10 ⁻⁴)-(32)-(Adam)	0.0409	0.2023	0.1151	0.6432

Table 4.1: Performance of model of different variations of hyperparameters (Cont'd)

4	(60:20:20)-(Sigmoid)- (10 ⁻⁴)-(32)-(Adam)	64.1116	8.007	4.5464	0.0357
5	(60:20:20)-(ReLU)-(10 ⁻³)-(32)-(Adam)	0.0199	0.1413	0.0852	0.4456
6	(60:20:20)-(ReLU)-(10 ⁻²)-(32)-(Adam)	62.7089	7.9189	4.5537	0.0315
7	(60:20:20)-(ReLU)-(10 ⁻⁴)-(64)-(Adam)	0.5564	0.7459	0.2336	0.5384
8	(60:20:20)-(ReLU)-(10 ⁻⁴)-(128)-(Adam)	1.7076	1.3067	0.5277	0.5211
9	(60:20:20)-(ReLU)-(10 ⁻⁴)-(32)-(RMSprop)	0.0313	0.1769	0.0944	0.5943
10	(60:20:20)-(ReLU)-(10 ⁻⁴)-(32)-(Adagrad)	44.664	6.6831	3.7223	0.1321

Note:

¹ represents the data split in different percentages (training: validation: testing)

² Activation function

³ Learning rate

⁴ Bath size

⁵ Optimizer

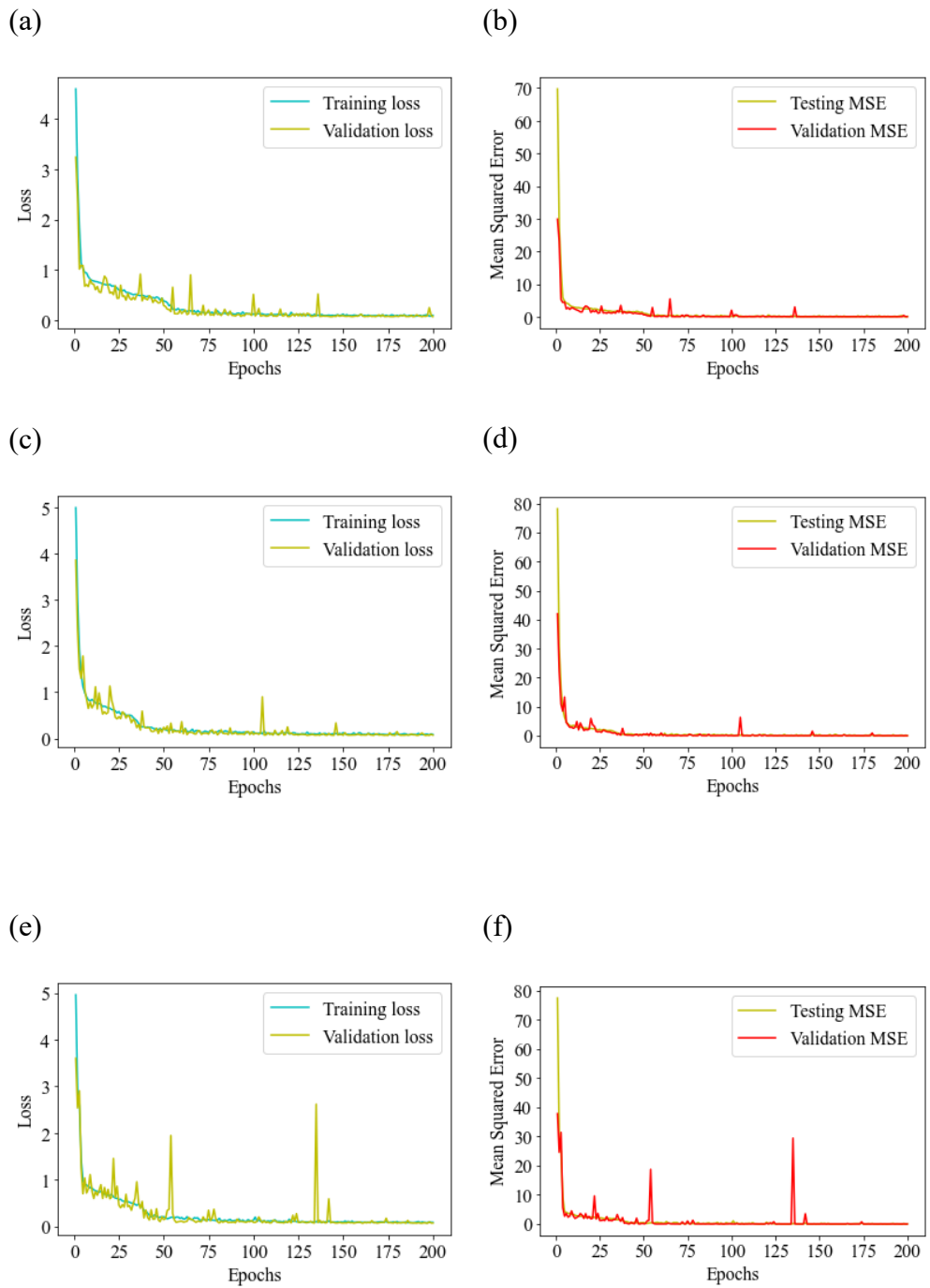


Figure 4.4: Training and testing of the model based on different data split ratios (a) 60:20:20 training; (b) 60:20:20 testing; (c) 70:15:15 training; (d) 70:15:15 testing; (e) 80:10:10 training; (f) 80:10:10 testing

4.3.2 Number of Hidden Layers and Neurons

The initial model architecture started with a single layer with 5 hidden neurons because there were 5 different types of input data. However, the initial model was unable to perform well in the prediction. Hence, the number of hidden neurons and layers was increased in order to achieve promising results. Hence, the model was able to perform with satisfactory results when the architecture of the neural network was increased to 25, 30, 35, 40, 45, 50, 55, 60, 65, 70 in each of the 10 hidden layers respectively. Due to a large amount of data, a high number of hidden neurons and layers is required for the model to learn the pattern of the data and extract useful information to train the model (Goodfellow et al., 2016).

4.3.3 Activation Function in Hidden Layers

Figure 4.5 compares the training and testing of the model using the sigmoid and ReLU activation function. Based on Figures 4.5a and 4.5b, the mean absolute error of the model was reduced to 0 during the training as well as the testing; the curves converged at 0 after 150 epochs and this explained that the model can learn from the dataset; As for Figures 4.5c and 4.5d present that the curves were not able to converge at 0 and remained constant; the mean absolute error for the data validation stopped updating at 4.5 and the mean squared error was not reduced once it reached 60 during the testing of the model.

Table 4.1 demonstrates the model performance using the ReLU and sigmoid activation function. Model 1 had the lowest MSE of 0.0166, RMSE of 0.1288, MAE of 0.0775 and R-squared of 0.67; whereas model 4 had MSE of 64.116, RMSE of 8.007, MAE of 4.5464 and R-squared of 0.0357. This is due to the vanishing problem in which the gradient vanishes or size reduction, and any significant change could not be made since its value is minimal. Under the circumstance, the model was learning drastically slowly or unable to learn further. The results proved that the ReLU activation function was able to converge more quickly and it is more suitable to be applied in the model with a large dataset (Loy, 2019; Campesto, 2020).

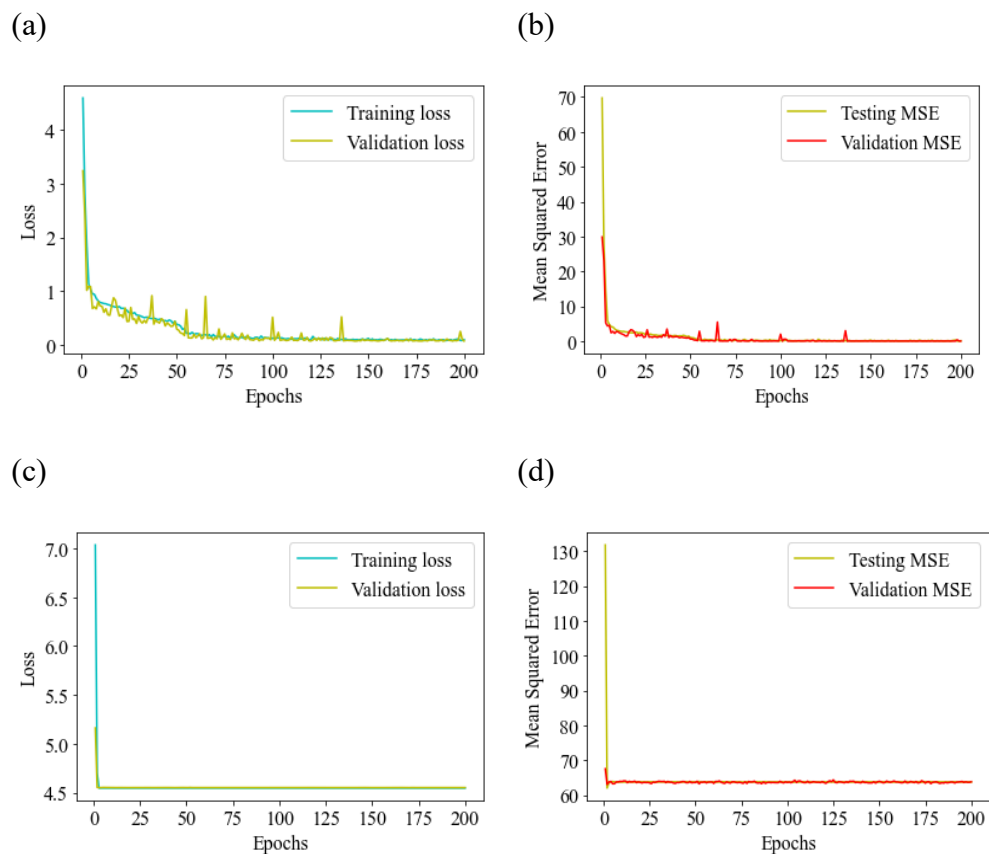


Figure 4.5: Comparison of testing and training of the model using different activation functions in the hidden layers (a) validation curve using ReLU;

(b) testing curve using ReLU; (c) validation curve using Sigmoid; (d) testing using Sigmoid

4.3.4 Number of Epoch

Figures 4.4a and 4.4b show the oscillation of the training and testing curve from 0 epochs to 200 epochs. The number of epochs was initiated from 50 but the curves were oscillating and unable to converge at 0 which indicated that more training, validation and testing were required to learn from the prediction error of the model. Hence, the number of epochs was increased by 25 upon every unsatisfactory outcome. The maximum number of epochs was 200 for consistency of the results. As the epochs were configured as 200, both the training and validation loss keeps reducing and converging which shows the learning process was effective. Hence, the number of epochs of 200 was determined as the optimal value to configure the other models with different hyperparameters.

4.3.5 Learning Rate

The experimented learning rates in this study were 10^{-2} , 10^{-3} and 10^{-4} using Adam optimizer. Figure 4.6 compares the training and the test of the models using different learning rates. Figures 4.6a and 4.6b illustrate the training and testing of the model using the learning rate of 10^{-4} and the fluctuation of the curve was mild as the loss function was updated optimally. As for Figures 4.6c and 4.6d, the learning rate was configured as 10^{-3} but both the testing and

validation curves were oscillating resulting in drastic change that leads to a disparate pattern. Next, the curves as depicted in Figures 4.6e and 4.6f were fluctuating intensively.

For model 1, the initial mean absolute error of the model training was 4 and after 200 epochs, the mean absolute error was reduced to 0; whereas the mean squared error of the testing data started from 50 and the error was then minimized to 0 as shown in Figures 4.6a and 4.6b. The initial high mean squared error in the testing set was because the testing split was only 20 % of the entire dataset. The mean absolute error in the model training fluctuated within the range of 0.3 and 3.5; whereas the mean squared error in the model testing oscillated from 0 to 40 at 200 epochs for model 5. For model 6, the changes of both the mean absolute and mean squared error was the highest in every comparison of different learning rate. This can be explained as a high learning rate leading to the new estimation exceeding the local or global minimal point and therefore the loss function was unable to be updated (Ketkar, 2017; Chollet, 2018; Campesato, 2020; Kinsley and Kukiela, 2020). Overall, the experimental results indicated that the learning rate of 10^{-4} was more effective in the training, validation and testing of the model.

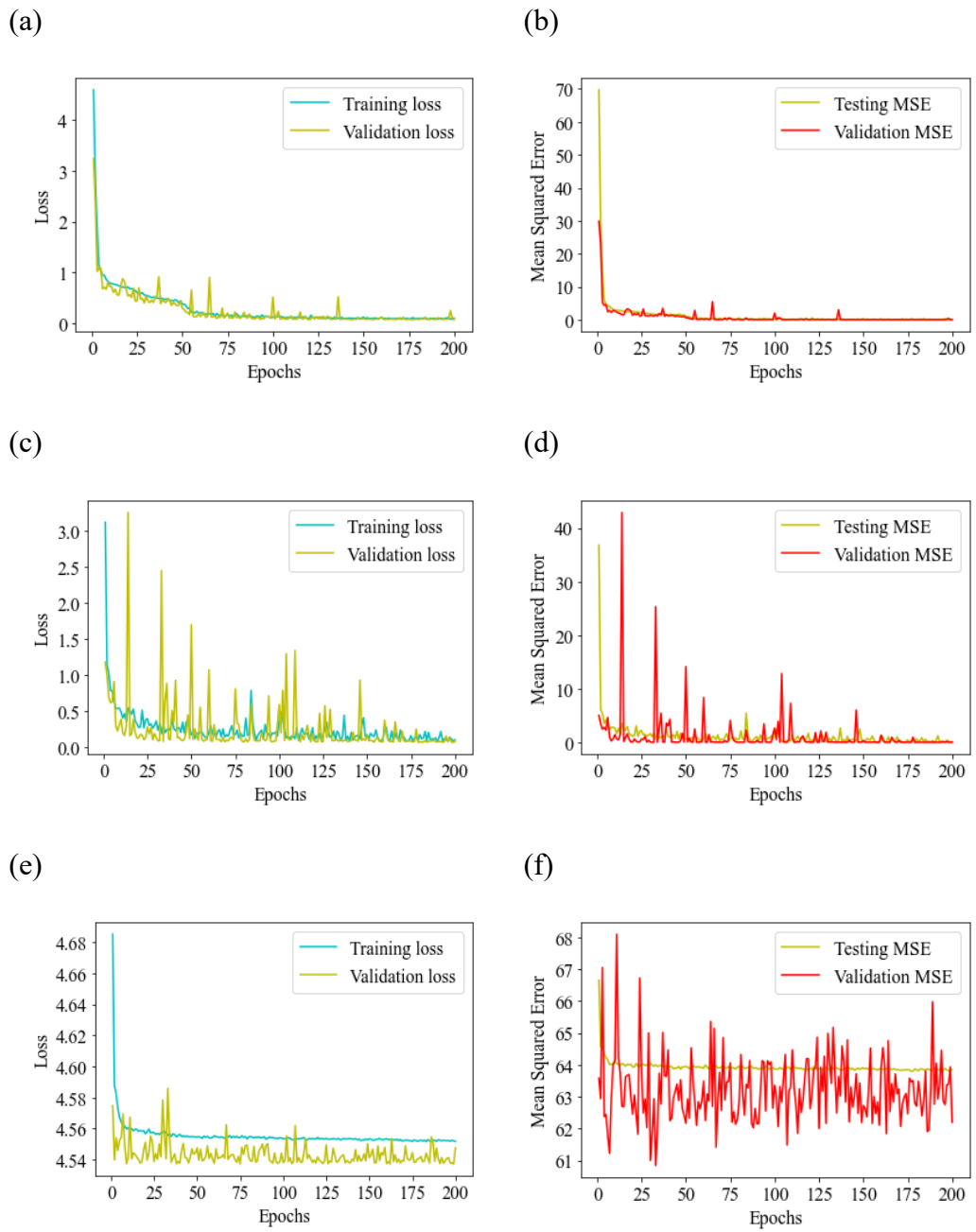


Figure 4.6: Comparison of different learning rates in training and testing of the model (a) lr of 10^{-4} on training; (b) lr of 10^{-4} on testing; (c) lr of 10^{-3} on training; (d) lr of 10^{-3} on testing; (e) lr of 10^{-2} on training; (f) lr of 10^{-2} on testing

Note: lr = learning rate

4.3.6 Batch Size

The comparison of the difference between training and testing of the models by using the batch size of 32, 64 and 128 along with the Adam optimizer in different models are depicted in Figure 4.7. From the results in Table 4.1, model 1 with a batch size of 32 had the best performance among the others. For a batch size of 64, The mean squared error for the batch size of 64 and 128 models were 0.5564 and 1.7076 respectively; whereas the root mean squared error for both models 7 and 8 were 0.7459 and 1.3067. Next, the mean absolute error for both the model were 0.2336 and 0.5277; followed by the R-squared of 0.5384 and 0.5211 correspondingly as presented in Table 4.1. The results showed that enlarging the batch size resulted in a higher error and lower R-squared during the training, validation and testing of the model. Montavon et al. (2012) mentioned that the batch size of 32 was able to generate a promising prediction and this statement was validated by the experimental results. Kandel and Castelli (2020) stated that choosing a small batch size (32) with a low learning rate was a good combination to develop a model with high performance.

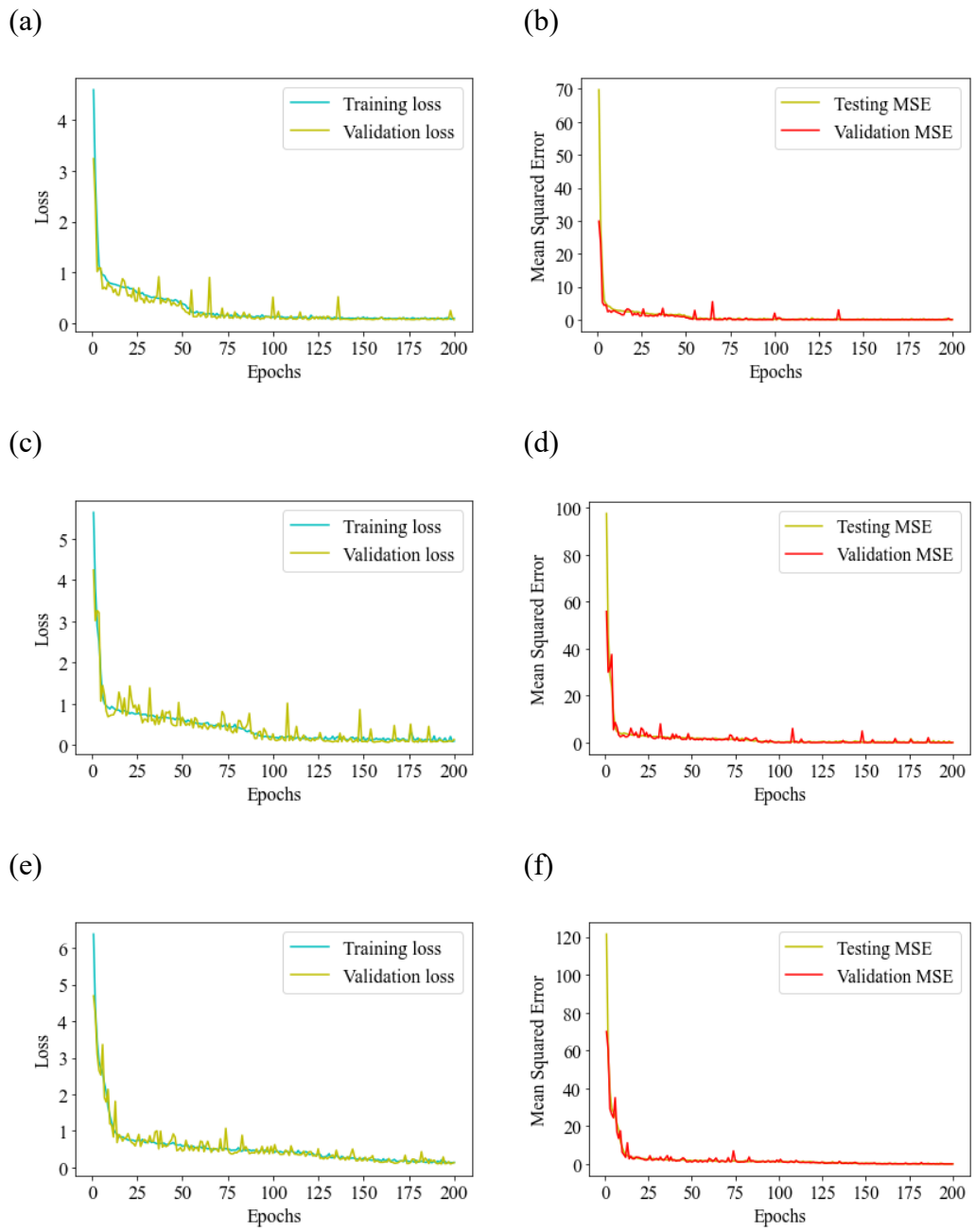


Figure 4.7: Comparison of validation and testing of the model using different batch size (a) batch size 32 on validation; (b) batch size 32 on testing; (c) batch size 64 on validation; (d) batch size 64 on testing; (e) batch size 128 on validation; (f) batch size 128 on testing

4.3.7 Optimizer

The selected optimizers used in models 1, 9 and 10 in this study were Adam, RMSProp and AdaGrad with the fixed learning rate of 10^{-4} correspondingly. Figure 4.8 depicts the plotted graphs representing the curves of validation and testing of the models by using different optimizers. The training and testing curve of model 1 were shown in Figures 4.8a and 4.8b; indicating that the training loss and testing started from the mean squared error of 70, mean absolute error of 4 then converged at 0 at the epochs of 200. Next, Figures 4.8c and 4.8 d show the curves of the validation and testing of model 9 with a mean squared error of 60 and a mean absolute error of 4.5. Initially, the curves fluctuated intensively to update the loss function; nevertheless, model 9 was able to converge to 0 at the 200th epoch. Following by model 10 using AdaGrad optimizer, although the learning, validation and testing errors were moving towards a smaller value, the process may take a longer duration and more epochs to be completed.

As for model 9, the errors and R-squared were 0.0313, 0.1769, 0.0944 and 0.5943 sequentially; whereas, for model 10, the values were 44.664, 6.6831, 3.7223 and 0.1321 as shown in Table 4.1. As compared to models 9 and 10 using AdaGrad and RMSProp optimizer respectively, model 1 had the lowest errors and highest R^2 . The performance of model 1 can be explained as the Adam optimizer leveraging the combination of the momentum and variance of the loss gradient to update the weight parameters leading to a shorter duration for the learning process and also a smooth learning curve (Aggarwal, 2018;

Moolayil, 2019). The high initial errors in model 9 were due to a high bias early in the training due to its initialization (Kinsley and Kukiela, 2020). As for model 10, the purpose of AdaGrad was to converge quickly in a convex function, but apparently, it is a nonconvex function in this problem, and that leads to the learning path passing through several different structures and eventually being trapped in the local convex region (Goodfellow et al., 2016).

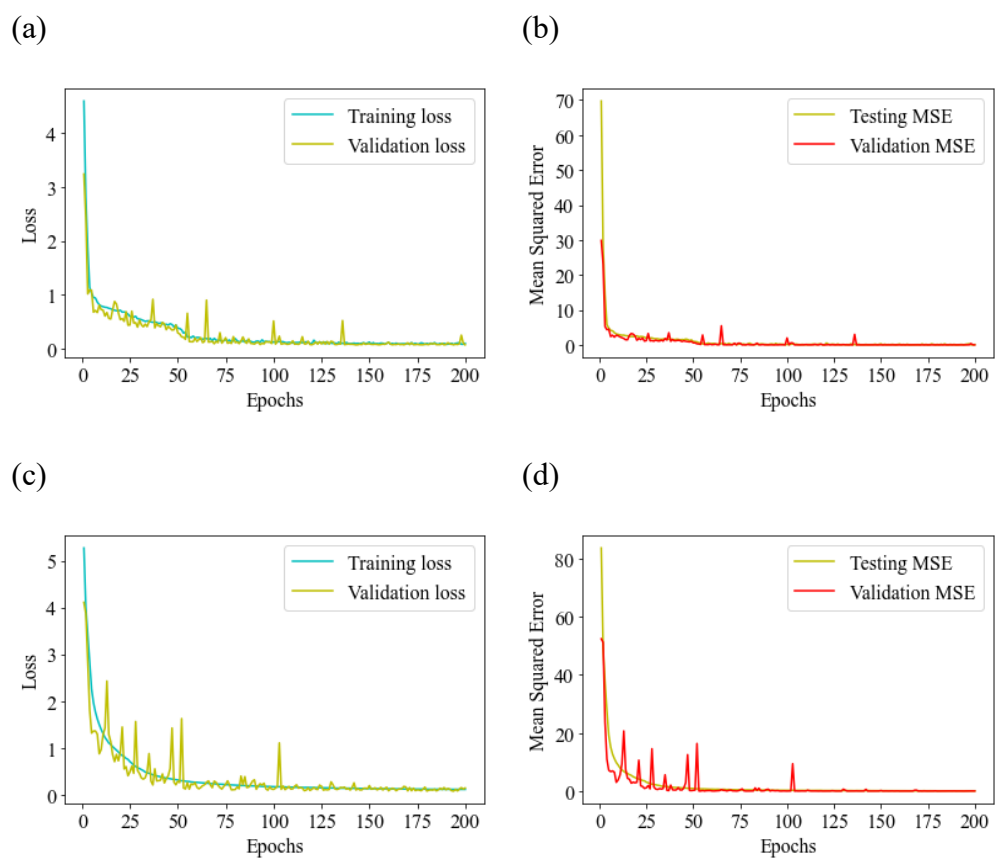


Figure 4.8: Comparison of validation and testing of the model using different optimizers (a) Adam on validation; (b) Adam on testing; (c) RMSprop on validation; (d) RMSprop on testing; (e) Adagrad on validation; (f) Adagrad on testing

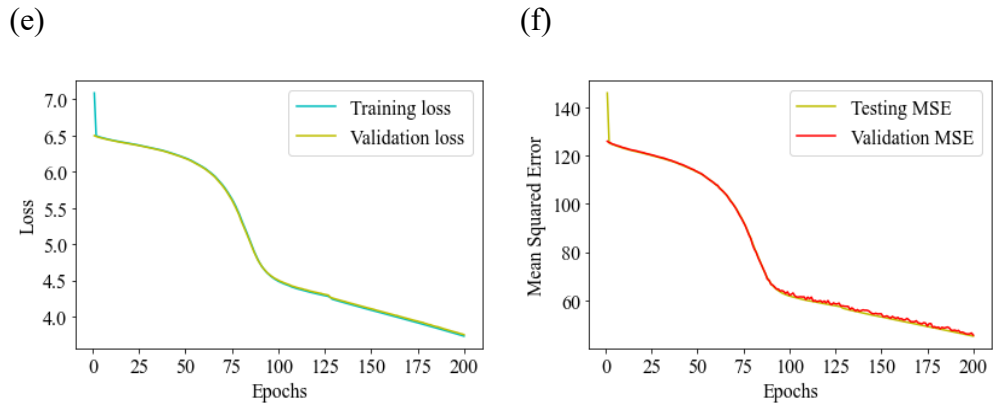


Figure 4.8: Comparison of validation and testing of the model using different optimizers (a) Adam on validation; (b) Adam on testing; (c) RMSprop on validation; (d) RMSprop on testing; (e) Adagrad on validation; (f) Adagrad on testing (Cont'd)

4.4 Performance of Stochastic Deep Learning Models

Therefore, the selected hyperparameters of the six remaining models with the aspect ratios of 1:2, 1:4, 1:8, 2:1, 4:1 and 8:1 were data split ratios of 60:20:20, 10 hidden layers with 25, 30, 35, 40, 45, 50, 55, 60, 65, 70 hidden neurons in each layer correspondingly, batch size of 32, ReLU activation function, 200 epochs, Adam optimizer, learning rate value 10^{-4} . The experimental hyperparameters were optimal for the six models except for the number of hidden neurons and layers; hence the models were re-configured with a dissimilar architecture.

For the model with the aspect ratio of 1:2, ten hidden layers were configured with 50, 55, 60, 65, 70, 75, 80, 85, and 90 hidden neurons in each hidden layer respectively. On the other hand, the hidden layers for the model

with the aspect ratio of 1:4 were 10 with 55, 60, 65, 70, 75, 80, 85, 90, 95, and 100 hidden neurons in each layer consequentially. Followed by the model with the aspect ratio of 1:8, the hidden neurons numbers in each hidden layer were 60, 65, 70, 75, 80, 85, 90, 95, 100, and 105. Next, the hidden neurons and layers and numbers were identical for the models with the aspect ratio of 2:1, 4:1 and 8:1. The hidden layers numbers were 11 and the numbers of hidden neurons were 50, 55, 60, 65, 70, 75, 80, 85, 90, 95, and 100. The increment of hidden layers and hidden neurons was due to the complexity of the data distribution as presented in section 4.2.3.

Table 4.2 shows the performance of the stochastic deep learning models that have been assessed using the MSE, RMSE, MAE and R-squared for the models ranging from 0.0114 to 0.0179, 0.1068 to 0.1339, 0.0619 to 0.0728 and 0.9716 to 0.9977. The results of the models presented the accuracy and the reliability of the stochastic deep learning model indicating that the models were ready to be deployed for the construction noise prediction.

Table 4.2: Performance of the stochastic deep learning models

Aspect ratio	Model name	Mean	Root Mean	Mean	R²
		Squared Error	Squared Error	Absolute Error	
1:1	1-1	0.0166	0.1288	0.0775	0.9720
1:2	1-2	0.0151	0.1229	0.0709	0.9716
1:4	1-4	0.0179	0.1339	0.0728	0.9937
1:8	1-8	0.0118	0.1087	0.0656	0.9977
2:1	2-1	0.0114	0.1068	0.0619	0.9860
4:1	4-1	0.0141	0.1189	0.0673	0.9882
8:1	8-1	0.0149	0.1224	0.0752	0.9976

4.5 Concluding Remarks

Ten configurations of the experimental hyperparameters were developed to determine the effectiveness of different hyperparameters in enhancing the noise model predictive performance. The following findings are concluded from this preliminary study:

- i) The data split ratio of 60: 20: 20 was the optimum ratio to train the model, 60 %, 20 % and 20 % of the data were applied in the training, validation and testing. The results implied that sufficient data were required for the validation and testing of the model to train the model effectively.

- ii) The hidden layers and neurons numbers were increased to 10 layers and each layer consisted of 25, 30, 35, 40, 45, 50, 55, 60, 65, 70 hidden neurons respectively. Broad (hidden layers number) and deep (hidden neurons number) were required because it was essential for the model to determine the attribute of the dataset and infer the information from the data and apply the information in the training.
- iii) The results showed that the ReLU activation function outperformed the Sigmoid activation function. This is because of the occurrence of a vanishing problem when the sigmoid activation function was applied in the model causing the model unable to learn further.
- iv) The training, validation and testing curves converged at 0 when they reached the 200th epoch; and it was chosen to configure all the models for the consistency of the results.
- v) The model was trained with the learning rates of 10^{-4} , 10^{-3} and 10^{-2} using the Adam optimizer. The model with the learning rate value of 10^{-4} was chosen as the best model as it outperformed the others in terms of consistency of model during the training, validation and testing as well as the predictive performance. This can be explained as a high learning rate leading to the new estimation exceeding the local or global minimal point and therefore the loss function was unable to be updated.

- vi) Configuration of the model using the batch size of 32 showed satisfactory results. The batch size of 64 and 128 were rejected because they resulted in a higher error during the training, validation and testing; the curves were unable to converge at 0 as well.

- vii) The best optimizer was Adam in the experimental results. The results indicated that the training, validation and testing curves had minimal fluctuation and converged at 0 more quickly than the other optimizers. This can be explained as the Adam optimizer utilising the association of the momentum and variance of the loss gradient to update the weight parameters producing a smooth learning curve and speeding up the learning process.

- viii) The outcome of the experimental model presents the association between stochastic modelling and artificial neural network is capable of predicting sound pressure level at a construction site with satisfactory performance as the highest absolute difference between DL prediction and actual value was 1.5 dBA. The highest standard deviation value was 3.7 dBA due to the variation in duty cycle and coverage area of the machine. Moreover, the R-squared value was 1.0 in case study 1 indicating the strong strength of association between the prediction and actual measurement. Therefore, the optimal hyperparameters were acceptable and applied in the configuration of the noise prediction model for the remaining 6 different aspect ratios (1:2, 1:4, 1:8, 2:1, 4:1, 8:1).

CHAPTER 5

RESULTS AND DISCUSSION

5.1 Introduction

The preliminary results in the previous chapter indicated that the optimal hyperparameters used in the model with the aspect ratio of 1:1 were able to achieve satisfactory predictive performance. Hence, the optimal hyperparameters were applied in the configuration of the stochastic deep learning model with the aspect ratios of 1:2, 1:4, 1:8, 2:1, 4:1, and 8:1.

In this chapter, extensive fieldwork was conducted at the construction sites with different activities to evaluate the stochastic deep learning model performance in construction noise prediction. Besides, discussion of the earth-moving machine, the condition of the construction activity for each case study and the noise exposure level of the employees were presented as well.

This section discusses the predicted noise levels using the simple prediction charts and deep learning model, as well as the actual noise levels of different case studies. The disparities between the predicted and actual results will be assessed by using absolute difference and relative error for accuracy, as the reliability of the models was based on the R-squared value and Pearson's correlation coefficient.

5.2 Proposed Case Studies

Fieldworks were carried out to validate the stochastic deep learning model's reliability and accuracy. The determination of the sound power level of 14 earth-moving machines in the fieldwork was following British Standards Institution (2010). However, the types of construction activities were limited to the preliminary construction stage as this stage was the noisiest stage. Ten case studies namely CS1 to CS10 with respect to different site aspect ratios of (1:1, 1:2, 1:4, 1:8, 2:1, 4:1, 8:1) and configuration (different distances and angles) were conducted in this study. CS1 was applied in the preliminary phase of this study to validate the experimental model with the aspect ratio of 1:1. The coverage angle of the control points for the simple prediction charts technique and stochastic deep learning model was different but the position of the control points was identical because the objective of this study was to cover the angles from 0° to 360° but the simple prediction charts only covered up to 0°, 15°, 30° and 45°.

5.2.1 Noise Emission Levels from Individual Machine

The sound power level (L_w) of the machines for earthmoving machinery was determined by using British Standards Institution (2008). The sound power level was the most important parameter as it was the main noise source; it was applied in the calculation to predict the equivalent continuous noise level (L_{Aeq}) at a selected location. To perform the calculation of sound power level, determination of the basic length (l) of the earth-moving machine is required as

shown in Appendix A. The measurement radius of the machine was 16 m if the basic length of the machine was greater than 4.0 m, whereas if the basic length falls in the range of 1.5 m to 4.0 m, then the measurement radius will be determined as 10.0 m. Then, the coordinates of the six receiving points were calculated by using Table 3.3. The machine was requested to be operated at full power throughout the measurement duration of 30 seconds for each point per the British Standards Institution (2008). All the data were recorded by using a Larson Davis Type 1 sound level meter that conforms with the recommendations of the International Electrotechnical Commission (2002) stipulated by the Department of Environment (2019).

The important information about the machines such as the machine manufacturer, machine model number, engine net power at corresponding revolution per minute was recorded and presented in Table 5.1 as stated in British Standards Institution (2008) and the information was verified by the personnel of the construction sites. Table 5.2 tabulated the input data of sound power level and the results of calculation for each machine's sound power level. All the machine emitted noise levels were recorded during the lunch break so that the irrelevant noise sources were excluded during the measurement. The machine emitted noise levels were applied in Equation 3.3 to calculate the $L'_{p(ST)}$ of the machines. Next, ΔL_p was computed by finding the difference between the $L'_{p(ST)}$ and the mean equivalent background noise, $\overline{L_{p(B)}}$. The ΔL_p of all the machines are greater than 15 dBA, which indicated that the loudness of the background noise was insignificant to cause an impact on the determination of sound power level. Consequently, the background noise

correction factor, K_1 for all the machines was determined as 0 by referring to Table 3.4.

There were six crawler excavators with excavator buckets (CE1, 2, 3, 4, 5, 6), three crawler excavators with rock breakers (CERB1, 2, 3), one back pusher (BP1), one road roller (RR1), and three rotary piling machines (PM1, 2, 3) involved in ten case studies. The sound power level of the machines ranged between 101.4 dBA and 110.5 dBA. The crawler excavators with excavator bucket were involved in case studies 1, 2, 3, 4, 5, 6 and 7 while the back pusher and road roller were only used in case studies 5 and 6; as for case study 8, three crawler excavators with rock breakers were involved. Lastly, three rotary piling machines were operated during the activities in case studies 9 and 10 and generated the highest sound power level (110.5 dBA, 109.8 dBA and 109.2 dBA) among the case studies; this was due to the larger machine engine power (194 kW – 302 kW) as compared to other machines (54 kW – 200 kW). Moreover, the rotary shaft of the rotary piling machine may induce additional noise. Lastly, the average age of all the machines ranged between 3 to 6 years.

Table 5.1: Construction activities and sound power level of the machines

Case Study	Types of Machines	Brand of the Machine	Model of Machine	Engine Power (kW)	Engine speed (RPM)
1	Crawler Excavator (CE1)	Hitachi	Zaxis 200LC	118	2000
2, 3	Crawler Excavator (CE2)	Komatsu	PC300	180	1900
4	Crawler Excavator (CE3) (CE4)	Komatsu Hitachi	PC300 Zaxis 200LC	180 118	1900 2000
	Crawler Excavator (CE5)	Volvo	EC250B	168	1600
5, 6	Back-Pusher (BP1)	New Holland	5610	54	1900
	Road Roller (RR1)	Caterpillar	CS54B	98	1800
7	Crawler Excavator (CE6)	Hitachi	Zaxis 200LC	118	2000
8	Crawler excavator with rock breaker (CERB1) (CERB2) (CERB3)	Doosan Sumitomo Kobelco	DX300LCA SSH330 SK250	147 200 137	1900 2000 2100
9	Rotary Piling Machine (PM1) (PM2)	Sinovo Sinovo	TR400F TR400F	302 302	2300 2300
10	Rotary Piling Machine (PM3)	Bauer	BG 25	194	220

Table 5.2: Input data for the sound power level of the earth-moving machine

Machine	l (m)	Radius (m)	L_{Aeq} at Different Points (dBA)						$L'_{p(ST)}$ (dBA)	$\overline{L_{p(B)}}$ (dBA)	ΔL_p (dBA)	L_w (dBA)
			1	2	3	4	5	6				
CE1	4.2	16	75.4	75.5	75.8	75.1	76.7	76.5	75.9	54	21.9	107.9
CE2	4.2	16	76.8	76.7	77.2	77.1	77.7	77.9	77.3	47	30.3	105.2
CE3	4.2	16	72.8	73.1	72.7	72.9	75.8	76.0	74.5	47.1	27.4	106.2
CE4	4.1	16	72.7	71.2	73.4	72.8	76.2	76.2	74.2	47.1	27.1	106.2
CE5	4.6	16	71.7	73.4	72.5	72.7	74.5	74.9	73.4	51.1	22.3	101.4
BP1	2.8	10	76.4	76.3	75.9	75.7	82.8	82.9	79.6	51.1	28.5	107.6
RR1	2.8	10	75.9	76.3	76.1	76.3	76.7	76.7	76.3	51.1	25.2	104.3
CE6	4.6	16	75.1	75.8	75.3	75.4	76.5	76.9	75.9	54.1	21.8	107.9
CERB1	4.9	16	75.4	76.5	77.2	76.7	80.3	79.4	77.9	57.7	20.2	109.9
CERB2	4.9	16	74.5	74.7	74.5	73.5	76.5	77.0	75.3	57.7	17.6	107.3
CERB3	4.9	16	75.2	75.5	75.8	75.3	76.5	76.9	75.9	57.7	18.2	107.9
PM1	5.1	16	75.9	76.6	76.5	76.2	78.9	78.6	77.3	61.8	15.5	109.2
PM2	5.1	16	76.8	76.4	76.9	76.2	79.7	79.6	77.2	61.8	15.4	109.8
PM3	4.4	16	78.3	78.2	77.5	77.7	79.3	79.8	78.5	61.8	16.7	110.5

5.2.2 Construction Activity of the Case Studies

The types of construction work and machines, site aspect ratio and the number of employees involved in different case studies are tabulated in Table 5.3. The activity of the crawler excavator (CE1) in case study 1 was to excavate trenches with a width of 2.0 m and relocate the precast concrete drain channel to the designated area. Followed by case studies 2 and 3, the crawler excavator (CE2) excavated the sewerage trench with a width of 1.5 m and installed the sanitary pipe at the trench. As for case study 4, two crawler excavators (CE3 and CE4) were operated to construct the water distribution system involving trench excavation, sheet piles installation, hoisting and placement of the water pipe.

Next, a crawler excavator with an excavator bucket (CE5) for minimal excavation, a back pusher (BP1) to push the crusher run on the path, and a road roller (RR1) to smoothen and compact the crusher run was operated in case study 5 and 6. Next, the activity of case study 7 was site clearance and one crawler excavator (CE6) was involved. The activity in case study 8 consisted of three crawler excavators with a rock breaker to break and extract the rocks on the mountain. Lastly, three piling machines (CERB1, 2 and 3) were operated in case studies 9 and 10 to bore the piling hole with the dimension of 1200 mm and 750 mm.

Table 5.3: Description of the case studies

Case Study	Types of Construction Works	w:d ratio	Types of Machines	Construction Activity	No. of employees involved
1	Drainage System	1:1	CE1	Excavation of trench, hoisting and placing the precast drain	4
2, 3	Sewerage System	1:2, 2:1	CE2	Excavation of trench and hoisting of sanitary sewer	5
4	Water Distribution System	4:1	CE2	Hoisting water pipe Excavating trench and installing sheet pile	6
			CE4	Minimal excavation	
5, 6	Road Construction	1:8, 8:1	BP1	Pushing the crusher run on the path	3
			RR1	Rolling and compacting the crusher	

Table 5.3: Description of the case studies (Cont'd)

7	Site Clearance	4:1	CE 6	Removing debris	2
					1
8	Rock Breaking	2:1	CERB1 CERB2 CERB3	Rock breaking	1
					1
9	Bored Pile	1:2	PM1 PM2	Pile Boring	4
10	Bored Pile	1:4	PM 3	Pile Boring	2

5.3 Background Noise of Construction Site

The background noise of each construction site was recorded before the commencement of any construction activities; the measurement was conducted at 7.00 a.m and lasted for 30 minutes. The background noise of the construction sites was tabulated in Table 5.4. Based on the measurement, the highest background noise among all the case studies was 61.8 dBA from case studies 9 and 10 because the construction site was located right next to a highway and railway track. Case studies 9 and 10 were both conducted at the same construction site and hence, the background noise was identical. Followed by case study 8, the background noise was 57.7 dBA as the site was a confined area and surrounded by buildings which created a reflection noise effect. Case study 7 had a background noise of 54.1 dBA because there were existing buildings located 30 m away from the sub-area that may reflect the noise. Next, case study 1 had the background noise of

54.0 dBA because it was due to the traffic noise as the sub-area was located 20 m away from the entrance of the construction site. Next, the background noise for both case studies 5 and 6 was 51.1 dBA due to the loud natural ambient noise of the animals and birds at the same construction site. For case study 4, the background noise is slightly lower than in the previous case studies because the construction activity was located in a residential area. Lastly, case studies 2 and 3 had the lowest background noise of 47.0 dBA because the sub-area was an isolated area located 50 m away from other construction activities and the background noise of both case studies was taken at the same construction site.

Table 5.4: Background noise of the construction sites

Case Study	Background Noise (dBA)	L_{min} (dBA)	L_{max} (dBA)	L_{10} (dBA)	L_{50} (dBA)	L_{90} (dBA)
1	54.0	32.7	80.0	52.0	41.1	37.3
2	47.0	39.2	60.9	49.4	45.5	43.0
3	47.0	39.2	60.9	49.4	45.5	43.0
4	47.1	43.9	70.8	48.6	45.7	45.0
5	51.1	40.2	74.6	53.1	49.9	44.7
6	51.1	40.2	74.6	53.1	49.9	44.7
7	54.1	43.2	77.6	56.1	52.9	47.7
8	57.7	54.6	67	58.8	57.4	56.3
9	61.8	56.4	78.6	61.8	59.4	58.1
10	61.8	56.4	78.6	61.8	59.4	58.1

5.4 Noise Emission Levels from Construction Activities

Table 5.5 summarizes the equivalent continuous A-weighted sound pressure level (L_{AFeq}), sound pressure level that exceeded 10 %, 50 % and 90 %

measurement duration (L_{10} , L_{50} , L_{90}) of the time of measurement duration, root mean squared maximum sound level (L_{max}), and root mean squared minimum sound pressure level (L_{min}), for each case study.

Based on the measurement, case study 8 had the highest equivalent continuous noise level of 86.9 dBA and a maximum sound level of 97.0 dBA among all the case studies. The main cause of the loud noise was due to the nature of the activity as it was breaking and extracting the rocks. On top of that, the noise levels were generated by three crawler excavators with rock breakers which broke the rock frequently and intensively during the activity and hence cause a high level of noise. Although, the operators were well-equipped with hearing protection equipment; however, they were exposed to noise levels that exceeded the permissible noise level stipulated by the Occupational Safety and Health Regulations (2019). Besides, exposure to loud noise may result in physiological issues such as high blood pressure and inconsistency of heartbeat rhythms of the operators (Geetha and Ambika, 2015).

Followed by the second and third noisiest activity, case study 9 had the equivalent continuous noise level of 83.0 dBA among the three control points and 100.3 dBA for the maximum noise level whereas the equivalent continuous and maximum noise levels of case study 10 were 81.6 dBA and 98.7 dBA. The loud noises were mainly induced by the rotary shaft and the engine of the piling machine during the piling boring process. Besides, the high impact noise was generated when the operator rotated the bored pile bucket back and forth repeatedly to remove the core rock and soil. For case study 9, two piling

machine operators and 2 general workers were executing the construction activity; although they were under the exposure to high noise levels that were close to the permissible noise level (85 dBA/ 8 hours) they did not wear hearing protection equipment, as the operators mentioned that the hearing protection equipment was not provided.

The noise levels of case studies 1, 2, 3 and 7 ranged between 69.3 dBA and 77.8 dBA, and a machine operator and two to five workers were involved in each case study. However, hearing protection devices were absent among the operators and workers as they mentioned that the noise levels were tolerable. Moreover, this phenomenon arose from a lack of personal safety concerns (Themann and Masterson, 2019) because they could not self-perceived the potential adverse effects of noise exposure. Although the obligation of the employer is stated by the Department of Occupational Safety and Health (2019), the hearing protection devices were not provided to the site personnel. For case study 4, the highest noise level of 79.8 dBA and a maximum noise level of 105.2 dBA were among the three control points of the case study. This has resulted from the high impact noise caused by the excavator during the sheet pile installation. The operators were equipped with earmuffs whereas the other four workers which were the supervisor, pipe welder, traffic controller and the general worker did not equip themselves with hearing protection equipment. According to the observation, the working duration of the employees was 8 hours per day. Prolonged exposure to high noise levels may result in workers suffering from noise-induced hearing loss problems (Johnson and Morata, 2010; Macca et al., 2015; Gan and Mannino, 2018).

The lowest noise levels among all the case studies were found to be 69.3 dBA for case studies 5 and 6. Besides that, the maximum sound level was only 82.2 dBA. Although three machines such as an excavator, road roller and back pusher were operated during the road construction activity, there was no high impact noise being generated during the activity. The noise was mainly induced by the machine engines during the soil compaction, placement of crusher run and minimal excavation works. There were three operators equipped with hearing protection devices and general workers were not involved in this activity. The noise levels of this case study were below the permissible level of 85 dBA (8 hours) indicating that the workplace was less harmful as compared to other case studies.

Table 5.5: Summary of the sound pressure levels at the control points for the case studies

Case Study	Control Points	$L_{A_{\text{F}_{\text{eq}}}}$ (dBA)	L_{min} (dBA)	L_{max} (dBA)	L_{10} (dBA)	L_{50} (dBA)	L_{90} (dBA)
1	1	75.5	59.5	101.0	78.1	71.1	63.8
	2	71.5	64.8	87.4	73.6	70.3	68.5
	3	70.1	56.3	96.8	74.0	65.3	62.7
2	1	75.4	66	94.1	76.7	74.1	71.2
	2	75.0	65	98.2	76.5	72.8	69.4
	3	69.9	61.7	87.0	71.9	68.3	64.5
3	1	75.6	66.2	91.2	78.4	73.2	71.2
	2	74.5	62.2	95.2	76.2	72.7	69.1
	3	69.3	59.1	90.9	71.4	66.9	67.0
4	1	79.8	65.8	103.2	78.9	77.2	68.9
	2	77.9	59.5	105.2	76.0	72.0	66.4
	3	75.2	62	99.5	75.3	71.3	66.0

Table 5.5: Summary of the sound pressure levels at the control points for the case studies (Cont'd)

5	1	73.2	61.1	94.7	78.1	74.3	69.3
	2	71.4	58.9	82.2	72.3	69.0	65.4
	3	69.3	62.9	87.7	70.9	68.6	66.5
6	1	70.4	63.2	91.3	75.3	71.5	66.8
	2	68.9	59.6	81.7	72.1	66.8	65.6
	3	66.8	63.2	85.3	68.1	65.4	61.3
7	1	77.8	65.9	94.9	81.3	75.3	67.5
	2	72.4	62.9	88.0	74.4	69.9	66.2
	3	72.2	68.6	86.1	72.1	71.6	71.1
8	1	86.9	69.6	97.0	92.3	88.7	82.5
	2	85.4	62.4	97.4	90.0	85.9	70.8
	3	82.9	65.5	94.9	89.0	82.8	68.4
9	1	79.9	66.9	95.5	82.5	77.7	75.1
	2	76.8	72.6	95.7	77.0	75.3	74.3
	3	83.0	71.9	100.3	82.2	78.9	74.8
10	1	81.6	66.3	98.7	87.8	83.4	81.5
	2	80.6	68.4	97.1	85.4	80.0	76.4
	3	76.0	71.5	94.9	82.3	77.5	74.4

5.5 Construction Noise Prediction using Simple Prediction Charts

The important parameters applied to predict the sound pressure level and standard deviation, such as the machine sound power level (L_w), width to depth ratio of the sub-area (w:d ratio), coverage angle (θ), the distance between the noise receiver and the site centre (r) were presented in Table 5.6. The first step of the simple prediction technique was to utilize the given parameters and obtain the standard deviation (σ) and mean level deviation (ΔL) from the simple prediction charts in Appendix B. Then, L_w and ΔL were applied in Equation 3.5

to compute the control point sound pressure level (L_p). When the sub-area consisted of more than one earth-moving machine, the L_p and σ were combined using Equations 3.6 and 3.7 respectively.

For CS1, CP1, 2 and 3 were selected to cover the angle of 29° , 34° and 0° as exemplified in Figure 5.1. The distance between the site centre and control points was 13.87 m, 23.25 m and 27.61 m. The predicted L_{AFeq} for CP1, 2 and 3 was 77.1 dBA, 72.6 dBA and 71.1 dBA whereas the standard deviations were 3.5 dBA, 2.3 dBA and 2.0 dBA. The selection of CP 1, 2 and 3 covering 0° , 34° and 44° for CS2 were located parallelly to the sub-area based on the varied distance of 8.00 m, 9.32 m and 19.87 m as depicted in Figure 5.2. The prediction of L_{AFeq} for each control point was 78.1 dBA, 77.1 dBA and 71.1 dBA whereas the standard deviation was 4.0 dBA for the control points.

The coverage angle of the control points in CS3 was 44° , 18° and 28° , at distances of 9.58 m, 12.85 m and 22.46 m; the condition of the sub-area was similar to CS2 as shown in Figures 5.2 and 5.3. At control point 1, 2 and 3, the predicted L_{AFeq} was 77.6 dBA, 75.8 dBA, 70.3 dBA; the σ was 2.0 dBA, 5 dBA, 3.8 dBA. For case study 4, the coverage angles of the control points were 38° , 28° and 44° as depicted in Figure 5.4. Control points 1 and 2 were located near the centre of the site at distances of 10.19 m and 13.20 m whereas control point 3 was placed at 17.52 m offset from the site centre., the sound pressure level and standard deviation of each control point were combined, providing the L_{AFeq} of 78.4 dBA, 76.7 dBA and 76.2 respectively; σ of 6.0 dBA at control point 1, and 4.0 dBA for control point 2 and 3.

The control points (CP1, CP2, CP3) of CS5 were placed approximately 12.0 m away from each other (20.49 m, 32.80 m and 44.36m), covering the angle of 44°, 27°, and 18° as demonstrated in Figure 5.5. The combined sound pressure level for CP1, CP2 and CP3 were 76.1 dBA, 73.0 dBA and 70.8 whereas the standard deviations were 7.0 dBA for CP1, 9.0 dBA for CP2 and CP3. Followed by case 6, the orientation of the site aspect ratio was rotated and the control points were set at different locations with coverage angles of 32°, 19° and 45° and distances of 18.08 m, 29.41 m and 47.15 m respectively as illustrated in Figure 5.6. Similar to CS5, the sound pressure level and standard deviation at each control point were combined providing the L_{AFeq} of 71.6 dBA, 69.9 dBA and 68.3 dBA at CP1, CP2, CP3 consecutively; 8.0 dBA, 7.0 dBA and 8.0 dBA of the σ at each control point sequentially.

Figure 5.7 shows that case study 7 consists of control 1 and 3 which covered 0° and the distance of 7.50 m and 18.64 m, whereas control point 2 covered 39° at 17.89 m away from the site centre. CP1 of CS7 had the L_{AFeq} of 78.4 dBA, 74.1 dBA and 73.8 dBA at CP2 and CP3. As for the standard deviation, the values were 4.0 dBA, 3.0 dBA and 1.5 dBA at CP1, CP2 and CP3. Next, the interval length between the noise receiver and the site centre for the control points 1, 2, 3 in case study 8 was 9.86 m, 9.86 m and 15.00 m covering the angle of 30° at CP1 and 2, whereas CP3 covered the angle of 0° as illustrated in Figure 5.8. The combined sound pressure level at CP1 and CP2 were 83.7 dBA, and at CP3 the sound pressure level was 81.0 dBA; whereas the standard deviations were 8.0 dBA for CP1, and 7.0 dBA for CP2 and CP3.

As for case study 9, the control points were located at the places with a hard ground surface covering the angle of 10°, 0°, and 40° at the distance of 19.61 m, 18.50 m and 11.63 m as shown in Figure 5.9. By combining the individual sound pressure level at each control point, the value of 77.9 dBA, 78.4 dBA and 82.5 dBA were obtained for CP1, CP2 and CP3. As for the combined standard deviation, the values were 7.0 dBA for CP1 and 2 whereas CP3 had a 6.0 dBA standard deviation. Lastly, the coverage angles of the control points in case study 10 were 0°, 41° and 29°; the location of control points was located at 7.00 m, 8.70 m and 21.51 m away from the site centre as depicted in Figure 5.10. The sound pressure level and standard deviation of 83.0 dBA and 4.5 dBA were obtained for CP1; L_{AFeq} of 80.6 dBA and σ of 5.5 dBA at CP2; L_{AFeq} of 76.8 dBA and σ of 1.0 dBA at CP3.

Table 5.6: Noise prediction using simple prediction charts

CS	CP	L_w	w:d ratio	θ	r	r/w ratio	σ	Combined σ	ΔL	L_p	Combined L_p
1	CP1	107.9	1:1	29	13.87	0.694	3.5	3.5	0.08	77.1	77.1
	CP2		1:1	34	23.25	1.163	2.3	2.3	0.08	72.6	72.6
	CP3		1:1	0	27.61	1.381	2.0	2.0	0.07	71.1	71.1
2	CP1	105.2	2:1	0	8.00	0.400	4.0	4.0	-1.40	78.1	77.7
	CP2		2:1	34	9.32	0.466	4.0	4.0	-0.75	77.1	77.1
	CP3		2:1	44	19.87	0.994	4.0	4.0	-0.10	71.1	71.1
3	CP1	105.2	1:2	44	9.58	0.958	2.0	2.0	0.00	77.6	77.6
	CP2		1:2	18	12.85	1.285	5.0	5.0	0.80	75.8	75.8
	CP3		1:2	28	22.46	2.246	3.8	3.8	0.10	70.3	70.3

Table 5.6: Noise prediction using simple prediction charts (Cont'd)

CS	CP	L_w	w:d	θ	r	r/w	σ	Combined	ΔL	L_p	Combined
			ratio					σ			L_p
4	CP1	106.2	4:1	38	10.19	0.255	4.0		-2.60	75.4	
	CP2		4:1	28	13.20	0.330	2.8	6.0	-2.00	73.8	78.4
	CP3		4:1	44	17.52	1.752	3.0	4.0	-0.1	73.2	76.7
	CP1	106.1	4:1	38	10.19	0.255	4.0	4.0	-2.60	75.3	76.2
	CP2		4:1	28	13.20	0.330	2.8		-2.00	73.7	
	CP3		4:1	44	17.52	1.752	3.0		-0.1	73.1	
5	CP1	105.5	1:8	44	20.49	1.205	4.0		-0.50	70.8	
	CP2		1:8	27	32.80	1.929	5.0		0.50	67.7	
	CP3		1:8	18	44.36	2.609	5.0		1.00	65.6	
	CP1	107.6	1:8	44	20.49	1.205	4.0	7.0	-0.50	72.9	76.1
	CP2		1:8	27	32.80	1.929	5.0	9.0	0.50	69.8	73.0
	CP3		1:8	18	44.36	2.609	5.0	9.0	1.00	67.7	70.8
	CP1	104.3	1:8	44	20.49	1.205	4.0		-0.50	69.6	
	CP2		1:8	27	32.80	1.929	5.0		0.50	66.5	
	CP3		1:8	18	44.36	2.609	5.0		1.00	64.4	
6	CP1	105.5	8:1	32	18.08	0.133	4.5		-6.00	66.4	
	CP2		8:1	19	29.41	0.216	4.3		-3.50	64.6	
	CP3		8:1	45	47.15	0.347	4.5		-1.00	63.0	
	CP1	107.6	8:1	32	18.08	0.133	4.5	8.0	-6.00	68.5	71.6
	CP2		8:1	19	29.41	0.216	4.3	7.0	-3.50	66.7	69.9
	CP3		8:1	45	47.15	0.347	4.5	8.0	-1.00	65.1	68.3
	CP1	104.3	8:1	32	18.08	0.133	4.5		-6.00	65.2	
	CP2		8:1	19	29.41	0.216	4.3		-3.50	63.4	
	CP3		8:1	45	47.15	0.347	4.3		-1.00	61.8	
7	CP1	107.9	4:1	0	7.50	0.188	4.0	4.0	-4.00	78.4	78.4
	CP2		4:1	39	17.89	0.447	3.0	3.0	-0.80	74.1	74.1
	CP3		4:1	0	18.64	0.466	1.5	1.5	-0.70	73.8	73.8

Table 5.6: Noise prediction using simple prediction charts (Cont'd)

CS	CP	L_w	$w:d$		r	r/w	σ	Combined		Combined	
			ratio	θ				σ	ΔL	L_p	L_p
	CP1	109.9	2:1	30	9.86	0.329	4.5		-1.75	80.3	
	CP2		2:1	30	9.86	0.329	4.0		-1.75	80.3	
	CP3		2:1	0	15.00	1.506	5.0		0.25	74.3	
8	CP1	107.3	2:1	30	9.86	0.329	4.0	8	-1.75	77.7	83.7
	CP2		2:1	30	9.86	0.329	4.5	7	-1.75	77.7	83.7
	CP3		2:1	0	15.00	1.506	5.0	7	0.25	71.7	81.0
	CP1	107.9	2:1	30	9.86	0.329	4.5		-1.75	78.3	
	CP2		2:1	30	9.86	0.329	4.0		-1.75	78.3	
	CP3		2:1	0	15.00	1.506	5.0		0.25	72.3	
9	CP1	109.2	2:1	10	19.61	0.654	5.0		-0.75	74.6	
	CP2		1:2	0	18.50	1.233	5.0	7.0	-0.80	75.1	77.9
	CP3		2:1	40	11.63	0.388	4.5	7.0	-0.75	79.1	78.4
	CP1	109.8	2:1	10	19.61	0.654	5.0	6.0	-0.75	75.2	82.5
	CP2		1:2	0	18.50	1.233	5.0		-0.80	75.7	
	CP3		2:1	40	11.63	0.388	4.5		-0.75	79.7	
10	CP1	110.5	4:1	0	7.00	0.175	4.5	4.5	-4.00	81.6	83.0
	CP2		1:4	41	8.70	0.218	5.5	5.5	0.00	83.7	80.6
	CP3		4:1	29	21.51	2.151	1.0	1.0	-0.20	75.6	76.8

Note:

CS = Case study

CP = Control point

L_w = Sound power level of the earth-moving machine (dBA)

$w : d$ ratio = width to depth ratio of the sub-area

θ = Angle ($^\circ$)

r = Distance between receiver and site centre (m)

r/w ratio = Ratio of distance to the width of the sub-area

σ = standard deviation (dBA)

Combined σ = Combined standard deviation where the number of the earth-moving machine was more than 1 dBA (dBA)

ΔL = Mean level deviation (dBA)

L_p = The predicted sound pressure level (dBA)

Combined L_p = The predicted sound pressure level where the number of the earth-moving machine was more than 1 dBA (dBA)

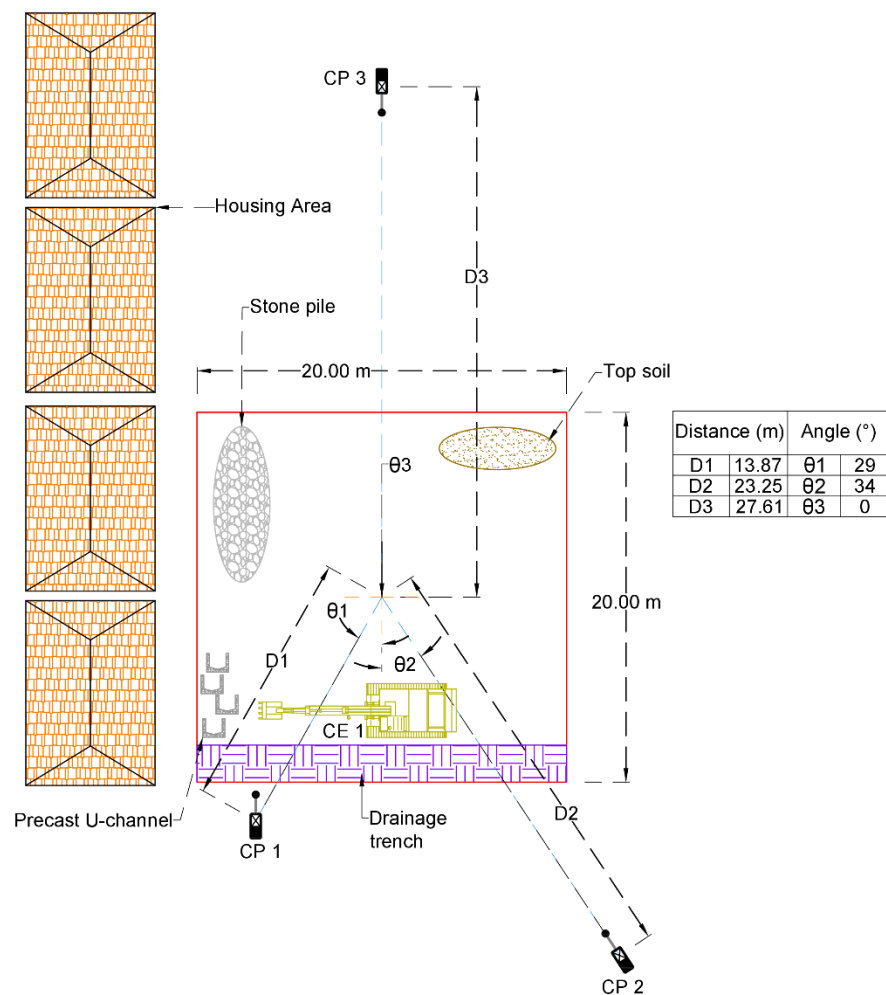


Figure 5.1: Case study 1 for the simple prediction charts technique

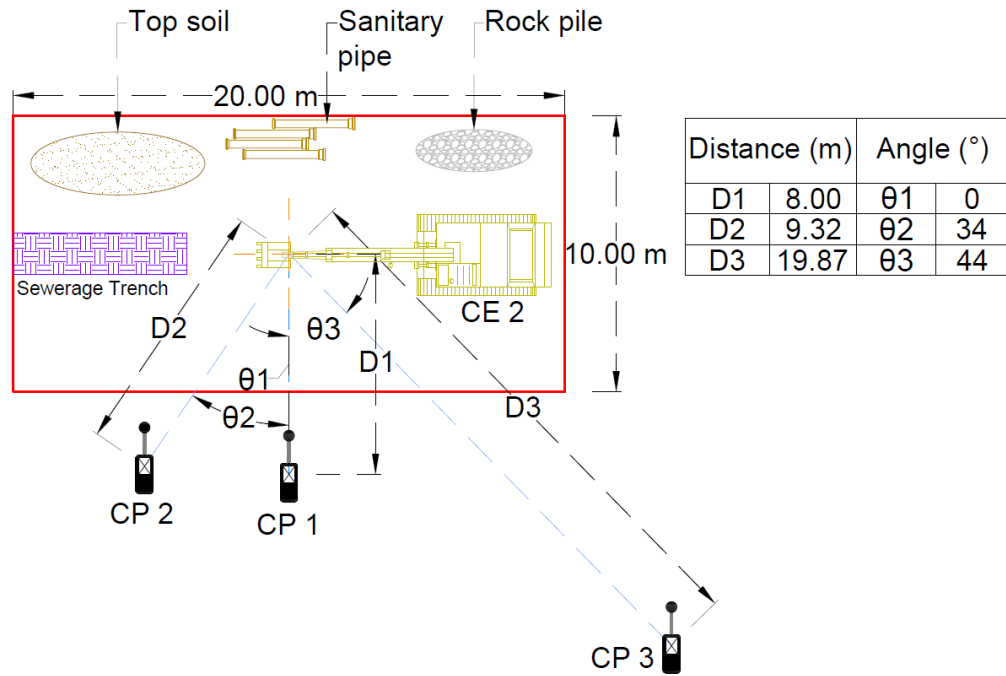


Figure 5.2: Case study 2 for the simple prediction charts technique

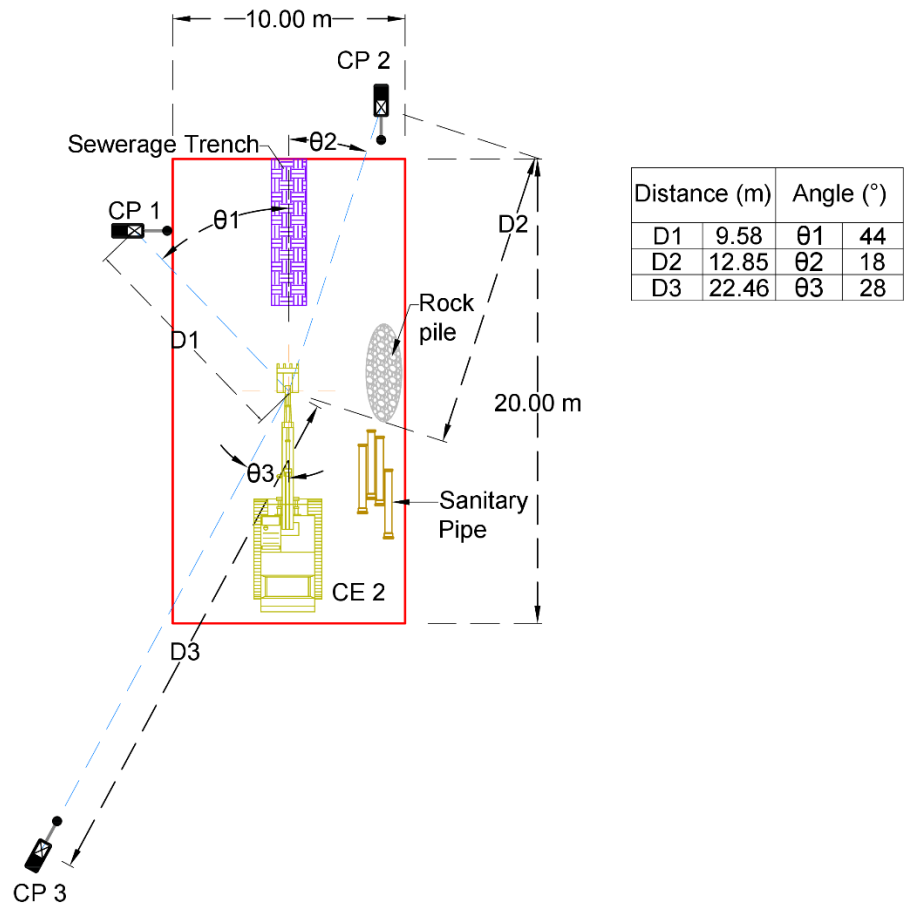


Figure 5.3: Case study 3 for the simple prediction charts technique

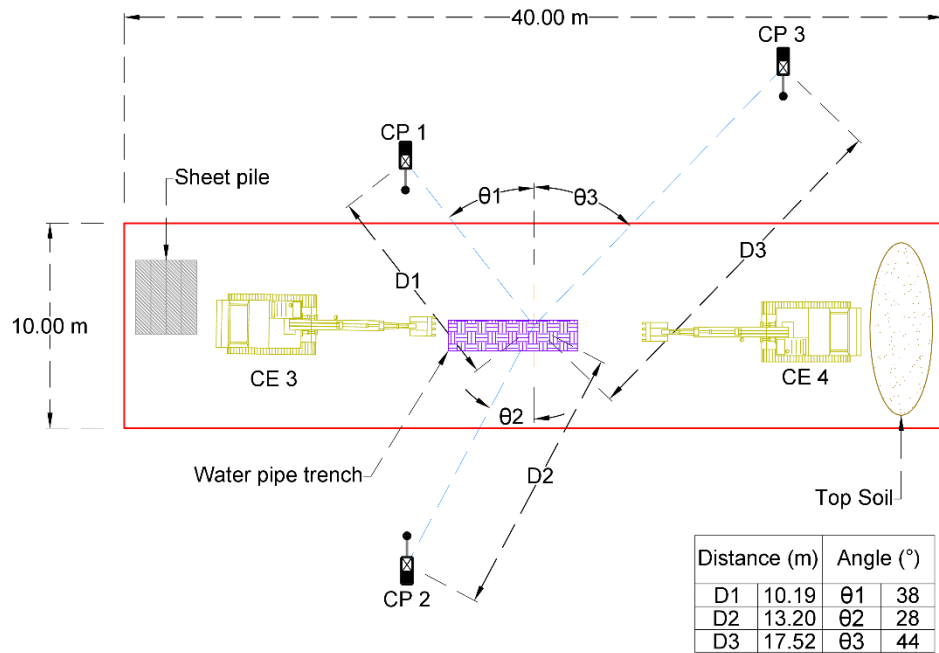


Figure 5.4: Case study 4 for the simple prediction charts technique

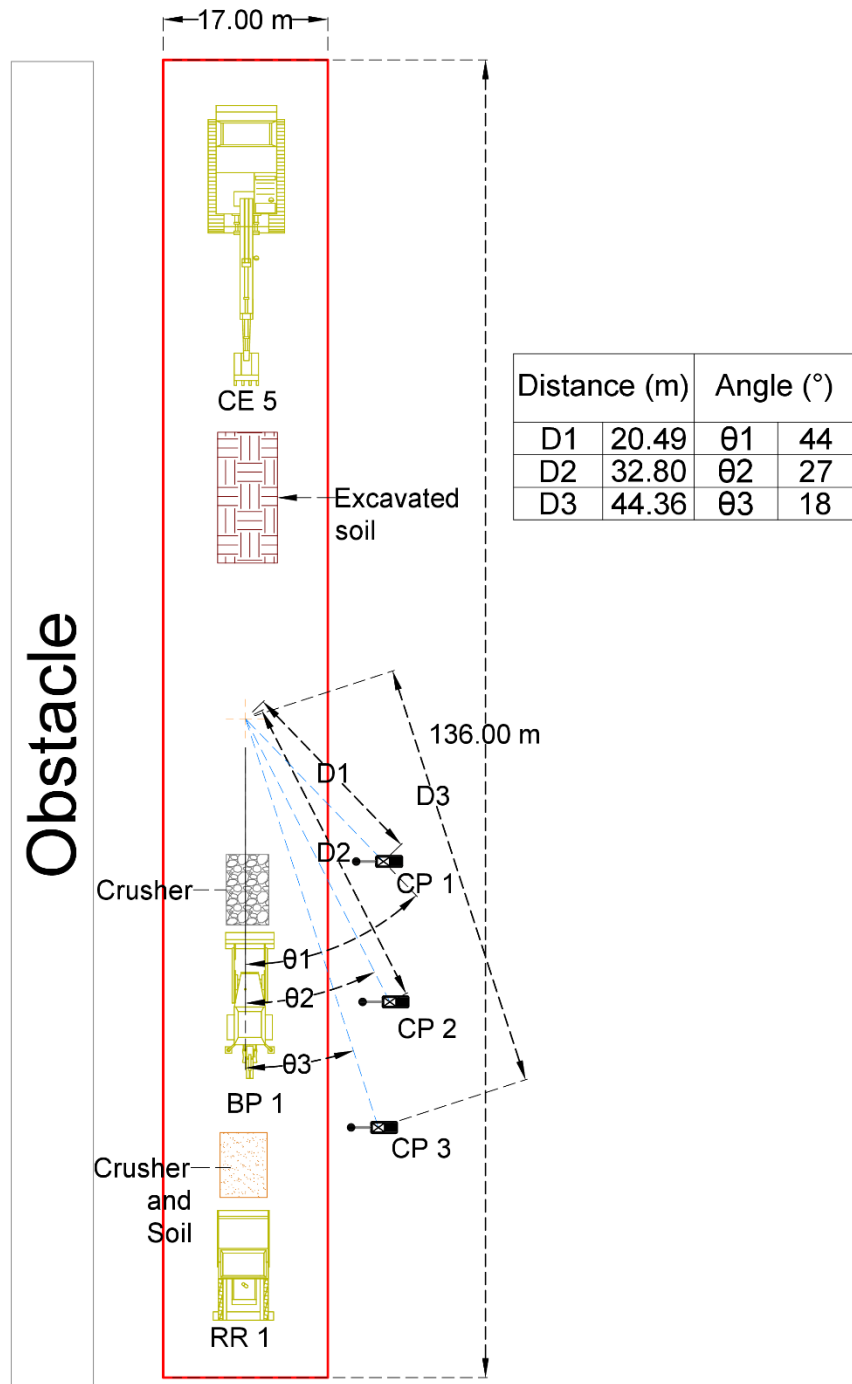


Figure 5.5: Case study 5 for the simple prediction charts technique

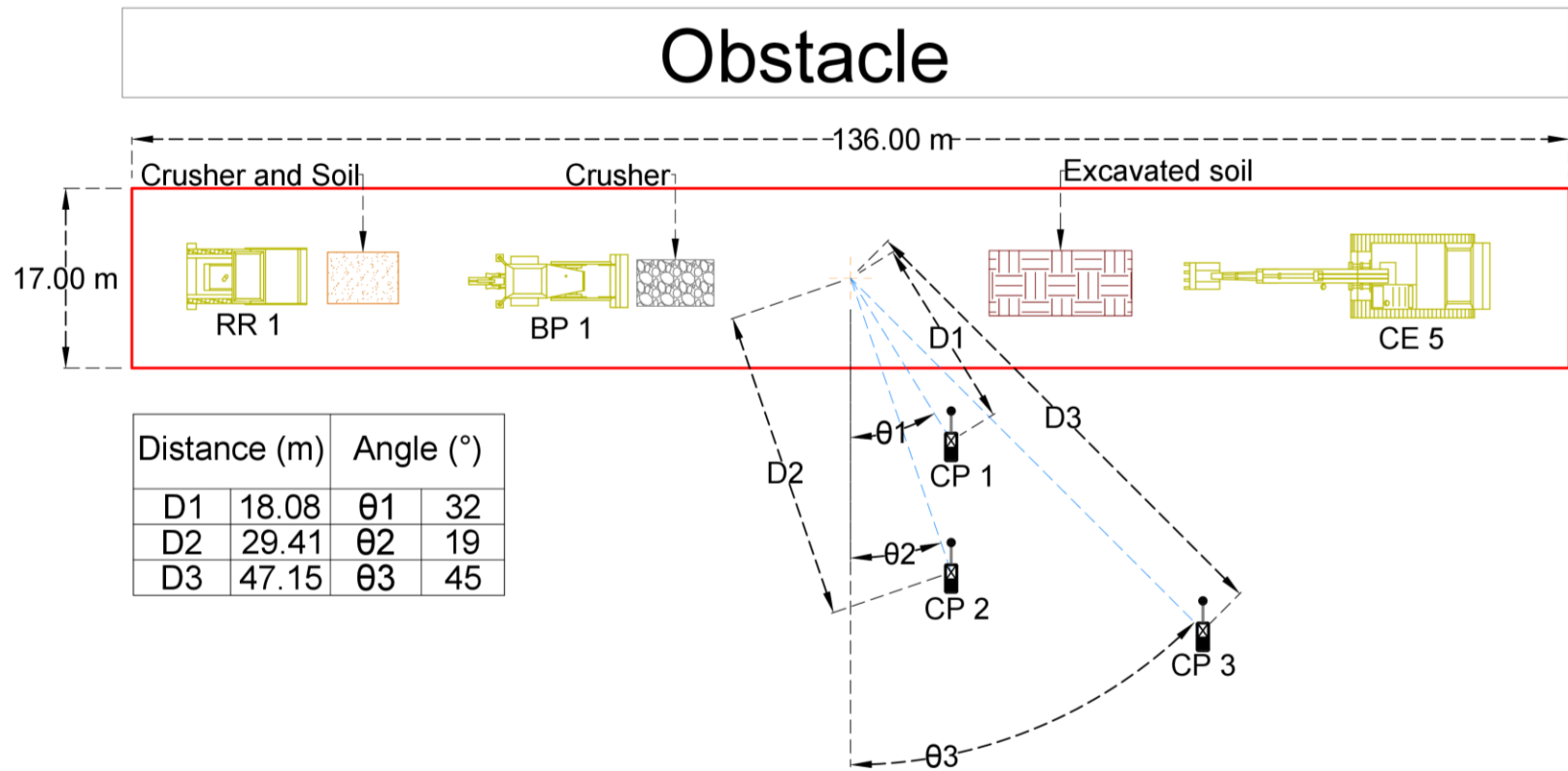


Figure 5.6: Case study 6 for the simple prediction charts technique

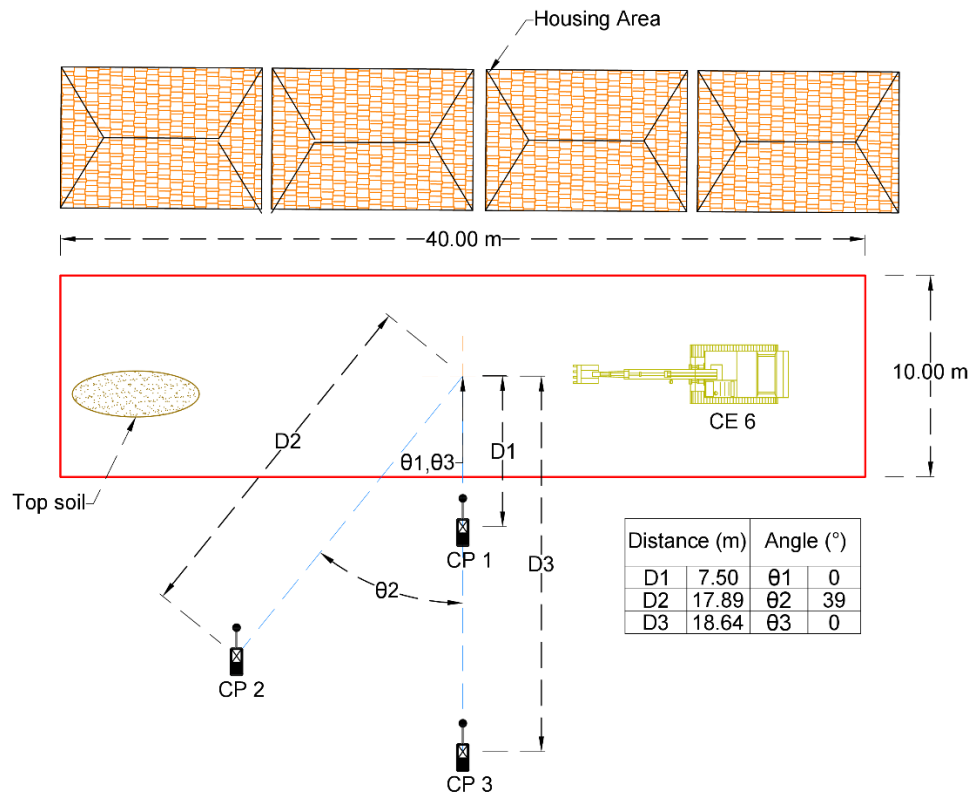


Figure 5.7: Case study 7 for the simple prediction charts technique

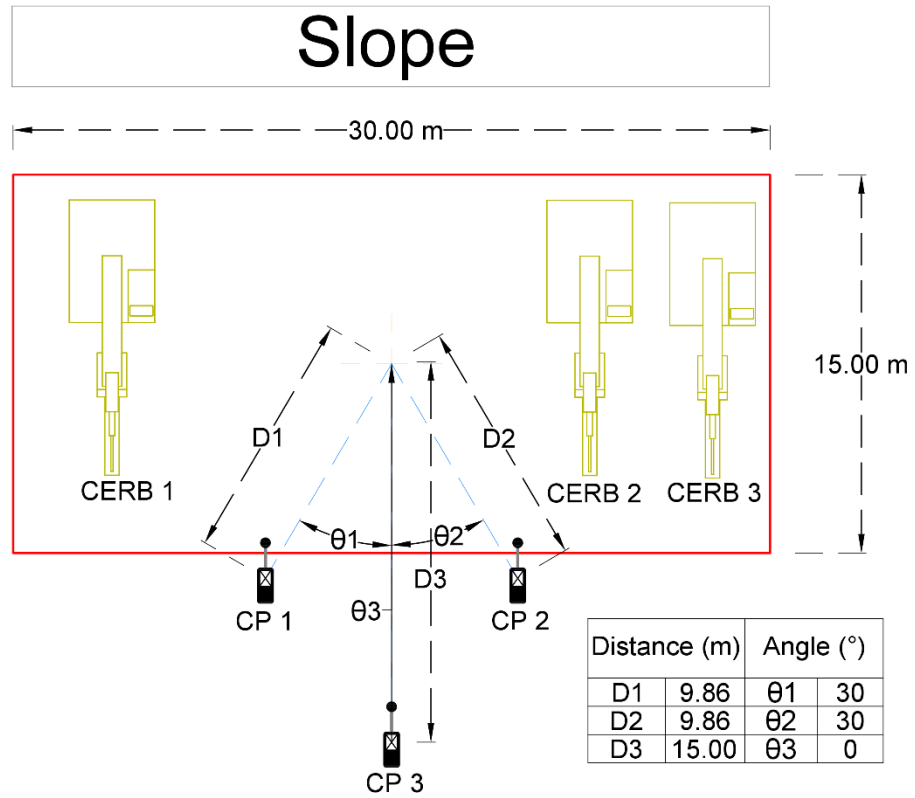


Figure 5.8: Case study 8 for the simple prediction charts technique

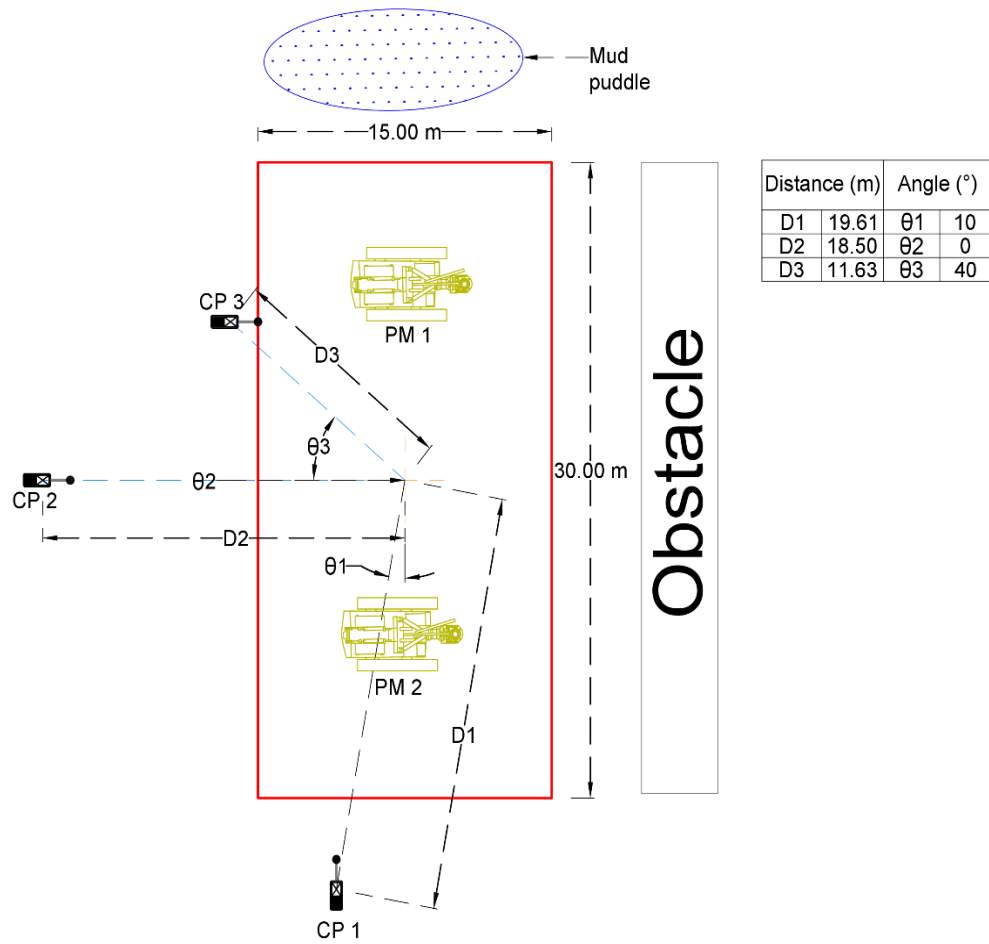


Figure 5.9: Case study 9 for the simple prediction charts technique

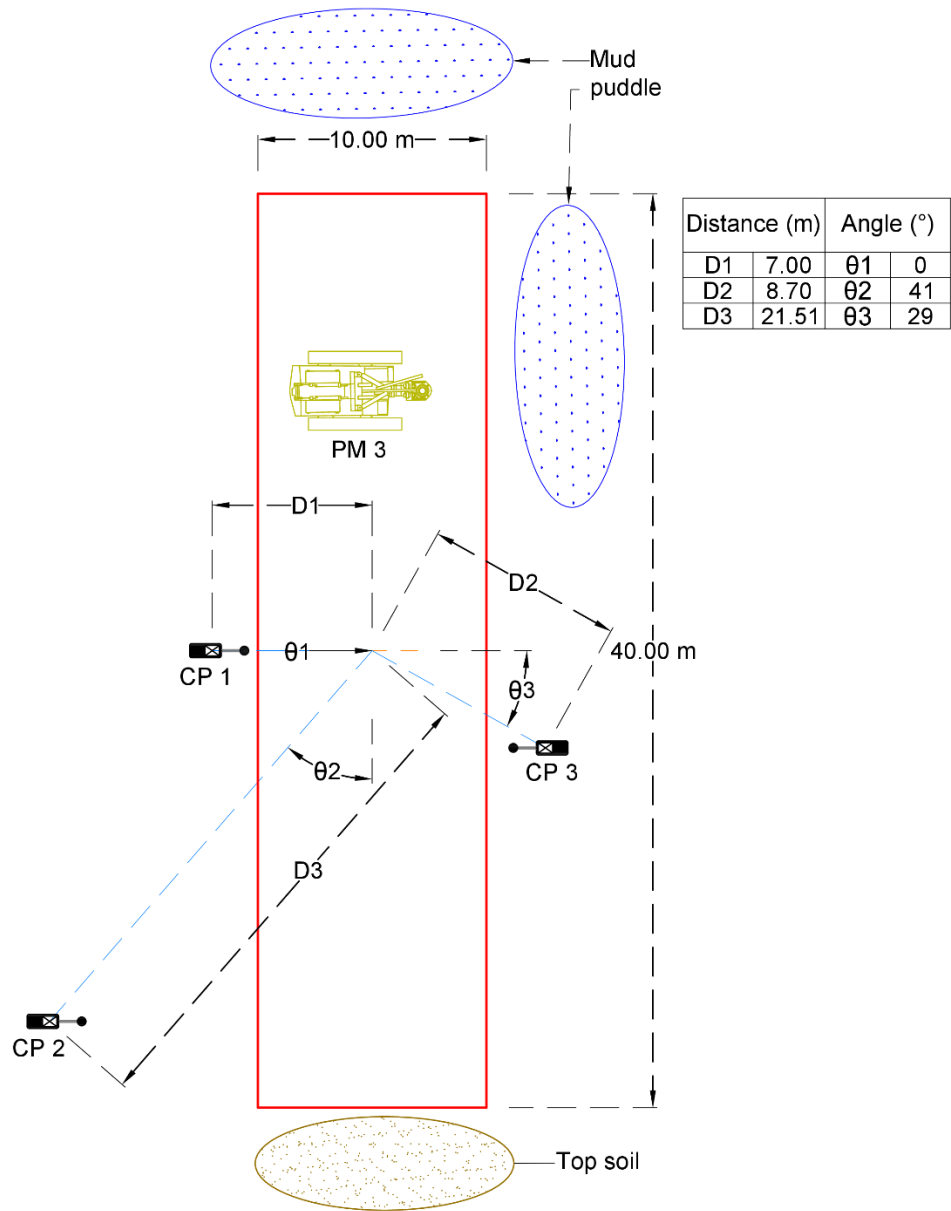


Figure 5.10: Case study 10 for the simple prediction charts technique

5.6 Construction Noise Prediction using Stochastic Deep Learning Model

To dictate the sound pressure level (L_{AFeq}) and the standard deviation (σ) at control points using the stochastic deep learning model, these parameters such as the number of machines in the sub-area, the machine sound power level (L_w), the distance between the noise receiver and the site centre (r), the width of the sub-area (w), coverage angle (θ), the probability of the machine duty cycle operating at full power, idling and off (P_{on} , P_{idle} , P_{off}) were presented in Table 5.7. The application of the model started by loading the trained model (.h5 file format) into Spyder and the execution of the program. Once the execution begins, the user is required to enter the parameters as stated. Upon the identification of the parameters, the model will predict the L_{AFeq} using Equation 3.5 and σ of the control point, and if there is more than one earth-moving machine involved within the sub-area, then the L_{AFeq} and σ of these control points (CP) will be combined using Equations 3.6 and 3.7 correspondingly.

The prediction from the stochastic deep learning model was compared with the actual measurement. The determination of site aspect ratio and control points were determined based on the activities and movement of the earth-moving machines. The operational duration for the earth-moving machines was recorded by using a stopwatch every 30 minutes. The proportion of the duty cycle was then converted to the probability values as P_{on} , P_{idle} and P_{off} having the maximum cumulative value of 1 as shown in Table 5.7. The duty cycle as presented in Table 5.7 was exemplified in case study 1 for clarification.

For CS1, CP1, CP2 and CP3 were selected to cover the angle of 241°, 304° and 90° as shown in Figure 5.11. This is because there were houses located on the left side of the sub-area, the chosen points were suitable for the measurement as the points were clear from the reflective structures and at least 30 m away from other irrelevant noise sources. At control points 1 and 2, CE1 operated at full power for 27 minutes, idled for 3 minutes and did not turn off during the observation providing the P_{on} of 0.9 and P_{idle} of 0.1 and P_{off} of 0.0. For control point 3, CE1 operated at full power throughout the observation providing P_{on} of 1.0. By utilizing the information, the predicted L_{AFeq} for CP1, 2 and 3 was 77.0 dBA, 72.6 dBA and 71.1 dBA whereas the standard deviations were 3.7 dBA, 3.7 dBA and 1.8 dBA.

The selection of CP1, 2 and 3 covering 270°, 236° and 314° for CS2 were located parallelly to the sub-area based on the varied distance of 8.00 m, 9.32 m and 19.87 m. This is because the top side of the sub-area was not suitable for the measurement as it was occupied by the topsoil, sanitary pipes and rock pile as illustrated in Figure 5.12. The prediction of L_{AFeq} for each control point was 77.7 dBA, 77.2 dBA and 71.3 dBA whereas the standard deviations were 4.2 dBA, 4.6 dBA and 3.7 dBA.

The objective of the configuration of each control point in CS3 was to cover the angle of three different quadrants of 134°, 72° and 242° at the distances of 9.58 m, 12.85 m and 22.46 m; the condition of the sub-area was similar to CS2 as demonstrated in Figure 5.12 and 5.13. At control point 1, 2 and 3, the predicted L_{AFeq} was 77.6 dBA, 75.6 dBA, 70.2 dBA; the σ was 3.9 dBA, 3.4

dB, 3.4 dB. For case study 4, the coverage angles of the control points were 128°, 242° and 46° as depicted in Figure 5.14. Control points 1 and 2 were located near the centre of the site at distances of 10.19 m and 13.20 m whereas control point 3 was placed at 17.52 m away from the site centre due to site constraints. Due to more than one machine involved, the sound pressure level and standard deviation of each control point were combined, providing the $L_{A_{\text{Feq}}}$ of 78.8 dBA, 77.2 dBA and 75.4 respectively; σ of 7.0 dBA at control point 1, and 5.8 dBA for control point 2 and 3.

The control points (CP1, CP2, CP3) of CS5 were placed approximately 12.0 m away from each other (20.49 m, 32.80 m and 44.36m), covering the angle of 314°, 297°, and 288°. The purpose was to measure the path covered by the machines throughout the observation duration as demonstrated in Figure 5.15. The combined sound pressure level for CP1, CP2 and CP3 were 72.5 dBA, 71.4 dBA and 70.7 whereas the standard deviations were 24.0 dBA for CP1 and CP2, 27.0 dBA for CP3. Followed by case 6, the orientation of the site aspect ratio was rotated and the control points were set at different locations with coverage angles of 302°, 289° and 315° and distances of 18.08 m, 29.41 m and 47.15 m respectively. The control points were located near the site centre to cover the noise levels from the machines due to the long travelling path of the machines (136.0 m) as shown in Figure 5.16. Similar to CS5, the sound pressure level and standard deviation at each control point were combined providing the $L_{A_{\text{Feq}}}$ of 72.1 dBA, 69.8 dBA and 68.3 dBA at CP1, CP2, and CP3 sequentially; 33.0 dBA, 28.0 dBA and 32.0 dBA of the σ at each control point consecutively.

Case study 7 consists of control 1 and 3 which covered 270° and the distance of 7.50 m and 18.64 m, whereas control point 2 covered 231° at 17.89 m away from the site centre. Figure 5.17 shows that the position of control points 1, 2 and 3 was selected because it was cleared from obstacles and the location of the control points was able to cover the area where the machine moved. CP1 of CE7 had the L_{AFeq} of 78.3 dBA, 74.3 dBA and 73.2 dBA at CP2 and CP3. As for the standard deviation, the values were 3.3 dBA, 3.1 dBA and 1.6 dBA at CP1, CP2 and CP3. Next, the distance between the noise receiver and the site centre for the control points 1, 2, 3 in case study 8 was 9.86 m, 9.86 m and 15.00 m covering the angle of 240° , 300° and 270° correspondingly, due to the constraints of topography at the construction site as illustrated in Figure 5.18. The combined sound pressure level at CP1, CP2 and CP3 were 84.0 dBA, 83.2 dBA and 80.8 dBA whereas the standard deviations were 13.0 dBA, 9.3 dBA and 6.5 dBA.

As for case study 9, due to the bad site condition, the soil was not suitable for setting up the instrument at a certain location. Hence, the control points were located at the places with a hard ground surface covering the angle of 260° , 180° , and 140° at the distance of 19.61 m, 18.50 m and 11.63 m as shown in Figure 5.19. By combining the individual sound pressure level at each control point, the value of 78.8 dBA, 77.1 dBA and 82.1 dBA were obtained for CP1, CP2 and CP3. As for the combined standard deviation, the values were 11.0 dBA for each control point. Lastly, the coverage angles of the control points in case study 10 were 180° , 331° and 229° ; the location of the control points was located at 7.00 m, 8.70 m and 21.51 m away from the site centre due

to accessibility constraints as topsoil pile and mud puddle were surrounding the sub-area as depicted in Figure 5.20. By using the given parameters, the sound pressure level and standard deviation of 81.7 dBA and 4.4 dBA were obtained for CP1; L_{AFeq} of 81.4 dBA and σ of 4.6 dBA at CP2; L_{AFeq} of 75.8 dBA and σ of 4.2 dBA at CP3.

Table 5.7: Noise prediction using stochastic deep learning models

CS	CP	Machine	L_w	$w:d$ ratio	θ	r	r/w ratio	P_{on}	P_{idle}	P_{off}	L_p	σ
1	CP1	CE1	107.9	1:1	241	13.87	0.694	0.9	0.1	0.0	77.0	3.7
	CP2			1:1	304	23.25	1.163	0.9	0.1	0.0	72.6	3.7
	CP3			1:1	90	27.61	1.381	1.0	0.0	0.0	71.1	1.8
2	CP1	CE2	105.2	2:1	270	8.00	0.400	0.8	0.2	0.0	77.7	4.2
	CP2			2:1	236	9.32	0.466	0.9	0.1	0.0	77.2	4.6
	CP3			2:1	314	19.87	0.994	0.9	0.1	0.0	71.3	3.7
3	CP1	CE2	105.2	1:2	134	9.58	0.958	0.9	0.1	0.0	77.6	3.9
	CP2			1:2	72	12.85	1.285	0.9	0.1	0.0	75.6	3.4
	CP3			1:2	242	22.46	2.246	0.9	0.1	0.0	70.2	3.4
4	CP1	CE3	106.2	4:1	128	10.19	0.255	0.9	0.1	0.0	77.2	5.8
	CP2			4:1	242	13.20	0.330	0.9	0.1	0.0		
	CP3			4:1	46	17.52	0.438	0.9	0.1	0.0		
5	CP1	CE4	106.1	4:1	128	10.19	0.255	0.9	0.1	0.0	75.4	5.8
	CP2			4:1	242	13.20	0.330	0.9	0.1	0.0		
	CP3			4:1	46	17.52	0.438	0.9	0.1	0.0		
5	CP1	CE5	105.5	1:8	314	20.49	1.205	0.7	0.1	0.2	72.5	24.0
	CP2			1:8	297	32.80	1.929	0.8	0.1	0.1		
	CP3			1:8	288	44.36	2.609	0.6	0.2	0.2		
5	CP1	BP1	107.6	1:8	314	20.49	1.205	0.6	0.4	0.0	71.4	24.0
	CP2			1:8	297	32.80	1.929	0.5	0.4	0.1		
	CP3			1:8	288	44.36	2.609	0.7	0.3	0		
5	CP1	RR1	104.3	1:8	314	20.49	1.205	0.9	0.1	0	70.7	27.0
	CP2			1:8	297	32.80	1.929	0.9	0.1	0		
	CP3			1:8	288	44.36	2.609	1.0	0	0		

Table 5.7: Noise prediction using stochastic deep learning models (Cont'd)

CS	CP	Machine	L_w	$w:d$ ratio	θ	r	r/w ratio	P_{on}	P_{idle}	P_{off}	L_p	σ
6	CP1	CE5	105.5	8:1	302	18.08	0.133	0.7	0.1	0.2		
	CP2			8:1	289	29.41	0.216	0.7	0.2	0.1		
	CP3			8:1	315	47.15	0.347	0.5	0.3	0.2		
	CP1	BP1	107.6	8:1	302	18.08	0.133	0.5	0.4	0.1	72.1	33.0
	CP2			8:1	289	29.41	0.216	0.5	0.5	0	69.8	28.0
	CP3			8:1	315	47.15	0.347	0.7	0.2	0.1	68.3	32.0
	CP1	RR1	104.3	8:1	302	18.08	0.133	0.8	0.2	0		
	CP2			8:1	289	29.41	0.216	0.8	0.1	0.1		
	CP3			8:1	315	47.15	0.347	0.9	0.1	0		
7	CP1	CE6	107.9	4:1	270	7.50	0.188	1.0	0.0	0.0	78.3	3.3
	CP2			4:1	231	17.89	0.447	1.0	0.0	0.0	74.3	3.1
	CP3			4:1	270	18.64	0.466	1.0	0.0	0.0	73.2	1.6
8	CP1	CERB1	109.9	2:1	240	9.86	0.329	0.9	0.1	0.0		
	CP2			2:1	300	9.86	0.329	0.9	0.1	0.0		
	CP3			2:1	270	15.00	0.753	0.9	0.1	0.0		
	CP1	CERB2	107.3	2:1	240	9.86	0.329	0.8	0.2	0.0	84.0	13.0
	CP2			2:1	300	9.86	0.329	0.9	0.1	0.0	83.2	9.3
	CP3			2:1	270	15.00	0.753	0.9	0.1	0.1	80.8	6.5
	CP1	CERB3	107.9	2:1	240	9.86	0.329	0.9	0.1	0.0		
	CP2			2:1	300	9.86	0.329	0.9	0.1	0.1		
	CP3			2:1	270	15.00	0.753	0.9	0.1	0.0		
9	CP1	PM1	109.2	1:2	260	19.61	0.654	1.0	0.0	0.0		
	CP2			1:2	180	18.50	0.617	0.9	0.1	0.0		
	CP3			1:2	140	11.63	0.388	0.8	0.2	0.0	78.8	11.0
	CP1	PM2	109.8	1:2	260	19.61	0.654	1.0	0.0	0.0	77.1	11.0
	CP2			1:2	180	18.50	0.617	0.9	0.1	0.0	82.1	11.0
	CP3			1:2	140	11.63	0.388	0.8	0.2	0.0		
10	CP1	PM3	110.5	1:4	180	7.00	0.700	0.9	0.1	0.0	81.7	4.4
	CP2			1:4	331	8.70	0.870	0.9	0.1	0.0	81.4	4.6
	CP3			1:4	229	21.51	2.151	0.9	0.1	0.0	75.8	4.2

Note:

CS = Case Study

CP = Control Point

L_w = Sound power level of the earth-moving machine (dBA)

θ = Angle (°)

r = Distance between receiver and site centre (m)

P_{on} = Ratio of the time when machine operated at full power

P_{idle} = Ratio of the time when the machine was idling

P_{off} = Ratio of the time when the machine was turned off

L_p = The predicted sound pressure level (dBA)

σ = standard deviation (dBA)

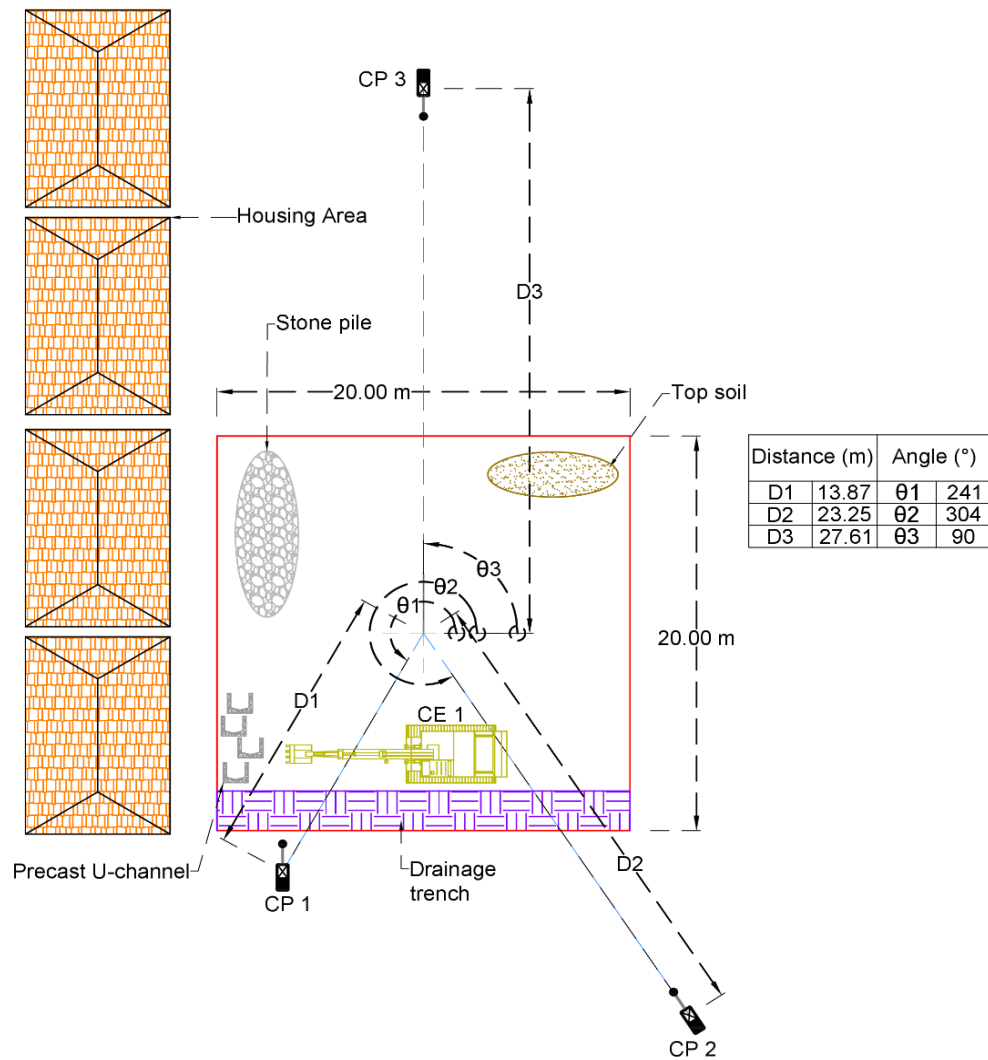


Figure 5.11: Case study 1 for stochastic deep learning model

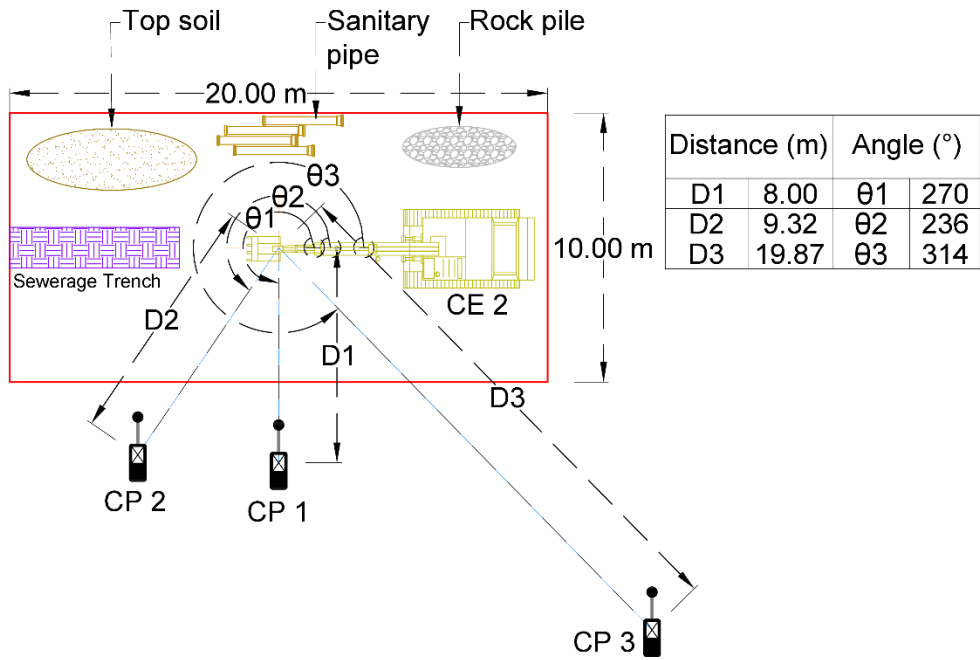


Figure 5.12: Case study 2 for stochastic deep learning model

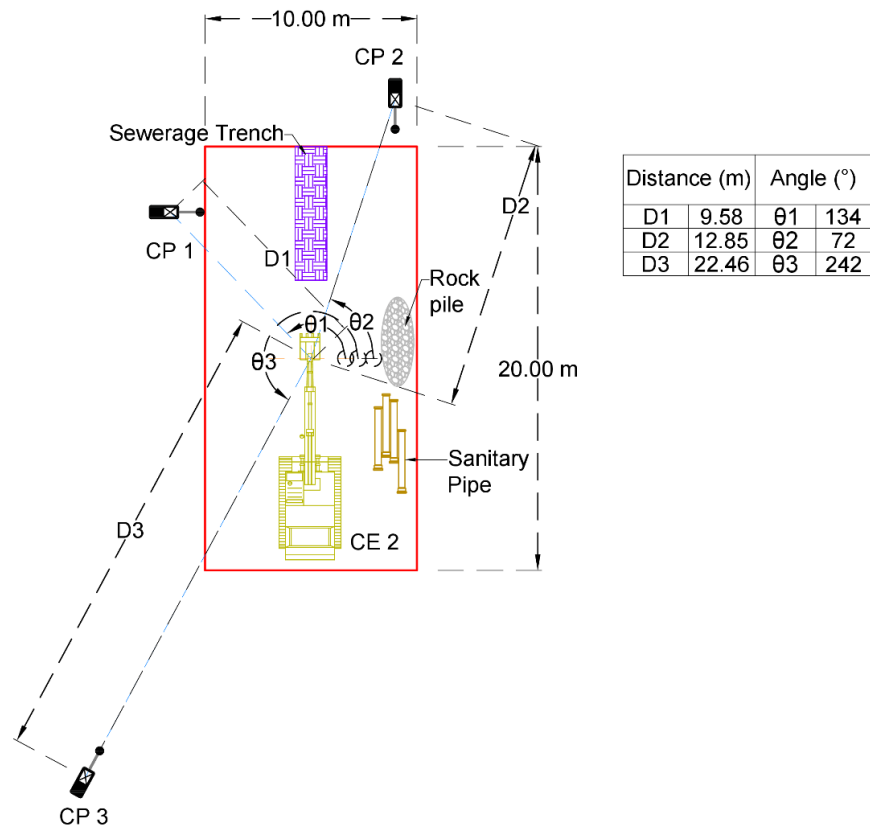


Figure 5.13: Case study 3 for stochastic deep learning model

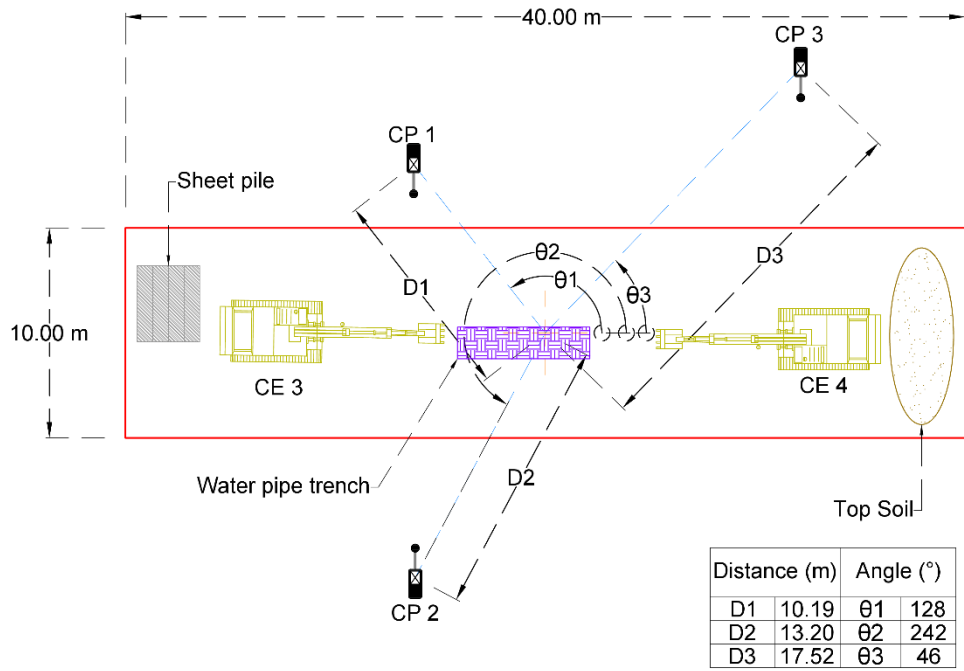


Figure 5.14: Case study 4 for stochastic deep learning model

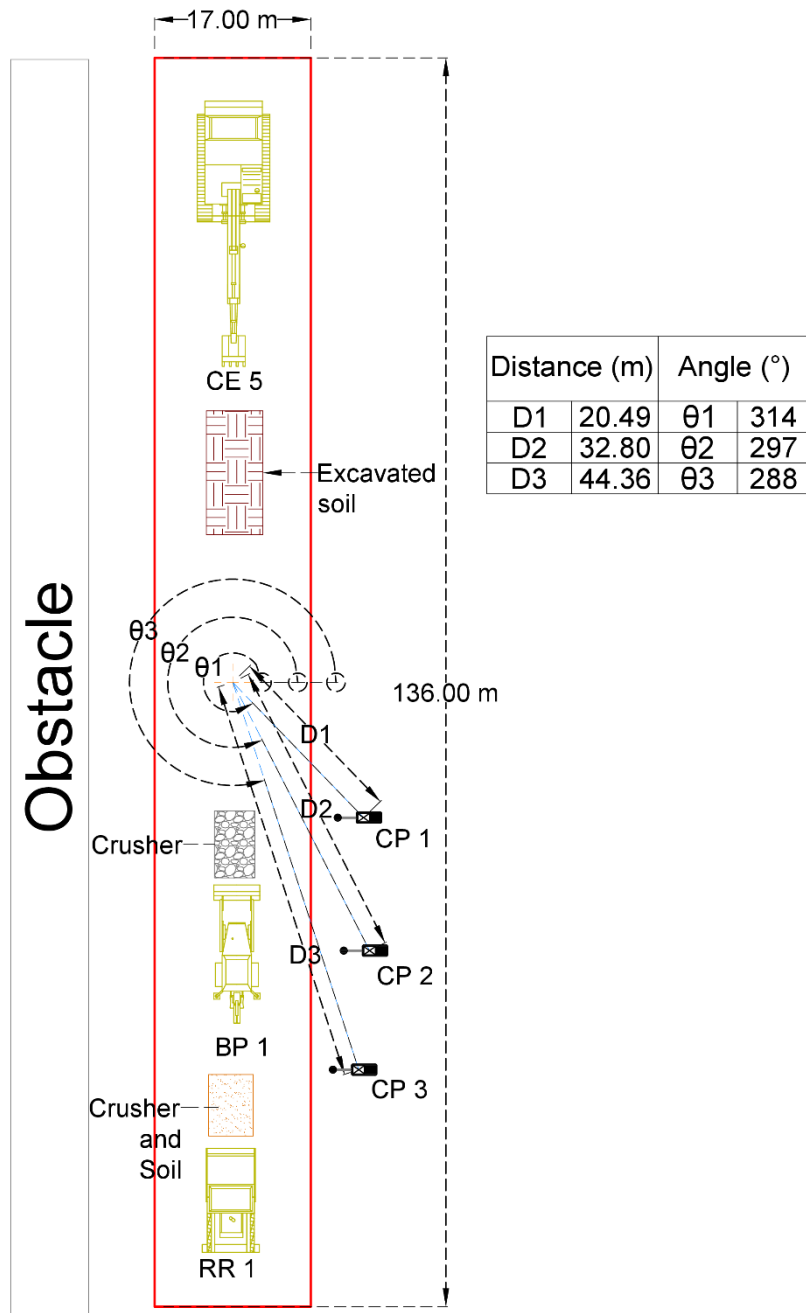


Figure 5.15: Case study 5 for stochastic deep learning model

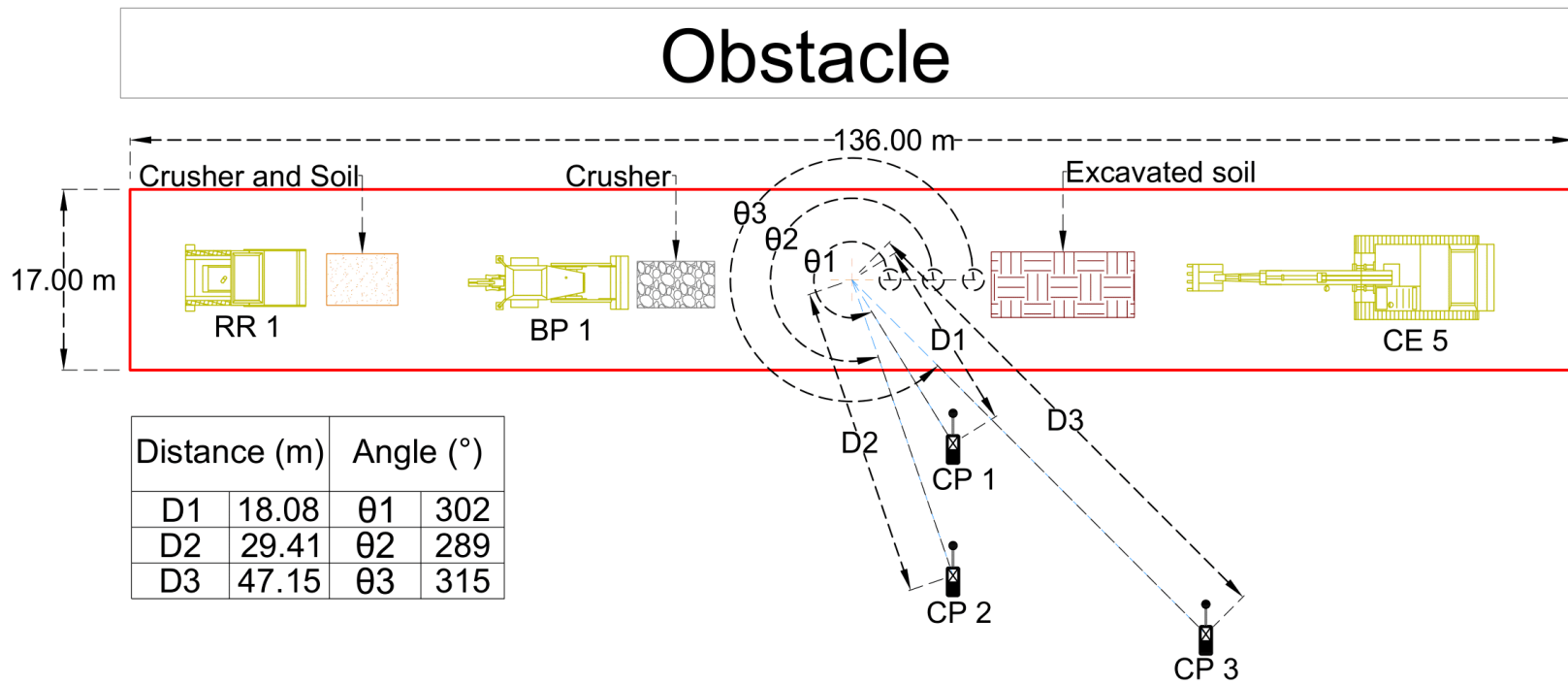


Figure 5.16: Case study 6 for stochastic deep learning model

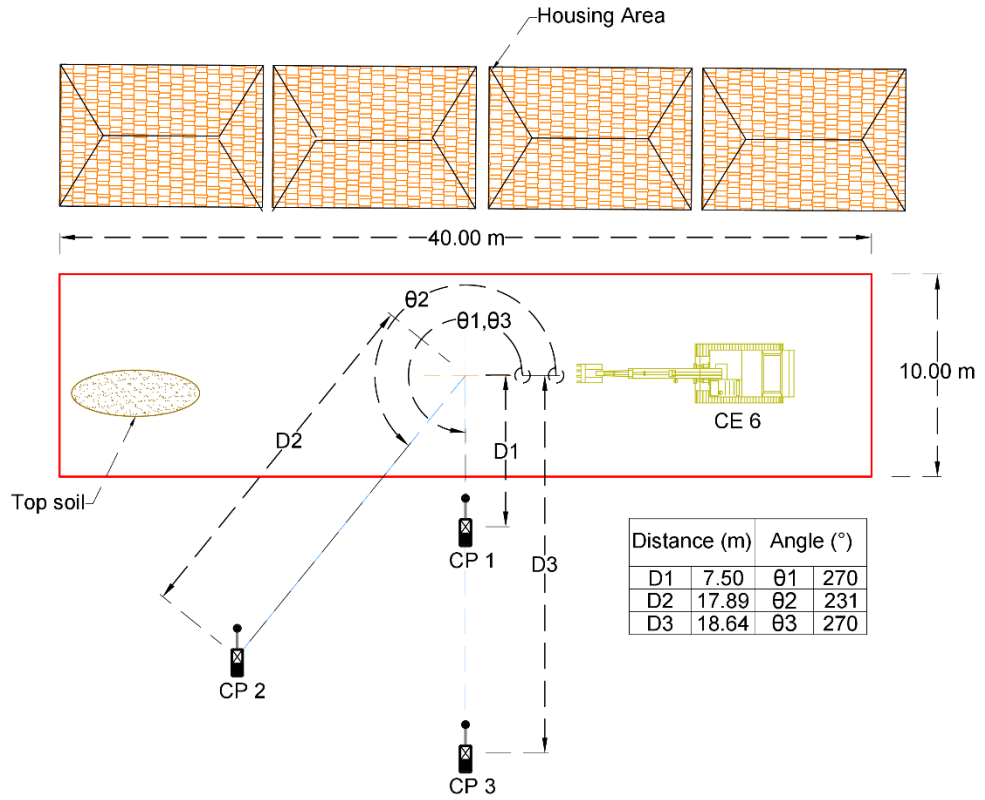


Figure 5.17: Case study 7 for stochastic deep learning model

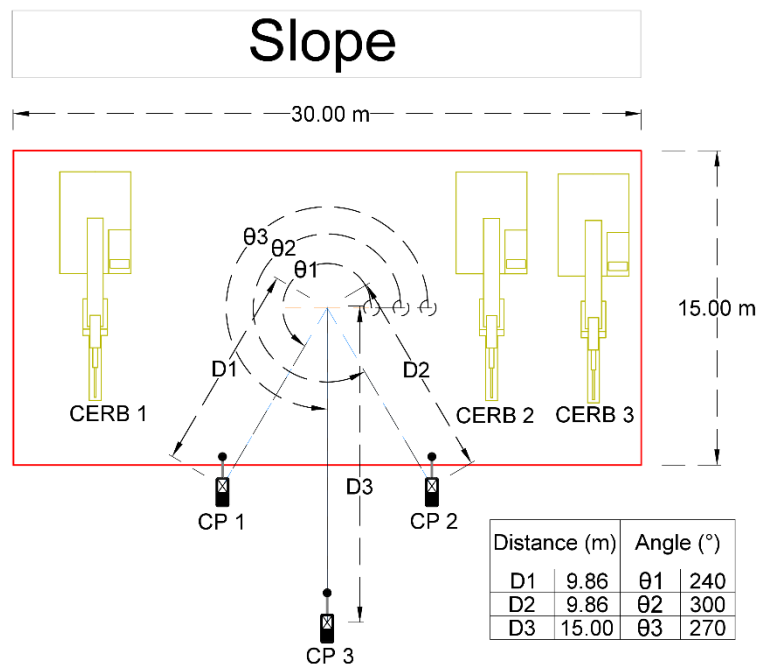


Figure 5.18: Case study 8 for stochastic deep learning model

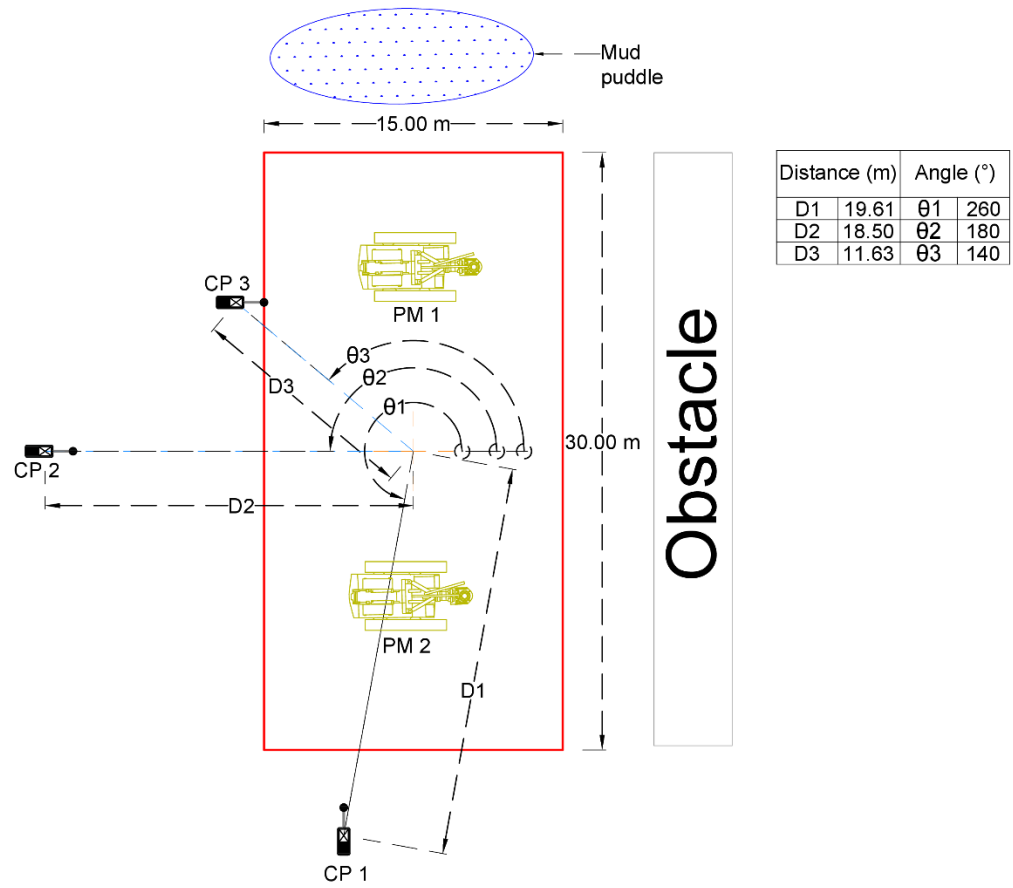


Figure 5.19: Case study 9 for stochastic deep learning model

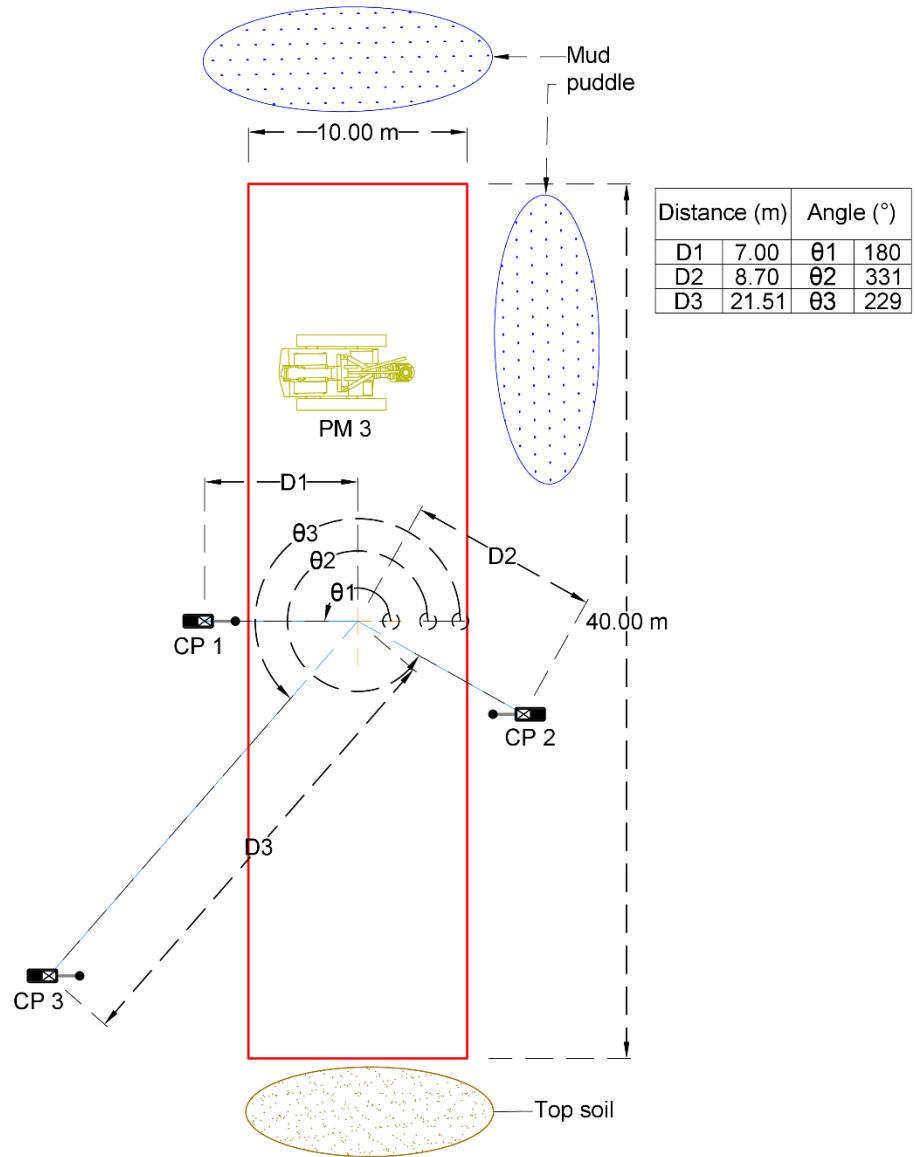


Figure 5.20: Case study 10 for stochastic deep learning model

5.7 Comparison of Simple Prediction Charts Technique (SPC) and Stochastic Deep Learning (SDL) Model Prediction

Table 5.8 shows the disparities of both predicted noise levels using the simple prediction chart and stochastic deep learning model of every control point for all the case studies. Besides, the accuracy of the prediction was tested by using the absolute difference and relative error. The reliability of the model was tested by using Pearson correlation and R-squared. Figure 5.21 presented the difference between the predictions from the simple prediction chart technique and the stochastic deep learning model.

The highest disparity of the comparison was 3.6 dBA and the relative error of 4.7 % in case study 5 and the average absolute difference for all the control points was 0.5 dBA and the average relative percentage error was 0.01 %. Overall, case study 1 contributed the lowest average absolute difference of 0.03 dBA and 0 % of relative error among the results whereas the average absolute difference of case study 5 was 1.8 dBA, the highest among all the case studies. Moreover, case study 1 has the highest value of Pearson correlation and R-squared of 1.000 indicating a strong association between the simple prediction chart technique and the stochastic deep learning model. However, the lowest Pearson correlation and R-squared value were identified from case study 9 having the value of 0.905 and 0.818.

The disparities were directly influenced by the inclusion of the earth-moving machine duty cycle. As mentioned earlier, the earth-moving machine

was assumed to operate at full power for the development of the simple prediction chart (Haron et al., 2008; Haron et al., 2009, Haron et al., 2012); but for the stochastic simulation in the current study, the earth-moving machine was assumed to have three different duty modes. Hence, the difference between the assumption resulted in the disparities between the stochastic deep learning model and the simple prediction chart technique. The relationship between the duty cycle and the disparities indicated that the higher the variation of duty cycles of the earth-moving machine, the higher the difference of prediction between the simple prediction charts technique and the stochastic deep learning model.

Furthermore, the introduction of the coverage angle of 0° to 360° from the site centre resulted in disparities in the prediction as well. Unlike the stochastic deep learning model, the simple prediction charts only covered up to 0° , 15° , 30° and 45° . As for the simple prediction charts, the angle equal to or less than 45° in the first quadrant can be symmetrically mirrored in the other quadrants (Q2, Q3, Q4) to determine the ΔL . For instance, the coverage angle of 45° in the simple prediction charts could be the coverage angle of 135° , 225° and 315° in the stochastic simulation. However, the sound pressure levels at these angles were different because of the inclusion of the different duty cycles of the earth-moving machine. In other words, if the earth-moving machine was simulated randomly to generate noise at full power mode in Q1, and produce noise at idling mode in Q3, then the sound pressure levels were not equivalent. Although the concept of the stochastic simulation in this study was derived from

the simple prediction charts, the outcome of prediction was different upon the inclusion of earth-moving machine duty cycles and complete coverage angle.

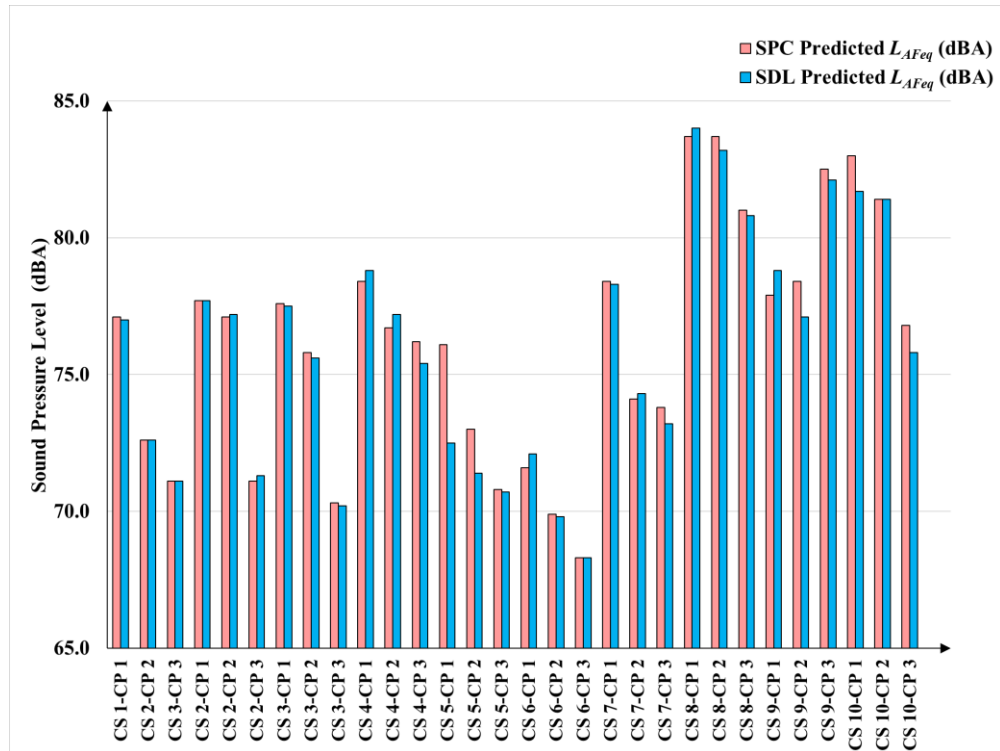


Figure 5.21: Comparison of sound pressure level between the SPC technique and SDL model

Table 5.8: Comparison between the prediction of SPC technique and SDL model

Case Study & aspect ratio	Control Points	SPC	SDL	Absolute Difference	Relative Error	Pearson Correlation	R Squared
		Predicted L_{AFeq} (dBA)	Predicted L_{AFeq} (dBA)				
CS1 (1:1)	CP1	77.1	77.0	0.1	0.1%	1.000	1.000
	CP2	72.6	72.6	0.0	0.0%		
	CP3	71.1	71.1	0.0	0.0%		
CS2 (2:1)	CP1	77.7	77.7	0.4	0.5%	0.998	0.996
	CP2	77.1	77.2	0.1	0.1%		
	CP3	71.1	71.3	0.2	0.3%		
CS3 (1:2)	CP1	77.6	77.5	0.0	0.0%	1.000	0.999
	CP2	75.8	75.6	0.2	0.3%		
	CP3	70.3	70.2	0.1	0.1%		
CS4 (4:1)	CP1	78.4	78.8	0.4	0.5%	0.943	0.889
	CP2	76.7	77.2	0.5	0.7%		
	CP3	76.2	75.4	0.8	1.0%		
CS5 (1:8)	CP1	76.1	72.5	3.6	4.7%	1.000	0.999
	CP2	73.0	71.4	1.6	2.2%		
	CP3	70.8	70.7	0.1	0.1%		
CS6 (8:1)	CP1	71.6	72.1	0.5	0.7%	0.995	0.989
	CP2	69.9	69.8	0.1	0.1%		
	CP3	68.3	68.3	0.0	0.0%		
CS7 (4:1)	CP1	78.4	78.3	0.1	0.1%	0.989	0.978
	CP2	74.1	74.3	0.2	0.3%		
	CP3	73.8	73.2	0.6	0.8%		
CS8 (2:1)	CP1	83.7	84.0	0.3	0.4%	0.971	0.942
	CP2	83.7	83.2	0.5	0.6%		
	CP3	81.0	80.8	0.2	0.2%		
CS9 (1:2)	CP1	77.9	78.8	0.9	1.2%	0.905	0.818
	CP2	78.4	77.1	1.3	1.7%		
	CP3	82.5	82.1	0.4	0.5%		
CS10 (1:4)	CP1	83.0	81.7	1.3	1.6%	0.979	0.958
	CP2	81.4	81.4	0.0	0.0%		
	CP3	76.8	75.8	1.0	1.3%		

5.8 Comparison of the Prediction and Actual Measurement

The comparison between the actual measurement and the prediction from both the simple prediction charts technique and stochastic deep learning model is presented in Figure 5.22; the absolute difference between all the case studies is exemplified in Figure 5.23. Table 5.9 shows the disparities in the predicted noise levels using the simple prediction chart and the actual measurement of every control point for all the case studies. Besides, the accuracy of the prediction was tested by using the absolute difference whereas the reliability of the model was tested by using R-squared. The highest disparity of the comparison was 3.2 dBA with a relative error of 3.8 % in case study 8. The average absolute difference for all the control points was 1.5 dBA and the average relative percentage error was 0.02 %. Overall, case study 1 contributed the lowest average absolute difference of 1.2 dBA among the results whereas the average absolute difference of case study 8 was 2.3 dBA, the highest among all the case studies. Moreover, case studies 1 and 2 had the highest value of R-squared of 1.000 indicating a strong association between the simple prediction chart technique and the measurement. However, the lowest R-squared value was identified in case study 9 having the value of 0.660.

The disparities were directly influenced by the inclusion of the earth-moving machine duty cycle. As mentioned earlier, the earth-moving machine was assumed to operate at full power for the development of the simple prediction chart (Haron et al., 2008); but in the actual scenario, the earth-moving machine operated at different duty modes. Hence, this resulted in the disparities

between the prediction and the actual measurement. The relationship between the duty cycle and the disparities indicated that the higher the variation of duty cycles of the earth-moving machine, the higher the difference between the prediction and the actual measurement. On the other hand, the reliability of the prediction was directly affected by the duty cycles as well. The inclusion of duty cycles in the construction noise prediction was suggested by previous researchers to improve the accuracy of the prediction (Haron et al. 2012; Lim et al. 2015)

Table 5.9 shows the absolute difference, relative error, Pearson correlation and R-squared of the predicted noise level using the stochastic deep learning model (SDL) and the actual noise level of every control point for all the case studies. Besides, the accuracy of the predicted results was tested by using the absolute difference and relative error; the reliability was tested by Pearson correlation and R-squared. The highest disparity of the comparison was 2.9 dBA with a relative error of 3.3 % and one of the control points had 0.0 dBA of absolute difference. Overall, case study 4 contributed the lowest average absolute difference of 0.63 dBA among the results whereas the average absolute difference of case study 8 was 2.4 dBA, the highest among all the case studies. The average absolute difference for all the control points was 1.2 dBA and the average relative percentage error was 0.02 %.

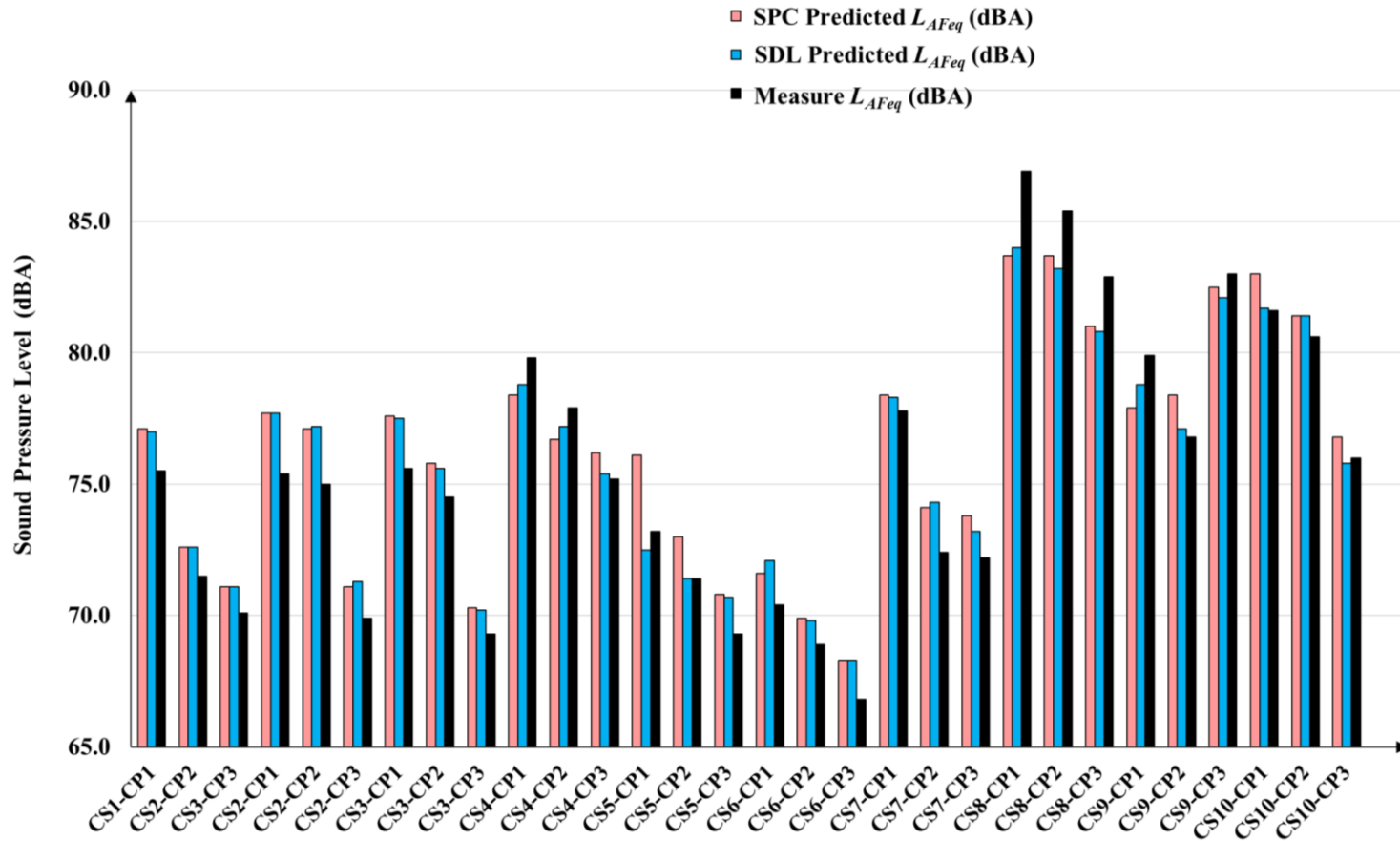


Figure 5.22: Comparison of sound pressure level between the SPC technique, SDL and actual measurement

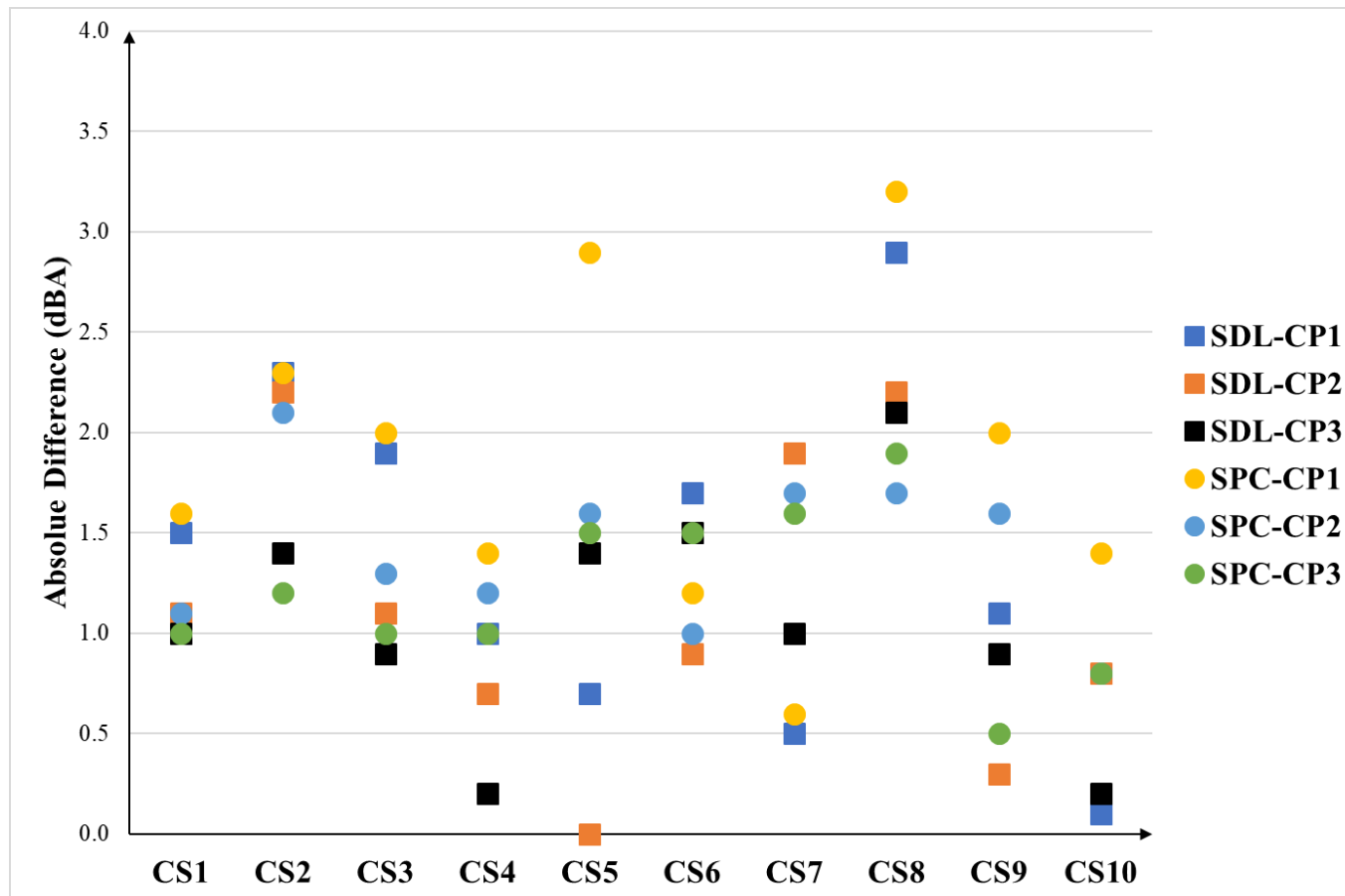


Figure 5.23: Absolute difference between the prediction and the actual measurement

Table 5.9: Comparison of the prediction and measurement

Case	Control	SPC Predicted L_{AFeq} vs. Measured L_{AFeq}				SDL Predicted L_{AFeq} vs. Measured L_{AFeq}							
		SPC Predicted L_{AFeq} (dBA)	SDL Predicted L_{AFeq} (dBA)	Measured L_{AFeq} (dBA)	Absolute Difference (dBA)	Absolute Difference (dBA)	Relative Error	Pearson Correlation	R Squared	Absolute Difference (dBA)	Relative Error	Pearson Correlation	R Squared
CS1 (1:1)	CP1	77.1	77.0	75.5	1.6	2.1 %				1.5	2.0 %		
	CP2	72.6	72.6	71.5	1.1	1.5 %	1.000	1.000	1.1	1.5 %	1.000	1.000	
	CP3	71.1	71.1	70.1	1.0	1.4 %			1.0	1.4 %			
CS2 (2:1)	CP1	77.7	77.7	75.4	2.3	3.0 %			2.3	3.1 %			
	CP2	77.1	77.2	75.0	2.1	2.7 %	1.000	1.000	2.2	2.9 %	1.000	1.000	
	CP3	71.1	71.3	69.9	1.2	1.7 %			1.4	2.0 %			

Table 5.9: Comparison of the prediction and measurement (Cont'd)

Case	Control	SPC Predicted L_{AFeq} vs. Measured L_{AFeq}				SDL Predicted L_{AFeq} vs. Measured L_{AFeq}							
		SPC Predicted L_{AFeq} (dBA)	SDL Predicted L_{AFeq} (dBA)	Measured L_{AFeq} (dBA)	Absolute Difference (dBA)	Absolute Difference (dBA)	Relative Error	Pearson Correlation	R Squared	Absolute Difference (dBA)	Relative Error	Pearson Correlation	R Squared
CS3 (1:2)	CP1	77.6	77.5	75.6	2.0	2.6 %				2.0	2.5 %		
	CP2	75.8	75.6	74.5	1.3	1.7 %	0.997	0.994	1.1	1.5 %	0.996	0.992	
	CP3	70.3	70.2	69.3	1.0	1.4 %			0.9	1.3 %			
CS4 (4:1)	CP1	78.4	78.8	79.8	1.4	1.8 %			1.0	1.3 %			
	CP2	76.7	77.2	77.9	1.2	1.6 %	0.919	0.845	0.7	0.9 %	0.998	0.996	
	CP3	76.2	75.4	75.2	1.0	1.3 %			0.2	0.3 %			

Table 5.9: Comparison of the prediction and measurement (Cont'd)

Case	Control	SPC Predicted L_{AFeq} vs. Measured L_{AFeq}				SDL Predicted L_{AFeq} vs. Measured L_{AFeq}						
		SPC Predicted L_{AFeq} (dBA)	SDL Predicted L_{AFeq} (dBA)	Measured L_{AFeq} (dBA)	Absolute Difference (dBA)	Absolute Difference (dBA)	Relative Error	Pearson Correlation	R Squared			
CS5 (1:8)	CP1	76.1	72.5	73.2	2.9	3.8 %			0.7	1.0 %		
	CP2	73.0	71.4	71.4	1.6	2.2 %	0.990	0.980	0.0	0.0 %	0.985	0.971
	CP3	70.8	70.7	69.3	1.5	2.1 %			1.4	2.0 %		
CS6 (8:1)	CP1	71.6	72.1	70.4	1.2	1.7 %			1.7	2.4 %		
	CP2	69.9	69.8	68.9	1.0	1.4 %	0.994	0.987	0.9	1.3 %	0.977	0.954
	CP3	68.3	68.3	66.8	1.5	2.2 %			1.5	2.2 %		

Table 5.9: Comparison of the prediction and measurement (Cont'd)

Case	Control	SPC Predicted L_{AFeq} vs. Measured L_{AFeq}				SDL Predicted L_{AFeq} vs. Measured L_{AFeq}							
		SPC Predicted L_{AFeq} (dBA)	SDL Predicted L_{AFeq} (dBA)	Measured L_{AFeq} (dBA)	Absolute Difference (dBA)	Absolute Difference (dBA)	Relative Error	Pearson Correlation	R Squared	Absolute Difference (dBA)	Relative Error	Pearson Correlation	R Squared
CS7 (4:1)	CP1	78.4	78.3	77.8	0.6	0.8 %				0.5	0.6 %		
	CP2	74.1	74.3	72.4	1.7	2.3 %	1.000	0.999	1.9	2.6 %	0.985	0.970	
	CP3	73.8	73.2	72.2	1.9	2.2 %			1.0	1.4 %			
CS8 (2:1)	CP1	83.7	84.0	86.9	3.2	3.8 %			2.9	3.3 %			
	CP2	83.7	83.2	85.4	1.7	2.0 %	0.929	0.862	2.2	2.6 %	0.991	0.981	
	CP3	81.0	80.8	82.9	1.9	2.3 %			2.1	2.5 %			

Table 5.9: Comparison of the prediction and measurement (Cont'd)

Case	Control	SPC Predicted L_{AFeq} vs. Measured L_{AFeq}				SDL Predicted L_{AFeq} vs. Measured L_{AFeq}							
		SPC Predicted L_{AFeq} (dBA)	SDL Predicted L_{AFeq} (dBA)	Measured L_{AFeq} (dBA)	Absolute Difference (dBA)	Absolute Difference (dBA)	Relative Error	Pearson Correlation	R Squared	Absolute Difference (dBA)	Relative Error	Pearson Correlation	R Squared
CS9 (1:2)	CP1	77.9	78.8	79.9	2.0	2.6 %				1.1	1.4 %		
	CP2	78.4	77.1	76.8	1.6	2.0 %	0.812	0.660	0.3	0.4 %	0.983	0.967	
	CP3	82.5	82.1	83.0	0.5	0.6 %			0.9	1.1 %			
CS10 (1:4)	CP1	83.0	81.7	81.6	1.4	1.7 %			0.1	0.1 %			
	CP2	81.4	81.4	80.6	0.8	1.0 %	0.997	0.993	0.8	1.0 %	0.992	0.985	
	CP3	76.8	75.8	76.0	0.8	1.0 %			0.2	0.3 %			

By interpreting the data, the SDL has high accuracy in each case study with the mean absolute difference ranging from 0.0 dBA to 2.9 dBA. The disparities between the actual measurement and prediction of the case studies 2, 3, 5, 6 and 7 can be explained by the coverage area of the machine during the activities was insufficient because the simulation assumed the earth-moving machines to cover all the areas within the well-defined sub-area (Haron et al., 2008). Besides, a study revealed that the accuracy of the prediction is directly affected by the coverage area of earth-moving machines (Lim et al., 2015). For case studies 1 and 4, the earth-moving machines covered almost every area within the sub-site and hence resulted in a low value of absolute difference but it has a low possibility that it will occur in a real case scenario.

Additionally, the accuracy of the prediction was very dependent on the variation of duty cycles. Based on the observation, earth-moving machines that were being operated at all times resulted in a low absolute difference value between the comparison of predicted and measured noise levels. Even though three different duty cycles were covered in this study but the operation cycle of earth-moving machines tends to have more different duty cycles in reality (Lim et al., 2015). Hence, the predicted values from SDL were slightly higher than the actual noise levels overall if the earth-moving machine was a crawler excavator that was attached to excavating bucket. As for case studies 8, 9 and 10, the majority of the predicted sound pressure levels at the control points were an averagely of 1.2 dBA lower than the actual measurement. This is because the impulsive noise was generated by the collision between the rock breaker and

the rock in case study 8. As for case studies 9 and 10, the impulsive noise was generated during the rock coring activities.

Based on the data analysis, the range of the standard deviation for each of the case studies varied from 1.6 dBA to 33.0 dBA. The standard deviation in the SDL was to explain the noise level distribution within the sub-area and also the variation of sound pressure levels at a different operational duty cycle. The standard deviation of all the case studies is tabulated in Table 5.7. Case study 6 had the highest average standard deviation of 31.0 dBA due to the width to depth ratio of 8:1 (136 m : 17 m). When a sub-area has a greater difference in ratio between the width and depth, the range between the maximum and minimum noise levels tends to be larger because of the inverse square law (Haron *et al*, 2008). Additionally, when the earth-moving machine is involved more often in different duty cycles, the standard deviation will be higher as well. Nonetheless, the reason that caused case study 6 to have a high standard deviation value is due to the high variation of duty cycles and dynamic properties of three machines during the road construction activity. On the contrary, case study 7 with an aspect ratio of 1:1 had the lowest average standard deviation of 2.7 dBA which the earth-moving machine operated at full power throughout the measurement having a smaller standard deviation value in the prediction. This explains the accuracy of the prediction highly relies on the operational duty cycle and the coverage area (Haron *et al.*, 2008; Haron and Yahya, 2009; Haron *et al.*, 2012; Lim *et al.*, 2015).

The lowest R-squared value of 0.954 which indicated the SDL was highly reliable; the highest R-squared value lies between case studies 1, 2 and 4 whereas case study 6 has the lowest R-squared value of 0.954 followed by case study 9 with the R-squared value of 0.967. In addition, the Pearson correlation value for case study 6 was the lowest among the case studies with a value of 0.977. Case studies with the highest Pearson correlation value of 1.000 were CS1 and CS2. In summary, the stochastic deep learning model is capable of providing good reliability in noise level prediction with an R^2 value ranging from 0.954 to 1.000 and the Pearson's correlation ranging from 0.977 to 1.000 indicating a strong association between the prediction and measurement (Henseler et al., 2009).

5.9 Concluding Remark

This chapter presents the results of fieldwork to investigate the stochastic deep learning model performance. Besides, the outcome of the model was compared to the simple prediction charts to determine the model performance based on the concept of stochastic modelling. Then, the stochastic deep learning model and the simple prediction chart technique were compared to the actual measurement to determine the performance of both the SPC technique and SDL models. The following conclusions can be drawn from this study:

- i) The disparities between the stochastic deep learning model and the simple prediction chart technique were directly influenced by the inclusion of the earth-moving machine duty cycle. As mentioned earlier,

the earth-moving machine was assumed to operate at full power for the development of the simple prediction chart; but for the stochastic simulation in the current study, the earth-moving machine was assumed to have three different duty modes. The relationship between the duty cycle and the disparities indicated that the higher the variation of duty cycles of the earth-moving machine, the higher the difference of prediction between the simple prediction charts technique and the stochastic deep learning model.

- ii) The difference in coverage angle from simple prediction chart technique and stochastic deep learning model resulted in the disparities between the prediction as well. The sound pressure levels at different coverage angles were different mainly because of the inclusion of the different duty cycles of the earth-moving machine at different random locations.
- iii) The coverage area of the earth-moving machines in the actual construction activities contributed to the disparities in the prediction for both simple prediction charts and deep learning models. In the simulation, the earth-moving machine was assumed to cover all the areas within the sub-site. However, the earth-moving machine was only able to cover certain areas with high intensity due to the type of work in the actual construction activities.
- iv) Although the overall absolute difference from the stochastic deep learning model was below 1.2 dBA with an average relative error of

0.01 %. Some case studies like pile boring activities contributed a higher absolute difference as well as relative error, compared to other case studies due to the impulsive noise generated from certain works which indicates that more parameters such as the generated noise types (steady-continuous noise, steady non-continuous noise, intermittent noise, impulsive noise, fluctuating noise) can be included in the simulation.

CHAPTER 6

CONCLUSION AND RECOMMENDATION

6.1 Introduction

Based on the objectives formulated in Chapter 1, conclusions are contemplated in this study. The explanation for each conclusion is explained with clarity in the following sections. The limitation and recommendations are covered in the following sections as well.

6.2 Conclusion

6.2.1 Feasibility of using Artificial Neural Network to Predict Construction Noise Levels

In conclusion, this study validated the predicted and actual noise levels from different construction activities. Actual noise levels measurement was conducted following BS 5228-1:2009 and BS ISO 6395:2008. The predicted noise levels were computed correctly by using the simple prediction chart technique and the stochastic deep learning model. The prediction from the stochastic deep learning model was proven to be accurate and reliable. To support the statement, the highest absolute difference value and the relative error compared to the measurement was less than 3.0 dBA and smaller than 4.0 %. Furthermore, the highest mean absolute difference values compared with the SPC and the measurement were 0.5 dBA and 1.2 dBA with an average

relative error of 0.01 %. Furthermore, the lowest R^2 value and Pearson's correlation coefficient among the case studies were 0.954 and 0.977 which indicates strong strength of association. Hence, the stochastic deep learning model has the potential to be adopted in the construction industry as a managerial and planning tool.

The stochastic deep learning framework was developed with the association of stochastic modelling and the artificial neural network. The framework aims to clarify the execution of every step in the stochastic deep learning model. The programming algorithms for stochastic modelling were developed in MATLAB to validate and compare the outcome of the previous studies and the current stochastic modelling. The deep learning models were established in Python programming language using Spyder 3.6. Seven sets of stochastic data based on different aspect ratios were generated. The purpose of stochastic modelling was to generate input data as the training data for the seven deep learning models for different aspect ratios. The deep learning models were trained and assessed according to the stochastic data. The performance evaluation for each stochastic deep learning model was satisfactory.

Ten case studies were successfully conducted in this study. The stochastic deep learning models predicted the construction noise based on different given parameters, and then the accuracy and reliability of the prediction were validated by using the actual measurement from construction sites. In conclusion, this study validated the predicted and actual noise levels from different construction activities. Actual noise levels measurement was

conducted following BS 5228-1:2009 and BS ISO 6395:2008. The predicted noise levels were computed correctly by using the stochastic deep learning model and the simple prediction chart method. The prediction from the stochastic deep learning model was proven to be accurate and reliable. To support the statement, the highest absolute difference value compared to the measurement was less than 3.0 dBA. Furthermore, the highest mean absolute difference values compared with the SPC and the measurement were 0.5 dBA and 1.2 dBA. The average relative error between the simple prediction chart technique and the stochastic deep learning model was 0.01 % whereas the relative error was 0.02 % by comparing the prediction from the stochastic deep learning model and the actual measurement. However, the lowest R^2 value among the case studies was 0.954 which indicates strong strength of association. Hence, the stochastic deep learning model is environmental modelling that has the potential to be adopted in the construction industry managerial and planning tool.

6.2.2 Limitation

This study is bounded by several limitations which may have directly affected the accuracy of the deep learning model. These limitations were identified as factors that would potentially influence the outcome in future research:

- i. This study only covered steady-continuous noise. However, some construction machines such as breakers and pile boring machines will generate different types of noise that would affect the sound pressure level during the measurement. This may crucially affect the

absolute difference between the deep learning model and actual measurement.

- ii. The machine sound power level in the stochastic model was determined as 120 dBA during the data generation. In reality, the machine sound power level varies due to different construction activities.
- iii. The aspect ratio for case studies was limited to 1:1, 1:2, 1:4, 1:8, 8:1, 4:1, and 2:1 only, which may constrain the flexibility of the fieldwork. This is because of the space limitation and inaccessibility of the construction site.
- iv. The case studies were mostly focused on infrastructure activity, the deep learning model accuracy and reliability were biased to infrastructure activities when the prediction is compared to the actual measurement.

6.3 Recommendation

Several study areas are recommended to be investigated to further improve the application of the stochastic deep learning model practically:

- i. Study the noise patterns of the machine during different stages of the construction activities, and include more operational modes during

the fieldwork and the prediction. Thus, it is worthwhile to further study the influence level based on different types of noise and operational modes that may affect the performance of the deep learning model.

- ii. The sound pressure level in the environment is mainly from the earth-moving machines during construction activities. Hence, including varieties of sound power levels during the data generation may significantly affect the performance of the stochastic deep learning model.
- iii. Study more aspect ratios so that the site configuration for each prediction will not only be limited to 7 aspect ratios as stated. Nonetheless, the user can configure the dimension of the sub-site depending on the accessibility and space in the harsh construction environment.
- iv. This study is feasible and has the potential to be applicable in all kinds of construction activities. With that being said, a comparison between varieties of case studies from different construction activities and the deep learning model would validate the accuracy and reliability of the model.

REFERENCES

- Aggarwal, C.C., 2018. *Neural networks and deep learning*. Cham: Springer Nature Switzerland.
- Aliabadi, M., Golmohammadi, R., Khotanlou, H., Mansoorizadeh, M. and Salarpour, A., 2015. Artificial neural networks and advanced fuzzy techniques for predicting noise levels in the industrial embroidery workrooms. *Applied Artificial Intelligence*, 29(8), pp. 766-785.
- Aliabadi, M., Golmohammadi, R., Mansoorizaddeh, M., Khotanlou, H., Hamadani, A.O., 2013. An empirical technique for predicting noise exposure levels in the typical embroidery workrooms using artificial neural networks. *Applied Acoustics*, Volume 74, pp. 364-374.
- Al-Mosawe, H.M., Alobaydi, D., Albayati, A., 2018. Development of traffic noise prediction model in an educational urban area. *Civil Engineering Journal*, 4(11), pp. 2588-2595.
- Arora, J.K. and Mosahari, P.V., 2012. Artificial neural network modelling of traffic noise in agra-firozabad highway. *International Journal of Computer Applications*, 56(2), pp. 1-10.
- Ballesteros, M.J., Fernandez, M.D., Quintana, S., Ballesteros, J.A. and Gonzalez, I., 2010. Noise emission evolution on construction sites. Measurement for controlling and assessing its impact on the people and the environment. *Building and Environment*, Volume 45, pp. 711-717.
- Beranek, L.L. and Mellow, T.J., 2012. *Acoustics: Sound fields and transducers*. 1 ed. Oxford: Elsevier.

- Bhosale, D., 2017. Noise pollution in construction industry and its adverse effects on construction workers. *Imperial Journal of Interdisciplinary Research*, 3(8), pp. 447-449.
- Brandimarte, P., 2014. *Handbook in Monte Carlo simulation, applications in financial engineering, risk management and economics*. New Jersey: John Wiley and Sons.
- British Standard Institution, 2008. *BS ISO 6395:2008 Earth-moving machinery - determination of sound power level - dynamic test conditions*, Geneva: British Standard Institution.
- Brownlee, J., 2016. *Deep learning with python*. Vermont Victoria: Machine Learning Mastery.
- Brownlee, J., 2016. *Machine learning mastery with python: understand your data, create accurate models, and work projects end-to-end*. 1 ed. Vermont Victoria: Machine Learning Mastery.
- British Standard Institution, 2009. *BS 5228:1 code of practice for noise and vibration control on construction and open sites-part 1: Noise*. London: British Standard Institution.
- British Standard Institution, 2008. *BS ISO 6395:2008: earth-moving machinery-determination of sound power level-dynamic test conditions*. London: British Standard Institution.
- British Standard Institution, 2010. *BS EN ISO 3744:2010: Acoustics-determination of sound power levels of noise sources energy levels of noise sources using sound pressure-engineering methods for an essentially free field over a reflecting plane*. London: British Standard Institution.

- Buduma, N., 2017. *Fundamentals of deep learning*. Sebastopol: O'Reilly Media, Inc.
- Campestrato, O., 2020. *Artificial intelligence machine learning and deep learning*. Dulles: Mercury Learning and Information.
- Cantley, L.F. et al., 2014. Does tinnitus, hearing asymmetry, or hearing loss predispose to occupational injury risk?. *International Journal of Audiology*, 54, pp. 30-36.
- Carpenter, F., 1997. Construction noise prediction at the planning stage of new developments. *Building Acoustics*, 3(4), pp. 239-249.
- Chollet, F., 2018. *Deep learning with python*. New York: Manning Publications Co.
- Cirianni, F. and Leonardi, G., 2015. Artificial neural network for traffic noise modelling. *ARPJ Journal of Engineering and Applied Sciences*, 10(22), pp. 10413-10419.
- Cowan, J. P., 2016. *The effects of sound on people*. 1 ed. West Sussex: John Wiley & Sons, Limited.
- Crocker, J. M., 2007. *Handbook of noise and vibration control*. Hoboken, New Jersey: John Wiley & Sons, Inc.
- Darus, N., Haron, Z. and Yahya, K., 2015. Comparison of noise prediction and measurement from construction sites. *Malaysian Journal of Civil Engineering*, 27(1), pp. 19-33.
- Das, H.S. and Roy, P., 2019. A deep dive into deep learning techniques for solving spoken language identification problems. In: Dey, N, (ed). *Intelligent Speech Signal Processing*. San Diego: Academic Press, pp. 81-100.

- Das, K. and Behera, R.N, 2017. A survey on machine learning: concept, algorithms and applications. *International Journal of Innovative Research in Computer and Communication Engineering*, 5(2), pp. 1301-1309.
- Dasgupta, A. and Nath, A., 2016. Classification of machine learning algorithms. *International Journal of Innovative Research in Advanced Engineering*, 3(3), pp. 2349-2763.
- Depart of Environment Malaysia, 2019. *Guidelines for environmental noise limits and control*. 3rd ed. Putrajaya: Department of Environment Malaysia.
- Department of Occupational Safety and Health, 2019. *Department of Occupational Safety and Health*. [Online] Available at: <http://tpg2.dosh.gov.my/index.php/ms/occupational-diseases-and-poisoning-statistic> [Accessed 25 June 2020].
- Department of Occupational Safety and Health, 2019. *Occupational and Safety Health (Noise Exposure) Regulations*. [Online] Available at: <https://www.dosh.gov.my/index.php/legislation/eregulations/regulations-under-occupational-safety-and-health-act-1994-act-514/3174-00-occupational-safety-and-health-noise-exposure-2019/file> [Accessed September 2021].
- Do, L.N.N, Neda, T. amd Vu, H.L., 2018. Survey of neural network - based models for short - term traffic state prediction. *WIREs Data Mining and Knowledge Discovery*, 9(1).

- Duchi, J., Hazan, E. and Singer, Y., 2011. Adaptive subgradient methods for online learning and stochastic optimization. *Journal of Machine Learning Research*, 12, pp. 2121-2159.
- Fan, C., Xu, J. and Di, S., 2014. Lane detection based on machine learning algorithm. *TELKOMNIKA Indonesian Journal of Electrical Engineering*, 12(2), pp. 1403-1409.
- Feder, K. et al., 2017. Prevalence of hazardous occupational noise exposure, hearing loss and hearing protection usage among a representative sample of working Canadians. *Journal of Occupational and Environmental Medicine*, 59(1), pp. 92-113.
- Fernández, M.D., Quintana, S., Chavarría, N. and Ballesteros, J.A., 2009. Noise exposure of workers of the construction sector. *Applied Acoustics*, 70, pp. 753-760.
- Firdaus, S. and Uddin, M.A., 2015. A survey on clustering algorithms and complexity analysis. *International Journal of Computer Science Issues*, 12(2), pp. 62-85.
- Foo, K.Y., 2014. A vision of the environmental and occupational noise pollution in Malaysia. *Noise Health*, 16(73), pp. 427-436.
- Freedman, D., Pisani, R. and Purves, R., 2007. *Statistics*. 4 ed. New York: W. Norton & Company, Inc.
- Gan, W.Q. and Mannino, D.M., 2018. Occupational noise exposure, bilateral high-frequency hearing loss, and blood pressure. *Journal of Occupational and Environmental Medicine*, 60(5), pp. 462-468.

- Geetha, M. and Ambika, D., 2015. Study on the impact of noise pollution at construction site. *International Journal of Latest Trends in Engineering and Technology (IJLTET)*, 5(1).
- Genaro, N. et al., 2010. A neural network based model for urban noise prediction. *Acoustical Society of America*, 128(4), pp. 1738-1746.
- Gilchrist, A., Allouche, E.N. and Cowan, D., 2003. Prediction and mitigation of construction noise in an urban environment. *Canadian Journal of Civil Engineering*, 30(4), pp. 659-672.
- Golmohammadi, R., Mohammadi, H., Bayat, H., Mohraz, M.H. and Soltanian, A.R., 2013. Noise annoyance due to construction worksites. *Journal of Research in Health Sciences*, 13(2), pp. 201-207.
- Goodfellow, I., Bengio, Y. and Courville, A., 2016. *Deep learning*. Cambridge: Massachusetts Institute of Technology.
- Goulet, J.A., 2020. *Probabilistic machine learning for civil engineers*. Cambridge: MIT Press.
- Guo, J., Wang, M., Kang, Y., Zhang, Y. and Gu, C., 2019. Prediction of ship cabin noise based on RBF neural network. *Mathematical Problems in Engineering*, 2019, pp. 1-21.
- Halim, H., Abdullah, R., Abang Ali, A.A. and Mohd. Nor, M.J., 2015. Effectiveness of existing noise barriers: comparison between vegetation, concrete hollow block, and panel concrete. *Procedia Environmental Sciences*, 30, pp. 217-221.

- Haron, Z., Oldham, D., Yahya, K. and Zakaria, R., 2008. A probabilistic approach for modelling of noise from construction site for sustainable environment. *Malaysian Journal of Civil Engineering*, 20(1), pp. 58 - 72.
- Haron, Z., Yahya, K. and Jahya, Z., 2012. Prediction of noise pollution from construction sites at the planning stage using simple prediction charts. *Energy Education Science and Technology, Part A: Energy Science and Research*, 29(2), pp. 989-1002.
- Haron, Z. and Yahya, K., 2009. Monte Carlo analysis for prediction of noise from a construction site. *Journal of Construction in Developing Countries*, 14(1).
- Harrington, P.B., 2017. Multiple versus single set validation of multivariate models to avoid mistakes. *Critical Reviews in Analytical Chemistry*, 48(1), pp. 33-46.
- Hastie, T., Tibshirani, R. and Friedman, J., 2009. *The elements of statistical*. 2nd ed. New York: Springer.
- Haugeland, J., 1985. *Artificial Intelligence: The Very Idea*. 1 ed. Cambridge: MIT Press.
- Haycraft, W.R., 2011. History of Construction Equipment. *Journal of Construction Engineering and Management*, 137(10), pp. 720-723.
- Henseler, J., Ringle, C.M. and Sinkovics, R.R., 2009. The use of partial least squares path modelling in international marketing. *Advances in International Marketing*, 20, pp. 277-319.
- Hewitt, P.G., 2014. *Conceptual Physics*. 12 ed. London: Pearson Education Limited.

- Hinton, G. and Tieleman, T., 2012. *Computer science university of toronto*.
[Online] Available at:
[https://www.cs.toronto.edu/~tijmen/csc321/slides/lecture_slides_lec6.p
df](https://www.cs.toronto.edu/~tijmen/csc321/slides/lecture_slides_lec6.pdf)[Accessed 22 April 2021].
- Huang, T., Kecman, V. and Kopriva, I., 2006. *Kernel based algorithms for mining huge data sets*. 1 ed. New York: Springer-Verlag Berlin Heidelberg.
- Hunashal, R. B. and Patil, Y. B., 2012. Assessment of noise pollution indices in the city of Kolhapur, India. *Procedia - Social and Behavioral Sciences*, 37, pp. 448-457.
- Idris, N., 2012. *Automated prediction of noise from construction site using stochastic approach*, Universiti Teknologi Malaysia: Master Thesis.
- International Electrotechnical Commission, 2002. *Sound level meters: part 1: specifications*. Geneva: International Electrotechnical Commission.
- Jahya, Z., 2014. *Automated construction noise prediction by considering the variability of noise sources and outdoor sound propagation*. Universiti Teknologi Malaysia: Master Thesis.
- Jo, T., 2021. *Machine Learning Foundations*. Cham: Springer.
- Johnson, A.C. and Morata, T.C., 2010. Occupational exposure to chemicals and hearing impairment. *The Nordic Expert Group for Criteria Documentation of Health Risks from Chemicals.*, 44(4), p. 177.
- Kandel, I. and Castelli, M., 2020. The effect of batch size on the generalizability of the convolutional neural networks on a histopathology dataset. *ICT Express*, 6(4), pp. 312-315.
- Ketkar, N., 2017. *Deep Learning with Python*. New York: Apress.

- Khan, K., Attique, M., Syed, I. and Chung, T., 2020. A multi-task framework for facial attributes classification through end-to-end face parsing and deep convolutional neural networks. *Sensors*, 20(2), pp. 328.
- Kim, P., 2017. *MATLAB Deep Learning*. New York: Springer.
- Kingma, D.P. and Ba, J.L., 2015. *Adam: A method for stochastic optimization*. San Diego, 3rd International Conference for Learning Representations.
- Kinsley, H. and Kukiela, D., 2020. *Neural Networks from Scratch in Python*. Cambridge: MIT.
- Koi, H.S.F.I.A., Tamura, H. and Hiramatsu, K., 1993. Regional noise prediction and management system using remote sensing. *International Journal of Remote Sensing*, 14(13), pp. 2427-2443.
- Konbattulwar, V., Velaga, N.R., Jain, S. and Sharmila, R.B., 2016. Development of in-vehicle noise prediction models for Mumbai metropolitan region, India. *Journal of Traffic and Transportation Engineering*, 3(4), pp. 380-387.
- Kroese, D.P., Taimre, T. and Botev, Z.I., 2011. *Handbook of Monte Carlo Methods*. New Jersey: John Wiley & Sons.
- Kurniawan, F., Umayah, B., Hammad, J., Nugroho, S.M.S. and Hariadi, M., 2018. Market basket analysis to identify customer behaviours by way of transaction data. *Knowledge Engineering and Data Science (KEDS)*, 1(1), pp. 20-25.
- Kurzweil, R., 1999. *The Age of Spiritual Machines*. 1 ed. New York: Viking Penguin.

- Lago, J., Ridder, F.D. and Schutter, B.D., 2018. Forecasting spot electricity prices: Deep learning approaches and empirical comparison of traditional algorithms. *Applied Energy*, 221, pp. 386-405.
- Lan, Y., Soh, Y. and Huang, G., 2010. Constructive hidden nodes selection of extreme learning machine for regression. *Neurocomputing*, 73, pp. 3191-3199.
- Lee, H.P., Wang, Z. and Lim, K.M., 2016. Assessment of noise from equipment and processes at construction sites. *Building Acoustics*, 24(1), pp. 21-34.
- Lee, S.H., Chan, C.S. and Remagnino, P., 2018. Multi-organ plant classification based on convolutional and recurrent neural networks. *IEEE Transactions on Image Processing*, 27(9), pp. 4287-4301.
- Lee, S.C., Hong, J.Y. and Jeon, J.Y., 2015. Effects of acoustic characteristics of combined construction noise on annoyance. *Building and Environment*, 92, pp. 657-667.
- Li, D. and Dong, Y., 2014. Deep learning: Methods and applications. *Foundations and Trends*, 7(3-4), pp. 198-349.
- Li, X., Song, Z., Wang, T., Zheng, Y. and Ning, X., 2016. Health impacts of construction noise on workers: a quantitative assessment model based on exposure measurement. *Journal of Cleaner Production*, 135, pp. 721-731.
- Lim, M.H., Haron, Z., Yahya, K., Bakar, S.A. and Dimon, M.N., 2015. A stochastic simulation framework for the prediction of strategic noise mapping and occupational noise exposure using the random walk approach. *PLoS ONE*, 10(4), p. e0120667.

- Lim, M.H., 2017. *Continuous noise mapping prediction techniques using the stochastic modelling*, Skudai, Johor, Malaysia: Doctor in Philosophy.
- Lord R., 1972. *Safety and Health at Work*, London: House of Commons Parliamentary Papers Online.
- Loy, J., 2019. *Neural network projects with python*. Birmingham: Packt Publishing Ltd.
- Lutz, M., 2013. *Learning Python*. 5 ed. Sebastopol: O'Reilly Media, Inc.
- Lydia, A. and Sagayaraj, F., 2019. Adagrad -An optimizer for stochastic gradient descent. *International Journal of Information and Computing Science*, 6, pp. 566-568.
- Macca, I. et al., 2015. High-frequency hearing thresholds: effects of age, occupational ultrasound and noise exposure. *International Archives of Occupational and Environmental Health*, 88(2), pp. 197-221.
- Majaj, J.N. and Pelli, D.G., 2018. Deep learning—using machine learning to study biological vision. *Journal of Vision*, 18(13), pp. 1-13.
- Mallampti, D., 2018. An efficient spam filtering using supervised machine learning techniques. *International Journal of Scientific Research in Computer Science and Engineering*, 6(2), pp. 33-37.
- Mansourkhaki, A., Berangi, M., Haghiri, M. and Haghani, M., 2018. A neural network noise prediction model for Tehran urban roads. *Journal of Environmental Engineering and Landscape Management*, 26(2), pp. 88-97.

- Mansourkhaki, A., Berangi, M. and Haghiri, M., 2018. Comparative application of radial basis function and multilayer perceptron neural networks to predict traffic noise pollution in tehran roads. *Journal of Ecological Engineering*, 19(1), pp. 113-121.
- Marsland, S., 2015. *Machine learning an algorithm perspective*. New York: Taylor and Francis Group.
- Mohd Bakhori et al., 2017. Noise Measurement and awareness at construction site – A case study. *Journal of Advanced Research Design*, 31(1), pp. 9-16.
- Montavon, G., Orr, G.B. and Müller, K.B., 2012. *Neural network: Tricks of the trade*. 2 ed. New York: Springer.
- Moolayil, J., 2019. *Learn Keras for Deep Neural Networks*. New York: Springer.
- Morata, T.C., 2016. Uncovering effective strategies for hearing loss prevention. *Acoust Aust*, 44(1), pp. 67-75.
- Murphy, E. and King, E., 2014. *Environmental noise pollution, noise mapping, public health, and policy*. 1 ed. San Diego: Elsevier Inc.
- Navarro, J.M., Martinez-Espana, R., Bueno-Crespo, A., Martinez, R. and Cecilia, J.M., 2020. Sound levels forecasting in an acoustic sensor sound levels forecasting in an Acoustic Sensor. *Sensors*, 20, p. 903.
- Nelson, D.I., Nelson, R.Y., Barrientos, M.C. and Fingerhut, M., 2005. The global burden of occupational noise-induced hearing loss. *American Journal of Industrial Medicine*, 48, pp. 446-458.
- Nelson, P.M., 1973. The combination of noise from separate time varying sources. *Applied Acoustics*, 6(1), pp. 1-21.

- Nilsson, N.J., 1998. *Artificial intelligence: A New Synthesis*. Beijing: Morgan Kaufmann Publishers Inc.
- Olatunji, O.O., Akinlabi, S., Madushele, N., Adedeji, P.A. and Felix, I., 2019. Multilayer perceptron artificial neural network for the prediction of heating value of municipal solid waste. *AIMS Energy*, 7(6), pp. 944-956.
- Passchier-Vermeer, W. and Passchier, W.F., 2000. Noise exposure and public health. *Environmental Health Perspectives*, 108, pp. 123-131.
- Patel, A.A., 2019. *Hands-on unsupervised learning using python*. Sebastopol: O'Reilly Media, Inc.
- Petrovici, A., Tomozei, C., Flores, R.G., Nedeff, F. and Irimia, O., 2015. Noise prediction, calculation and mapping using specialized software. *Journal of Engineering Studies and Research*, 21, pp. 59-64.
- Pierce, A. D., 2019. *An introduction to its physical principles and applications*. 3 ed. Cham: Springer.
- Pohlmann, K.C. and Everest, F.A., 2015. *Master Handbook of Acoustics*. 6 ed. New York: McGraw-Hill Education.
- Rafique, D. and Velasco, L., 2018. Machine learning for network automation: overview, architecture, and applications. *Journal of Optical Communications and Networking*, 10(10), pp. D126-D143.
- Raschka, S. and Mirjalili, V., 2017. *Python machine learning*. 2 ed. Birmingham: Packt Publishing.
- Rosenblatt, F., 1958. The perceptron: A probabilistic model for information storage and organization in the brain. *Psychological Review*, 65(6), pp. 386-408.

- Said, K.M., Haron, Z., Saim A.A., Abidin, M.Z., Yahyah, K. and Lim, M.H., 2014. Occupational Noise Exposure among Road Construction Workers. *Jurnal Teknologi*, 70(7), pp. 15-19.
- Shubhendu S.S. and Vijay, J., 2013. Applicability of artificial intelligence in different fields of life. *International Journal of Scientific Engineering and Research*, 1(1), pp. 2347-3878.
- Silver, L., Wren, B. and Loudon, D., 2013. *The essential of marketing research*. 3rd ed. New York: Taylor and Francis.
- Singh, P. and Manure, A., 2020. *Learn TensorFlow 2.0 implement machine learning and deep learning models with python*. New York: Springer.
- Singh, P., 2021. *Deploy machine learning models to production*. New York: Springer.
- Skansi, S., 2018. *Introduction to deep learning*. Cham: Springer.
- Social Security Organization, 2020. *Pertubuhan Keselamatan Sosial*. [Online] Available at: <https://www.perkeso.gov.my/index.php/ms/laporan/laporan-tahunan> [Accessed 25 6 2020].
- Soydaner, D., 2020. A comparison of optimization algorithms for deep learning. *International Journal of Pattern Recognition and Artificial Intelligence*, 34(13), p. 2052013.
- Suhartono, Ashari, D.E., Prastyo, D.D., Kuswanto, H. and Lee, M.H., 2019. Deep neural network for forecasting inflow and outflow in Indonesia. *Sains Malaysiana*, 48(8), p. 1787–1798.
- Suter, A.H., 2010. Construction noise: exposure, effects, and the potential for remediation; a review and analysis. *AIHA Journal*, 63(6), pp. 768-789.

- Taylor, H.M. and Karlin, S., 1998. *An introduction to stochastic modelling*. San Diego: Academic Press Limited.
- Themann, C.L. and Masterson, E.A., 2019. Occupational noise exposure: a review of its effects, epidemiology, and impact with recommendations for reducing its burden. *The Journal of the Acoustical Society of America*, 146(5), pp. 3879-3905.
- Towers, D.A., 2001. Mitigation of community noise impacts from nighttime construction. *Construction and Materials Issues*, pp. 106-120.
- Vijaya, Aayushi, S. and Ritika, B., 2017. A review on hierarchical clustering algorithms. *Journal of Engineering and Applied Sciences*, 12(24), pp. 7501-7507.
- Wang, P., Chan, C.Y. and La Fortelle, A., 2018. A Reinforcement learning based approach for automated lane change manoeuvres. *IEEE Intelligent Vehicles Symposium (IV)*, 71, pp. 1379-1384.
- Wang, X., Song, L., Wu, Z. and Wu, P., 2018. Development of a road shoulder's equivalent sound source traffic noise prediction model. *Proceedings of the Institution of Civil Engineers – Transport*, pp. 1-10.
- Weisberg, S., 2014. *Applied Linear Regression*. 4 ed. Hoboken: John Wiley & Sons, Inc.
- Winston, P.H., 1992. *Artificial Intelligence*. 3 ed. Reading, Massachusetts: Addison-Wesley.
- Witten, I.H., Frank, E., Hall, M.A. and Pal, C.J., 2017. *Data mining practical machine learning tools and techniques*. 4 ed. Cambridge: Morgan Kaufmann.

- World Health Organization, 2011. *Burden of Disease from Environmental Noise: Quantification of healthy life years lost in Europe*. Denmark: World Health Organization.
- Xu, Y. and Goodacre, R., 2018. On splitting training and validation set: A comparative study of cross-validation, bootstrap and systematic sampling for estimating the generalization performance of supervised learning. *Journal of Analysis and Testing*, 2, pp. 249-262.
- Yang, Z., Wang, C., Zhang, Z. and Li, J., 2019. Mini-batch algorithms with online step size: *Knowledge-Based Systems*, 165, pp. 228-240.
- Zaccone, G. and Karim, M.R., 2018. *Deep learning with TensorFlow*. 2 ed. Birmingham: Packt.
- Zanin, P.H.T., do Nascimento, E.O., da Paz, E.C. and do Valle, F., 2018. Application of artificial neural networks for noise barrier optimization. *Environment*, 5(12), pp. 135.
- Zao, C., Zhu, R., Tao, Z., Ouyang, D. and Chen, Y., 2020. Evaluation of building construction-induced noise and vibration impact on residents. *Sustainability*, 12(4), pp. 1579.
- Zhang, X., Zhao, M. and Dong, R., 2020. Time-series prediction of environmental noise for urban IoT based on long short-term memory recurrent neural network. *Applied Sciences*, 10, pp. 1144.
- Zhao, H., Liu, F., Zhang, H. and Liang, Z., 2019. Research on a learning rate with energy index in deep learning. *Neural Network*, 110, pp. 225-231.

- Zhao, Y., Wong, Z.S.Y. and Tsui, K.L., 2018. A framework of rebalancing imbalanced healthcare data for rare events' classification: a case of look-alike sound-alike mix-up incident detection. *Hindawi Journal of Healthcare Engineering*, pp. 1-11.
- Zolfagharian, S., Nourbakhsh, M. and Irizarry, J., 2012. Environmental impacts assessment on construction sites. *Construction Research Congress 2012*.
- Zulifqar et al., 2017. Forecasting drought using multilayer perceptron artificial neural network model. *Advances in Meteorology*, 2017, pp. 1-9.

APPENDIX A

APPENDIX A: Basic Length, l , of the machine

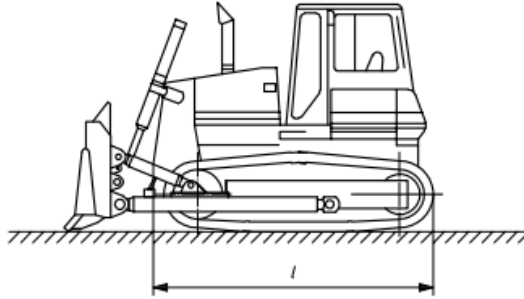


Figure A.1: Crawler dozer (British Standard Institution, 2008).

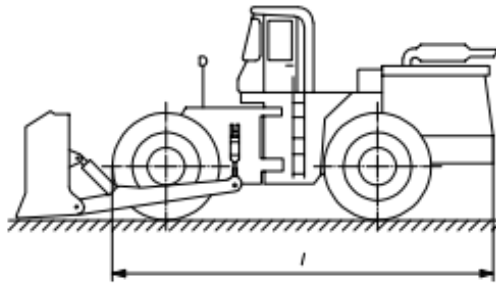


Figure A.2: Wheeled dozer (British Standard Institution, 2008).

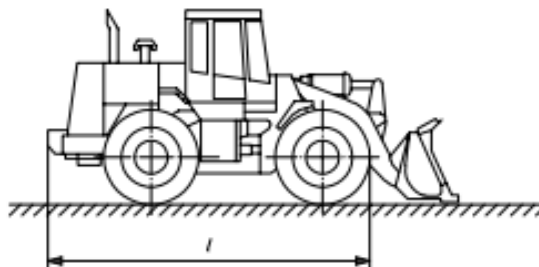


Figure A.3: Wheeled loader with an operating mass more than 4500 kg (British Standard Institution, 2008).

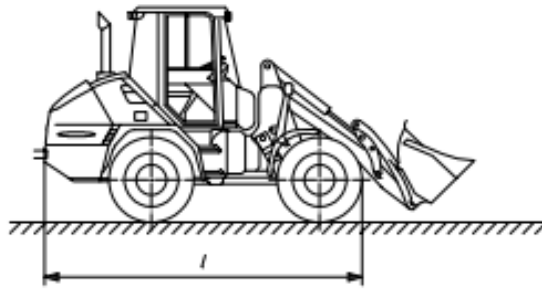


Figure A.4: Crawler loader with an operating mass less than or equal to 4500 kg (British Standard Institution, 2008).

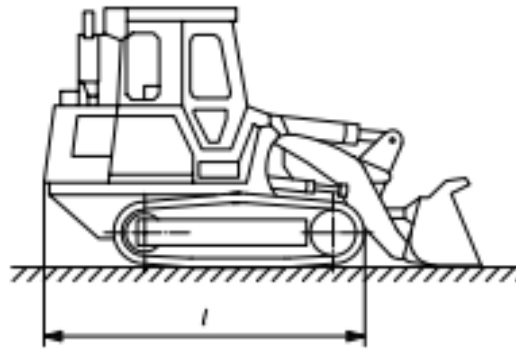


Figure A.5: Crawler loader (British Standard Institution, 2008).

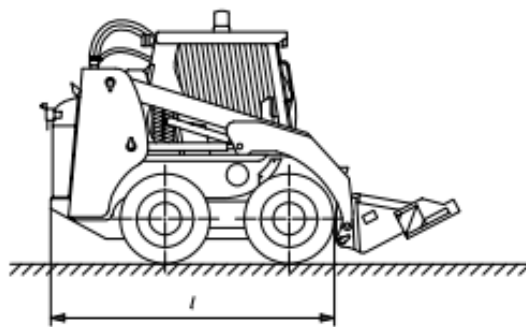


Figure A.6: Skid steer loader (British Standard Institution, 2008).

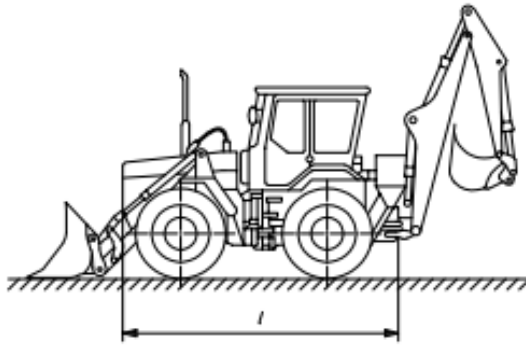


Figure A.7: Wheeled backhoe loader (British Standard Institution, 2008).

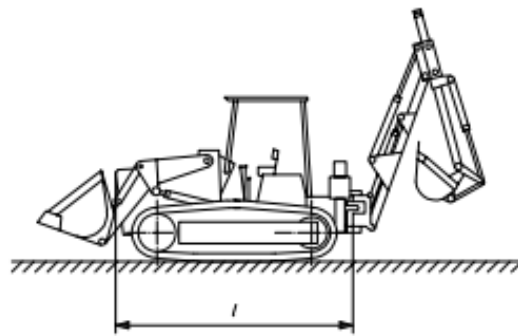


Figure A.8: Crawler backhoe loader (British Standard Institution, 2008).

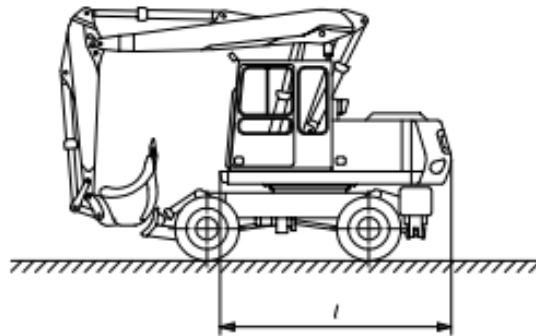


Figure A.9: Wheeled excavator (British Standard Institution, 2008).

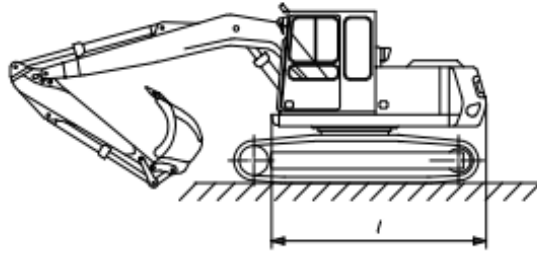


Figure A.10: Crawler excavator (British Standard Institution, 2008).

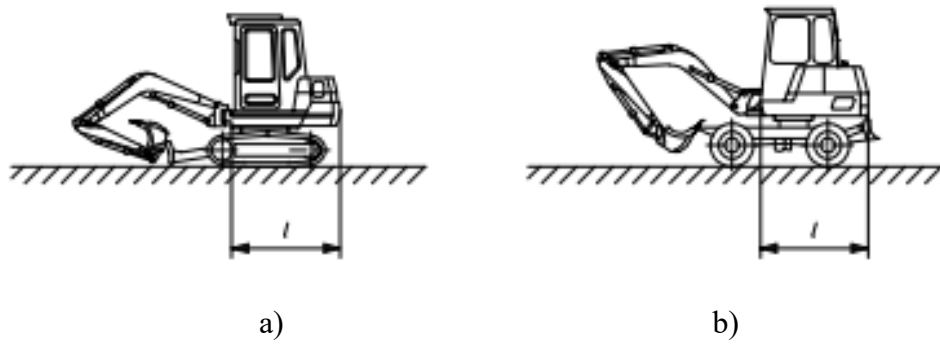


Figure A.11: Compact excavator with an operating mass less than or equal to 6000 kg (British Standard Institution, 2008).

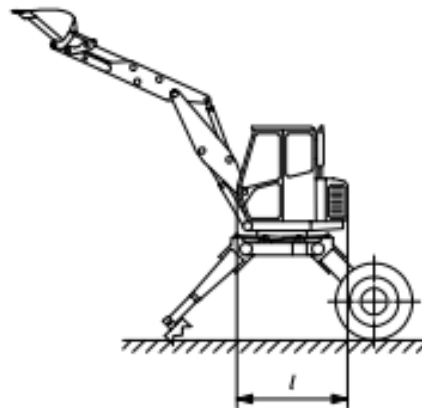


Figure A.12: Walking excavator (British Standard Institution, 2008).

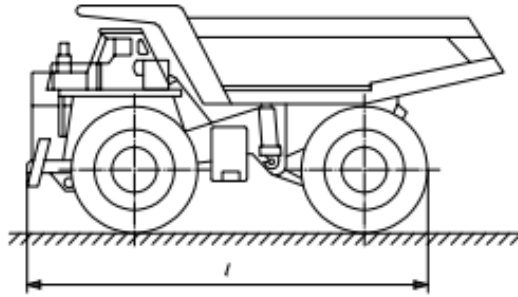


Figure A.13: Wheeled rigid-frame dumper (British Standard Institution, 2008).

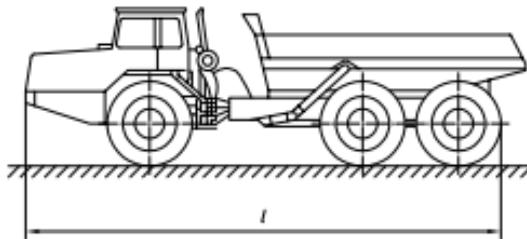


Figure A.14: Articulated-frame dumper (British Standard Institution, 2008).

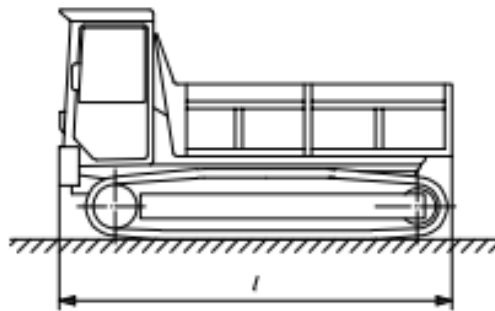


Figure A.15: Crawler dumper (British Standard Institution, 2008).

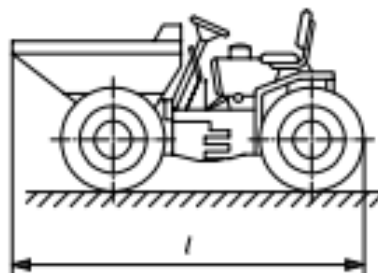


Figure A.16: Wheeled dumper with an operating mass less than or equal to 4500 kg (British Standard Institution, 2008).

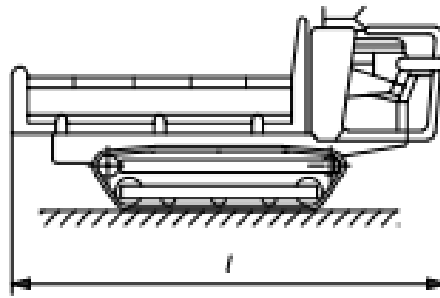


Figure A.17: Crawler dumper with an operating mass less than or equal to 4500 kg (British Standard Institution, 2008).

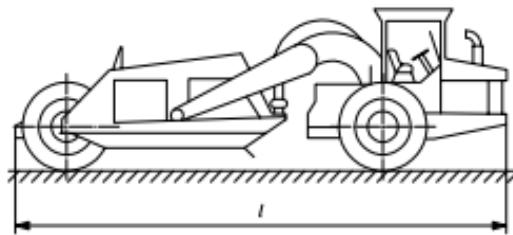


Figure A.18: Scraper with one engine (British Standard Institution, 2008).

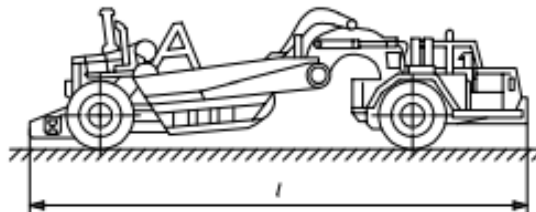


Figure A.19: Scraper with two engines (British Standard Institution, 2008).

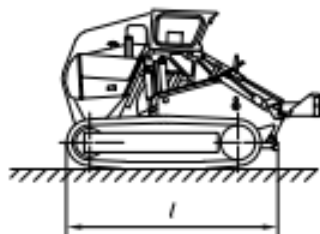


Figure A.20: Crawler scraper (British Standard Institution, 2008).

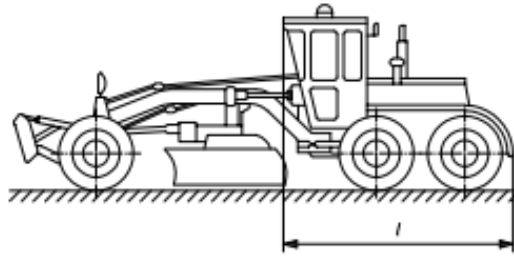


Figure A.21: Grader (British Standard Institution, 2008).

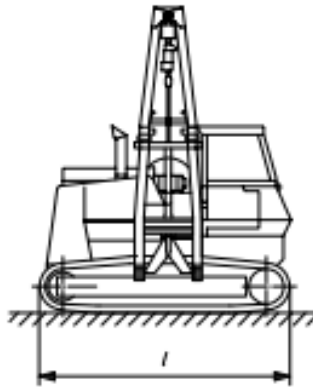


Figure A.22: Pipelayer (British Standard Institution, 2008).

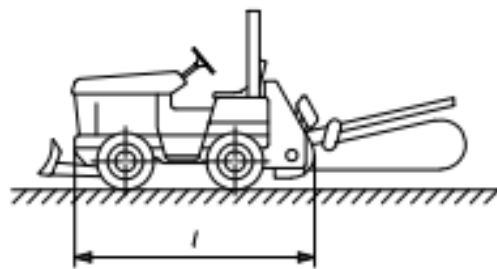


Figure A.23: Wheeled ride-on trencher (British Standard Institution, 2008).

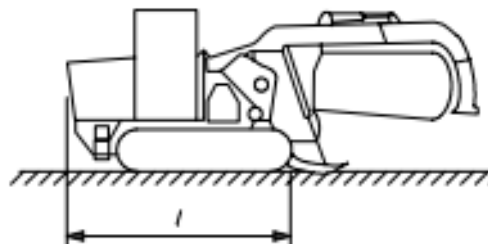


Figure A.24: Crawler ride-on trencher (British Standard Institution, 2008).

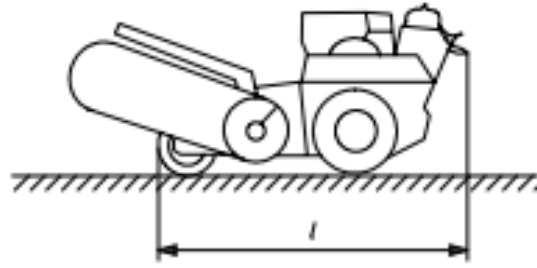


Figure A.25: Walk-behind trencher (British Standard Institution, 2008).

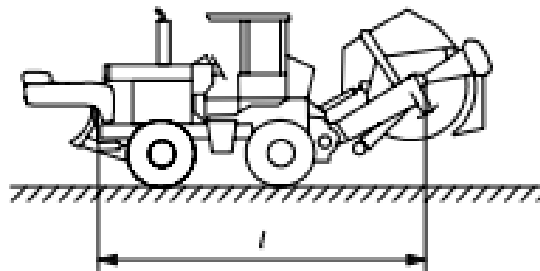


Figure A.26: Disk trencher (British Standard Institution, 2008).

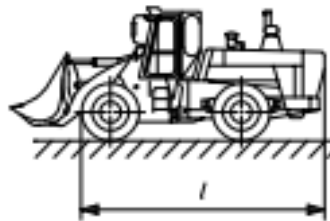


Figure A.27: Landfill compactor with loading equipment (British Standard Institution, 2008).

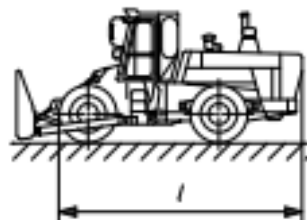
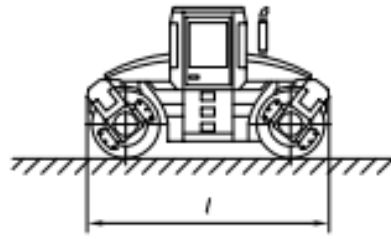
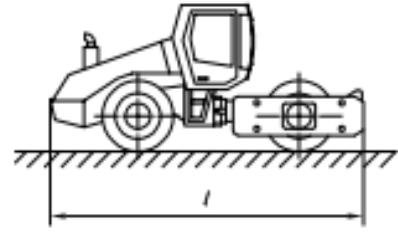


Figure A.28: Landfill compactor with loading equipment (British Standard Institution, 2008).



a)



b)

Figure A.29: Rollers (British Standard Institution, 2008).

APPENDIX B

Appendix B

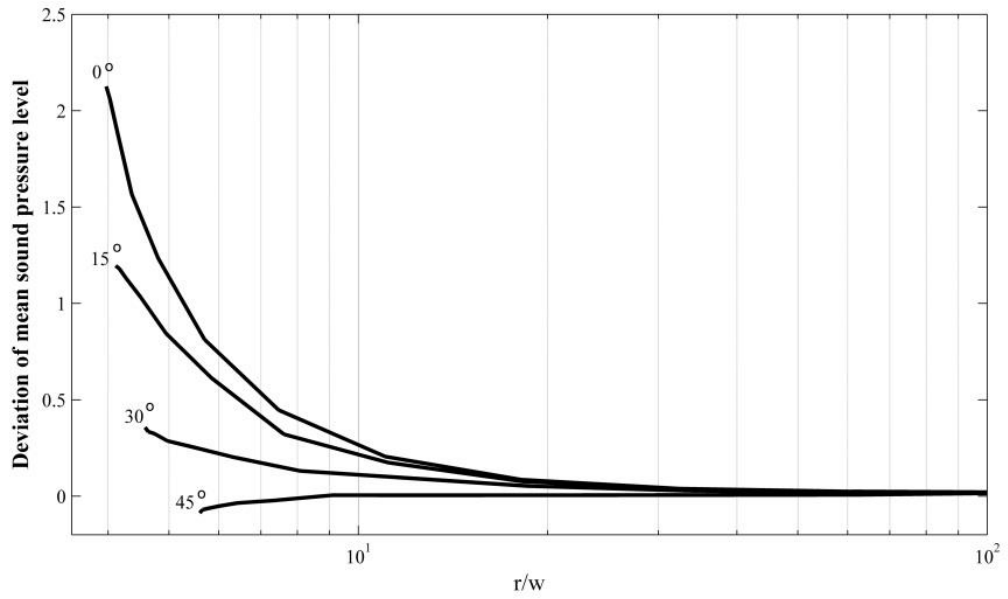


Figure B.1 Simple Prediction Chart for mean level deviation 1:1 aspect ratio (Haron et al., 2012).

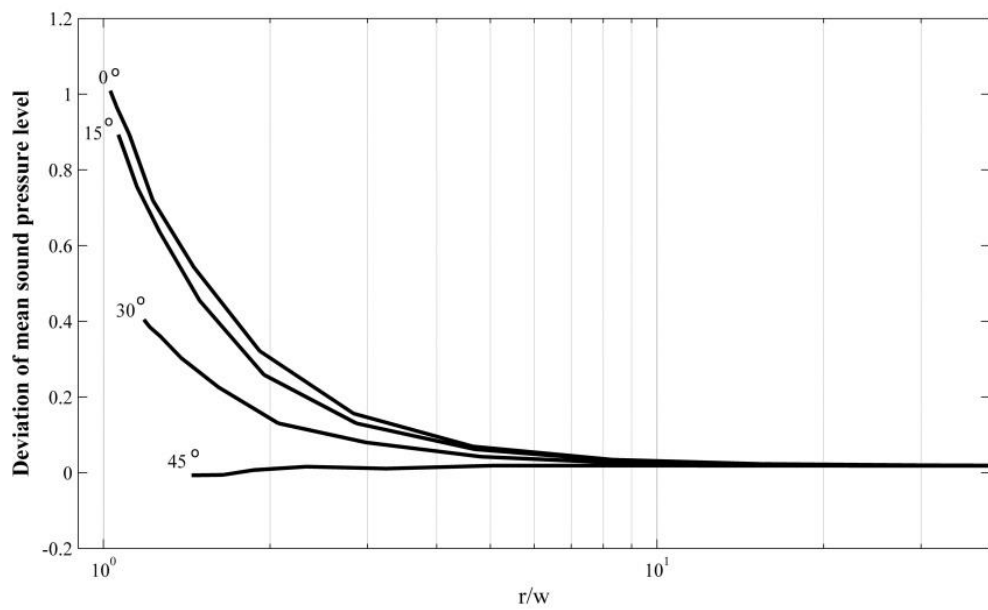


Figure B.2 Simple Prediction Chart for mean level deviation 1:2 aspect ratio (Haron et al., 2012).

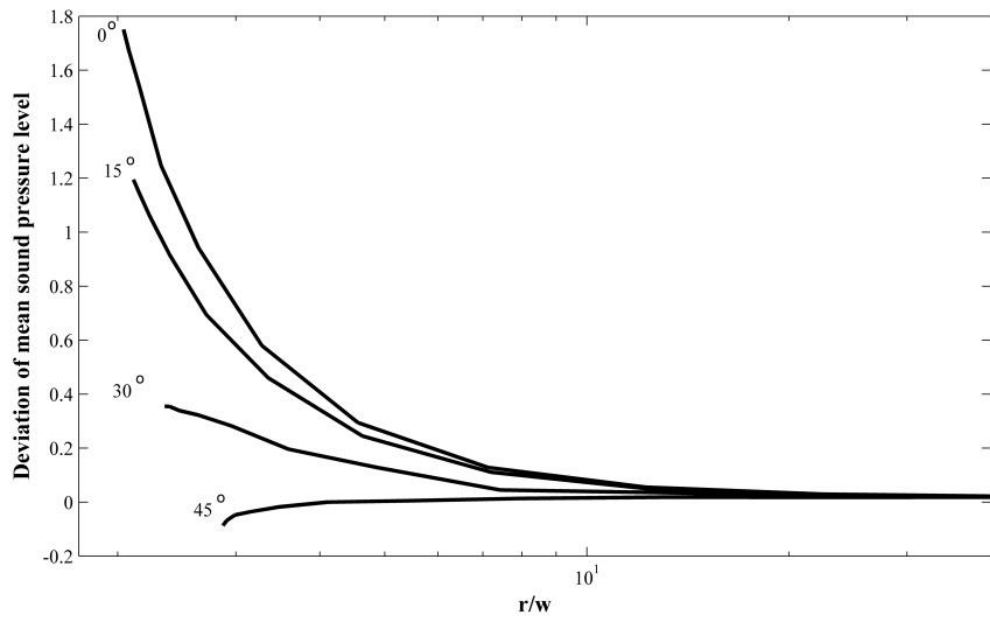


Figure B.3 Simple Prediction Chart for mean level deviation 1:4 aspect ratio (Haron et al., 2012).

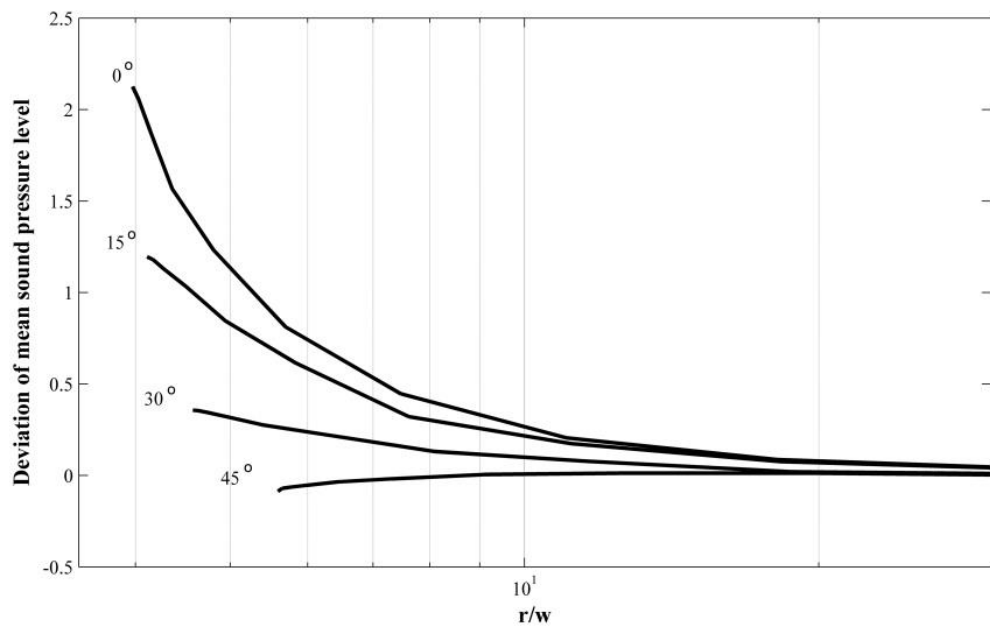


Figure B.4 Simple Prediction Chart for mean level deviation 1:8 aspect ratio (Haron et al., 2012).

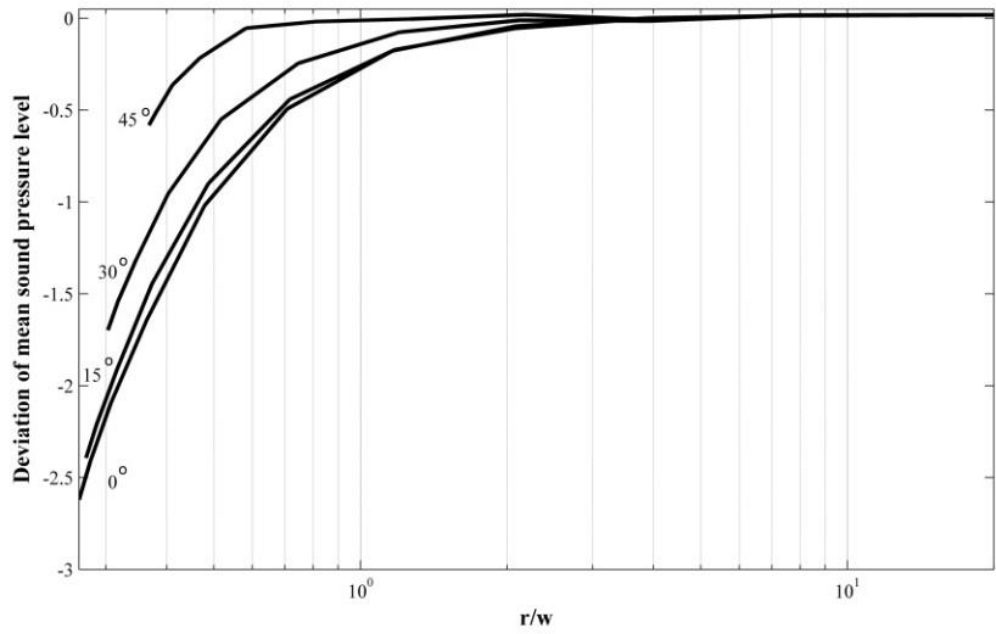


Figure B.5 Simple Prediction Chart for mean level deviation 2:1 aspect ratio (Haron et al., 2012).

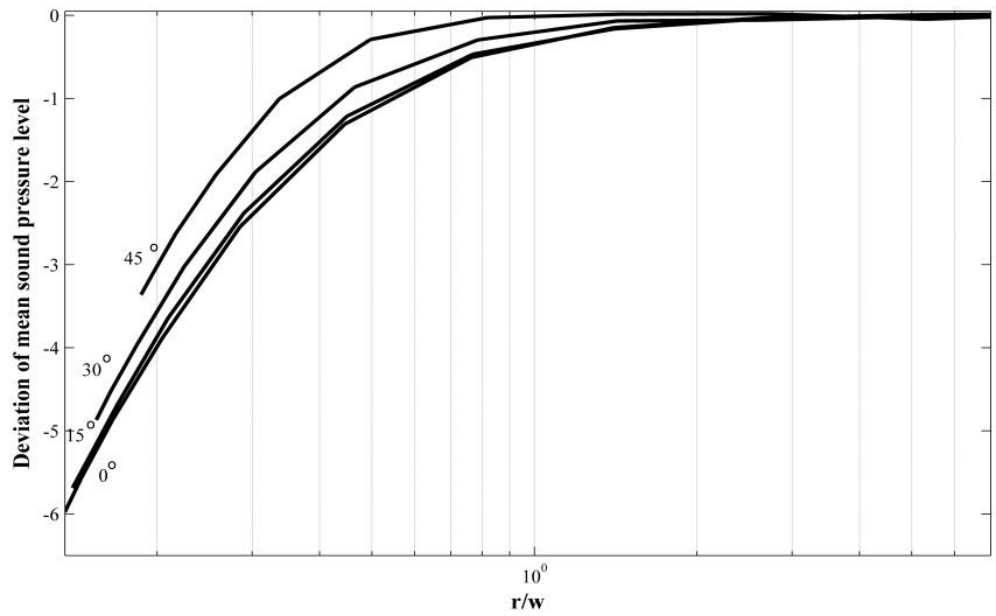


Figure B.6 Simple Prediction Chart for mean level deviation 4:1 aspect ratio (Haron et al., 2012).

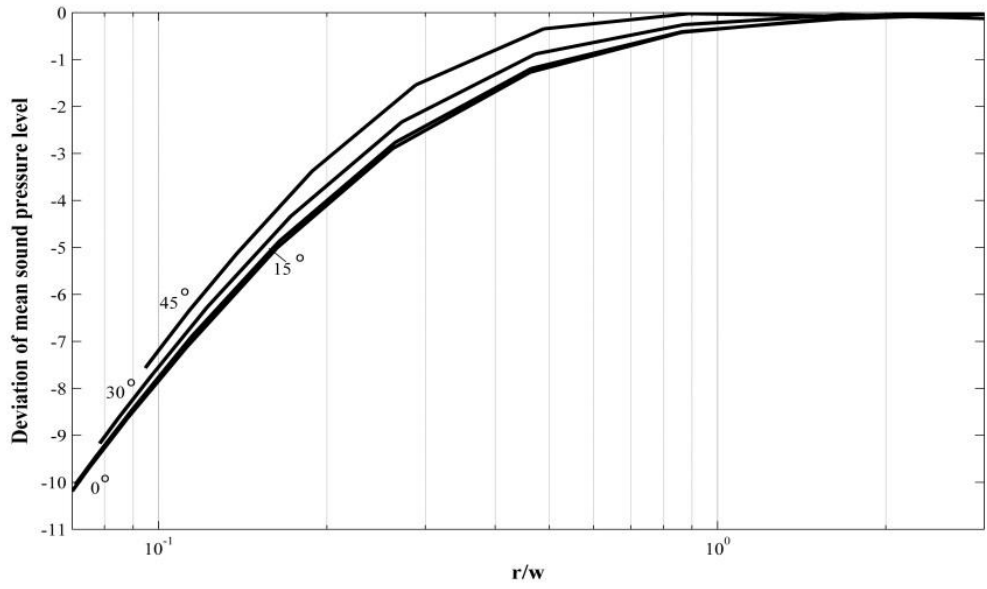


Figure B.7 Simple Prediction Chart for mean level deviation 8:1 aspect ratio (Haron et al., 2012).

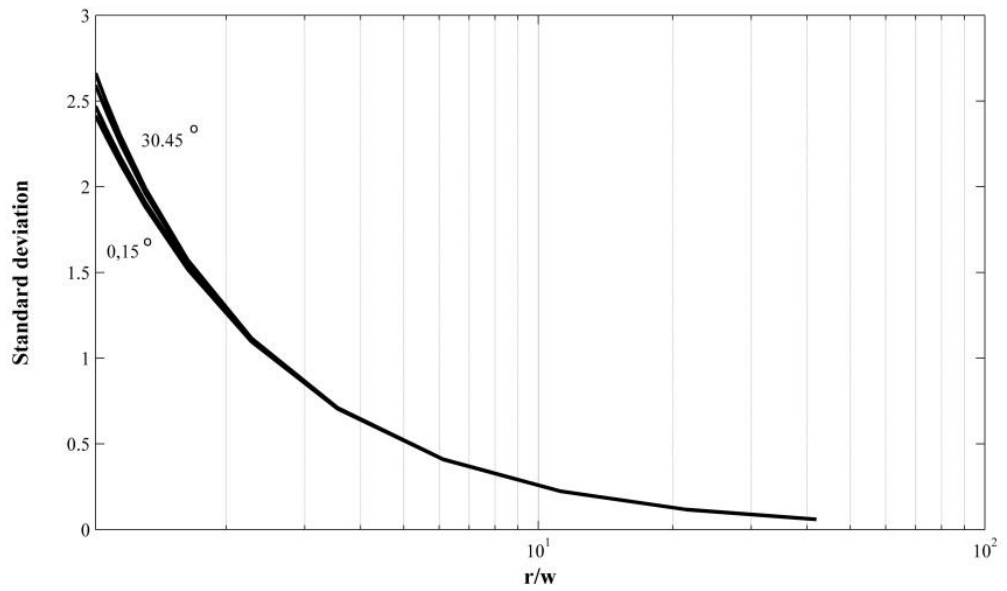


Figure B.8 Simple Prediction Chart for standard deviation 1:1 aspect ratio (Haron et al., 2012).

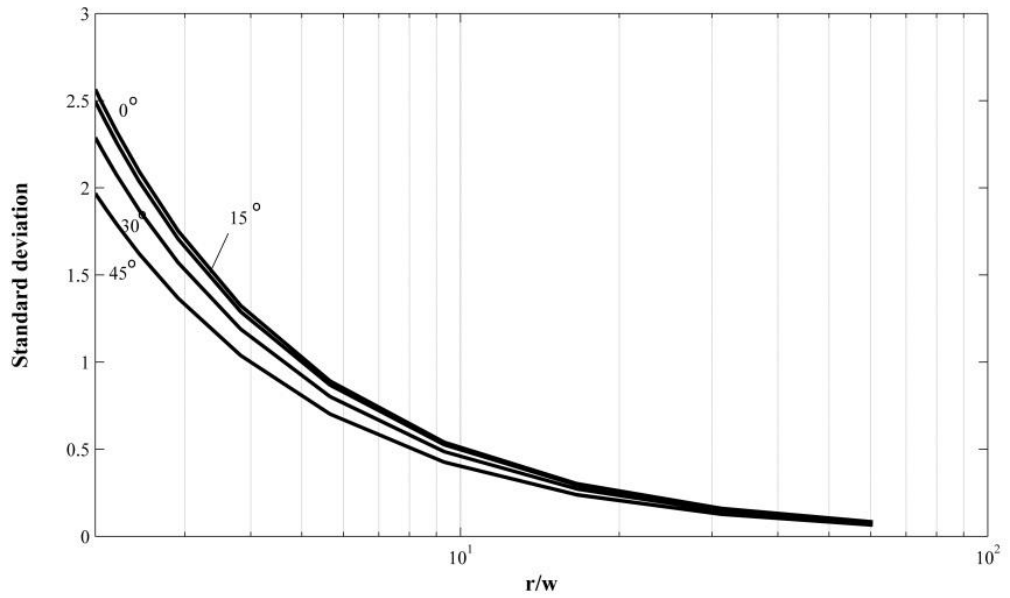


Figure B.9 Simple Prediction Chart for standard deviation 1:2 aspect ratio (Haron et al., 2012).

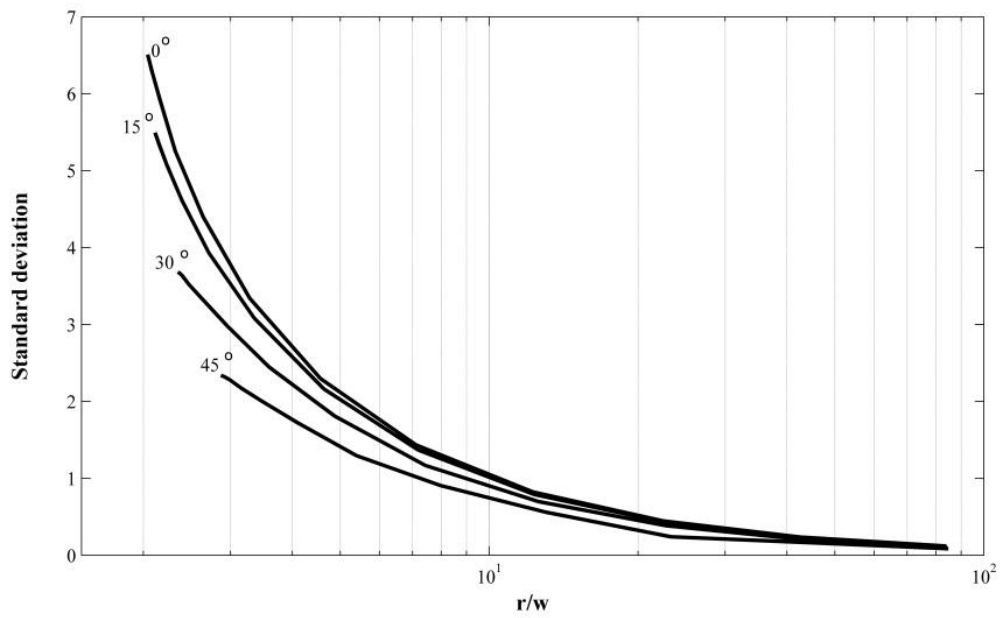


Figure B.10 Simple Prediction Chart for standard deviation 1:4 aspect ratio (Haron et al., 2012).

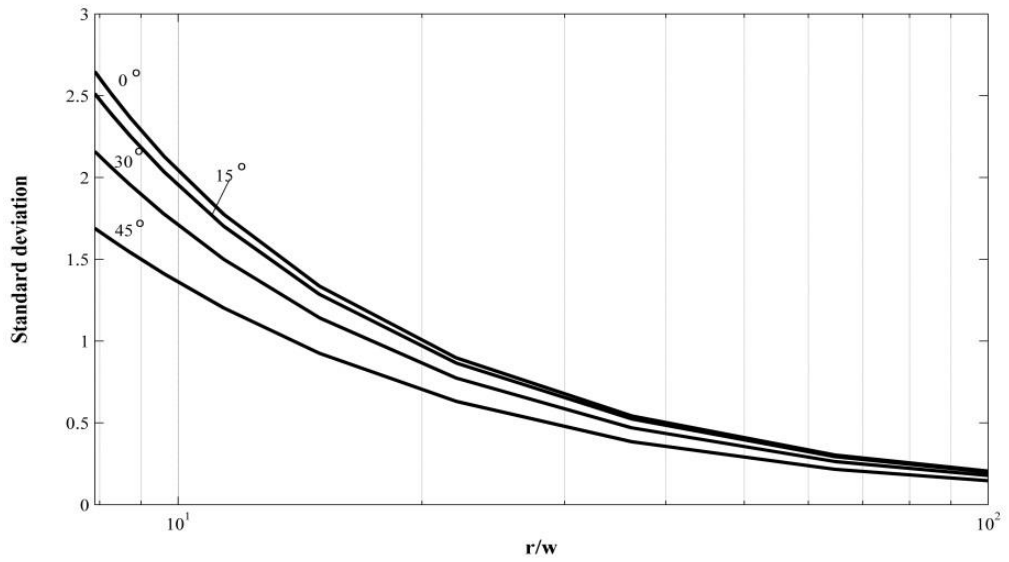


Figure B.11 Simple Prediction Chart for standard deviation 1:8 aspect ratio (Haron et al., 2012).

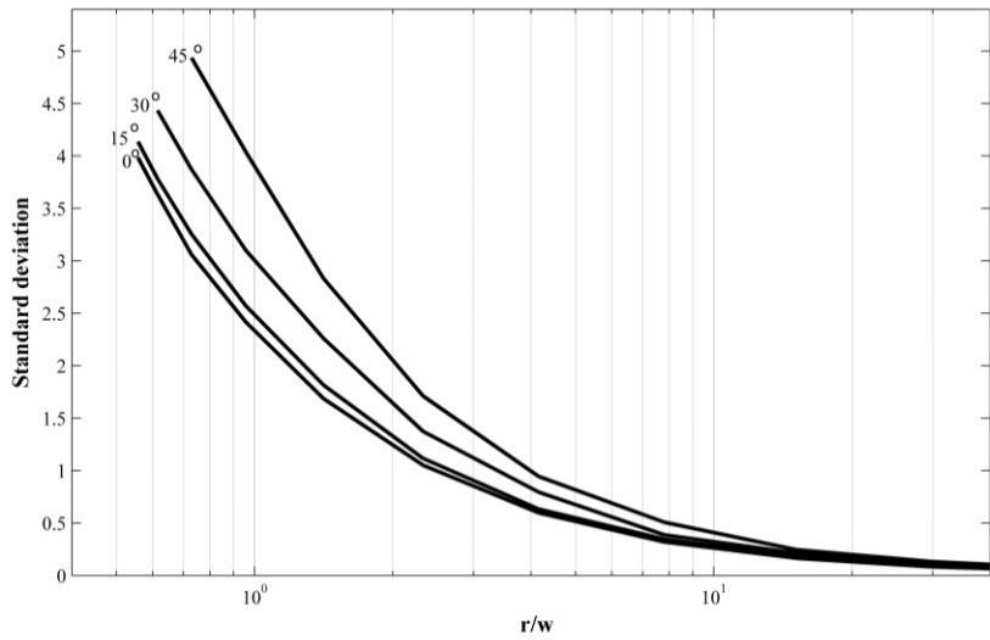


Figure B.12 Simple Prediction Chart for standard deviation 2:1 aspect ratio (Haron et al., 2012).

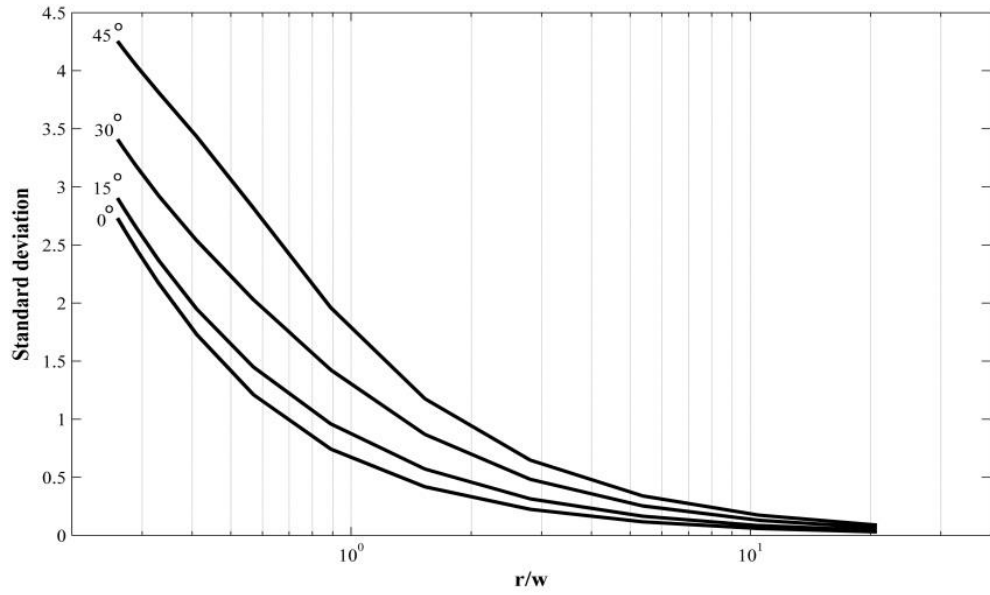


Figure B.13 Simple Prediction Chart for standard deviation 4:1 aspect ratio (Haron et al., 2012).

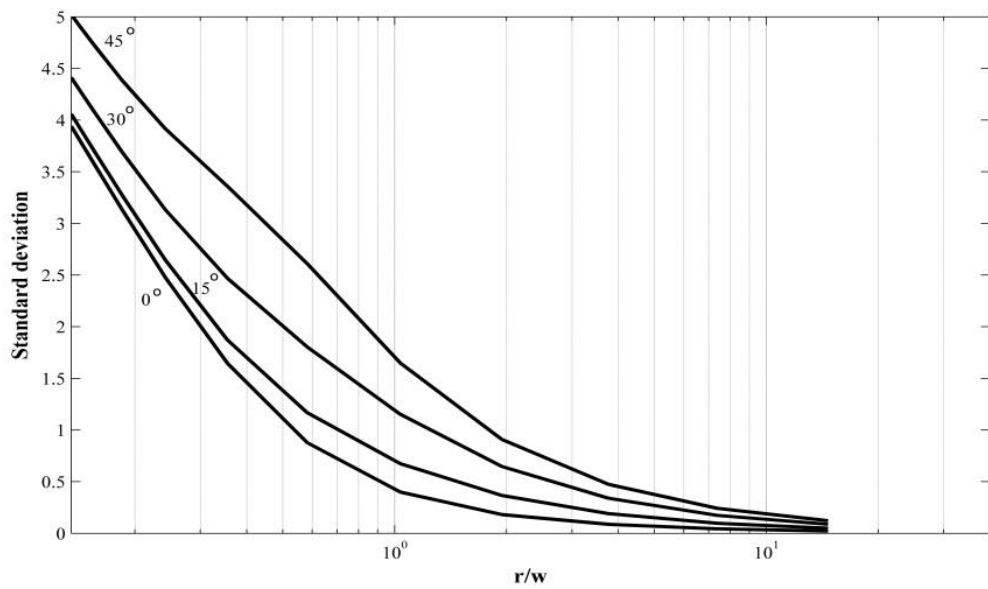


Figure B.14 Simple Prediction Chart for standard deviation 4:1 aspect ratio (Haron et al., 2012).